Seismic Behavior and Retrofitting of Steel Frames under the Sequence of Mainshock and Aftershock

Ph. D. Thesis

Shashi Narayan
2015RNC9021

NATIONAL CENTER OF DISASTER MITIGATION AND MANAGEMENT

MALAVIYA NATIONAL INSTITUTE OF TECHNOLOGY, JAIPUR

OCTOBER 2019

Seismic Behavior and Retrofitting of Steel Frames under the Sequence of Mainshock and Aftershock

Submitted in

fulfillment of the requirements of the degree of

Doctor of Philosophy

By

Shashi Narayan
2015RNC9021

Under the Supervision of

Prof. M. K. Shrimali (Supervisor)
Prof. S. D. Bharti (Supervisor)
Dr. Pradeep K. Goyal (Supervisor, External)

NATIONAL CENTER OF DISASTER MITIGATION AND MANAGEMENT

MALAVIYA NATIONAL INSTITUTE OF TECHNOLOGY JAIPUR

OCTOBER 2019

DECLARATION

I, Shashi Narayan, declare that this thesis titled "*Seismic Behavior and Retrofitting of Steel Frames under the Sequence of Mainshock and Aftershock*" and the work presented in it, are my own. I confirm that:

- This work was done wholly or mainly while in candidature for a research degree at this university.
- Where any part of this thesis has previously been submitted for a degree or any other qualification at this university or any other institution, this has been clearly stated.
- Where I have consulted the published work of others, this is always clearly attributed.
- Where I have quoted from the work of others, the source is always given. With the exception of such quotations, this thesis is entirely my own work.
- I have acknowledged all main sources of help.
- Where the thesis is based on work done by myself, jointly with others, I have made clear exactly what was done by others and what I have contributed myself.

Date:

Shashi Narayan
2015RNC9021

CERTIFICATE

This is to certify that the thesis entitled "***Seismic Behavior and Retrofitting of Steel Frames under the Sequence of Mainshock and Aftershock***", being submitted by **Mr. Shashi Narayan (2015RNC9021)** is a bonafide research work carried out under our supervision and guidance in fulfillment of the requirement for the award of the degree of **Doctor of Philosophy** in the National Center of Disaster Mitigation and Management, Malaviya National Institute of Technology, Jaipur, India. The matter embodied in this thesis is original and has not been submitted to any other University or Institute for the award of any other degree.

Place: Jaipur

Date:

Prof. M. K. Shrimali	Prof. S.D. Bharti	Dr. Pradeep K. Goyal
Professor	Professor	Associate Professor
NCDMM	NCDMM	Dept. of Civil Engg.
MNIT Jaipur	MNIT Jaipur	DTU, Delhi

ACKNOWLEDGEMENT

Among the countless people who have helped me during my Ph.D. journey, my supervisors, Prof. M. K. Shrimali, Prof. S. D. Bharti and Dr. Pradeep K. Goyal deserve the first mention. I am and will always be indebted to the two of them for their unfailing support and guidance.

Besides my advisors, I would like to thank Prof. T. K. Datta for providing all the necessary help, support, encouragement and critical advices throughout this work. His words of reassurance and motivation are gratefully acknowledged.

My sincere thanks also goes to members of DREC, Prof. Gunwant Sharma and Dr. P. V. Ramana for their invaluable suggestions.

I would also like to acknowledge the contribution of entire team of National Center of Disaster mitigation and management of MNIT-Jaipur, which has been kind enough to make this process smooth, providing me with the best laboratory facilities and research database. I also thank the eminent members of the department for assisting me with the right guidance and friendly advices at numerous points during the last few years.

I am grateful to my employer, National Institute of Technology, Uttarakhand for sponsoring me for the Ph. D. program. My colleagues at NIT Uttarakhand have also been very understanding and cooperative during this journey.

I have also been very fortunate to have the support and reinforcement of colleagues and seniors such as Dr. Arnav Anuj Kasar, Dr. Pankaj Kumar, Dr. Vishisht Bhaiya, Dr. Nishant Roy and Dr. Ambika Singh. Other friends from MNIT and NITUK, Saurabh, Kedar, Vijay, Sunita, Vishal, Vijay, Mohit, Devesh, Surendra, Laiju Amardeep, Bibhash and Durgesh have also been there throughout to make this work a success.

Last but not the least, my parents, siblings, and life partner who have always been there unconditionally. There are perhaps no words in which I can ever thank them enough for their unflinching love and tireless support.

ABSTRACT

During an earthquake, it is quite commonly observed that two similar building frames constructed at the same time and at the same site behave differently; one might have collapsed entirely, and the other might have survived with considerable damages. One of the possible causes for this is that the nature and location of the prevailing damages in the two were such that the sidesway collapse of the structure was initiated by the earthquake for the one, while for the other the collapse did not occur; progression of the damage was arrested at a specific damaged state. Apart from the above cause, there could be several other causes that might contribute to the failure of the one structure with the other structure not undergoing the collapse. They include the number of mainshocks and aftershocks the two withstood, any local retrofitting done on the structures and uncertainties of the materials or loss of strength over the time. Considering the above possibilities, the present study investigates the vulnerability of the damaged and undamaged (but weak) building frames to sway collapse under seismic excitations. The study is divided into four parts. In the first part, the side sway collapse of the building frames under different simulated damage scenarios is investigated using a novel technique comprising of the plastic analysis and genetic algorithm to identify the critical damage scenarios. In the second part, the building behaviour of the steel MRF frames under a sequence of artificially generated mainshock and aftershock events is studied in detail. In the third part, the optimum retrofitting of damaged frames to withstand a sequence of the mainshock and aftershock satisfying a set of performance criterion is presented. In the fourth part, the fragility analysis of both retrofitted and unretrofitted MRFs under a sequence of recorded mainshock and (a single) aftershock is carried in order to investigate the vulnerability of steel MRFs to aftershocks effects.

The vulnerability of damaged building frames to sway collapse under seismic excitation is investigated in the first part of the study. Crucial to the investigation is the identification of the critical damage scenario that triggers complete or partial sway collapse of the frame. This is accomplished by a simulation procedure aided by the genetic algorithm, plastic analysis, and pushover analysis of the frame. The procedure, genetic plastic pushover analysis (GPPA), enables the identification of the critical

damage scenario that leads to the collapse of the frame under the response spectrum compatible earthquakes. The damage scenario, which requires the least value of the PGA for the collapse, is identified as the critical damage scenario. If a frame has a damage scenario the same as the critical damage scenario, then it is likely to collapse under a similar earthquake having a PGA equal to the least value of PGA as described above. A 10-story steel building frame is used as an illustrative example to demonstrate the application of the method. The result of the study is validated by performing a nonlinear time history analysis under response spectrum compatible ground motion, and by comparing analytical prediction with the existing test result available in the literature. The numerical results show that there exist certain localized damages in a building frame that may trigger collapse, leading to the complete failure under an earthquake. If the damage of the building can be evaluated beforehand, the building's vulnerability to collapse under future earthquakes can be predicted using the methodology presented here.

Seismic design of buildings is made without paying much attention to the repeated sequence of mainshock-aftershock events. It has been found that a building frame may sustain the mainshock, but is damaged significantly during the aftershock. Most of the studies related to the above topic are confined to the evaluation of the performance of the frame after only one aftershock. In the second part of the study, the performance of steel building frames is evaluated by nonlinear time history analysis for a sequence of aftershocks followed by the mainshock. For this purpose, 4-, 8- and 12-story steel building frames are considered and are subject to the response spectrum compatible mainshock-aftershock sequences. For making the variety of sequences, Bath's law is applied and implemented by selecting a maximum of seven aftershocks followed by each mainshock of an ensemble of 8 mainshocks. Time history record used for the analysis is developed by joining the artificially generated earthquakes in series keeping a gap of 40s between two events. The performance parameters used in the study are the maximum inter-story drift ratio during an event (MIDR), residual inter-story drift ratio after the event (RIDR), maximum transient and residual top story displacements and number of plastic hinges. The performances of the three building frames are compared in the study. It is seen that the 12-story frame is damaged to

collapse level after 3 aftershocks, while the 4- and 8-story building frames survive all the seven aftershocks.

The enhanced seismic performance of a retrofitted 12-storey building frame is investigated by considering the effect of a sequence of the mainshock and aftershocks in the third part of the study. The seismic performance of the frame is studied in terms of a number of seismic demand parameters including the transient maximum inter-storey drift ratio, residual inter-storey drift ratio, transient maximum top storey displacement and residual top storey displacement. The frame is retrofitted using 'X'-bracings made of hollow steel sections and placed strategically to meet a set of performance criteria, namely, the retrofitted frame shall withstand all aftershocks and damages in the beams and the columns will remain within the specified performance level. The strategic placement of the bracings is accomplished by two techniques, namely, an iterative technique and an optimization technique. In the optimization technique, a genetic algorithm is used for obtaining the optimum locations of the bracings in the frame so that the desired performance criteria are met. In both techniques, the nonlinear time history analysis of the frame is performed for a synthetically generated sequence of the mainshock and aftershocks to obtain the seismic demand parameters. The results of the numerical study show that using a small number of bracings placed at the two bottom-most stories, the structure may be strengthened sufficiently to withstand all aftershocks. The performance of the optimally braced frame is elevated significantly compared to the arbitrarily placed bracings in withstanding the sequence of the mainshock and aftershocks.

Finally, the probability of seismic collapse in terms of specified damage states of unretrofitted and retrofitted building frames subjected to a (recorded) mainshock and (single) aftershock sequence is evaluated. The frame is optimally braced to create the retrofitted frame. An ensemble of 18 sequence of the mainshock- aftershocks is utilized to carry out the fragility analysis with respect to different PGA levels. The damage states are considered as the maximum transient and residual top floor displacements. Three damage levels defined for the analysis include IO, LS, and CP. The uncertainties are modelled as lognormal variables. The damage states are determined by the

incremental nonlinear time history analysis. The results of the study indicate that the probability of the seismic collapse for the aftershock event is much higher as compared to the mainshock. Further, the probability of the collapse is considerably reduced for the retrofitted frame. Even for a PGA level of 0.6g, the probability of the collapse of the retrofitted frame under aftershock remains within an extremely small level, of the order of 10-2.

TABLE OF CONTENTS

LIST OF TABLES

List of Figures

CHAPTER-1
INTRODUCTION

1.1 GENERAL

Recent earthquakes have caused enormous damages of infrastructures, loss of life and financial losses. Despite the seismic resistant design of buildings following the code provisions, the buildings are found to collapse during earthquakes. For new buildings, the reasons for such failures may be attributed to several factors such as the poor construction, lack of due consideration of the local soil effects and uncertainties inherent in the earthquakes. For the old or damaged buildings in previous earthquakes, the main reason is due to the lack of proper retrofitting of structures. The limitation of the code provisions also contributes to this cause. One of the major limitations of the code is that it assumes negligible probability of the structure to be exposed to more than one ground shocks in its lifespan. In fact, most of the major earthquakes consist of a series of foreshocks and aftershocks associated with the major shock. The records of the past earthquakes demonstrate that some of the aftershocks could be as severe as the main ground shock. Thus, structures, in reality, have a high probability of being exposed to a number of ground shocks during its life span. Properly designed structures for earthquakes usually sustain the mainshock with few members undergoing nonlinear excursion and eventual damage. However, this leads to the decrease in the overall strength of the structure and makes it more vulnerable to subsequent ground shocks. The reduction of overall strength of structures may also be caused due to several other factors than earthquakes. They include environmental effects such as the fatigue, shrinkage or creep etc. Sometimes, the strength of structures may get reduced due to some man-made events such as gas explosions or blast in a portion of the structure.

The above concerns lead to the motivation of the present study. A few investigations associated with this concern are taken up as the main focus of the present study. The investigations may be broadly classified as i) Seismic behaviour

of damaged buildings under earthquake; ii) Response of buildings under a sequence of the mainshock and aftershocks; iii) Performance-based seismic retrofitting of damaged structures; and iv) Seismic reliability analysis of undamaged and retrofitted structures. A brief background of the related literature on the topics is presented below in order to highlight the need of the present investigations and to formulate the objectives of the study. A detailed review of the literature is presented in the next chapter in order to bring out the gap areas in the subject.

1.1.1 SIDESWAY COLLAPSE

A number of investigations have been conducted on the progressive collapse related to the vertical load carrying capacity. Some of the recent studies on the subject included various nonlinear effects associated with the problem. Kwasniewski evaluated the progressive collapse potential of an eight-storey steel frame structure under column removal using nonlinear dynamic finite element model based on the GSA guidelines (Kwasniewski 2010). Kim et al. (2011) investigated the sensitivity of design variables of steel buildings subjected to progressive collapse. Fu conducted a nonlinear dynamic analysis of a three dimensional (3D) 20-storey composite steel frame under consecutive column removal conditions using the general-purpose ABAQUS software (Fu 2012). Numerical modelling of semi-rigid connections using the SAP2000 software package has been discussed in detail by Bandyopadhyay et el (Bandyopadhyay et al. 2008). They considered the geometric nonlinearity and debris loading.

Relatively much less studies have been carried out on the lateral sway collapse. Domingues Costa et al. (2007) proposed a new seismic design procedure for RC structures corresponding to a particular sway collapse mechanism of failure under earthquake. Zareian et al. (2010) presented the concept of collapse fragility curve in estimating the collapse performance of building frames under the earthquake ground motion. Lignios et al. (2011) predicted and validated the sideway collapse of a scale model of a steel moment frame using the earthquake simulator test. Plastic hinges conforming to component deterioration levels were

simulated in a four-storey steel frame and tested under simulated earthquake to validate the analytically predicted collapse behaviour. Malaga-Chuquitaype et al. (2016) studied the contributions of the bracing in steel building frames to augment their lateral and vertical load carrying capacities. They (Malaga-Chuquitaype et al. 2009) also studied the rigid plastic model for the seismic design and assessment of steel frame structures to increase the lateral load capacity due to concentrically braced frames for the sway mechanism of failure under earthquakes. Del Carpio et al. (2016) evaluated the seismic performance of a hybrid model consisting of a four-storey frame and a moment frame subassembly experimentally. The failure mechanism of the model confirmed to the partial sway mechanism of failure. Lopez et al. (2015) presented an innovative seismic based design procedure for a regular frame structure considering the sidesway collapse prevention.

Most of the above studies deal with experimental tests on model steel frames for investigating the sway collapse behaviour of structures under earthquakes, coupled with the nonlinear time history analysis for the analytical study. Only one study by Domingues Costa et al. (2007) used the theory of plasticity for the determination of required structural strength of the members for predefined performance parameter using a rigid-plastic response spectrum.

1.1.2 MAINSHOCK-AFTERSHOCK EVENTS

Evaluation of existing structures (e.g., FEMA 356, FEMA 355f American Society of Civil Engineers (ASCE) 2000; Federal Emergency Management Agency (FEMA) 2000) are based on the estimation of peak lateral displacement demands that structures could suffer under seismic excitation. These evaluation procedures are not explicit about the aftershock effects. In real life, a structure located in high seismic regions not only experiences a single seismic event (i.e., mainshock), but also to a seismic sequence consisting of foreshocks, mainshock, and aftershocks.

Recent evidence of aftershocks of significant magnitudes are those associated with the Kathmandu valley earthquake and Mexico earthquake. There were nearly 150 earthquakes in 450 km radius of Matias Romero between 2nd September 2017 and 13th October 2017 including an earthquake of M_w =8.1. Post-

1994 Northridge earthquake, research on the response of a structure subjected to mainshock and aftershock event has gained momentum. After a seismic event, damage assessments are performed visually by trained professionals which may not be accurate. Different professionals may take different decisions. Therefore, the confirmed decision is unachievable. Nevertheless, most of the current seismic risk assessment tools only consider mainshock effects without considering aftershocks. After the mainshock, the threat to the life safety for building occupants and risk of building damage are higher than before the occurrence of the mainshock due to permanent deformation or hinge formation in the building during a mainshock. Collapse in successive earthquakes because of the damage from the mainshock has been demonstrated by van de Lindt on a shake table (Han et al. 2016; Nazari et al. 2015). Most of the building codes on earthquake resistant design of structures do not provide any clear-cut guideline for the aftershock effect. The value of the reduction factor 'R' specified in the code for different types of buildings might cater to this effect. However, no explicit recommendation is available on this issue.

In this connection, several application frameworks for the seismic loss estimation have also been proposed. For example, Salami and Goda (2014); Pei and van de Lindt (2010) developed a seismic loss estimation methodology for the wood frame construction that applied Baye's theorem for updating information. Three methods of intensity, scenario, and time-based assessments for structural performance quantification were developed by the ATC-58 project (American Society of Civil Engineers (ASCE) 2000; Federal Emergency Management Agency (FEMA) 2000). However, in these approaches, the unrealistic assumption was made that the building was rebuilt to its integral state immediately after an earthquake (Carreño et al. 2010; Gee Liek Yeo and C. Allin Cornell 2012). Luco et al. (2004) investigated the residual capacity against collapse for mainshock-damaged buildings and recommended a statistically calibrated approach for computing residual capacity, which could be adopted to develop a fragility curve for a mainshock-damaged building. An assessment procedure considering only one aftershock instead of many have been proposed for concrete structures by Han et al. (2015, 2016).

In the literature, the response of a building subjected mainshock-aftershock sequence has been evaluated using three approaches, namely, a) back to back b) randomized and c) stochastic. In the back to back approach the real mainshock, scaled or unscaled, is repeated as an aftershock (Amadio et al. 2003; Fragiacomo et al. 2004; Hatzigeorgiou and Beskos 2009). In the second approach, an ensemble of real mainshock is chosen, and artificial aftershock is generated by scaling a randomly selected mainshock from the ensemble (Goda 2015; Goda et al. 2013; Li and Ellingwood 2007; Ruiz-García 2012, 2014; Ruiz-García and Negrete-Manriquez 2011). In the third approach, a sequence of stationary Gaussian random process modulated by an envelope function is used as a mainshock-aftershock sequence (Moustafa and Takewaki 2011, 2012).

1.1.3 RETROFITTING OF DAMAGED BUILDINGS

Earthquake resistant design of the building is based on the concept of strong column-weak beam design. The strength of a column is higher than that of the adjoining beam. The beam column joint has higher strength than that of the column and beam. Recent earthquakes, Northridge, Kobe and Chi-Chi, have shown that the inability of the building to resist an earthquake is due to yielding of connections failure and buckling of braces (Broderick et al. 1994; Elnashai et al. 1995). The strong column-weak beam design enables this yielding to be localized at the beam ends and bottom of the column. This localized yielding of members is termed as the formation of hinges. These damages have attracted a significant amount of attention on how can damaged steel buildings be made safer by the retrofitting techniques.

Seismic Retrofitting is defined as "judicious modification of the structural properties of an existing building in order to improve its performance in a future earthquake" (Wyllie 1983). Several techniques such as the local modification of components, removal or reduction of existing irregularities, global structural stiffening, global structural strengthening, mass reduction, seismic isolation and energy dissipation devices are currently available to retrofit and strengthen buildings (ASCE 41-13 2014). Addition of new structural elements such as

structural walls or steel braces; and selective strengthening of deficient structural elements such as the use of concrete or steel jackets and fibre reinforced polymers are two main retrofitting approaches to upgrade the seismic performance of existing structures (Li et al. 2009; Di Sarno and Elnashai 2009).

Among several seismic retrofit techniques, the bracing system is being widely used to enhance the global stiffness and strengthen the unbraced steel moment resisting frames (MRFs) as well as reinforced concrete structures (Di Sarno and Elnashai 2006, 2009; Youssef et al. 2007). Moment resisting frames are not efficient in resisting sequences of earthquakes (mainshock and a sequence of aftershocks) for tall steel buildings (above12 storey MRFs). Truss members such as diagonals are often used to brace steel frameworks to maintain lateral drifts within acceptable limits (Liang et al. 2000). Diagonal bracing that connects the brace concentric to the beam-column joint includes X-bracing, chevron bracing and V-bracing configurations. Other different types of bracing system are eccentric braces, knee braces (Roeder and Popov 1978). Hou and Tagawa (2009) used wire rope (cable) as the bracing for steel moment-resisting frames. The frame retrofitted using the wire rope (cable) as bracing system restrains unacceptably large storey drift and exhibit ductile behavior.

The building retrofitted using steel braces has higher strength and stiffness than that of retrofitted with energy dissipation devices (Tena-colunga and Vergara 1997). Higher stiffness significantly reduces both the deformation and acceleration demands of the structure during an earthquake. Lower demands of retrofitted MRFs reduce the risk of brittle failures in the structure (Tena-Colunga and Vergara 1997). Di Sarno and Elnashai 2009 investigated the seismic performance of steel MRFs retrofitted with different bracing systems such as concentrically braced frames (SCBFs), buckling-restrained braces (BRBFs) and mega-braces (MBFs). Tremblay et al. (2003) investigated the seismic performance of concentrically braced steel frames under cyclic loading. Özel and Güneyisi (2011) investigated the seismic reliability of the mid-rise R/C buildings retrofitted by D, K, and V type eccentric steel bracing systems with four different spatial distributions in the structure. (Patil and Sangle 2015) performed a nonlinear static analysis for different

storied buildings varying from 15 to 35 retrofitted using CBF, VBF, XBF and ZBF. For preventing buckling occurrence in the bracing members, buckling-restrained braces have been investigated (Xie 2005). A non-compression brace (Tamai and Takamatsu 2005) and a dissipative bracing system (Renzi et al. 2007) have been proposed to improve the seismic resistance with bracings. Some researchers have also examined the efficacy of the application of braces to retrofitting frames (Bartera and Giacchetti 2004; Hueste and Bai 2007).

Most of the above studies have focused on retrofitting of structures to withstand a single shock (Mainshock). The mainshock is usually followed by a number of aftershocks which may be severe and generally cause further damage to buildings (Huang et al. 2008; Li et al. 2014a) and can increase the seismic demand (deformation or acceleration) for a structure. It has been found that a structure may sustain the mainshock but is damaged during the aftershock. Several authors have evaluated the seismic effect of the mainshock-aftershock sequence for an unbraced MRF. (Ruiz-García and Aguilar 2015; Ruiz-García and Negrete-Manriquez 2011). In general, the retrofitting of buildings is done without paying much attention to the repeated sequence of mainshock-aftershock events.

1.1.4 SEISMIC RELIABILITY ANALYSIS

The damage to the structure during strong ground motion depends upon the dynamic property of the structure and characteristics of seismic waves. There are uncertainties in the characteristics of strong ground motion such as spectral shape, duration and frequency content. These uncertainties lead to a probabilistic assessment of the collapse risk of structures using Epsilon, an indicator of the spectral shape of the ground motion that affects the response of a structure (Baker and Cornell 2005). Raghunandan and Liel (2013) performed incremental dynamic analysis to study effects of the strong motion duration on the collapse of reinforced concrete buildings. Montejo and Kowalsky (2008) studied the effect of frequency content on the behaviour of the structure using incremental dynamic analysis taking the frequency content as the intensity measure of the ground motion. Champion and Liel (2012) described a method to quantify the effect of the near-

fault directivity in the probabilistic assessment of the collapse risk through incremental dynamic analysis of the building. Ellingwood and Kinali (2009) illustrated how above-mentioned uncertainties, both inherent and knowledge-based, effects the estimates of the probability of exceeding pre-defined performance levels (collapse) for a steel frame building structure.

Other than the uncertainty of the earthquake ground motion, the uncertainty of the characteristics of damaged buildings after the mainshock is complex. A systematic methodology to integrate the uncertainty in building characteristics due to mainshock and aftershock needs to be incorporated in the probabilistic risk assessment of the building frame to a seismic event consisting of the mainshock and aftershock (Li et al. 2014b).

A probabilistic assessment of the structural damage before and after an aftershock using enhanced uncoupled modal response history analysis (EUMRHA) method was developed by Li and Ellingwood (2007). Damage accumulation in terms of "damage ratio" defined in terms of the maximum inter-story drift ratio was used as damage measure for the probabilistic analysis. Song et al. (2014) investigated the collapse risk of post mainshock events. Structures, which have sustained one strong ground motion with damage states beyond immediate occupancy are more fragile when subjected to other ground motions. As the damage level increases, the influence of aftershocks increases (Song et al. 2014). Park et al. (2018) proposed a quantitative assessment model for selecting critical earthquake sequences to evaluate risk assessment of a damaged structure subjected to the aftershock.

The nonlinear static analysis with Monte Carlo simulation is used to determine structural response and to obtain probabilistic seismic risk of the structures (Vargas et al. 2013). Fereshtehnejad et al. (2016) developed Bayesian probability network (BPN) in order to identify all possible failure modes using multiple sets of pushover analysis to model random variables together with appropriate criteria for the plastic hinge formation of the structural components. Mai et al. (2017) computed the fragility curves for a three-storey steel frame using two non-parametric approaches, Monte Carlo simulation and kernel density,

rather than the parametric lognormal assumption. Burton et al. (2017) described statistical models such as best subset regression and the Gaussian kernel ridge regression for estimating the aftershock collapse vulnerability of buildings using the incremental dynamic analysis.

Kumar and Gardoni (2014) developed a probabilistic model to predict the seismic vulnerability of reinforced concrete structures incorporating the seismic degradation of the reinforced concrete structure during past earthquakes. Muntasir Billah and Shahria Alam (2015) compared different methods available for the fragility analysis and gave guideline for the development of fragility curves. Jalayer et al. (2015) proposed Bayesian cloud analysis method, which uses a simple regression in logarithmic space of damage measure versus intensity measure, for the effective and efficient risk assessment for collapse during a seismic event. Baker (2015) proposed a fitting approach for the fragility function using the stripe method and incremental dynamic analysis. It was deduced that stripe method is more efficient than the incremental dynamic analysis.

1.2 NEED FOR THE PRESENT STUDY

Structures are locally damaged during its lifespan due to several factors such as earthquakes, aging of the structure, local damages caused due to accidents and poor maintenance. The locally damaged building behaves differently during a strong ground motion. It is quite commonly seen that during the earthquake, two identical buildings built at the same time and at the same site behaved differently; one may collapse globally and the other may survive with considerable damages. There is no literature exclusively on the global collapse of structures under earthquake forces which are defined as the spread of some initial localized damages in the structure caused due to earthquakes or some other factors mentioned before, leading to the partial or complete failure of the structure.

Even a virgin structure damaged by the mainshock is subjected to ground motions comprising of a series of aftershocks following the occurrence of the mainshock. In that case, the aftershocks act on a damaged structure. Thus, the structure behaves differently in the aftershock than in the mainshock (when it is

virgin), even if the two shocks have more or less the same intensity. Coupled with this phenomenon is the recurrence of aftershocks i.e. the number of aftershocks the structure encounters. As a consequence, the sequence of the mainshock-aftershock events is extremely important in assessing the damages caused by the earthquake. Current code focuses primarily on the mainshock in the seismic design of structures and in the evaluation of its damages. Current literature on the effects of aftershocks in the structures focuses only on a single aftershock after the mainshock. Not much literature exists on the damage assessment of structures subjected to a sequence of mainshock-aftershocks events. The techniques employed for the same in literature use scaled mainshock as an aftershock, whereas, the aftershock may have completely different characteristics than that of the mainshock. It has been observed that characteristics of an aftershock may be very weakly related to the characteristics of the mainshock.

Significantly damaged structures under earthquake are usually retrofitted to withstand future earthquakes. There are many retrofitting techniques, available in the literature, which are used to strengthen the building for lateral loads. Base isolation and dampers are the popular technologies to make buildings strong enough to resist seismic vibrations. Through base isolation, the building or the superstructure are decoupled from its substructure which rests on the ground, thus protecting the building during an earthquake. Dampers, on the other hand, work as shock absorbers and minimize the magnitude of vibrations transmitted to the building from the ground. Other than dampers, structural concepts such as bracing, where X-shaped braces strengthen the buildings and help in absorbing movement during an earthquake, are also in use. All these techniques are expensive and have no consideration for aftershocks. The research on optimal placement of the isolators, dampers, braces is still in its primitive stage. The validation of retrofitted building to withstand aftershocks along with the mainshock requires a special attention. Along with that, the seismic risk assessment of structures for the mainshock and as-recorded aftershocks forms a research topic of current interest.

1.3 SCOPE AND OBJECTIVES OF THE WORK

Keeping the above background in view, the present study is undertaken. Sidesway collapse of damaged steel Moment Resisting Frames during an earthquake is first investigated. A new technique involving Genetic Algorithm, Plastic Analysis and Pushover Analysis is developed to investigate the sidesway collapse. Then, an extensive study on the behavior of steel building frames subjected to a sequence of mainshock-aftershock events is carried out. Finally, the performance and reliability analyses of retrofitted frames with the help of stiffness bracing are presented. Specific objectives of the study include:

I. To investigate the sidesway collapse of damaged steel building frames under earthquake having localized damages in the building that trigger further damages leading to complete or partial failure of the frames.
II. To investigate the seismic behavior of steel building frames subjected to a sequence of mainshock-aftershock events.
III. To develop an optimal retrofitting strategy with the help of stiffness bracings, that withstands a sequence of mainshock-aftershock events maintaining a pre-decided performance level.
IV. To determine the probability of occurrence of different damage states of steel building frames, undamaged and retrofitted, produced due to a single mainshock-aftershock episode using fragility analysis.

In order to achieve the above objectives, a moment resisting steel frame (MRF) having 3 bays and 10 storeys with each storey of 3.0m height is considered for the analysis. For evaluating the seismic performance of the building frame, it is subjected to one mainshock and seven aftershocks. Also, the PGA of the mainshock is considered as 0.394g and those of aftershocks ranging from 0.289g to 0.410g with an average value of the PGA of 0.34g. The performance of the steel frame is evaluated in terms of the maximum inter storey drift ratio (MIDR), residual inter-storey drift ratio (RIDR) after the event, maximum top storey displacement, residual top storey displacement and number of plastic hinges. The optimal

solution of the retrofitting strategy is achieved using cross bracings of different sections and by searching their optimum locations in order to identify their performance states namely, IO, LS, and CP. The optimization problem is solved using an iterative technique and genetic algorithm. The performances of their retrofitted building frames obtained by both optimization strategies are compared in terms of the performance levels, namely, IO, LS, and CP.

1.4 ORGANIZATION OF THE THESIS

An extensive study on the behavior of damaged building frames during earthquakes in presented in this thesis. The thesis is divided in seven chapters.

Chapter 1 provides the brief background information of the present work. Sidesway collapse of building frames are briefly discussed. Effects of the mainshock and aftershocks on moment resisting frame are also highlighted. Motivation for the present work is outlined in the chapter. Finally, the major objectives are enlisted.

Chapter 2 provides an extensive literature review on the behavior and sidesway collapse of damaged steel moment resisting frames. The literature review is split into following subparts: i) Sidesway collapse of building frames; ii) Damages caused during mainshock-aftershock events; iii) Retrofitting of building frames to withstand sidesway collapse; and iv) Sidesway collapse risk probability of structures. In sidesway collapse of building frames, the literature on the collapse of building frames by forming sway mechanism is discussed. In damages caused during the mainshock-aftershock, the occurrence of aftershocks and their characteristics are reviewed. The building behavior under the action of the mainshock and aftershocks estimated by analytical methods are also reviewed. In retrofitting of structures to withstand sidesway collapse, the retrofitting strategies developed to protect building frames to any seismic event are presented. Retrofitting using bracings to strengthen the building frame is also extensively discussed. In sidesway collapse risk probability of frames, different techniques to evaluate the seismic risk probability of structures is outlined. The seismic risk probability of building frames under the action of the mainshock and aftershocks

are reviewed extensively. Based on the review of literature, the precise objectives are highlighted at the end of the chapter 2.

A method called Genetic Plastic Pushover Analysis (GPPA) to evaluate the vulnerability of damaged building frames to collapse under an earthquake is developed and presented in **Chapter 3.** The method uses the Genetic Algorithm, Plastic Analysis and Pushover analysis to identify most vulnerable localized damage state which leads to the collapse of the frame under an earthquake. The proposed method is validated by the nonlinear time history analysis. A ten-storey steel building frame is taken as an illustrative example. Different damage scenarios in the frame are synthetically generated. Out of all the damage scenarios, the proposed method identifies the one, which requires the least value of the PGA of an earthquake to collapse. That damage scenario called the critical damage scenario.

In **Chapter 4,** the behavior of building frames subjected to the mainshock and a series of aftershocks is investigated using nonlinear time history analysis. For the purpose of analysis, the time histories of the mainshock and aftershocks are connected back to back, with sufficient time gaps created with zeros, for allowing the structure to come to rest before it is acted upon by the next time history of earthquake. For generating the sequence of mainshock and aftershocks, Bath's law is applied and implemented by selecting a maximum of seven aftershocks followed by each mainshock of an ensemble of 8 mainshocks. A time history record of 40s with zeros is inserted between the two earthquake records. For studying the behavior of building frames under the sequence of the mainshock and aftershocks, three steel building frames having 4, 8 and 12 storeys are considered as the numerical examples. The performance parameters used for investigating the behavior of the frames include the maximum inter-story drift ratio (MIDR), residual inter-story drift ratio after the event (RIDR), maximum top story displacement, residual top story displacement and number of plastic hinges. The performances of the three building frames in terms of the above parameters are compared in the study.

In **chapter 5**, the 12-storey steel building frame is retrofitted with cross bracings. Two different techniques are applied to retrofit the moment resisting frame i) iterative method and ii) optimization. In the iterative method, the bracing is first provided in the central bay ground storey. The braced frame is subjected to the sequence of the mainshock and aftershocks and the response is observed. If the response is beyond the specified acceptable limit, then the next storey of the central bay is retrofitted, and the process is repeated until the response is within the specified limit. In the optimization method, optimum locations of bracings are determined using the genetic algorithm. Roof displacement is considered as the objective function and the number of bracings is put as the constraint. The performances of both retrofitted (by both methods) and un-retrofitted building frames are compared. The performance of the optimally retrofitted bracing configuration in the frame is compared with that of the bracing configuration of the frame with the arbitrary choice of the locations of the bracings.

In **chapter 6**, the fragility analysis of the optimally braced and un-retrofitted building frame of 12 storey subjected to the mainshock and single aftershock is performed. For this purpose, the building frames are subjected to 18 sequences of the mainshock and single aftershock. The PGA of the seismic sequence is varied from 0.1g to 1.25g. The probability of exceedance of some predetermined threshold values of the response quantities is obtained by considering only the uncertainty the ground motion. The response quantities of interest or damage measures include the maximum transient roof drift and permanent roof drift.

Chapter 7 provides a summary of the present study and summarizes the important conclusions drawn from the study. The limitations of the present work and further possible extensions of the present study as future researches are also listed in the chapter.

CHAPTER-2
LITERATURE REVIEW

2.1 INTRODUCTION

The collapse of structures signifies that the structure or a part of it cannot withstand the load superimposed on it. The part which is incapable of bearing its load collapses. Based on the functionality of the structure, the collapse can be defined as the structure or a part is unable to bear the applied load. In other words, collapse constitutes a limit state associated with the complete loss of the strength of the structure, its contents and functions. If the structure, as a whole, fails, then the collapse is global. There are instances when the localized collapse in a small segment of the structure leads to the collapse of a substantial portion of the structure. This small damage leading to the disproportionate damage is termed as progressive collapse (Liu 2010; Marjanishvili 2004).

Progressive collapse of a structure may be traced back to the collapse of Ronan Point Apartment, London in 1968. Subsequently, much attention has been paid to the subject of progressive collapse, and several studies have been carried out. The main thrust of the works was to randomly remove one or more vertical members of the structure to model the initial damage done by a random loading event. The sudden removal of a structural member has the same effect as the sudden application of force in the direction opposite to the internal force of the member leading to a transient dynamic response (Powell 2005). As a consequence, forces redistribute in the system, and the damaged structure either comes to a new equilibrium point, or the collapse occurs.

Progressive collapse is related to vertical load carrying capacity. In regard to earthquake engineering, collapse is defined as the inability of the structure or its part to withstand any seismic load (Ibarra and Krawinkler 2005). The inability of the structure to withstand lateral load is termed as the side sway collapse (Lignos et al. 2013; Wittrick 1968). The thesis is focused on the side sway collapse of damaged building frames and their retrofitting. The damages may be caused due

to environmental effect, strength deterioration due to aging or any abnormal loading or a previous earthquake. An extensive review of literature considering the sidesway collapse of damaged building frames is presented here. The literature review is split into following parts; i) side sway collapse of building frames; ii) damages caused in building frames during mainshock-aftershock events; iii) retrofitting of building frames against side sway collapse; and iv) probabilistic risk assessment of side sway collapse of building frames.

2.2 SIDE SWAY COLLAPSE OF BUILDING FRAMES

A number of recent studies are reported in the literature on the side sway collapse of frames under earthquake. These studies relate to (i) damage observed in the sway collapse mode under earthquakes, and (ii) strengthening and design of frames to prevent the sway collapse. These studies are relevant in the context of the present investigation since it deals with the sway collapse mode of failure of the structure under earthquakes showing different degrees of damages.

Domingues Costa et al. (2007) proposed a seismic design method for reinforced concrete structures based on the theory of plasticity. The method was based on the nonlinear time history analysis with the expectation that the reinforced concrete structures can undergo the nonlinear excursion in its lifetime when subjected to an extreme earthquake. The performance parameters are a priori selected using rigid-plastic response spectrum and the mechanism it can form. The capacity demand varied with the intensity of ground shaking. A 4-storey reinforced concrete building was designed using the method, and its performance was compared with that of design methods prevailing.

Lignos et al. (2011) predicted the collapse of a 4-story steel frame structure numerically and validated experimentally through 1:8 scale model. The building was designed based on seismic design provisions of the 2003 IBC for vertical and lateral loads. Two 1:8 scale prototype steel building frames, whose property closely match with the designed building, were fabricated. In order to accurately simulate the dynamic properties based on the similitude rule, the aluminum was selected in place of the steel. Based on the probable locations of the nonlinear excursion,

plastic hinge elements were placed at the beam and column ends. The scaled model was tested to collapse. In the analytical model, deterioration properties of the rotational springs were idealised by the Ibarra-Medina-Krawinkler (IMK) model. The study concluded that the side sway collapse could occur in realistic combinations of the structural framing and earthquake ground motion.

Krishnan and Muto (2012) explored the collapse mechanism of an 18-storey steel building frame under the earthquake excitation through three-dimensional nonlinear analysis using FRAME 3D. The plastic analysis in the form of the energy balance equation was exploited to identify all the collapse mechanisms ranging from localized combined storey to side sway collapse. The peak transient IDR, normalised by its height, was used as an indicator of the damage to both structural elements as well as many types of non-structural elements. For the peak transient IDR, the larger of the peak values at two diagonally opposite corners of each story was taken to include the effects of torsion in the performance assessment accurately. The author concluded that only the long-period excitation imparts energy to tall buildings large enough to cause collapse. Long period ground motion was the ground movement during an earthquake with a period longer than 1 second (frequency of such waves was 1 Hz or lower).

Lignos et al. (2013) Determined vital factors essential for the collapse assessment of steel frame structures subjected to strong earthquakes based on the modified IK deterioration model. The modified IK model can simulate the strength and stiffness deterioration of steel components under cyclic loadings. The deterioration model has been validated with the response of full-scale 4-storey building test at the E-Defense shake table facility. The 2-bay by 1-bay steel building frame was subjected 1995 Kobe earthquake. The test frame was subjected to a sequence of 20% (Level 1), 40% (Level 2), 60%, and 100% of the originally recorded time history in all three directions. The test results showed that the Y-direction frame sustained more significant deformation than that of the X-direction frame. The author investigated collapse mitigation strategies for the plastic deformation and strength enhancement of the frame so that its first-story collapse mechanism

would be delayed or shifted to a complete-story mechanism and withstand different levels of the earthquake.

Karamanci and Lignos (2014) proposed a computational approach to assess the side sway collapse of concentrically braced frames. For the collapse assessment, the author also developed a hysteresis model to represent the strength and stiffness deterioration of braces. The strength and stiffness deterioration of beams and columns were modelled by modifying Ibarra-Medina-Krawinkler (IMK) deterioration model incorporating the pinching model for gusset plates. Open Sees was used to simulate the concentrically braced steel frame model for the incremental dynamic analysis. It was shown that to assess the side sway collapse of CBFs subjected to the ground motion, information on the storey shear along with the storey drift was necessary.

Hamidia et al. (2014a) developed a procedure to estimate the side sway collapse capacity of building frames. The procedure was based on obtaining similar viscously damped SDOF system by bi linearization of the pushover curve using the nonlinear static analysis. The response parameters of the building were determined by a database of already conducted nonlinear time history analysis of different modelled SDOF systems. The collapse level spectral acceleration was thus determined to form the response. On similar lines, Hamidia et al. (2014b, 2015) developed a procedure to estimate the side sway collapse capacity of building frames incorporating the linear and nonlinear viscous dampers.

López et al. (2015) proposed a displacement-based seismic design procedure for regular planar framed structures considering the side sway collapse. In order to adequately consider the P-Δ effects, an MDOF system was characterised by an equivalent SDOF using modal analysis. This characterization allowed the identification of the side sway collapse of the structure during any given seismic demand. Deterioration of the members was not considered during the study. The method allowed the design of structures for either deformation control or the prevention of the actual side sway collapse.

Malaga-Chuquitaype et al. (2016) investigated the effect of extreme loading conditions in terms of multi-hazards on steel building frames. Two multi-hazard

cases were investigated in the study, namely, a) earthquake and fire and b) earthquake and blast. The side sway collapse along with the structural inability to withstand the vertical load was considered in the study. The authors also evaluated the effects of the secondary frame (gravity frame) in mitigating the multi-hazards. It was observed that the gravity frames provide good resistance to the side sway collapse. A brief provision of simplified approaches for the design of secondary frames in order to resist multi-hazards were also presented in the study.

2.3 DAMAGES CAUSED DURING MAINSHOCK-AFTERSHOCK EVENTS

Post-1994 Northridge earthquake, research on the response of a structure subjected to mainshock and aftershock events has gained momentum. After a seismic event, damage assessments are performed visually by the trained professional which may not be accurate. Different professionals may take different decisions. Therefore, confirm decision is unachievable. Nevertheless, most of the current seismic risk assessment tools only consider mainshock effects without considering aftershocks. Collapse in successive earthquakes because of damage from the mainshock has been demonstrated by van de Lindt on a shake table (Han et al. 2016; Nazari et al. 2015a). Most of the building codes on the earthquake resistant design of structures do not provide any clear-cut guidelines for aftershock effects. The value of the reduction factor 'R' specified in the code for different types of buildings might cater to this effect. However, no explicit recommendation is available on this issue.

the observation shows that there can be a number of aftershocks and of varying magnitude after a mainshock. After the Mainshock, the threat to life safety for building occupants and risk of building damage is higher than before the occurrence of the mainshock due to the permanent deformation or hinge formation in the building during a mainshock. There are several examples of mainshock and aftershock events. An Earthquake hit Mexico City on 19th September 1985 having magnitude 8.0. The mainshock caused severe damage to the Greater Mexico City area. The sequence of events included a foreshock of magnitude 5.2 that occurred

before the main shock on 19 September and two large aftershocks. The first of these occurred on 20th September with a magnitude of 7.5 and the second occurred seven months later on 30th April 1986 with a magnitude of 7.0 (Anderson et al. 1986).

After the 1994 Northridge earthquake (Mw = 6.7) that affected the Los Angeles Area in California, an Mw of 6.0 aftershock was felt approximately 1 min later (Dreger 1997). The 1999 İzmit earthquake also known as the Kocaeli earthquake occurred on 17th August 1999 having a magnitude of 7.6. More than 2000 aftershocks were observed in 2 months following the mainshock (Ito et al. 2002). On 12th May 2008, a strong ground motion having a magnitude 8.0 hit Chengdu, China which is also known as the Wenchuan earthquake or Sichuan earthquake. After the Wenchuan earthquake, 1070 aftershocks of more than M 3.0 hit the region nearby. The largest aftershock was having a magnitude 6.4 which hit on 25th May 2008 (Hua and Chen 2009).

After the earthquake on 25th April 2015 (Mw=7.8) that violently shook the Kathmandu valley causing the collapse of several structures, several earthquakes of magnitude higher than Mw =4.0 were observed within the first 45 days (Adhikari et al. 2015). On 12th May 2016, weeks after the main event, an earthquake of Mw=7.3 hit the region. One of the very recent examples is of Mexico earthquake, on 19th September 2017 in which an earthquake of M_w=7.1 having an epicentre at 2km NE of Ayutla, Mexico was observed. A few days later of the event on 23rd September 2017, an earthquake of M_w= 6.1 was observed having epicentre at 15km SE of Matias Romero, Mexico. The distance between both the epicentres was within 450km radius. There had been nearly 150 earthquakes in a radius of 450 km radius of Matias Romero from 2nd September 2017 and 13th October 2017. An earthquake of M_w =8.1 was observed in the same region on 8th September 2017. (USGS website cited on 13th October 2017).

2.3.1 MAINSHOCK AND AFTERSHOCK CHARACTERISTICS

Earthquakes are usually caused by a sudden slip on a fault. Fault slip is resisted by asperities that are distributed on a much weaker fault that continuously creeps in response to the tectonic stress. The sudden fault slip releases energy

waves that travel through the earth's crust and cause the shaking. The spot underground where fault slip occurs is called the focus of the earthquake. The place right above the focus on the earth's surface is called the epicenter of the earthquake. Aftershocks are caused by an increase in local stresses resulting from the mainshock (Shcherbakov et al. 2005). Local stress concentrations resulting from "asperities" and "barriers" also contribute to the generation of aftershocks in the vicinity of the mainshock rupture (Scholz 2002). If the asperity area which causes the ground motion shaking is large, then the magnitude of an earthquake is large. If the asperity area of the aftershock is larger than that of the mainshock, then the aftershock is the mainshock, and the previous earthquake is the foreshock. So, a seismic event comprises of foreshocks, mainshock, and aftershocks. Aftershocks are located over the full area of fault rupture and occur within the volume affected by the strain associated with the mainshock. In the literature, there are different laws relating to the mainshock and aftershocks.

Shcherbakov et al. (2005) combined three empirical laws relating the mainshock and aftershocks to obtain a relation for the aftershock time decay rate. The three empirical laws are i) Gutenberg-Richter frequency-magnitude scaling, ii) Bath's law, and iii) the modified Omori's law. The combined empirical laws were employed to study the statistical properties of several large earthquakes having an epicentre in and around California. The author also explained the reasons for the occurrence of several shocks during and after an earthquake event. The foreshock, mainshock and aftershocks are explained by asperities and barriers for the stress field. The larger is the asperities large is the ground shaking magnitude. The continuous ground shakings relax the excess localized stress.

Goda (2012) emphasized the consideration of aftershocks along with the seismic effects of mainshocks. Large mainshock was generally followed by a number of damaging aftershocks. The aftershock effect on the ductility demand was investigated using the nonlinear seismic assessment of the single degree of freedom system subjected to the mainshock and aftershock sequence. The SDOF system was subjected to real seismic sequence from the Japanese earthquake database and artificially generated seismic sequence based on Omori's law

considering the magnitude, distance, and site classification. The artificially generated aftershocks are validated by comparing the ductility demand of the real aftershocks with that of artificial aftershocks.

Goda and Taylor (2012) investigated the effects of aftershocks by using real as well as artificially generated mainshock-aftershock sequences. Pacific Earthquake Engineering Research Centre—Next Generation Attenuation (PEER-NGA) database were used to gather the real mainshock-aftershock sequence. Due to the limited number of real sequences, the artificial mainshock-aftershock sequence was generated based on Omori's law. Nonlinear dynamic analysis of a single degree of freedom system subjected to the mainshock-aftershock sequence was evaluated. The results indicated that the aftershock imposed higher ductility demand than that of the mainshock. Aftershocks caused additional damages to the mainshock damaged building frame.

Ruiz-García (2012) presented the correlation between the mainshock and aftershock of a seismic sequence. The author examined the characteristics of 184 real mainshock-aftershock sequences from the PEER-NGA database and Mexican Database of Strong Motions (MDSG). The primary parameters compared were the predominant period, bandwidth and effective duration. It was concluded that the predominant period, bandwidth and effective duration of the largest aftershock were shorter than those of the mainshock. The predominant period and bandwidth were linearly related. The PGA of the mainshock and aftershocks had no relation at all. There were instances that the PGA of aftershock was more than that of the mainshock.

Salami and Goda (2014) performed probabilistic seismic hazard analysis and structural vulnerability assessment during an earthquake event. The probability of occurrence of an aftershock did not follow the poisons distribution as that of the mainshock. Moreover, the occurrence, magnitude and temporal decay of an aftershock were given by different laws. Seismic vulnerability of the wooden structure subjected to a set of real mainshock-aftershock sequences was extensively examined by the author using incremental dynamic analysis. It was

concluded from the results that the aftershocks moderately affected the maximum response of the structure and damage probability.

Song et al. (2014) investigated the post mainshock collapse probability of the building frame subjected to aftershocks. The effects of aftershock characteristics on the collapse probability were also emphasized in the study. Different parameters considered in the study were the significant duration and mean period, which represented the duration and frequency content respectively. The author also evaluated the relationship for both parameters for the mainshock and aftershock. Statistical analysis was performed to understand the trend and the frequency distribution of the parameters considered. The author also conducted a multivariate regression analysis to quantify the influence of the parameters on the damage states of the structure. The strength and stiffness degradation were modelled by the modified Ibarra–Krawinkler (IK) hysteretic model. The building frame was subjected to a suite of 62 mainshock-aftershock sequences. It was concluded that the duration and frequency content of mainshocks, as well as aftershocks, contribute significantly to the structural collapse capacity. It was also observed that the aftershock characteristics significantly affected the damages as damage states due to the mainshock increased.

2.3.2 MODELLING OF AFTERSHOCKS

In the literature, the response of a building subjected the mainshock-aftershock sequence has been evaluated using three approaches, namely a) back to back b) randomized and c) stochastic. In the back to back approach, the real mainshock, scaled or unscaled, is repeated as an aftershock (Amadio et al. 2003; Fragiacomo et al. 2004; Hatzigeorgiou and Beskos 2009). In the second approach, an ensemble of real mainshocks is chosen, and artificial aftershocks are generated by scaling a randomly selected mainshock from the ensemble (Li and Ellingwood 2007; Ruiz-García 2012; Ruiz-García 2014; Ruiz-García and Negrete-Manriquez 2011; Goda 2015; Goda et al. 2013). In the third approach, a sequence of stationary Gaussian random process moderated by an envelope function is used as a mainshock-aftershock sequence (Moustafa and Takewaki 2011; Moustafa and

Takewaki 2012). Some researchers also simulated artificially generated earthquakes following different laws discussed in the previous section. Few authors are in favor of actual recorded mainshock-aftershock events to be used.

Li et al. (2014) investigated the damage probability at different damage states in steel building frames subject to aftershocks which sustained the mainshock with little damage. Two techniques, namely, repeated and randomized were employed to obtain the aftershocks. In the repeated technique, the mainshock was scaled down by some factors and utilized as the aftershock to the same mainshock. In the randomized technique, randomly selected mainshock was employed as the aftershock to the mainshock. Aftershocks with magnitudes less than those of the mainshock have a higher potential to cause severe damage once the structure is slightly damaged during the mainshock event. The study was validated on a 4-storey steel moment resisting frame with structural deterioration model available in the NEES hub database during those times.

Hashemi and Naserpour (2014) proposed a tool for the seismic analysis of steel moment resisting frame damaged during the mainshock. The steel building frame was designed using AISC 360-10 (AISC 2010) and modelled to evaluate the seismic response of a 3D special moment resisting frame subject to the mainshock-aftershock sequence. The building was subject to seven different mainshock-aftershock events in both X and Y directions. Instead of using the mainshock aftershock as one-time history, the damages caused by the mainshock were modelled as plastic hinges. The hinge property duly incorporated the permanent deformation caused by the mainshock using the nonlinear dynamic analysis of the 3D modelled frame. The performance of the mainshock damaged 3D building frame was evaluated by the nonlinear dynamic analysis.

Goda (2015) investigated different approaches for recorded selection for aftershocks. Among the three methods, the author emphasized the back to back method for the incremental dynamic analysis. In the back to back approach, it is assumed a priori that the characteristics of the mainshock and aftershock remain the same. From the numerical investigation for a wood-frame structure, it was

concluded that the fragility was affected by the characteristics of the aftershocks as well as the mainshock.

Han et al. (2015) evaluated the seismic response of the reinforced concrete building frame subjected to mainshock and aftershock events. Two three-bay non-ductile building frames having an identical plan consisting of different storeys (3-storey and 6-storey) was used as the test frame for the seismic performance evaluation. The building was subjected to as recorded ground motions suites comprising of the mainshock and different aftershocks. The total number of seismic events considered were 5 in which a number of aftershocks varied from 2 to 13. The mainshock and following aftershocks were combined in chronological order with a gap of the 30s. Thus, obtaining a long duration earthquake time history which was employed as an input to the nonlinear time history analysis of the famed structures. Financial losses due to the earthquake with and without the contribution of aftershocks were evaluated and compared.

2.3.3 STRUCTURAL RESPONSE DURING MAINSHOCK-AFTERSHOCK EVENTS

In the literature, different structures have been subjected to a sequence of mainshock-aftershock events. Different software used for the analysis are Open Sees, Frame3D, Drain-2DX, ANSR-I and ABAQUS. Most researches performed the nonlinear time history analysis duly incorporating the mainshock effects to evaluate the seismic response of structures during the aftershocks.

Luco et al. (2004) evaluated the capacity of a 4-storey building frame damaged during the mainshock to withstand an aftershock. Both nonlinear static analysis and nonlinear dynamic analysis were conducted on the building frame to determine the residual capacities. Three different hysteresis models, namely, a) bilinear, b) peak-oriented and c) pinching were employed to obtain the dynamic responses of the building frame. A dynamic analysis was performed for an intact building subjected to 30 different mainshocks and 30 different aftershocks following the mainshocks. In total 900 different analyses were performed for each hysteresis model. A nonlinear static procedure was proposed and validated with

the results of the dynamic analysis for the test building frame. The proposed nonlinear static method duly considered the residual drift of the building frame damaged by the mainshock.

Carreño et al. (2010) proposed a computational method to compute damaged states of building frames after the mainshock. The method was based on computationally intelligent neuro-fuzzy technique. The hybrid technique based on three-layer feedforward artificial neural network and the fuzzy rule provided definite conclusions about the safety and reparability of the building frame. This method provided a profound insight into the occupancy (whether to permit or not) of the building. The method could be used by the building inspector, who, after visual inspections decides on the permission to occupy the building or not.

Ruiz-Garcia and Negrete-Manriquez (2011) utilized 64 recorded seismic sequences to analyze the effect of as-recorded mainshock-aftershock sequences on a structure. Although the correlation of frequency content between aftershocks and mainshocks was performed by using data, no clear tendency was observed. The estimation results of structural responses for the recorded sequences were analyzed by randomizing and repeating the set of mainshocks. The study argued that the effect of aftershocks should be analyzed by means of recorded sequences. An analysis was conducted by combining the existing data or by using sequences where the same earthquake was repeated. It appeared that the estimation of structural responses to aftershocks using recorded sequences had limitations.

Sarno (2013) investigated the effects of mainshock- aftershock sequences on the response of structures incorporating the inelastic effects. As an example, the problem of the two-storey two-bay frame was subjected to a seismic sequence of Tohoku (Japan), starting on March 2011. Seismic sequence records from five different stations were chosen to study the effect of multiple strong earthquakes on structures. The strength and stiffness degradation of the building frame was modelled with a modified clough model. The response spectra were developed for the reinforced concrete frame subjected to multiple earthquakes. It could be seen that the responses of the structure subjected to multiple earthquakes were more

than that of the single mainshock. It was concluded from the study that extensive study is required for aftershock effects on the building frames.

Nazari et al. (2015a) emphasized the need to consider the aftershock effects in the seismic design of the building frames. The primary objective of the study was to include the aftershock effects into performance-based earthquake engineering. The study duly incorporated the strength and stiffness degradation models during the incremental dynamic analysis. The seismic response of the building frame damaged due to the mainshock was evaluated for different intensity levels of aftershocks. The study was validated on wood frame building damaged by the different intensity of the mainshock. The collapse probability of the wood building frame was computed using the mainshock-aftershock sequence with varying intensity and random aftershocks. It was concluded that the aftershock damage probability was weakly related to the damage probability of the building frame during the mainshock, indicating that aftershock hazard would play a significant role in the performance-based seismic design of building frames.

Ruiz-García and Aguilar (2015) proposed a seismic evaluation of building frames subjected to aftershocks taking into the residual inter-storey drift ratio (RIDR) after the mainshock event. The methodology was validated for a 4-storey steel moment resisting frames calibrated with the reported experimental results of the 1:8 scale model (Lignos et al. 2011). The incremental dynamic analysis was performed for determining the collapse resisting capacity of the building frame. The Building frame was assumed to collapse (irreparable damage) when the residual inter-storey drift ratio exceeded 2%. The author also examined the effect of the polarity of the aftershock on the collapse capacity.

Dulinska and Murzyn (2016) performed a dynamic analysis of one-storey reinforced concrete building frame subjected to the mainshock-aftershock seismic sequence using ABAQUS. Concrete was modelled using concrete damaged plasticity model available in ABAQUS. The building frame was subjected to all the three components of the mainshock-aftershock seismic event recorded in central Italy. The magnitude of the mainshock was 6.1, and that of the aftershock was 5.7. Both the time histories were scaled to a ground acceleration of 0.5g. In the dynamic

analysis, three components of the registered mainshock and aftershock were considered. It was concluded that the aftershocks could significantly affect the dynamic behavior of the concrete model in terms of damage states.

Han et al. (2016) discussed the aftershock effects on seismic performance of building frames. Currently, the seismic assessment in terms of loss estimation and damage identification methods was based on building behavior during single shock events. The damage probability during an aftershock was higher than that of the mainshock. The author proposed a performance-based design methodology to incorporate the aftershock effects. The method was validated by 18 near-fault and 60 far-field mainshock-aftershock sequences. It was concluded that the effects of multiple aftershocks were minimal than that of a single aftershock.

Kojima and Takewaki (2016) presented a method to evaluate the seismic performance of two residential buildings made of steel subjected to two consecutive earthquakes. The building frames were subjected to 2016 Kumamoto earthquake in Japan occurred on April 14 and 16 having a magnitude greater than VII on the Mercalli scale to evaluate their seismic performances. The hysteresis behavior of steel was modelled with the bilinear hysteresis having a negative second slope considering p-Δ effects. The sequence of the near-field earthquake was modelled with two sine pulse of velocity. The method was based on energy criteria.

Song et al. (2016) proposed a methodology to estimate the seismic loss of steel structures subjected to mainshock-aftershock sequences. The methodology incorporated the seismic hazard, structural response and damage analysis. The 4-story steel frame was chosen as the example problem. The material nonlinearity was modelled by the IMK hysteresis model. The steel building frame was subjected to the mainshock-aftershock sequence at two different levels of PGA design level, and maximum considered earthquake. The uncertainty in the loss estimation was examined by using Monte Carlo Simulation. It was concluded that the aftershocks had produced a significant role in the estimation of the seismic loss due to different damage states during the aftershocks.

Sun et al. (2016) investigated the single degree of freedom system subjected to the mainshock-aftershock sequence. The paper emphasized on the strength reduction factor "R" required for the seismic design of the building frame. The aftershock altered the ductility demand of the structure and thus, the strength reduction factor. The results were based on nonlinear time history analysis of SDOF systems subjected the mainshock-aftershock sequence. It was concluded that in order to consider the aftershock effects, the strength reduction factor should be 0.6 to 0.9 times of that required for the ductility-based factor as existing in seismic codes of different countries.

2.4 RETROFITTING OF STRUCTURES TO WITHSTAND SIDESWAY COLLAPSE

Old buildings may not have been built keeping earthquake resistance parameters in mind, even though that may not necessarily make them unsafe. Retrofitting strategies are employed to achieve a desired overall performance of a building frame using retrofitting techniques. Several retrofitting techniques such as increasing the global strength and stiffness using bracing systems, reduction of the seismic demand by using energy dissipating devices such as a base isolator or dampers are currently available to retrofit the building frames.

Base isolation and dampers are employed to make buildings strong enough to resist seismic vibrations. Through base isolation, the building or the superstructure is decoupled from its substructure which rests on the ground, thus protecting the building during an earthquake. To make a building earthquake-resistant, the building base is strengthened in such a way that during an earthquake, the building's load is borne by the base alone, and the upper storeys do not experience much quaking. The part of the base that is above the ground is cut and rested on bearings. The bearings are a combination of roller bearings and elastomer bearings. Higher floors of a building retrofitted by base isolation may not feel any shaking in the event of an earthquake. Dampers, on the other hand, work as shock absorbers and minimize the magnitude of vibrations transmitted to the building from the ground.

2.4.1 OTHER RETROFITTING STRATEGIES

A number of retrofitting strategies are now available and have been implemented in practice. Every retrofitting strategy has its own merits and demerits and is judiciously selected to retrofit a damaged structure. The condition of the damage and nature of the load for which retrofitting is to be carried out are the primary deciding factors for the choice. For steel building frames, variuos types of bracings are preferred for retrofitting as they involve least constructional effort.

Tena-Colunga and Vergara (1997) evaluated the seismic performance of a building frame retrofitted using steel braces and building retrofitted using added damping and stiffness (ADAS). ADAS is a passive energy dissipation device, and steel braces are global stiffness and strength enhancement techniques. The retrofitting technique was used to retrofit a building constructed in 1950 and damaged during the 1985 Mexico City earthquake. The ADAS energy dissipation device was used instead of the conventional steel braces to retrofit the building frames to withstand a higher level of earthquakes. The retrofitted building frame was analyzed by using the elastic analysis, limit analysis and nonlinear time history analysis. For the nonlinear time history analysis, the building was retrofitted using both techniques and was subjected to artificial earthquakes confirming to empirical formulae for the Mexico City earthquake having a magnitude 8.1. The empirical formulae generate acceleration time histories based on transfer function of the site and previous earthquake database. It was concluded from the response of analysis that the building retrofitted using ADAS devices performed better than that of braced building frames in terms of lateral displacement, whereas the braced building frames had shown high strength and low cost compared to its counterpart.

Maheri et al. (2003) conducted an experiment in a 1:3 scaled model of the unbraced and braced reinforced concrete frames. Two different configurations of braces namely, X-braces and Knee Braces were considered for the experimental study. Experimental pushover analysis considering both gravity load as well as horizontal load was conducted. Experimental results indicated that the yield capacity and strength could be enhanced using the bracing of the reinforced

concrete frames. The global displacement could also be decreased by adding braces in the virgin frames. Bracing also drastically decreased the ductility of the frames. It was concluded from the experimental results that both X-bracing and Knee bracing could be employed to improve the seismic behavior of the framed structure.

Zhao and Zhang (2007) presented a review of the retrofitting of steel structures using fiber reinforced polymer. The review paper discussed the bond strength between the steel and fiber reinforced polymer. The paper also discussed different failure modes of the fiber reinforced polymers. The paper emphasized on strengthening of the hollow steel section using the FRP. Enhancement of the compressive strength and flexural strength of the hollow sections using FRP was also considered in the review. The author highlighted the fatigue crack propagation for the fiber reinforced polymer wrapped on the hollow steel sections.

Di Sarno and Elnashai (2009) evaluated the seismic performance of different retrofitted steel moment resisting frames. Three different configurations of braces, namely, special concentrically braces (SCBFs), buckling-restrained braces (BRBFs) and mega-braces (MBFs) were considered in the study. A 9-storey moment resisting frame was retrofitted with a different configuration of bracing at different locations as a design example. The retrofitted building frame was subjected to a suite of response-spectrum compatible earthquakes. The nonlinear time history analysis of the braced frames was carried out on DRAIN-2DX to evaluate the seismic performance considering the P-Δ effects. The unconditionally stable Newmark-β method with $\beta=0.25$ and $\gamma=0.25$ was employed for numerical integration of the equation of the motion. The lateral inelastic deformations were compared for different bracing configuration. It was concluded that the lateral deformation was a function of the earthquake characteristics, bracing configuration and location. As a result, buckling restrained braces were superior to other braces.

Hou and Tagawa (2009) presented a seismically retrofitted technique for building a frame using cables. The building frame was retrofitted using cables as braces. An experimental test was carried out for the one storey steel building frame

retrofitted using cables. The test frame was subjected to cyclic load using 1000KN capacity hydraulic jack with the stroke of 300mm. The experimental test results were used to characterize the building frame braced with cables. The results of the experimental test were applied for the analytical study. A three-storey building frame retrofitted by the technique was subjected to El-Centro earthquake. Characterization of the building frame was carried out using the cyclic pushover analysis of the building frame. The results implied that the building frame could be retrofitted efficiently by the cables.

Di Sarno and Manfredi (2010) evaluated the seismic performance of reinforced concrete structures designed for gravity loads only. The building frame was highly vulnerable during the seismic event due to the limited ductility of the structure. A retrofitting technique was proposed to strengthen the building frame based on energy balance. The method was iterative and based on effective hysteretic global response of the structure. For an example problem, a retrofitting scheme by strategically placed buckling restrained braces along the perimeter of the building frame was developed. Pushover analysis and nonlinear response history analysis were conducted for both the as built and retrofitted structures. The structures were subjected to a set of seven earthquake records compatible with the response spectrum of the code. The inelastic response of both structures was compared, and the results indicated that lateral displacements are within the allowable limits for the retrofitted structure. It can also be concluded that buckling restrained braces enhance the ductility of the structure and in turn, the seismic performance of the building frames.

2.4.2 BRACES AS RETROFITTING TECHNIQUE

Koboevic et al. (2012) investigated the seismic response of eccentrically braced 3-storey and 8-storey building frames. The building frame was designed as per the national building code of Canada 2005 (NBCC 2005). The designed bracing complied with seismic provisions of Canada. Three different modelling software, namely, ANSR-I, Drain-2DX and Open Sees were employed for the nonlinear time history analysis of the building frame. The building frame modelled in different

software yielded different inelastic response to the set of applied ground motions on the eccentrically braced frames. The results indicated that modelling techniques significantly alters the inelastic response of the eccentrically braced frames. Flexural buckling was observed in both braces and columns. It was also concluded that even a small change in the section property of the braces altered the response drastically.

Safarizki et al. (2013) evaluated the seismic performance of the retrofitted reinforced concrete building frames using steel braces. Pushover analysis and nonlinear time history analysis were utilized for the evaluation of the seismic performance of the structure. The seismic design of building frame was based on the Indonesian code of seismic resistant building (SNI 03-1726-2002, Nasional 2002). Target displacements in X-direction and Y-direction were 0.188m and 0.132m respectively. El-Centro earthquake was used for the nonlinear dynamic analysis. From the analytical study, it was concluded that the target displacement demand reduced for the retrofitted building. Moreover, the storey drifts for the retrofitted building was below the allowable limits. It was also concluded the bracing size did not make significant alterations to the seismic performance of the retrofitted building frame.

Lai and Mahin (2014) presented experimental results for one-bay, two-storey concentrically braced steel frames. Hollow sections, both square and circular, were used as bracing members. The braced building frame was designed based on the AISC 2005 seismic provisions (ANSI 2005). The building frame was tested for displacement controlled cyclic pushover test. The bracing strength and its cyclic deterioration property were simulated on Open Sees. The experimental results were validated with numerical modelling on Open Sees. The experimental and numerical results confirmed that the circular hollow sections perform superior to that of the square hollow sections of the similar property of both sections. The results also demonstrated that further study is recommended on the behavior of braced frames.

Vafaei and Eskandari (2014) examined the seismic performance of buckling restrained braced steel frames subjected to near-source ground motions. Near field

earthquakes imposed higher displacement demands than that of the far- field earthquakes. The forward directivity in terms of high amplitude pulses at the beginning of the ground motion was considered for simulation of 4-, 8-, 12- and 15- storey buckling restrained braced building frames. High amplitude pulses at the beginning of the earthquake records imposed large energy demand on the building frames. Nonlinear time history analysis using Open Sees was conducted on the braced frames. The results indicated that the displacement demands on the lower storey are maximum for the example problems. It was also concluded that the higher modes didn't contribute to the seismic demand of the retrofitted building subjected to near-field earthquakes.

Patil and Sangle (2015) compared the seismic behavior of braced building frames. Four different configurations of bracing were used: chevron braced frames (CBFs), V-braced frames (VBFs), X-braced frames (XBFs) and zipper braced frames (ZBFs) along with the moment resisting frame. 15-, 20-, 25-, 30- and 35-storey building frames were used as examples for high rise building frames. The building frames were designed as per Indian standard code for the seismic design of buildings (IS 1893-2007). Nonlinear static analyses were carried out on different building frames with different configurations. The capacity curves of all the analyses were compared. The results of analyses revealed that different configurations of the building frame behaved differently in terms of the storey displacement, inter-storey drift ratio, base shear and performance point. It was concluded from the results that the CBF, VBF and ZBF enhanced the seismic performance of the building frames.

Haddad (2018) modelled different concentric hollow structural section (HSS) using ABAQUS. The true stress-strain behavior was modelled based on the coupon test on the specimens. The true stress-strain behavior was idealized with exponential functions. The modelling parameters of the strain-stress were validated with the experimental results given by Haddad et al. 2011; Shaback and Brown 2003. The hysteresis behavior of the bracing members was obtained from the true stress-strain behavior of the bracing members. A damage accumulation hysteresis behavior was obtained from the study of ultra-low cycle fatigue. The

refined behavior was used to model an eight-storey concentrically braced steel frame on Open Sees. The building frame was designed for site class-C as per the national building code of Canada 2010. The concentrically braced frame was subjected to four ground motions. The designed concentrically braced frames sustained the earthquakes without any fracture in the bracing members.

2.5 SIDESWAY COLLAPSE RISK PROBABILITY OF STRUCTURES

Collapse risk of structues are determined using fragility curves. Fragility curves are commonly used to assess the vulnerability of structures to earthquakes. The probability of failure associated with a prescribed criterion known as damage measure is represented as a function of the intensity of the earthquake ground motion known as intensity measure. The classical approach relies on assuming a lognormal shape of the fragility curves. There are different approaches to obtain fragility curves.

2.5.1 DIFFERENT METHODS FOR COLLAPSE RISK ANALYSIS

Baker and Cornell (2005) proposed a vector-valued ground motion intensity measure, consisting of a spectral acceleration and epsilon. The proposed intensity measure incorporated the shortcoming of the other intensity measures such as the peak ground acceleration and spectral acceleration. The author emphasized on the use of epsilon as the intensity measure and its ability to significantly predict the structural response. Epsilon was defined as "the number of standard deviations by which an observed logarithmic spectral acceleration differed from the mean logarithmic spectral acceleration of a ground-motion prediction (attenuation) equation". For numerical illustration, fifteen generic frames of 3-, 7-, 9 and 15-story with different time periods were considered. The buildings were modelled with different material behavior, namely, the Ibarra-Krawinkler with peak oriented, MIK with peak oriented and pincheira model. The building frames were subjected to 40 different sets of earthquakes scaled to 16 levels of 5% damped spectral acceleration corresponding to the fundamental period. Inter-storey drift angle in

present study was considered as a damage measure criterion. The study revealed that the epsilon was a necessary parameter considering the structural response.

Zareian et al. (2010) summarized different damage measures for collapse performance and the probabilistic basis for developing fragility curves. Two methods for incremental dynamic analysis, namely, Engineering Demand Parameter (EDP) and Intensity Measure (IM) based method were discussed and evaluated. The EDP based method utilized EDP for the estimation of the probability of collapse for a certain level of ground motion intensity. The IM based method used the ground motion intensity measure for the estimation of the probability of collapse. Collapse performance for both methods was compared with that of the guidelines recommended by SAC/FEMA. In the study, 8-storey moment resisting frame was considered as the case study. The building frame was modelled on Open Sees. The material nonlinearity was modelled using the IMK hysteresis model. The probability of collapse at discrete levels of seismic hazard levels was drawn as a fragility curve. It was concluded that the IM-based approach for developing the fragility curve has a better accuracy than the EDP based method. It was also concluded that the EDP based method overestimates the probability of collapse.

Baker (2013) presented a review of the impact of the ground motion characteristics on the fragility analysis of the building frame. The ground motion selection could affect the collapse capacity of the structure. Improper selection could lead to the under or overestimation of the collapse probability. The study emphasized the selection of a sufficient number of ground motions and their characteristics for efficient fragility analysis of the structure. The study also compared multiple stripe analysis (MSA) and incremental dynamic analysis (IDA). It was concluded from the study that a proper selection of single ground motion suite and their scaling based on an intensity measure was sufficient for incremental dynamic analysis, whereas, multiple suites at each ground motion intensity was required for the multiple stripe analysis.

Baker (2015) Discussed different approaches for the evaluation of the fragility function. The study also discussed the applicability of different statistical

methods for the risk analysis. Incremental dynamic analysis truncated incremental dynamic analysis and multiple stripe analysis were discussed in detail. In all the method, θ and β were determined by solving an optimization problem to determine the probability of collapse corresponding to different intensity measures. The method minimizes the likelihood estimation from the set of nonlinear dynamic analysis for earthquakes scaled at different seismic levels. The study revealed that the multiple stripe analysis was more effective than the incremental dynamic analysis. The multiple stripe method was superior to the incremental dynamic analysis as the method utilized different ground motions at varying intensity levels which represented different characteristics.

Zentner et al. (2017) reviewed a number of different approaches for the seismic reliability analysis and their applications. The Seismic reliability analysis gave the probability of attaining a damaged state during an earthquake with defined seismic hazard. Several methods were available to build fragility curves. Different methods investigated by the author in the study were i) safety factor method; ii) regression analysis; iii) maximum likelihood estimation and iv) incremental dynamic analysis. In the safety factor method, the safety margin was evaluated in terms of the fragility curve assuming that the seismic capacity and safety margins followed a lognormal distribution. In the regression analysis method, sets of input-output were evaluated using the nonlinear time history analysis wherein input was the intensity measure and output was the damage measure. The method required N different samples of input-output, which is assumed to represent the population. Linear regression analysis is performed to fit a curve between the probability of collapse and intensity measure. The maximum likelihood method also requires N different samples of input-output as in the regression analysis method. Instead of assuming a continuous distribution of the damage state, the method assumed the damage state to be binary. In the maximum likelihood estimation method, the damage was estimated. Finally, in the incremental dynamic analysis, the set of ground motion was scaled until the collapse of the structure took place. The structural capacity was determined using the nonlinear time history analysis. The analysis was performed until the building

frame collapsed. The fragility curve showed the probability of the collapse given by the number of ground motions for which the structure collapsed below the intensity measure. All the methods were compared for a 3-story reinforced concrete building frame.

2.5.2 FRAGILITY ANALYSIS OF DIFFERENT STRUCTURES

Ellingwood and Kinali (2009) emphasized on the uncertainty modelling effect on the seismic risk analysis and proposed a consequence-based risk analysis tool. The author also identified the issues which should be addressed for the enhanced decision during the event of the earthquake. For the numerical analysis, 2- 4- and 6- story steel building frames were modelled on finite element-based modelling software Open Sees. The material nonlinearity for beam and column were modelled as nonlinear beam-column with distributed plasticity. The geometric nonlinearity was also considered during the nonlinear time history analysis for the probabilistic analysis. The 2-and 4- storey frame were modelled as a partially restrained moment resisting frames, whereas the 6-story frame was modelled as braced frames. For the seismic risk analysis, 5% damped spectral acceleration corresponding to the fundamental period was taken as the intensity measure. The inter-storey drift angle was taken as the damage measure. For different collapse levels, different drift ratios were taken as the damage measure. Instead of the point estimate of the damage measure, interval bound was considered. The study revealed the benefits of the approach over the conventional ones for various risk mitigation strategies.

Pei and van de Lindt (2010) investigated the effect of the mainshock-aftershock on wood building frames for the financial loss. Due to a large number of wood frames in the united states, the cumulative financial loss for the building frame subjected to large earthquakes was alarming. A sensitivity analysis of the impact of the structural property and the ground motion magnitude of the financial loss was carried out. A two-storey residential building frame was chosen for the numerical investigation. Three different nailing patterns were adopted for the study. The wood shear-walls were modelled with hysteresis behavior

incorporating the strength and stiffness degradation. The detailed nonlinear dynamic analysis was performed for the building frame. The study concluded that the financial loss was not significantly depending on the structural property until the peak ground acceleration of 0.3g. It was also concluded that the long-term financial loss was significantly affected by the seismic hazard level.

Yin and Li (2010) evaluated the effect of aleatoric and epistemic uncertainty on the collapse probability of light wood frame structure. The uncertainties were considered in both the demand of the earthquake and capacity of the building frame. A one storey building frame with a fundamental period less than 0.5s was considered as a case study. The backbone curve of the wood structure defined by the hysteresis model was modelled as per Folz and Filiatrault (2004). A suite of ground motions developed by the SAC project was employed for the incremental dynamic analysis. Nonlinear time history analysis was carried out on Open Sees for the ground motion scaled at different levels. It was concluded from the study that the uncertainty in the capacity of a building frame and their modelling effects significantly the seismic collapse risk of the light frame wood structures.

Özel and Güneyisi (2011) conducted a seismic fragility analysis of steel braced reinforced concrete building frames. The building frame was designed based on the seismic code of turkey (Code 2007.). The building frame was retrofitted using different bracing configurations. Different bracing configurations considered in the study are D, K and V-type eccentric bracing systems with different spatial configurations. The effectiveness of the bracing system was examined using the fragility analysis. The building frame was subjected to 200 artificially generated earthquakes compatible with the response spectra based on the seismic design code of turkey (Code 2007.). Nonlinear time history analysis was performed on the retrofitted building frame subjected to the artificially generated earthquake with varying peak ground accelerations. The peak ground acceleration was used as an intensity measure for the fragility analysis. From the fragility curves for all the retrofitted building frames and the virgin frame, it was concluded that the seismic performance of the retrofitted building frame is superior to that of the un-retrofitted building frames.

Raghunandan and Liel (2013) investigated the influence of the ground motion duration on the seismic collapse probability of the reinforced concrete structures. The incremental dynamic analysis was conducted to determine the collapse risk probability. For the same, 17 different buildings were considered to represent both old and modern buildings. The buildings were subjected to 76 different earthquakes having different significant durations, representing the long and short duration earthquakes. The long duration earthquakes signified multiple cycles of spectral displacement during the earthquake. Inelastic spectral displacement corresponding to the fundamental period of the structure was taken as the intensity measure. The inelastic spectral displacement was computed for 5% damped SDOF system with the bilinear material property. Different damage measures were considered based on the roof drift ratio. It was concluded from the study that ground motion duration significantly affects the collapse risk probability of both high ductile as well as less ductile structures.

Fereshtehnejad et al. (2016) proposed a method to identify modes of failure. The failure mode was based on the mechanism after hinge formation. The method was based on the formation of the appropriate plastic hinge and push over analysis. Locations of plastic hinges were decided a priori using Bayesian probability network. These locations were utilized for incremental dynamic analysis. The methodology was applied to a two-story special steel moment resisting frames. The building was modelled on Open Sees incorporating P-Δ effects. The material nonlinearity was imposed by the MIK hysteresis model. The study revealed that most of the failure modes determined in pushover analysis are also observed in the incremental dynamic analyses.

Koopaee et al. (2017) investigated the effect of ground motion uncertainties in determining the seismic risk analysis of reinforced concrete building frames. A method for selecting the ground motion for probabilistic earthquake analysis was also developed. The reinforced concrete was modelled using fiber-element-strength and stiffness degradation hysteresis model which accounted for the cyclic fatigue, reinforcement buckling and crushing. The model incorporated P–Δ effects for the sidesway collapse of the building frame. The ground motions were selected

based on the conditional mean spectrum and generalized conditional intensity measures were used. The collapse fragility curves were drawn using the multiple stripe method. The study concluded that the ground motion selected using the conditional mean spectrum method was more suited than the other method.

2.5.3 FRAGILITY ANALYSIS FOR MAINSHOCK AFTERSHOCK EVENTS

Li and Ellingwood (2007) evaluated the damage probability caused by aftershocks to steel moment resisting frames. The enhanced uncoupled model response history analysis (EUMRHA) was developed as a technique to evaluate the stochastic nonlinear dynamic analysis. The method significantly reduced the computational time than that by the nonlinear time history analysis of a building frame subjected to an earthquake. This reduction in the computational time enabled a number of analyses required in less time. The seismic response of the structure was reported to be similar by both the methods. 9- and 20- storey building frame designed for gravity load as per 1994 uniform building codes was taken for the numerical illustration of the method proposed. The building frame was subjected to several earthquakes, and inter-story drift ratio was recorded and used as a damage measure for the probabilistic analysis. The damage probability for the building frame was evaluated for the mainshock as well as for the mainshock-aftershock sequence. The study revealed that the damage probability of both building frames corresponding to the mainshock-aftershock sequence was low if the damage caused by the mainshock is low. It was also concluded from the study that the response of a structure by repeating the mainshock as the aftershock was overestimated than the recorded mainshock-aftershock sequence.

Han et al. (2014) determined the seismic collapse probability of base-isolated reinforced concrete building frame due to the mainshock-aftershock sequence. The results of the fragility analysis of the base-isolated building frame were compared with that of the non-retrofitted ductile reinforced concrete building frames. The uncertainties considered in the study were structural property, uncertainty in the ground motion modelling and ground motion intensity. The author also examined the impact of different building parameters

on the fragility analysis of both retrofitted and un-retrofitted building frames. It was concluded from the study that the base isolation drastically reduced the seismic risk for higher damage levels. Moreover, the aftershock effects should not be neglected during the seismic risk analysis and seismic design of the building frame.

Raghunandan et al. (2015) computed the seismic risk analysis of reinforced concrete building due to aftershock using incremental dynamic analysis. 900 different mainshock and aftershock sequences with 11 scaling factors was considered for the study. The building frame was modelled on Open Sees. The nonlinear time history analyses for different cases were run on the Janus supercomputer comprising of 900 processors which reduced the computational time from 33 weeks to 12hrs. Fragility analysis of the building for aftershocks incorporating the damages caused by the mainshock was computed. The study revealed that the building undamaged after the mainshock had less probability of damage during the aftershock. This probability increased significantly once the building was damaged during the mainshock.

Nazari et al. (2015b) proposed a method, considered in the aftershock effects for seismic design of building frames. The method quantified the changes required for the structural design using the nonlinear model of the building frame subjected to the mainshock and aftershock sequence. The collapse probability of the building frame subjected to the mainshock and changes required for same collapse probability of building frame subjected to the mainshock and aftershock sequence were studied. The collapse probability for the mainshock and aftershock sequence was computed using the theory of conditional probability for the aftershock damage subjected to the damage during the mainshock. The method was validated for changes required in the structural design of a two-storey wooden building frame. The author emphasized the need to consider the effects of aftershocks in the seismic design of the building frame.

Burton et al. (2017) presented statistical models to estimate the collapse probability due to aftershocks based on the mainshock characteristic, response of the structure and damage indicators. The collapse probability for the mainshock

damaged building frame was evaluated using the incremental dynamic analysis for the mainshock-aftershock sequence. Different statistical tools were employed to determine reduced collapse capacity of the structure. A four-storey steel building frame designed as per Indian standard for the earthquake resistant design of structures, IS 1893, is taken as an example frame for the numerical illustration. The building frame was modelled on finite element software Open Sees. The strength and stiffness degradation was modelled by plastic hinges using Ibarra-Krawinkler hysteresis model. The model duly incorporates the P-Δ effects.

Hwang and Lignos (2017) quantified the seismic collapse risk of a building frame and economic losses during the earthquake. The author presented a probabilistic financial loss estimation subject to the damage, the building has sustained during the earthquake, for a given intensity measure. A dual parameter fragility curve generation was adopted as an alternative to the univariate fragility curve as given in the present guidelines for seismic evaluation by FEMA 2012. For numerical illustration, a steel building frame designed as per ASCE/SEI (7-05) was considered. The braces were designed as per ANSI/ASCE 341-05. Hollow steel sections were used as the braces. Incremental dynamic analysis by the nonlinear time history analysis is performed on Open Sees. 5% damped spectral acceleration corresponding to the fundamental period was chosen as the intensity measure. Drift based dual parameter was chosen as the damage measure. The study revealed that the loss during the low probability of occurrence of earthquakes was overestimated. It was also concluded that the dual-parameter instead of drift-based damage measure should be used for developing fragility curves.

Kiani et al. (2018) discussed the effect of the number of earthquakes considered in the fragility analysis. The study was aimed at determining the optimal number of earthquakes and their property for the seismic risk analysis. The number of earthquakes was varied from 3 to 100 at nine discrete points (100,40,30,25,20,15,10,7 and 3). An eight storey steel building frame with a fundamental period of 2.3s was taken as an example problem. The building was modelled on Open Sees. The beams and columns were modelled with the MIK hysteresis model. The building was subjected to different sets of ground motions.

The ground motion selected adhered to a generalized conditional intensity measure framework (GCIM) framework, i.e. ground motion followed the multivariate lognormal distribution. The study revealed that 25-hazard consistent ground motions were necessary for a reliable estimate of probable seismic response. It was also concluded that seven ground motions were adequate for the seismic response considered for the design of the structure.

Pang and Wu (2018) examined the aftershock effects on the seismic performance of the multi-span reinforced concrete bridges. A 3-span 2 column continuous girder bridge with sliding bearing was taken as an illustrative example. The bridge was designed as per the old Chinese bridge design specifications. The seismic performance was evaluated using a reliability analysis of the bridge. The reliability analysis was performed using the nonlinear time history analysis of the bridge on finite element software Open Sees. The reinforcement of the bridge was modelled as a multilinear hysteresis model to model the strength and stiffness degradation, and concrete was modelled using the uniaxial concrete model. 75 sequences of the mainshock and aftershocks were selected from 10 earthquakes occurred in different parts of the world. All the earthquake sequences selected for the reliability analysis were far field having a magnitude more than 4. The peak ground acceleration of the aftershock was less than 0.7 times that of the aftershocks. Fragility curves were drawn for both the mainshock as well as for the mainshock and aftershock sequence. The study revealed that the aftershock had higher damage capability than that of the mainshock.

Park et al. (2018) proposed a quantitative evaluation model for developing the fragility curve of a damaged building considering the aftershock effects. The aftershocks were artificially generated using EQ-maker software based on SIMOKE theory. The characteristics of the earthquakes considered were the mean period and effective duration. A 3-bay 2-storey and a 3-bay 4-storey reinforced concrete building frames were modelled on Open Sees. The model incorporated the strength and stiffness degradation using the bilinear hysteresis model. Nonlinear dynamic analysis of the building frames was performed for different ground motions. The incremental dynamic analysis used spectral acceleration at

the fundamental period as the intensity measure. The method efficiently evaluated the critical earthquake sequence for developing the fragility analysis using a limited number of aftershocks.

2.6 CONCLUDING REMARKS

Although there have been a number of studies on the behavior of building frames during earthquake and ample literature on the performance of building frames subjected to the mainshock and aftershock, there is a need for further research in certain areas which are evident from the literature review. They include the following:

1. The building frame may be damaged by several other factors than the earthquake. Such building frames were not examined for seismic excitation. Therefore, elaborate studies on the performance and side sway collapse of damaged (due to other causes) building frames under the earthquake is necessary.
2. There are several aftershocks associated with the mainshock. The previous studies revealed that the aftershocks are more devastating than the mainshock. There have not been many studies on the repeated sequence of aftershocks. Most of the studies had been carried out on single aftershock with a mainshock.
3. There have been studies on the retrofitting of building frames using bracings. There has not been much study on optimizing the location of the braces so as to withstand different levels of earthquakes efficiently.
4. Extensive studies on the fragility analysis of the retrofitted building frames by considering the uncertainty of mainshock-aftershock events are lacking. The consideration of aftershock is important as the building frame which sustained the mainshock are prone to collapse under the mainshock-aftershock sequence. Therefore, exhaustive studies on the seismic risk probability of retrofitted and virgin building frames during the mainshock aftershock event are required.

CHAPTER-3
SIDESWAY COLLAPSE OF DAMAGED STEEL BUILDING FRAMES

3.1 INTRODUCTORY REMARKS

In many earthquakes, it is seen that two identical buildings built at the same time and at the same site respond differently; one has collapsed, while the other has developed more damages, but they got arrested at a certain level. The reason for the collapse of the former may be ascribed to spreading of some initial localized damages leading to sway collapse of the structure. These localized damages are caused due to environmental and other ageing effects, such as the fatigue, shrinkage and creep. Since the collapse occurs due to the progression of some initially localized damages, the collapse may be termed as progressive collapse. Since this adds confusion to the terminology 'progressive collapse' as used in the current literature, it is better to be called the sidesway collapse of damaged frames under earthquakes.

Analysis techniques used for the 'progressive collapse' are a) linear and nonlinear static analyses and b) linear and nonlinear time history analyses. Significant research had been carried out in the recent past on the 'progressive collapse' of building frames (Ellingwood and Leyendecker 1978; Marjanishvili and Agnew 2006; Menchel et al. 2009; Kwasniewski 2010; Fu 2012; Bandyopadhyay et al. 2008; Haberland and Starossek 2009; & Pearson and Delatte 2005) which are presented in chapter 2. No literature exists exclusively on the collapse of structures because of the spreading of a few initial localized damages in the structure leading to the complete collapse in sway mode during earthquakes. However, a few associated studies have been carried out for the sidesway collapse of steel frames which are briefly reviewed again in chapter 2.

In this chapter, the spread of different patterns of localized damages in steel building frames during earthquakes is critically investigated to identify the potential damage scenario for the of the collapse of the frame. The quantification

of damages is obtained using a plastic analysis and genetic algorithm (GA). The detail of the plastic analysis of multi storey frames and the genetic algorithm are discussed in this chapter. With the help of the above techniques, different damage scenarios are simulated which have the same specified total damage expressed in terms of the reduction in total plastic moment carrying capacity of the system. Push over analysis is then used to identify the critical damage scenario which leads to the complete sway mechanism of failure for a response spectrum compatible earthquake with the least value of the PGA. The value of the PGA is obtained by making the performance point to coincide with the collapse point of the pushover curve. The pushover analysis is also used to verify the collapse load predicted by the mechanism method of the plastic analysis. The entire method is named as Genetic Plastic Pushover Analysis (GPPA), the results of which are validated by a nonlinear time history analysis of the frame under the simulated response spectrum consistent earthquake having the least value of the PGA as described above. A ten-storey building frame is taken as an illustrative example.

3.2 THEORY

A damaged structure, depending upon the nature and locations its damage behaves in different ways to future earthquakes. In order to trace the subsequent damages in the form of plastic hinges and the collapse of the structure during the earthquake, the following analytical tools are used:

I) Pushover analysis
II) Plastic analysis
III) Optimization using genetic algorithm
IV) Nonlinear time history analysis.

Brief backgrounds of the above analysis procedures in the context of the present study are outlined below:

3.2.1 PUSHOVER ANALYSIS

The non-linear static analysis, pushover analysis, has no strict theoretical base (Krawinkler 1996). It is mainly based on the assumption that the response of the structure is controlled by the first mode of vibration and mode shape. Several recent researchers (Mwafy and Elnashai 2001; Naeim and Lobo 1998; Goel and Chopra 2004) indicate that if the response of the structure is dominated by the first mode, then the response of multi-degree of freedom system can be estimated by the pushover analysis.

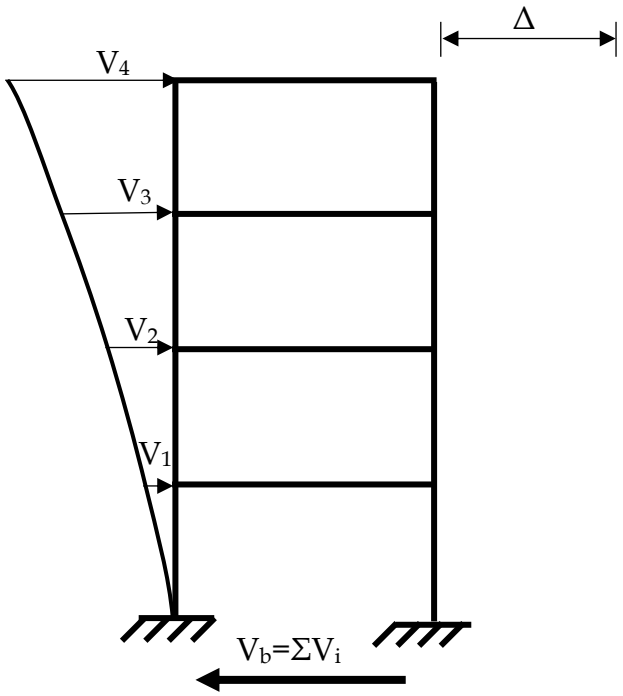

Fig. 3.1 Building frame subjected to lateral loads

In the pushover analysis, the structure is subjected to gravity loads and is laterally pushed by monotonically increasing displacement at a certain point. Fig. 3.1 shows the building subjected to a lateral load. A pattern of increasing lateral forces needs to be applied to the mass points of the system so as to be consistent with the incremental lateral displacement applied to the structure. The Lateral push may have different envelopes based on the requirement. The purpose of this is to represent all forces which are produced when the system is subjected to the earthquake excitation. The increment of the lateral push is continued until a predetermined displacement or collapse of the structure takes place. The method

incorporates the elastic as well as the inelastic property of the materials. By incrementally applying this pattern up to and into the inelastic stage, progressive yielding of the structural elements can be monitored. During the inelastic stage, the system will experience a loss of stiffness and a change in its vibration period. This can be seen in the force-deformation relationship of the system.

For the nonlinear static analysis, the compatibility equation is:

$$K_T \Delta X = \Delta P \qquad (3\text{-}1)$$

Where, K_T is the instantaneous stiffness matrix, modified after each increment of the displacement (ΔX). ΔX is the predetermined incremental displacement provided, generally at the top story. The incremental displacement at other storey levels conforms to the first deformation mode shape of the frame, starting from an initial elastic state. K_T, at any displacement level, is obtained by modelling the initial elastic stiffness along with the plastic hinges formed at that level. Eq. 3-1 provides the incremental force vector corresponding to the applied incremental displacement at the top storey. The incremental internal forces, for each member, are determined for ΔP and added to the total internal force prior to the application of incremental displacement ΔX. Required iterations are carried out if transition points are encountered by some members. SAP 2000 software package is used to carry out the nonlinear static pushover analysis. A displacement controlled non-linear static procedure is adopted.

3.2.1.1 MATERIAL NONLINEARITY

In the SAP 2000, the material nonlinearity is assumed at different points, where the member is expected to experience inelastic excursion. It is assumed that the behavior of the frame is elastic until a plastic hinge is formed. After the formation of a plastic hinge, stiffness of all the beams and columns decrease in a small percentage of their initial value (region B-C in Fig. 3.2). Hinges are assigned to a frame element (beam or column) at 5% length from the ends. A sudden loss of strength of the hinge is assumed as soon as the moments at the predefined point exceed the total failure or maximum rotation allowed as per the hinge properties. For each degree of freedom, a force and displacement behavior are assigned as

shown in Fig. 3.2. For each moment degree of freedom, a plastic moment and rotation behavior is assigned in a similar way as for the force-deformation behavior, where point B represents yielding. No deformation is assumed up to point B. Point C represents the ultimate capacity for the pushover analysis. Point D represents a residual strength of the members. Point E represents the total failure. Beyond this point, the hinge will drop the load to zero. The additional

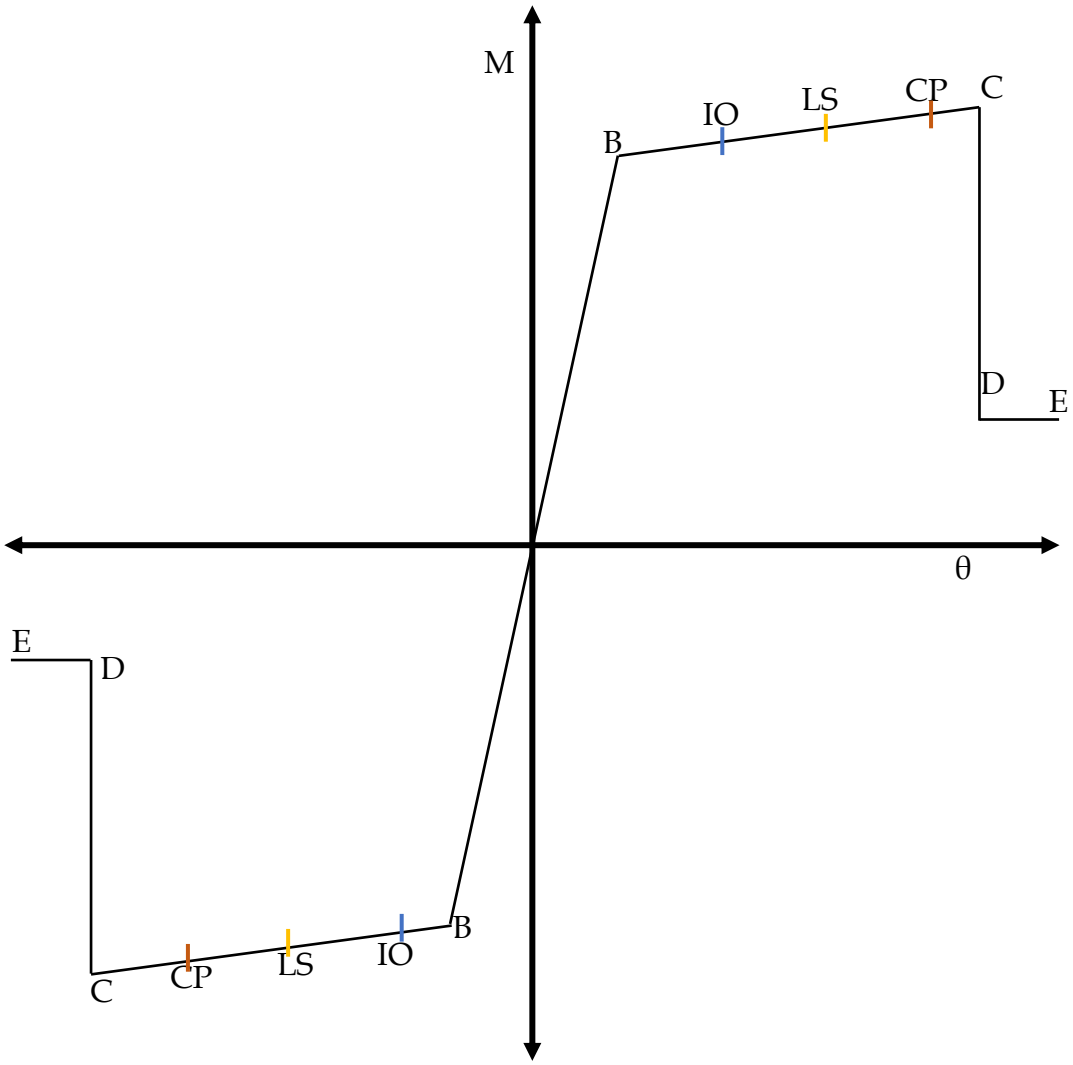

Fig. 3.2 Material Nonlinearity

deformation measure is provided at points (Intermediate occupancy) LS (life safety), and CP (Collapse prevention). The FEMA 356 default values are assumed for this purpose. The M3 hinge assigned for beams and the P-M3 hinge is provided in columns.

3.2.1.2 CAPACITY SPECTRUM METHOD

The capacity spectrum method was developed by Freeman et al. 1975. The capacity spectrum method is based on the capacity of the structure and response spectrum. The capacity of the structure is represented graphically in terms of global force versus displacement plot. A typical capacity curve is shown in Fig. 3.3. The response spectrum of the earthquake demand is superimposed on the capacity curve to determine the performance point. In order to superimpose the two curves, the capacity curve is converted into Acceleration Displacement Response Spectrum (ADRS) format.

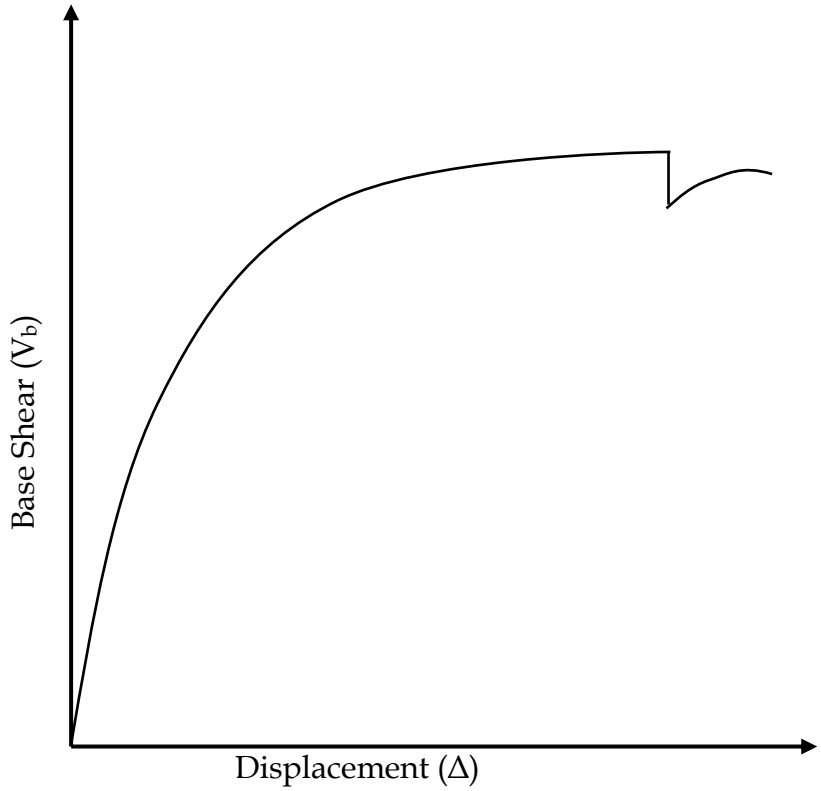

Fig. 3.3 Pushover curve

The building frame is statically pushed by applying the lateral load or displacement. The inelastic property can be defined as distributed plasticity or concentrated plasticity. In this study, concentrated plasticity is assumed. The building is pushed till the local or global collapse takes place. Since the global collapse of the building frame is desired, the building frame is designed such that the collapse is global. The curve is drawn for the base shear versus top floor

displacement. The curve for each increment of displacement or load is superimposed to form the capacity curve. The structure is assumed to take an infinite number of cycles along the capacity curve. The roof displacement and base shear are converted to the spectral displacement (S_d) and spectral acceleration (S_a) using Eq. 3-2 and Eq. 3-3.

$$S_a = \frac{V_b/W}{\alpha_1} \tag{3-2}$$

$$S_d = \frac{\Delta}{\Gamma_1 \cdot \phi_{1,m}} \tag{3-3}$$

Where, W is the total weight of the structure, V_b denotes the base shear, α_1 is the mass participation factor, Δ denotes the top floor displacement, Γ_1 is the mode participation factor and $\phi_{1,m}$ is the amplitude of the first mode of the top floor. Capacity curve in the ADRS format is shown in Fig. 3.4.

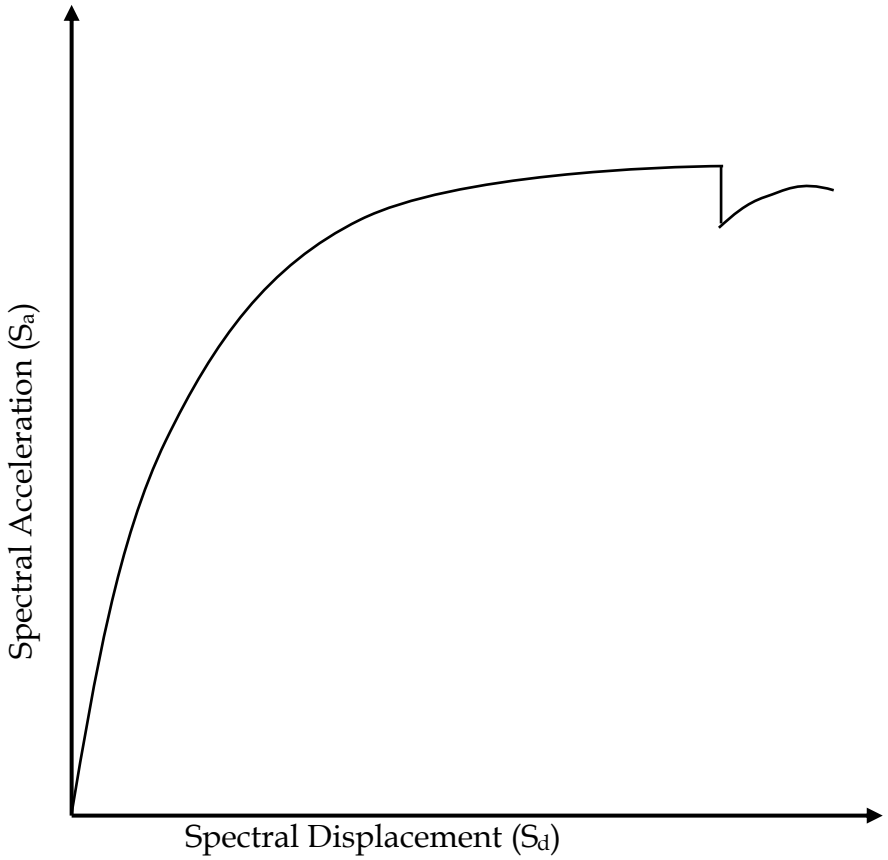

Fig. 3.4 Capacity Curve in ADRS Format

The demand curve is represented by the earthquake response spectrum. The response spectrum is presented based on the soil type of the site and damping of the structure. As the structure is loaded to its inelastic limit, the effective damping increases.

Generally, 5% is taken for the structure in the elastic limit. Higher damping is incorporated due to the hysteretic damping during the inelastic excursion of the structure. The increased damping is automatically incorporated by the SAP2000 iteratively. The response spectrum is the response of SDOF systems with varying time period (T) and plotted in $S_a\ versus\ T$ format. The $S_a\ versus\ T$ format is converted to $S_a\ versuss\ S_d$ format using $S_d = S_a\left(\frac{T}{2\pi}\right)^2$. The demand curve in $S_a\ versus\ S_d$ coordinate is superimposed on the capacity curve in the same format to determine the performance points.

3.2.2 PLASTIC ANALYSIS

The plastic analysis has been used extensively for the design of steel structures. The analysis is based on the idealization of the stress-strain curve as elastic-perfectly-plastic. The stress-strain curve for an elastic-perfectly plastic behavior is shown in Fig. 3.5. It is further assumed that sections of the structural elements are plastic as per IS 800-2007 which implies that the width to thickness ratio of members are such selected that local buckling is prevented. It is also assumed that the sections will undergo plastic rotation as they reach the plastic moment carrying capacity of the sections. The plastic collapse load is evaluated through virtual work formulation in which elastic the deflection is ignored. The method is applied to determine the collapse load factors for beams and frames. In this study, the plastic analysis of multi storey frames has is used.

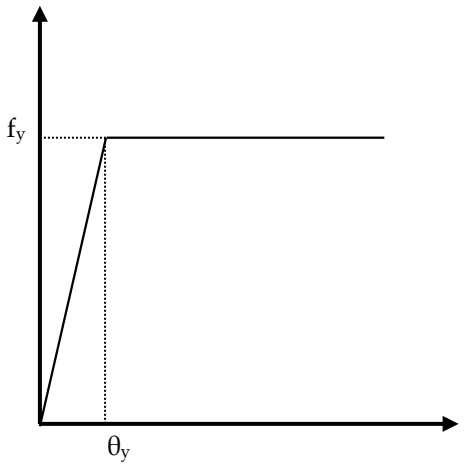

Fig. 3.5 Idealised Stress-strain curve

3.2.2.1 PLASTIC ANALYSIS OF MULTI-STOREY FRAME

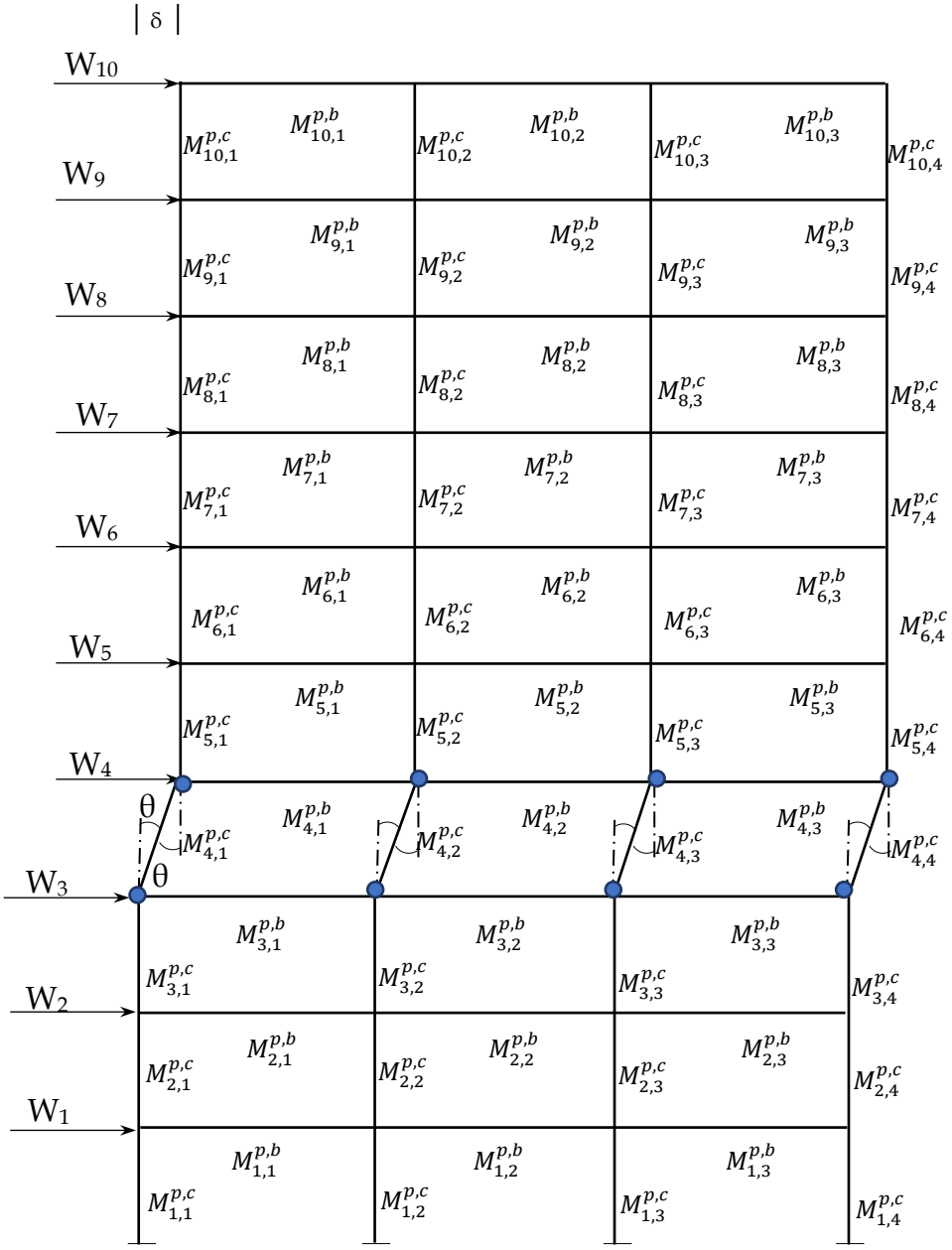

Fig. 3.6 sway mechanism for the 4th storey

In the case of frames, the basic anticipated modes of collapse mechanisms are i) the beam mechanism, ii) the sway mechanism, iii) the combined sway mechanism (storey mechanism) and iv) the combined sway and beam mechanism. Beam mechanism forms when any of the beams in the frame develops a minimum number of plastic hinges required to induce instability. Formation of the plastic hinge assumes that the external force is resisted only through the flexing of structural members; shear forces and axial forces are second order effects. The

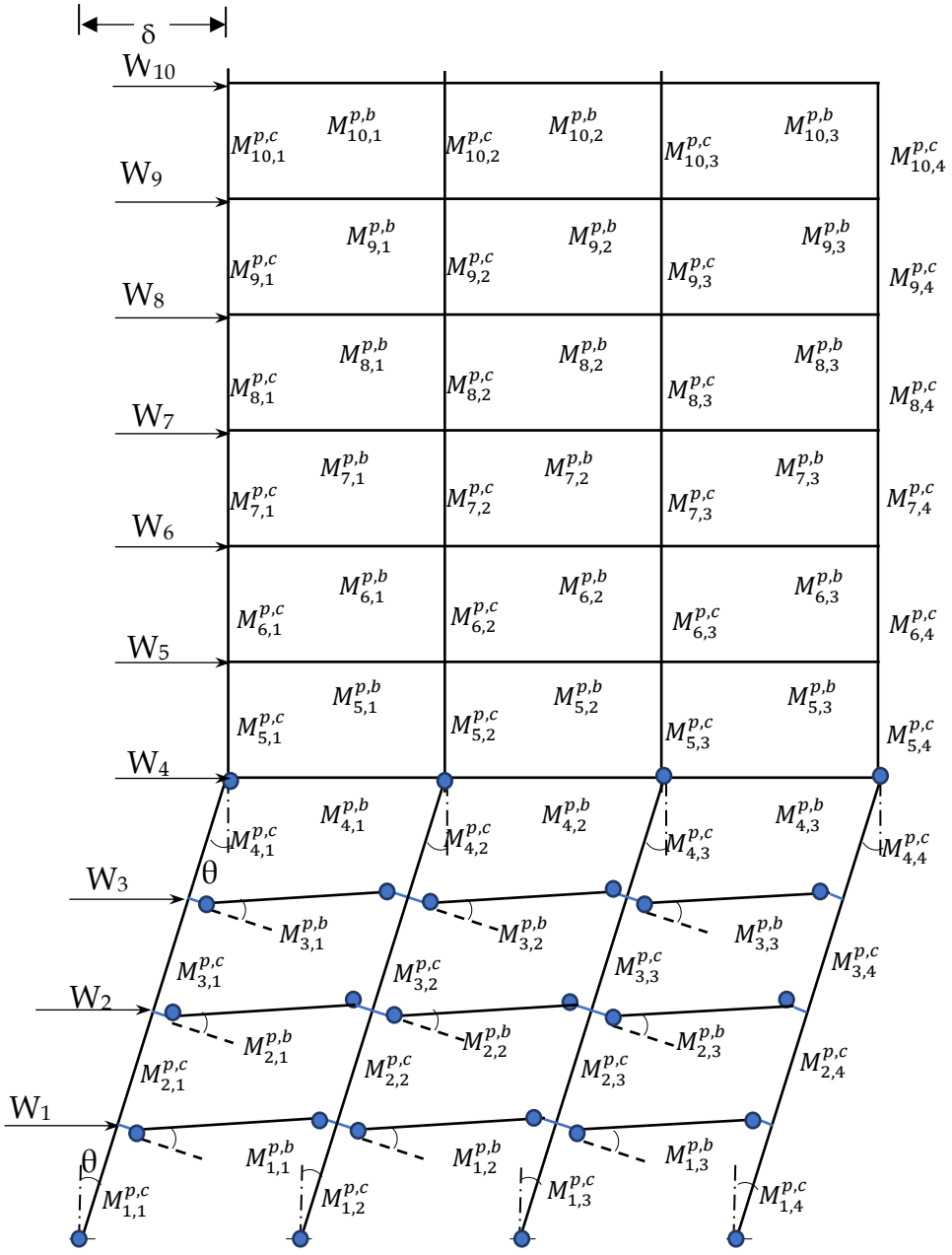

Fig. 3.7 Combined Mechanism for first 4 storey

frame is assumed to be subjected to lateral forces at beam-column joints as shown in Fig. 3.6. Under the influence of lateral forces, the possibility to form the beam mechanism and combined beam and sway mechanisms are absent. This is attributed to the absence of sufficient vertical load on the frame to develop these mechanisms. Thus, only two types of collapse mechanisms possible for such frames are sway mechanism (sway mechanism for the 4th storey is shown in Fig. 3.6) and storey mechanism (storey mechanism for first 4 storeys is shown in Fig. 3.7) for a few consecutive storeys. Thus, only sway and storey mechanisms are

considered in the analysis. The mechanism method, better called an upper bound method, assumes the formation of a sufficient number of plastic hinges to form a valid mechanism, and then obtains the collapse load factor using the virtual work method. For the purpose of illustration purpose, consider the 3-storey frame shown in Fig. 3.8. Different mechanisms possible for the 3storey - 2bay frame structure are, i) first sway mechanism (Fig. 3.9), ii) second sway mechanism (Fig. 3.10), iii) third sway mechanism (Fig. 3.11), iv) first storey mechanism (Fig. 3.12) and v) second storey mechanism (Fig. 3.13).Referring to the first sway mechanism, the work equation is given by

$$10\lambda W3\theta = 6M^p\theta \text{ or } \lambda = \frac{M^p}{5W} \qquad (3\text{-}4)$$

Similarly, λ can be obtained for the other two sway mechanisms as $\frac{2M^p}{9w}$ and $\frac{M^p}{4w}$.

The combined sway mechanisms to form a storey mechanism can be obtained by adding individual sway mechanisms and applying rotational mechanisms at the joints to transfer plastic hinges from the columns to the beams. The process leads to the cancellation of plastic hinges in columns and the addition of plastic hinges at the ends of the beams in a particular bay. As a consequence, two essential criteria are achieved. Namely, the column in the storey mechanism becomes straight, and there is a loss of total internal energy because of cancellation of hinges. Each storey mechanism thus formed provides a value for λ from the work equation. This is illustrated by combining the first two sway mechanisms (shown in Fig. 3.9 and Fig. 3.10).

Work equations for the first and second mechanisms are

$$10\lambda W3\theta = 6M^p\theta \qquad (3\text{-}5)$$

$$9\lambda W3\theta = 6M^p\theta \qquad (3\text{-}6)$$

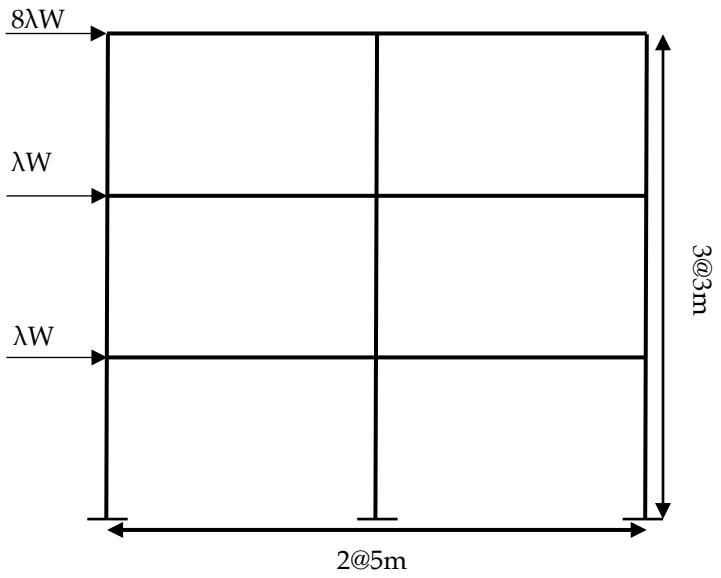

Fig. 3.8 3-storey 2-bay frame

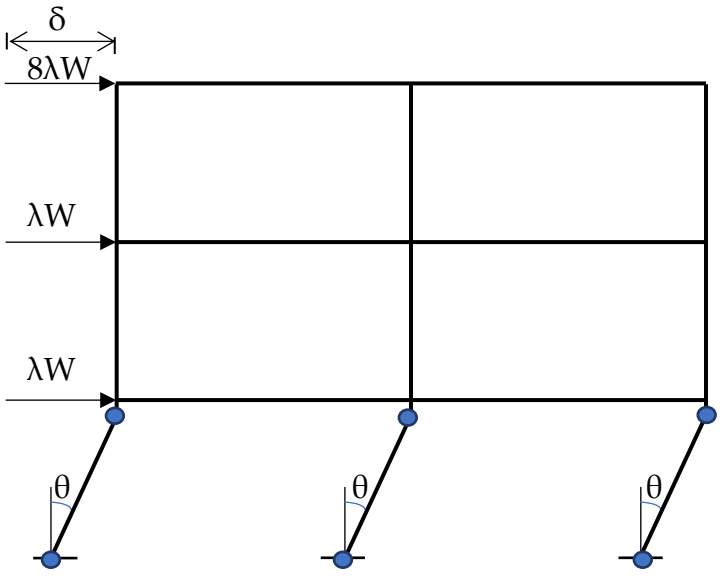

Fig. 3.9 First Sway Mechanism

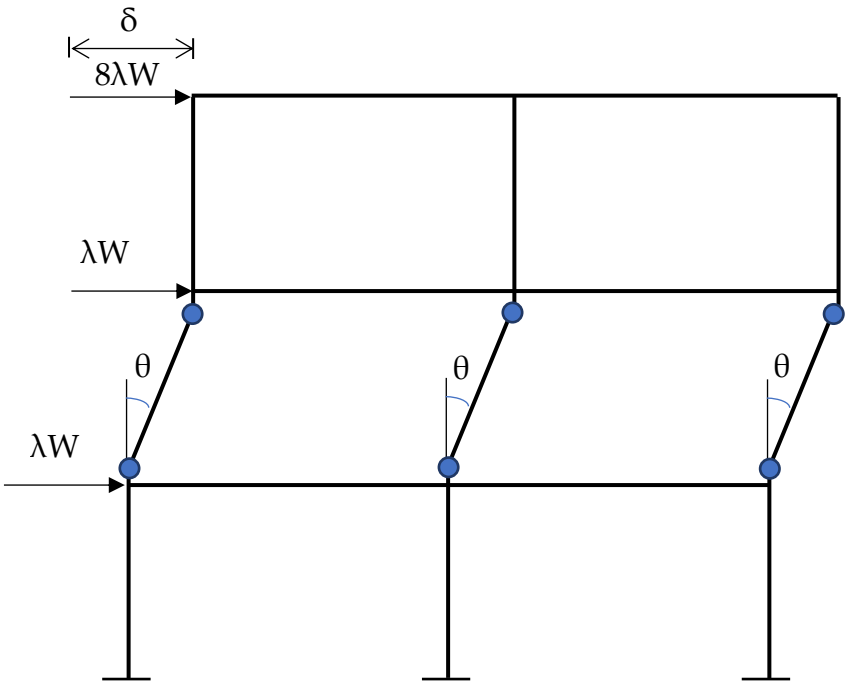

Fig. 3.10 Second Sway Mechanism

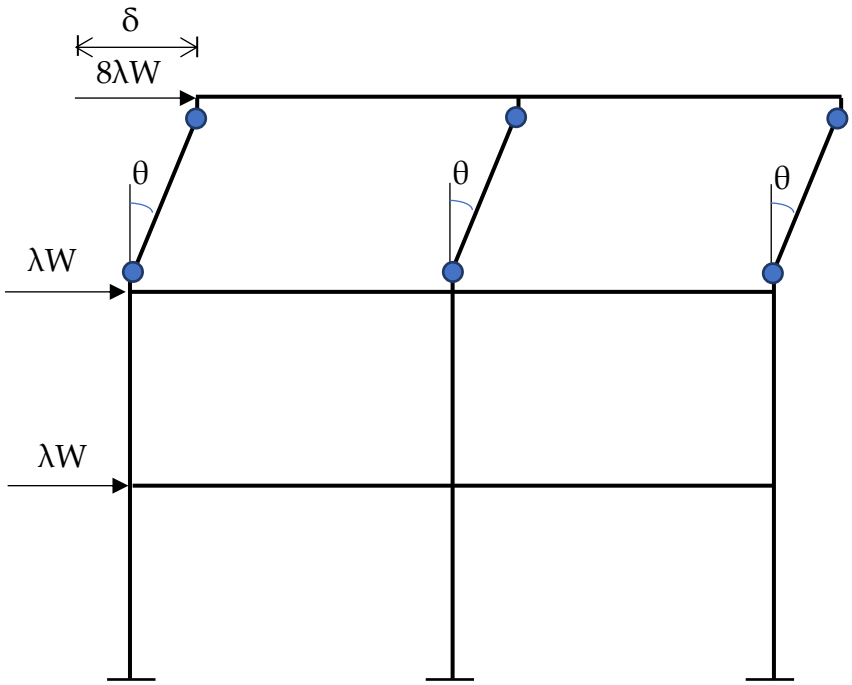

Fig. 3.11 Third Sway Mechanism

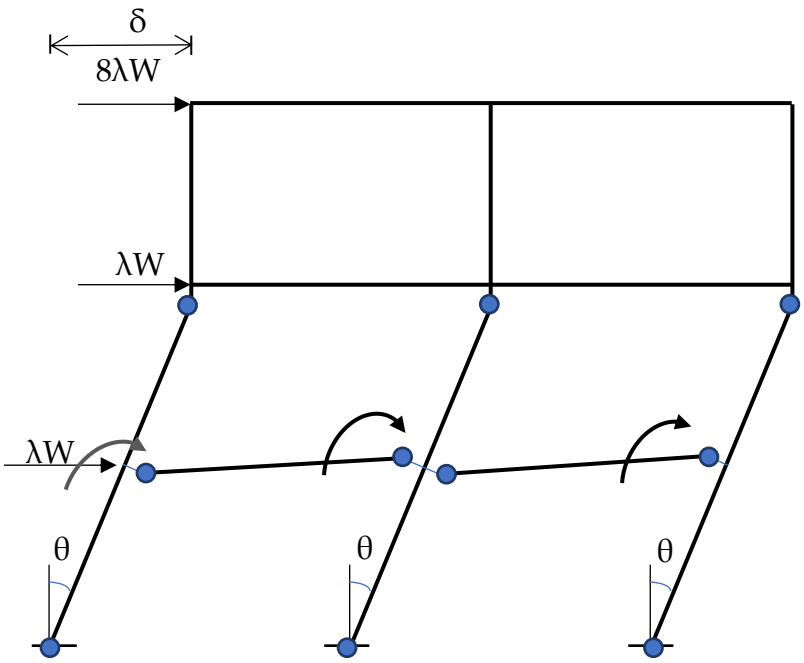

Fig. 3.12 First Storey Mechanism

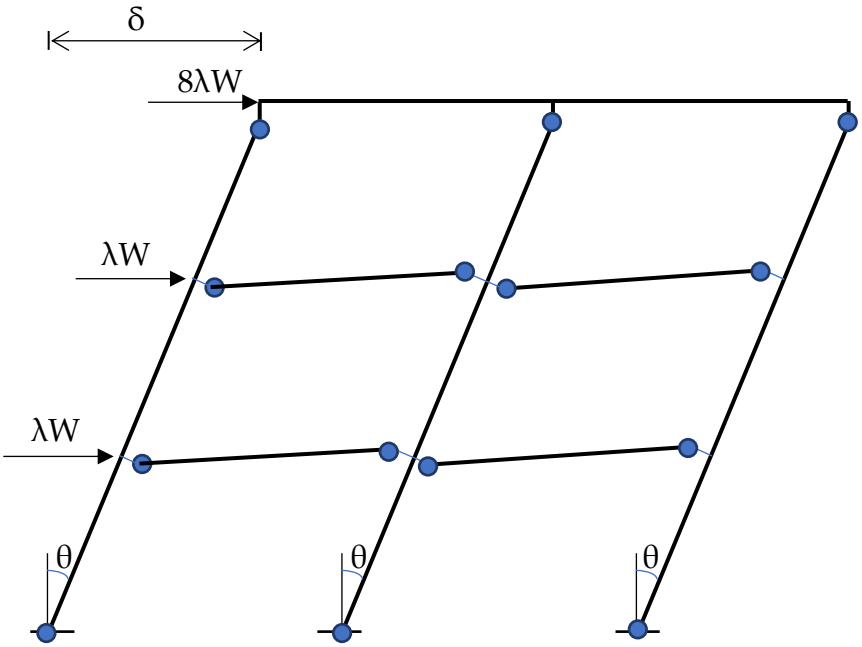

Fig. 3.13 Second Storey Mechanism

Combining mechanisms given by Eqs. 3-5 and 3-6, and applying a rotational mechanism as shown in Fig. 3.12, leads to the cancellation of 6 hinges in columns and the introduction of 4 new hinges in beams providing a net cancellation of 2 hinges. Therefore, the work equation for the first storey mechanism is given as

$$19\lambda W3\theta = 12M^p\theta \qquad (3\text{-}7)$$
$$\underline{\qquad -2M^p\theta} \quad \text{(Cancellation)}$$
$$19\lambda W3\theta = 10M^p\theta$$

$$\lambda = \frac{10M^p}{57W} \qquad (3\text{-}8)$$

Proceeding in the same way, the work equation for the second storey mechanism (as shown in Fig. 3.13) is

$$27\lambda W3\theta = 16M^p\theta \qquad (3\text{-}9)$$
$$\underline{\qquad -2M^p\theta} \quad \text{(Cancellation)}$$
$$27\lambda W3\theta = 14M^p\theta$$

$$\lambda = \frac{14M^p}{81W} \qquad (3\text{-}10)$$

Further, the application of the rotational mechanism at the joints of the top storey will lead to a net addition of one new hinge, and the work equation for the final combined mechanism is

$$27\lambda W3\theta = 14M^p\theta \qquad (3\text{-}11)$$
$$\underline{\qquad +1M^p\theta} \quad \text{(Addition)}$$
$$27\lambda W3\theta = 15M^p\theta$$

$$\lambda = \frac{15M^p}{81W} \qquad (3\text{-}12)$$

It is seen that λ is the least for the last but one combined mechanism as shown in fig 3.13.

Using the sequence of operation as illustrated for the 3 storey – 2bay frame, a N storey – M bay frame can be analyzed to obtain the least value of λ. Accordingly, a computer code in the MATLAB is developed.

3.2.3 OPTIMIZATION USING GENETIC ALGORITHM

3.2.3.1 GENETIC ALGORITHM

The concept of the Genetic Algorithm (GA) is based on the Darwin theory of natural selection. The GA is a metaheuristic optimization algorithm that is extensively used for solving the optimization problems in different fields of research. Robustness, parallel computation and constraint independence are some of the features of the GA that make it one of the most robust optimization techniques in the engineering field. GA was initially proposed by Holland (1975) and later developed by Goldberg and Holland (1988). Goldberg defined four different characteristics of the GA that differentiates the GA from the other optimization techniques. First is that the GA does not work with the parameters to be optimized. Instead, it operates with a coding of the parameter set. Second is that the GA searches the genetic solution from a population of points and not around a single point. The third is that the GA does not use any derivative or auxiliary knowledge for optimization, instead it uses the knowledge of the objective function and finally, the GA uses probabilistic transition rules for the optimization instead of the deterministic rules used by other optimization algorithms.

In the GA, a set of possible solutions to an optimization problem evolves towards the best solution. The GA is an iterative process, and initially, a group of individuals is selected by creating a random population of binary bits '0' and '1'. The binary bits are mapped to real design variables and are decoded as real values. The fitness of each decoded real value is evaluated using the objective (fitness) function. Based on the fitness values, the better individuals are selected and transferred into the mating pool for reproduction. The two most used selection algorithms are tournament selection and roulette wheel selection algorithms. Through the crossover and mutation operators, the selected individuals undergo reproduction. Hence, the genetic loop comprising of the fitness evaluation, selection, crossover and mutation is an iterative process, and it continues until some convergence criteria are satisfied. The flow chart of the GA is given in Fig. 3.14.

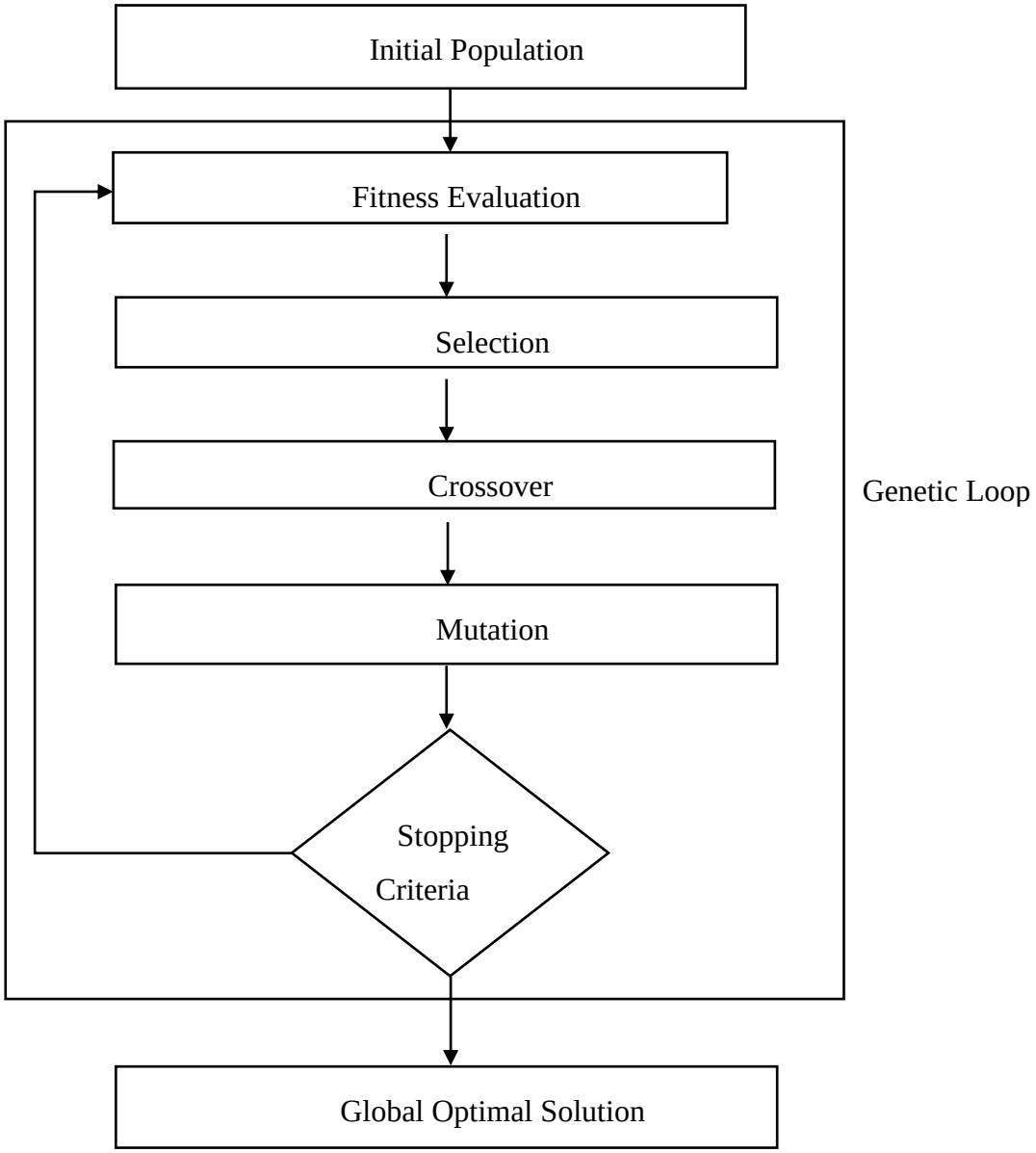

Fig. 3.14 Flow Chart of Genetic Algorithm

3.2.3.2 INITIALIZATION

Initially, in the GA, a group of individuals is selected from the set of possible solutions. The selection of individuals is random, but any particular selection procedure can be adopted for selecting. There are two primary methods to initialize a population in a GA. They are a) random initialization, and b) heuristic initialization. In the random initialization, the initial population are selected entirely by random solutions. During the heuristic initialization, the initial population is selected using a known heuristic for the problem.

3.2.3.3 SELECTION

The principle of "survival of fittest" states that the chance of survival is more for the individual which is well adapted to the environment. In each successive generation, a part of the current population is selected for breeding a new generation. The selection of individuals is based on their fitness values, i.e. individuals having higher fitness values have more chances of getting selected. The fitness function is always problem dependent and is defined over the genetic representation of the possible solutions. Various kinds of selection mechanisms such as the tournament, roulette wheel, fitness proportionate selection, reward-based selection etc. exist. For the study, the tournament selection is employed for the selection.

In tournament selection, a few individuals are selected randomly from the current population. The selected individuals compete against each other, and the one with the best fitness value is selected for the crossover. The selection process continues until the size of selected individuals become equal to the size of the initial population. Tournament selection is preferred over other selection algorithms because they can work on parallel architecture and are simple to code.

3.2.3.4 CROSSOVER

In the GA, the concept of reproduction through mating is achieved through the crossover operator. Crossover combines two individuals, or parents, to form a

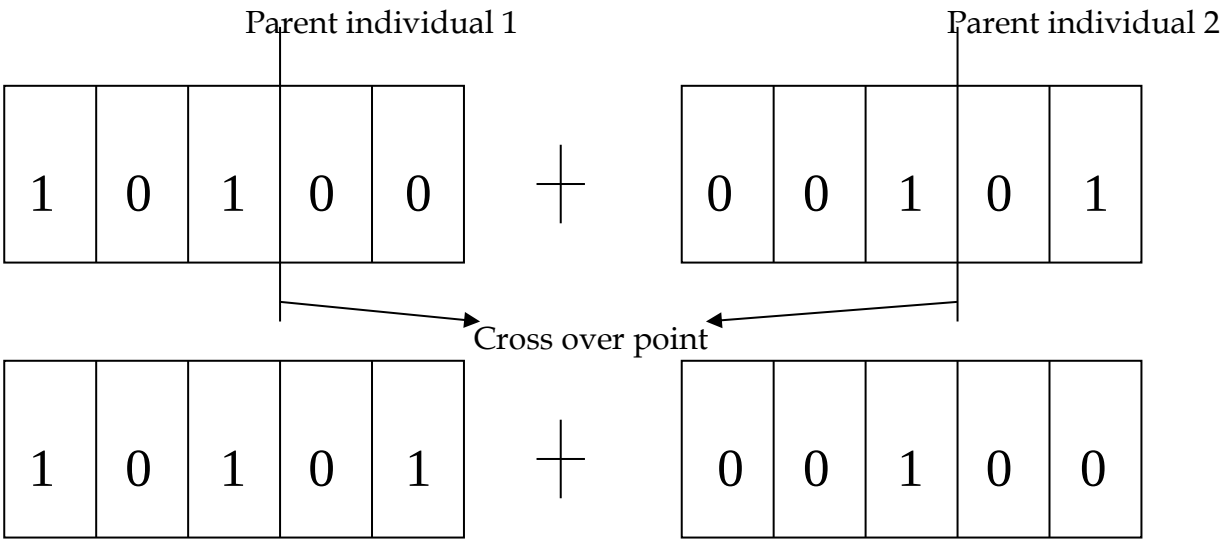

Fig. 3.15 Single point crossover

new individual, for the next generation. Different types of crossover mechanisms like the single point crossover, multi-point crossover (Eshelman et al., 1989), uniform crossover (Syswerda, 1989) and cycle crossover (Oliver et al., 1987) exist. The GA generally uses the single point crossover. In a single point crossover, randomly two parents are selected from the population selected for mating. Then a crossover point is selected on both parents. All the data beyond the crossover point is swapped in both the parents. As a result, two new offsprings are generated. Fig. 3.15 shows an example of a single point crossover mechanism. Two binary strings 10100 and 00101are selected from the mating pool. The crossover point is randomly picked on the two points as shown in the figure. The data beyond the crossover point in both the parents is exchanged and the two new individuals 10101 and 00100 are generated.

3.2.3.5 MUTATION

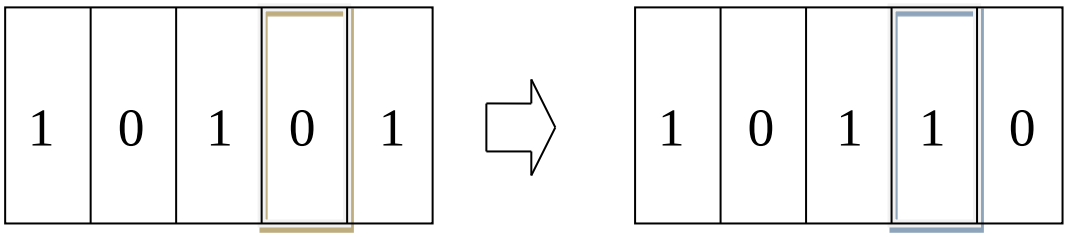

Fig. 3.16 Mutation operation

Mutation functions make small random changes in the individuals in the population, which provide the genetic diversity and enable the genetic algorithm to search a broader space. For a simple genetic algorithm, during the crossover operation, no new information is created. During the continuous generation, the selected chromosomes become robust to the problem environment, and as a result, the chromosomes start resembling each other over the time. Hence, it is a possibility that a globally optimized solution pre-converges to a local solution. To overcome the problem of premature convergence to a local solution, the mutation operation is introduced. The mutation operation prevents the loss of the gene information from the current population and sustains the diversity of the gene information. The process of mutation is shown in Fig. 3.16.

3.2.3.6 TERMINATION

The generation process is repeated until a terminating condition is reached. Common terminating conditions are like the fixed number of generations reached, allocated budget computation time reached, the highest-ranking solution's fitness is reaching or has reached a condition such that successive iterations no longer produce better results or combinations of the above.

3.2.4 NONLINEAR TIME HISTORY ANALYSIS

The equation of motion of the vibration of a building frame subjected to an earthquake is given by

$$\boldsymbol{m}\ddot{u} + \boldsymbol{c}\dot{u} + \boldsymbol{k}u = -\boldsymbol{m}I\ddot{u}_g(t) \qquad (3\text{-}13)$$

Where, $\boldsymbol{m}, \boldsymbol{c}, and\ \boldsymbol{k}$ are the mass, damping and stiffness matrices respectively, $u, \ddot{u}_g and\ I$ are the displacement, ground acceleration and influence vector respectively. During the earthquake, the ground acceleration varies irregularly with time. So, an analytical solution to Eq. 3-13 is not feasible. Numerical techniques are employed to solve Eq. 3-13. Further, if the elements of the structure undergo inelastic excursion, the stiffness matrix changes with the displacement. Hence, the incremental form of the equation of motion, as given below, is solved numerically to obtain the response quantities of interest.

$$\boldsymbol{m}\Delta\ddot{u} + \boldsymbol{c}\Delta\dot{u} + \boldsymbol{k}\Delta u = -\boldsymbol{m}I\Delta\ddot{u}_g \qquad (3\text{-}14)$$

Where, Δ denotes incremental values. Direct integration techniques such as Newmark-β, Wilson-θ, Hilbert-Hughes methods, etc. can be used to integrate the governing differential equation to determine the responses of the structure.

Most of the buildings are deformed beyond the linear elastic limit of the structure when subjected to a strong earthquake. Once the structural response is beyond the elastic limit, the inelastic response of the structure is governed by the idealized nonlinear stress-strain curve of the material. The material nonlinearity assumed in the modelling for the building frame is as explained in section-3.2.1.1. Moreover, the response of the structure is affected by the second-order $P-\Delta$ effects of the gravity loads acting on the laterally deformed state of the building

frame. Other effects that affect the response of the building frame are ductility, beam to column strength ratio and beam to column stiffness ratios. Considering the nonlinearity, the stiffness term and damping term in Eq. 3.14 contains the nonlinear term. The nonlinear governing equation, in more accurate form, is given by:

$$\boldsymbol{m}\Delta\ddot{u} + \boldsymbol{c}(\boldsymbol{u})\Delta\dot{u} + \boldsymbol{k}(\boldsymbol{u})\Delta u = -\boldsymbol{m}I\Delta\ddot{u}_g \qquad (3\text{-}15)$$

The numerical solution of the equation of motion given by Eq. 3-15 is commonly known as the nonlinear time history analysis and performed here using the SAP 2000 standard software.

3.2.5 GENETIC PLASTIC PUSHOVER ANALYSIS (GPPA)

GPPA has two phases. In the first phase, different damage scenarios of the frame are simulated such that complete collapse mechanisms are formed for each of the damage scenarios. For this purpose, the plastic analysis of the multi-storey frame is carried out to develop work equations of independent mechanisms, and combined mechanisms formed out of them, in terms of unknown plastic moment capacities of the damaged members assumed for a particular damage scenario. A genetic algorithm is used to obtain the unknown plastic moment capacities of the damaged members such that the collapse load factor corresponding to the complete collapse mechanism is minimized subject to the constraint that no other mechanism of failure than the complete collapse mechanism forms.

In the second phase, the pushover analysis of the frame for each of the damage scenarios is carried out to obtain the capacity curve, and the performance point for each case is made to coincide with the collapse point of the capacity curve by adjusting the PGA value of the assumed spectrum. The critical damage scenario is identified by finding the case which provides the least value of the PGA. Note that intensity measure for an earthquake is taken as the PGA. The intensity measure for earthquake could be defined by various parameters like the intensity, magnitude, PGA, and spectral ordinates. For the nonlinear time history analysis, the PGA is traditionally adopted as an intensity measure for an earthquake whereas, for a response spectrum method of analysis spectral ordinates are

routinely used. Further, the PGA of the assumed spectrum, used as a demand curve to find the performance point, is taken as the reference PGA for nonlinear time history analysis. Since, the proposed analysis uses the pushover analysis and nonlinear time history analysis, the performance point and PGA have been considered as the important parameters.

3.2.6 SIMULATION OF DAMAGE SCENARIOS (FIRST PHASE)

Different damage scenarios of a building frame are simulated using the plastic analysis and genetic algorithm as mentioned before. For the convenience of identifying the worst (critical) damage scenario, the damage scenarios are created such that the total percentage reduction of plastic moment capacities of beams and columns together remains the same for all cases. One of the damage scenarios (called reference damage state) is created by the uniform reduction of plastic moment capacities of all beams and columns. For each damage scenario, a plastic analysis of the frame is carried out. For the multi-storey frame, the basic anticipated modes of collapse mechanisms are considered as discussed in the section 3.2.2.1. The frame is assumed to be subjected to lateral forces at beam-column joints and it is assumed that the failure takes place primarily due to lateral forces produced by an earthquake. Thus, the possibility to form the beam mechanism and combined sway beam mechanism are precluded. Only two types of collapse mechanisms, namely, the sway mechanism (sway mechanisms are shown in Fig. 3.9-3.11) and combined sway mechanism (shown in Fig. 3.12 and 3.13) are considered in the analysis. The collapse load factor for each mechanism is expressed in terms of plastic moment capacities of all beams and columns, including reduced plastic moment capacities of damaged members. Since the latter are unknowns, the objective function λ (the collapse load factor) is minimized with respect to them. The constraints imposed are (i) the reduction of total plastic moment capacities in the damaged members is equal to a specific value, (ii) no other mechanism than the complete collapse mechanism can form and (iii) plastic moment capacities of the damaged members remain within the specified upper and lower bounds. The derivation of the objective function and the constraints are

explained with the help of a three storey- three bay frame with an assumed damage state.

Consider the three storey-three bay frames shown in Fig. 3.17. It is assumed that the middle bay of the frame is damaged and the $M_p$values of beams and columns are reduced by various degrees. The reductions in the M_p values of beams and columns add up to a value which is equal to $p\%$ of the total M_p values of all beams and columns of the undamaged structure. Let W_1 , W_2 and W_3 be the service loads acting on the frame and bear a proportion equal to the first mode distribution of the load following a base shear approach given by

$$W_i = \frac{V_b h_i^2}{\sum h_i^2} \qquad (3\text{-}16)$$

Where, V_b is the base shear in the first mode.

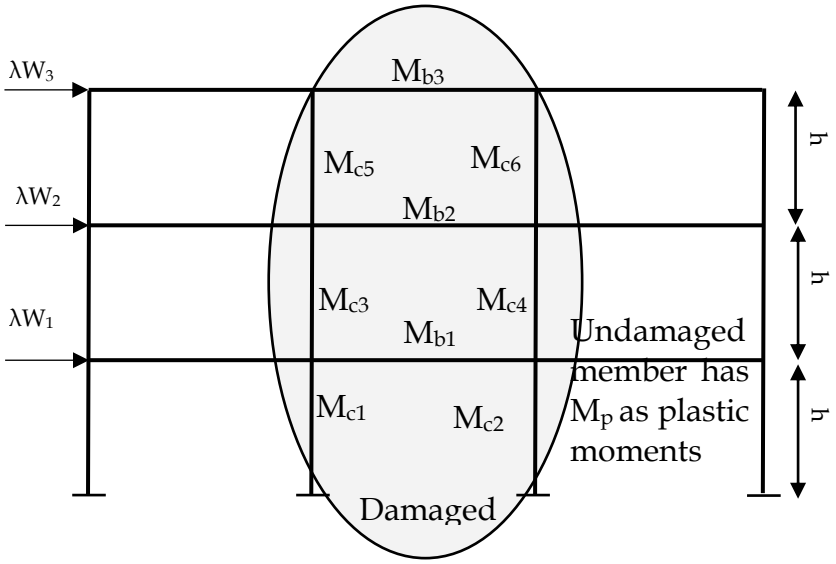

Fig. 3.17 Three bay three storey damaged framed structure.

Three sway mechanisms of the frame are shown in Fig. 3.9-3.11. Without loss of any generality, it is assumed that M_p values of beams and columns are the same for the undamaged structure. For the first sway mechanism, the work equation is given by

$$4M_P\theta + 2M_{c1}\theta + 2M_{c2}\theta = \lambda(w_1 + w_2 + w_3)h\theta \qquad (3\text{-}17)$$

$$\lambda = 4gM_p + 2gM_{c1} + 2gM_{c2};\ g = \big(h(w_1 + w_2 + w_3)\big)^{-1} \qquad (3\text{-}18)$$

in which, M_{c1} and M_{c2} are the unknowns.

For the second sway mechanism, the work equation is given by.

$$\lambda = 4g_1M_p + 2g_1M_{c3} + 2g_1M_{c4};\ g_1 = \left(h(w_2 + w_3)\right)^{-1} \quad (3\text{-}19)$$

in which, M_{c3} and M_{c4} are the unknowns.

For the third sway mechanism, the work equation is given by

$$\lambda = 4g_2M_p + 2g_2M_{c5} + 2g_2M_{c6};\ g_2 = (hw_3)^{-1} \quad (3\text{-}20)$$

in which, M_{c5} and M_{c6} are the unknowns.

For the first combined sway mechanism Fig. 3.12, there is a cancellation of plastic hinges in the columns due to the application of the rotational mechanism (Baker and Heyman, 1969). The work equation is given by

$$\begin{array}{c} 4M_P + 2M_{c1} + 2M_{c2} = \lambda(w_1 + w_2 + w_3)h \\ 4M_P + 2M_{c3} + 2M_{c4} = \lambda(w_1 + w_2)h \\ \hline 8M_P + 2M_{c1} + 2M_{c2} + 2M_{c3} + 2M_{c4} = \lambda(w_1 + 2w_2 + 2w_3)h \\ -4M_p + 4M_P - M_{C1} - M_{c2} - M_{C3} - M_{c4} + 2M_{b1} = 0\ (\ hinge\ Cancellation) \\ \hline 8M_P + M_{c1} + M_{c2} + M_{c3} + M_{c4} + 2M_{b1} = \lambda(w_1 + 2w_2 + 2w_3)h \end{array} \quad (3\text{-}21)$$

$$\lambda = 8g_3M_p + g_3(M_{c1} + M_{c2} + M_{c3} + M_{c4} + 2M_{b1});\ g_3 = \left(h(W_1 + 2W_2 + 2W_3)\right)^{-1} \quad (3\text{-}22)$$

For the second combined mechanism (Fig. 3.13), the work equation is given by

$$\begin{array}{c} 8M_P + M_{c1} + M_{c2} + M_{c3} + M_{c4} + 2M_{b1} = \lambda(w_1 + 2w_2 + 2w_3)h \\ 4M_P + 2M_{c5} + 2M_{c6} = \lambda(w_3)h \\ \hline 12M_P + M_{c1} + M_{c2} + M_{c3} + M_{c4} + 2M_{c5} + 2M_{c6} = \lambda(w_1 + 2w_2 + 3w_3)h \\ -4M_p + 4M_P - M_{C3} - M_{c4} - M_{C5} - M_{c6} + 2M_{b2} = 0\ (hinge\ Cancellation) \\ \hline 12M_P + M_{c1} + M_{c2} + M_{c3} + M_{c4} + M_{c5} + M_{c6} + 2M_{b1} + 2M_{b2} = \lambda(w_1 + 2w_2 + 3w_3)h \end{array} \quad (3\text{-}23)$$

$$\lambda = 12g_4M_p + g_4(M_{c1} + M_{c2} + M_{c3} + M_{c4} + M_{c5} + M_{c6} + 2M_{b1} + 2M_{b2});\ g_4 = \left(h(W_1 + 2W_2 + 3W_3)\right)^{-1} \quad (3\text{-}24)$$

The last combined mechanism that can form is obtained by combining the joint mechanisms. However, this mechanism does not lead to a less value of λ compared to that given by Eq. 3-20 as it adds two net plastic hinges over and above the mechanism. The net addition of plastic hinges in a combined mechanism increases the value of λ (Baker and Heyman, 1969).

For the complete collapse mechanism to form, the collapse load factor λ given by Eq. 3-23 is to be minimized with respect to the unknown plastic moments

$M_{c1}, M_{c3}, M_{c4}, M_{c5}, M_{c6}, M_{b1}\ and\ M_{b2}$. The set of constraints imposed on the minimization process are:

(i) Mechanisms given by Eq. 3-18 to Eq. 3-22 cannot form.

(ii) The value of M_{b3} should be such that the last combined mechanism has a λ value less than that given by Eq. 3-24.

(iii) All unknown plastic moments shall lie within the specified upper and lower limits.

The formulation shown for the three storey-three bay frames can easily be extended to *n* storey - *m* bay frame. A computer code in MATLAB is developed to form the expression for the collapse load factor of the complete mechanism (such as that given by Eq. 3-24) in terms of unknown plastic moments of the damaged members and the equations of the constraints for the minimization.

With the help of the GA toolbox of MATLAB, the collapse load factor is minimized to obtain the plastic moment capacities of the damaged members. Thus, different damage scenarios leading to complete collapse of the frame can be simulated in order to identify the most vulnerable one to an earthquake. The damage scenario which provides the least value of the collapse load factor is not necessarily the worst (critical) damage scenario. A pushover analysis is required to identify the critical one. Note that partial collapse mechanism like the sway mechanisms (Fig. 3.9-3.11) leading to failure of the structure are precluded from the study as they are too obvious to identify.

3.2.7 IDENTIFICATION OF CRITICAL DAMAGE SCENARIO (SECOND PHASE)

The minimization of the collapse load factor for each damage scenario provides the value of the collapse load factor for which the frame will collapse. The one having the least value of the collapse load factor is likely to be most vulnerable to an earthquake. However, the PGA value of the earthquake which will cause complete collapse for that damage scenario (called critical damage scenario) of the structure is not known. Further, the extent of the progress of damages in the

structure for other damage scenarios due to the same earthquake is also not known.

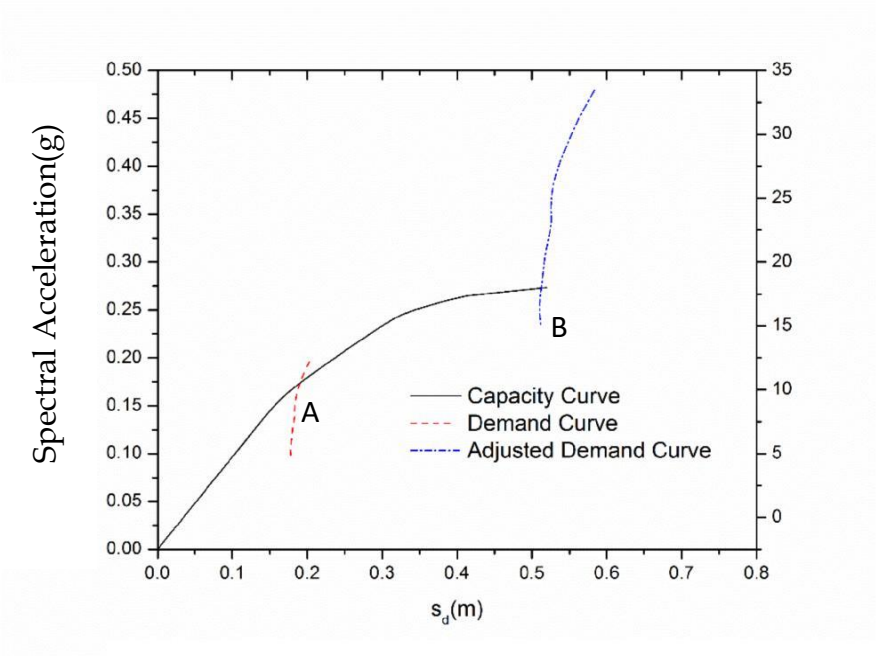

Fig. 3.18 Capacity Curve superimposed with demand curve.

In order to obtain them, a displacement pushover analysis is performed for the building frame for each damage scenario generated as above. Plastic moment capacities of different members (M_i^p) and M_i^p versus rotation (θ) curve for different cross-sections are provided as inputs for the analysis. The capacity curve showing the variation of the base shear with the top floor displacement of the frame is plotted in S_a(base shear divided by building weight) and S_d (S_d = *top displacement*) coordinates (in Acceleration-Displacement Response Spectrum (ADRS) format) for each case of the damage scenario as shown in Fig. 3.18

The seismic demand of an earthquake denoted by its bi-spectrum (response spectrum plotted on $S_a - S_d$ axes) is plotted in the same figure. The PGA value of the demand curve is so adjusted that it intersects the capacity curve at the point (*B)* denoting the complete collapse of the frame as shown in Fig. 3.18. Thus, for each damage scenario, a PGA value is obtained. The one which gives the least value of the PGA denotes the critical damage scenario. In other words, if a response spectrum consistent earthquake having the same PGA takes place, then the critical damage scenario of the frame described as above, will lead to the complete collapse

of the frame. For other damage scenarios, the frame will survive the earthquake with different degrees of damages. Thus, the critical damage scenario of the frame may be viewed as the one that will trigger a progression of initial damages of the frame to complete sway mechanism of failure for that specific earthquake.

The damage states of the frame with other damage scenarios under the same earthquake can be assessed from the results of the pushover analysis. Note that the critical damage scenario, as described above may not necessarily yield the least collapse load factor. The results of the pushover analysis are validated by the nonlinear time history analysis using the response spectrum compatible earthquakes.

3.3 NUMERICAL RESULTS AND DISCUSSION

A 10 storey 3 bay building frame having a storey height as 3m and a bay of 6m is considered for the current study. The building frame is made up of steel

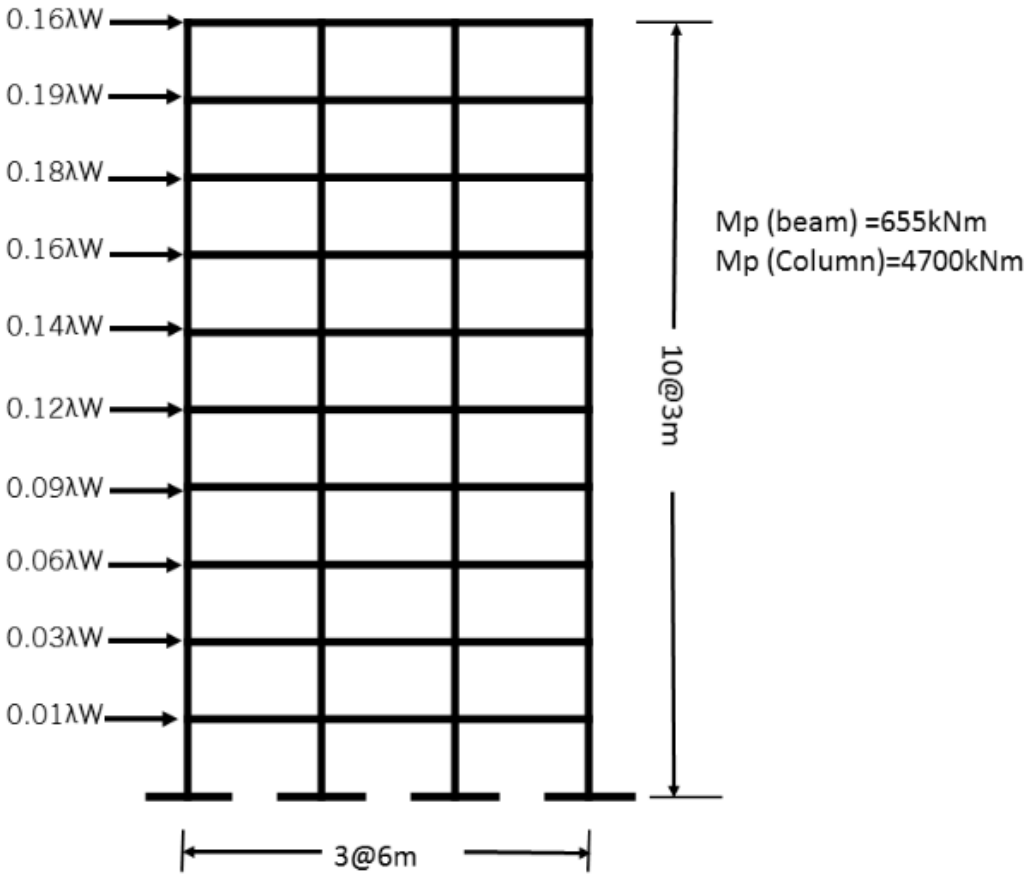

Fig. 3.19 Distribution of lateral loads for the plastic analysis of undamaged frame.

sections, W21X68 as beams W33X291 as columns shown in Fig. 3.19. Dead loads of the roof and other floors are 87.74kN/m and 94.20kN/m respectively. The live load of each floor is 70.124kN/m, and that of the roof is 17.55kN.

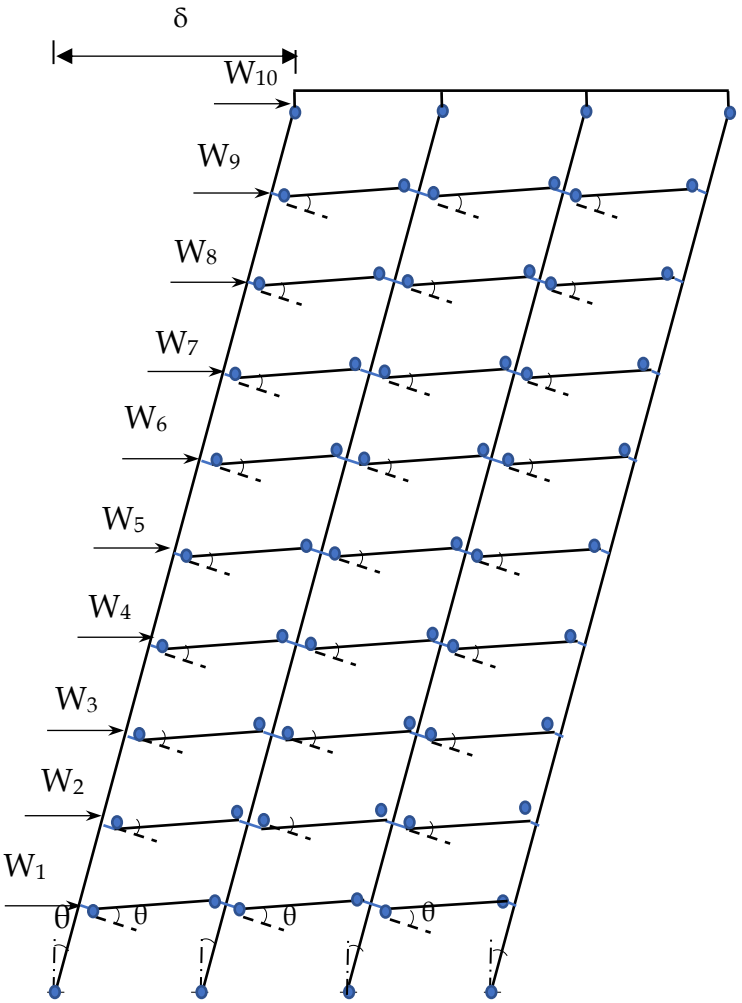

Fig. 3.20 Desirable Mechanism for ten Storey Building.

Lateral loads applied to the structure for the plastic analysis are assumed to be proportional loading. The lateral loads bear a relationship with the shear force developed in the first mode of the structure. Loading condition for the plastic analysis is shown in Fig. 3.19, where λ is the collapse load factor, and W is the weight of the structure. A plastic analysis is carried out to determine the collapse load factor λ for the undamaged frame. The collapse mechanism which provides the least collapse load factor is the last but one combined sway mechanism (Fig. 3.20). The corresponding collapse load factor is 0.2065. This collapse load factor is

utilized to find the base shear force for the collapse mechanism and is found to be 3675.4 kN.

The same structure is analyzed by the pushover analysis using SAP 2000. The hinge locations for the collapsed condition, which are as shown in Fig. 3.21, closely match with those obtained by the plastic analysis shown in Fig. 3.20. The maximum base shear by the pushover analysis is 3769kN which is 2.5% higher than the base shear obtained by the plastic analysis.

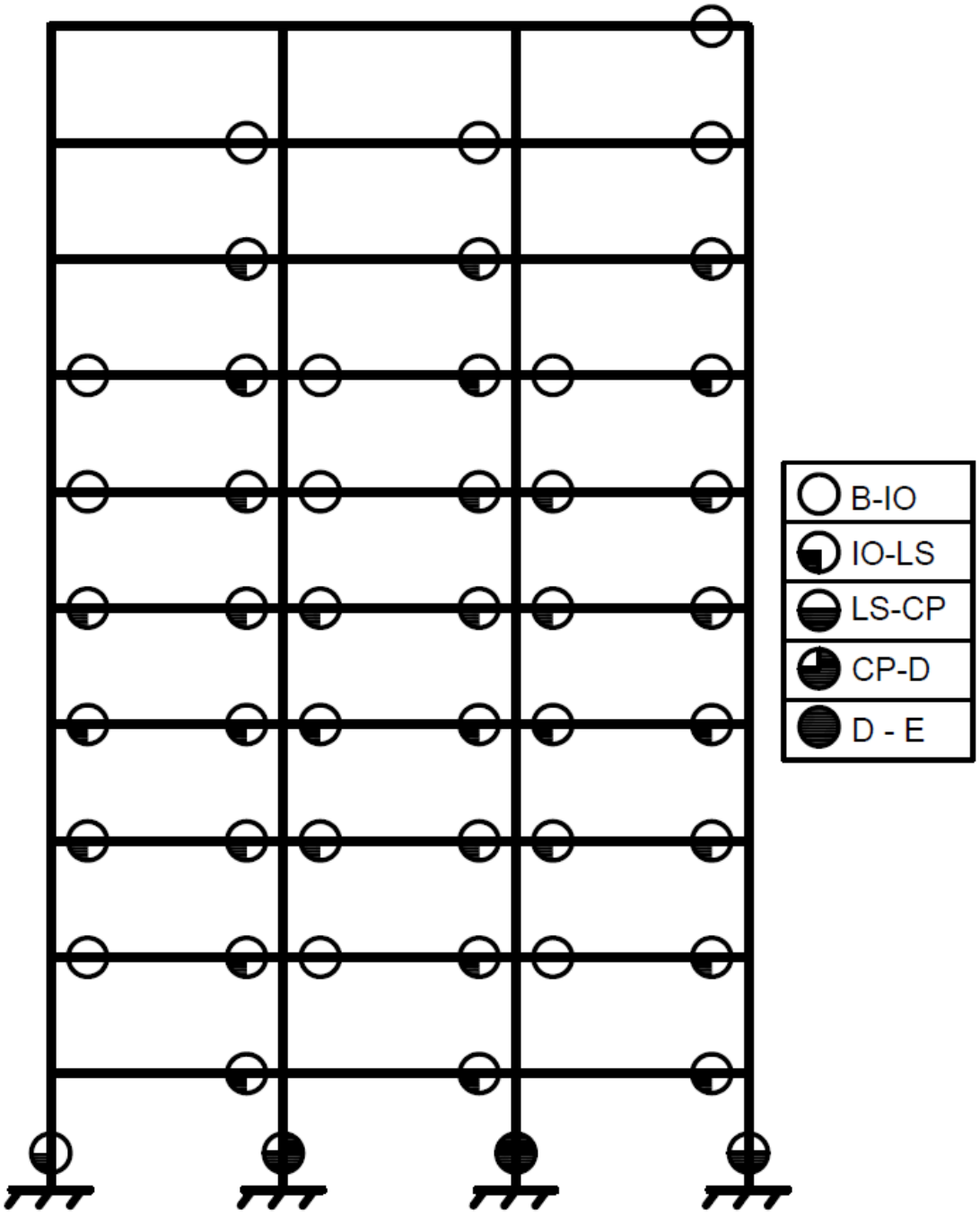

Fig. 3.21 Hinge Locations obtained by the pushover analysis for the undamaged frame.

3.3.1 *DAMAGE SCENARIOS*

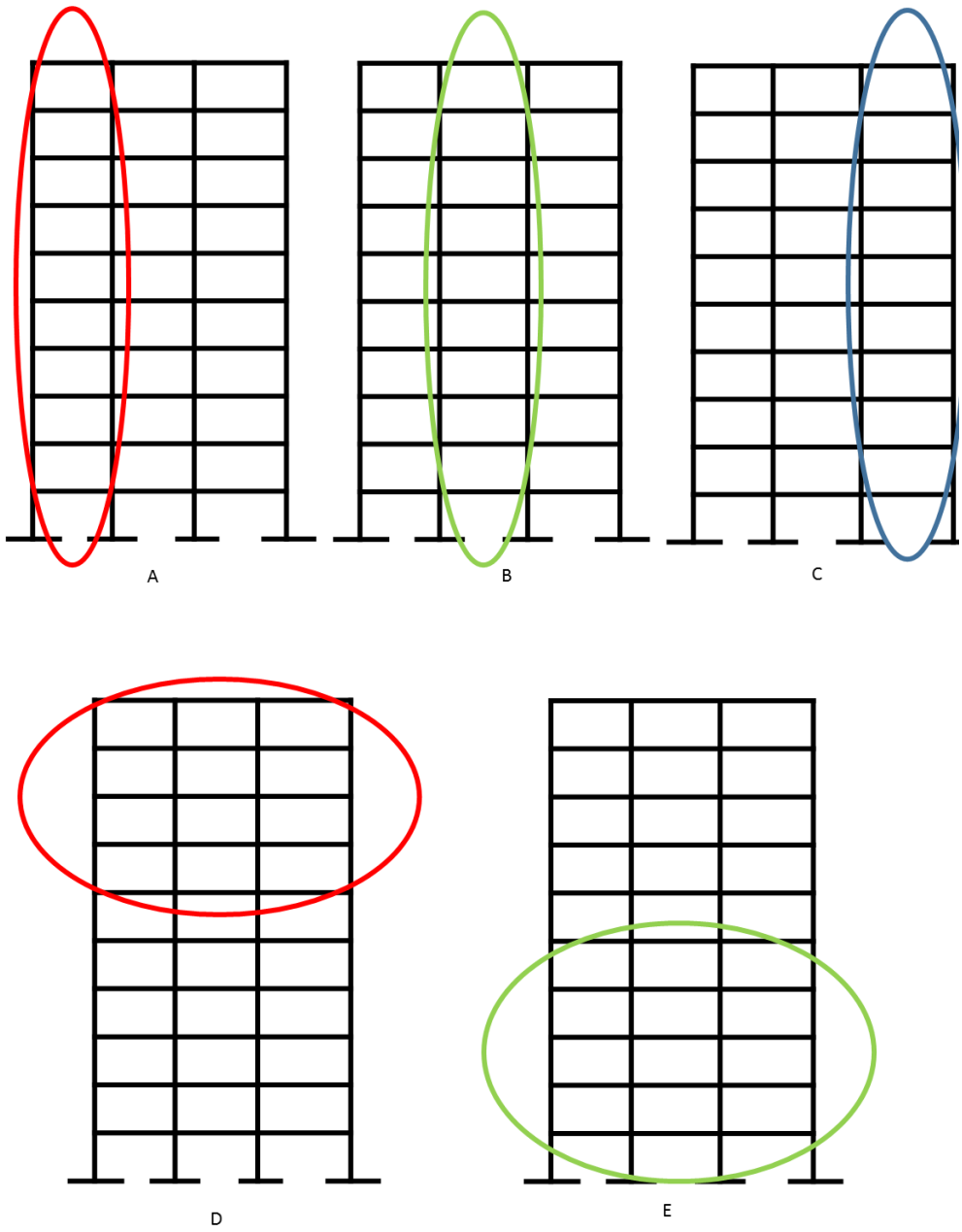

Fig. 3.22 Damage scenarios for a 10-storey building a) Case A; b) Case B; c) Case C; d) Case D; e) Case E.

It is possible to create a number of damage scenarios, keeping the total damage expressed in terms of percentage reduction of the total plastic moment capacity (sum of plastic moment capacities of beams and columns) of the frame to be the same. For the numerical example, 6 damage scenarios, including the uniform damage (reference damage state) are created. They are shown in Fig. 3.22 (a-e). In the case A, damages are localized in the first bay, in case B, damages are

localized in the second bay, in case C, damages are localized in the third bay, in case D, damages are localized in the upper storey and in case E, damages are localized in the lower storey. For the uniform damage scenario, plastic moment capacities of all members are uniformly reduced.

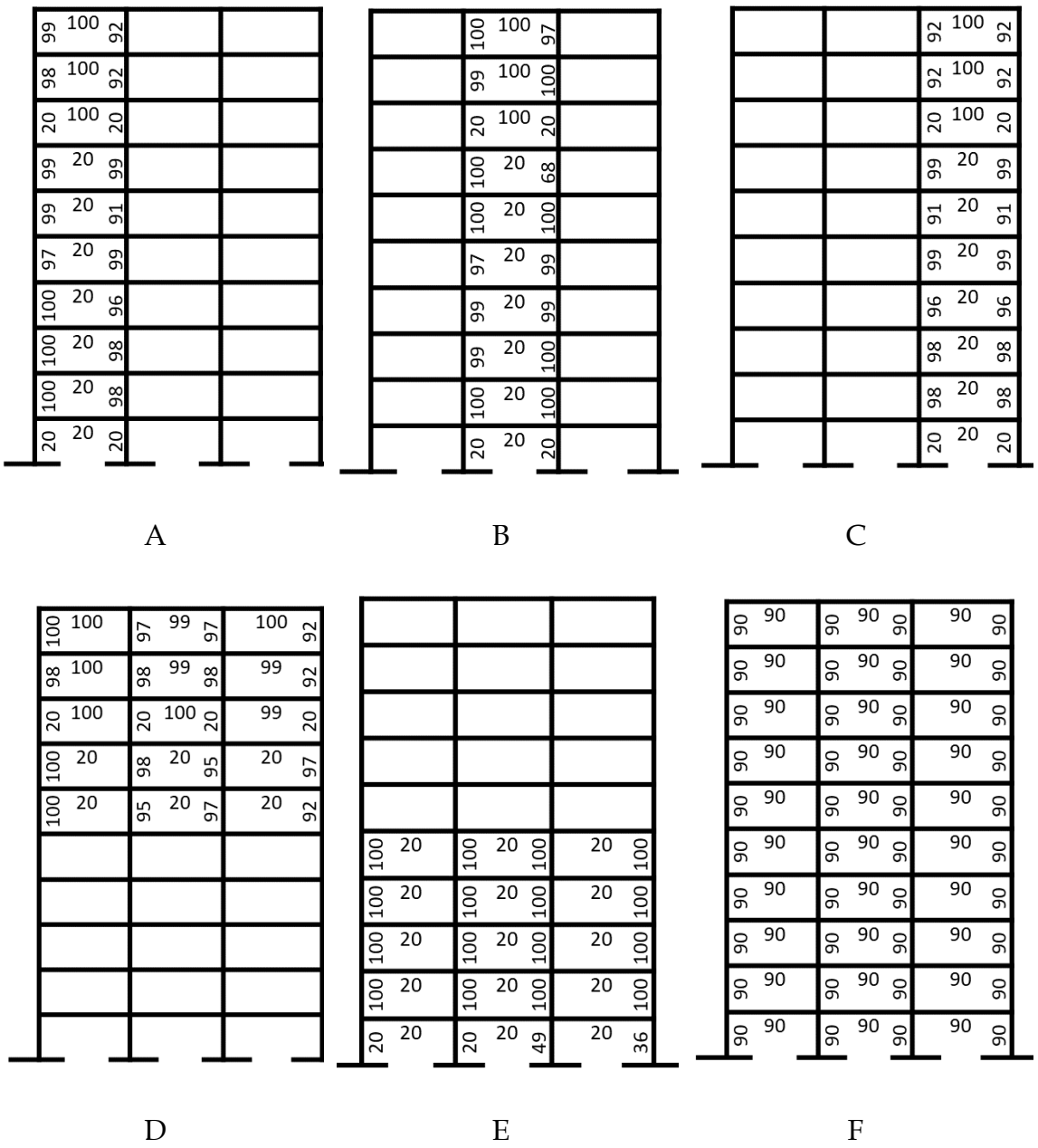

Fig. 3.23 Reduced moment carrying capacities of damaged members for; a) Case A; b) Case B; c) Case C; d) Case D; e) Case E; f) Uniform Damage.

The Plastic moment capacity of each damaged member is shown in terms of percentage of the undamaged plastic moment as indicated in Fig. 3.23 (a-f) for the 10% total reduction of the plastic moment capacities of all members. The

members without any number indicate undamaged members. In a similar way, percentage reductions of moment capacities of the members for 15% and 20% total reductions are achieved.

Table 3.1. Comparison of Plastic Analysis and Push Over Analysis

Damage Scenarios	10% Damage					15% Damage					20% Damage				
	Plastic Analysis			Pushover Analysis		Plastic Analysis			Pushover Analysis		Plastic Analysis			Pushover Analysis	
	br	λ	n	br	n	br	λ	n	br	n	br	λ	n	br	n
Case A	0.12	0.10	58	0.12	52	0.12	0.10	58	0.12	52	0.10	0.09	58	0.11	52
Case B	0.11	0.10	58	0.11	58	0.11	0.09	58	0.11	58	0.10	0.09	58	0.11	58
Case C	0.12	0.10	58	0.12	52	0.12	0.10	58	0.12	52	0.10	0.09	58	0.11	52
Case D	0.10	0.09	58	0.10	46	0.10	0.08	58	0.10	46	0.09	0.08	58	0.09	46
Case E	0.10	0.09	58	0.10	52	0.10	0.09	58	0.10	52	0.10	0.08	58	0.10	52
Uniform Damage	0.19	0.16	58	0.19	50	0.18	0.15	58	0.18	50	0.17	0.14	58	0.17	50

Note: br =base shear/total weight of frame; λ =Collapse Load Factor; n =Number of Plastic Hinges

It is seen from Table 3.1 that base shears obtained by the plastic analysis differ for different types of damage (a-e) and uniform damage. The base shear is found to be maximum for the uniform damage state. The Pushover analysis is carried out for all damaged scenarios. The base shears obtained by the plastic analysis and the pushover analysis compare well for all damage scenarios considered in the study. As it would be expected, the base shear decreases as the total percentage damage is increased.

For further study, the case of the 10% total reduction of plastic moment capacities is considered. The capacity curves for all cases of damage including the case of uniform damage are shown in Fig. 3.23. It is seen from the figure that compared to the case of uniform damage; all other damage scenarios provide lower capacity curves. The performance points obtained by superposing the seismic demand curves (using ADRS) with the capacity curves are pushed to coincide with the collapse points of different damage scenarios including the

uniform damage scenario by adjusting the PGA level. Table 3.2 shows the PGAs required to match the performance points with the collapse points of the capacity curves for each damage scenario. In the table, the spectral acceleration and spectral displacement corresponding to the performance point for each case are also shown.

Table 3.2. Adjusted PGAs for the performance point to match with collapse state for 10% total damage

Damage Scenarios	Performance Point		PGA(g)	No. of Plastic hinges at the PGA level of 0.493g
	Spectral Acceleration (g)	Spectral Displacement (m)		
Case A	0.165	0.284	0.545	46
Case B	0.144	0.255	0.493	58
Case C	0.165	0.284	0.545	46
Case D	0.143	0.312	0.545	40
Case E	0.156	0.425	0.70	48
Uniform Damage	0.240	0.380	0.855	36

From the table, it is seen that the damage scenario 'B' has the least PGA (PGA=0.493g). Therefore, if an earthquake with a PGA of 0.493g or slightly more occurs, then a progressive collapse leading to the complete failure of the frame having the damage scenario 'B' would take place. For the PGA level of 0.493g, the frames with other damage states will be damaged by different degrees of damage, but the frames would not collapse. Thus, from the point of the progressive collapse due to an earthquake, the damage scenario 'B' is the most vulnerable one. For other damage scenarios, the localized damages would progress to different states of damage, i.e. there would be spread of damages in the form of plastic hinges in the structure during that earthquake without a complete collapse of the structure. The extent of damage is indicated by the total number of plastic hinges formed for different damage scenarios. When an earthquake of PGA=0.493g is encountered, the number of plastic hinges formed for each case is also shown in Table 3.2.

Nonlinear time history analysis of the damaged frames was carried out with ATC40 compatible time history with PGA scaled to 0.493g, the PGA value for which the complete collapse of the structure with critical damage scenario was observed in the pushover analysis. A sample time history of acceleration compatible with ATC40 spectrum scaled to PGA 0.493g is shown in Fig. 3.25. The nonlinear time history analysis of the building frame with all damaged scenarios are carried out. Time histories of the top floor displacement for all the damaged frames are shown in Fig. 3.26.

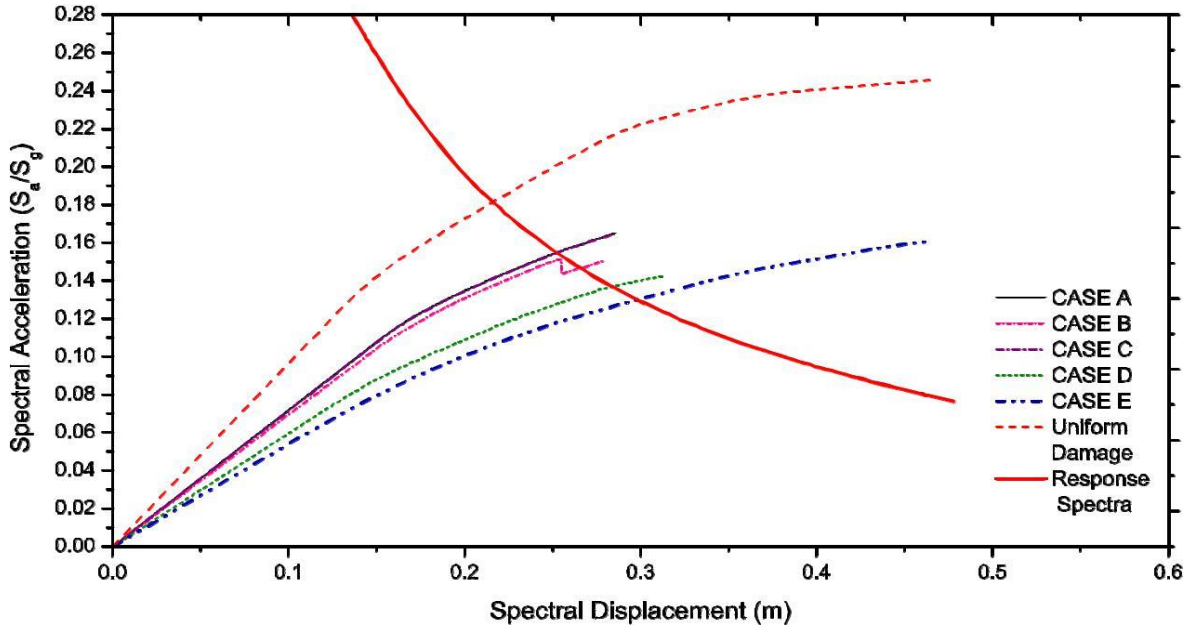

Fig. 3.24 Capacity Curve for Different Damage Scenarios Superimposed with ATC-40 Response Spectrum.

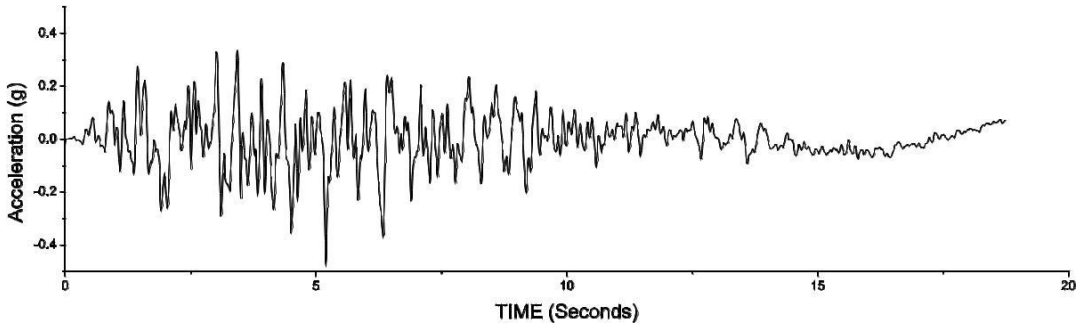

Fig. 3.25 ATC-40 Compatible Ground Motion.

Table 3.3 compares between the maximum top floor displacements and base shears obtained from the pushover and time history analyses. Note that performance points on the pushover curves for all cases are obtained for the

response spectrum with PGA of 0.493g. It is seen from Table 3.3 that the difference between time history results and those obtained from the pushover analysis are within 30%. Fig. 3.27 compares between the plastic hinges formed in the pushover and time history analyses for the building frame having different damage scenarios(a-e).

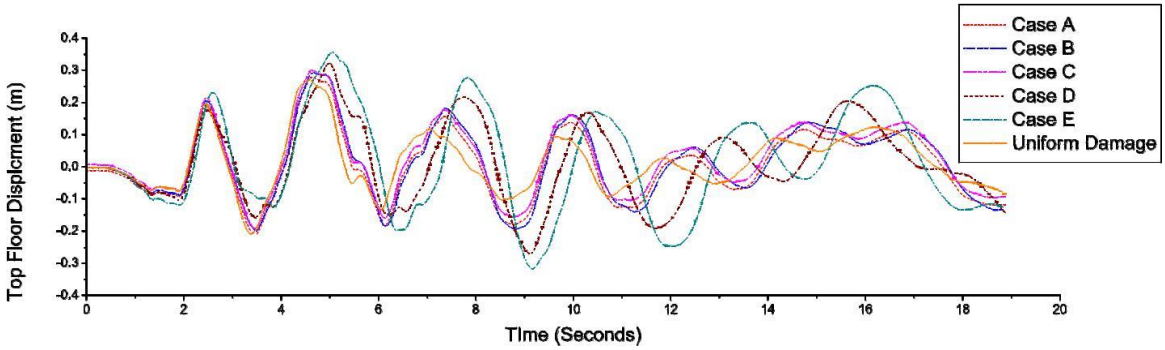

Fig. 3.26 Top Floor Displacement for Different Damage Scenarios.

Table 3.3. Comparison of Push Over Analysis and Time History Analysis

	Push Over Analysis		Nonlinear Time History	
Damage Scenarios	Top floor displacement(m)	Base Shear (kN)	Top floor displacement(m)	Base Shear(kN)
Case A	0.326	2007	0.280	2870
Case B	0.341	2012	0.294	2712
Case C	0.326	2007	0.280	2870
Case D	0.354	1771	0.322	2939
Case E	0.430	1425	0.357	2253
Uniform Damage	0.311	2669	0.271	3237

It can be seen from the figures that the pattern and number of plastic hinges formed for each damage scenario obtained by the pushover and nonlinear time history analyses are nearly the same. Number of plastic hinges required for the complete collapse of the frame is equal to 58 (Table 3.1). It is seen from the figures that except for the critical damage scenario, the number of plastic hinges are less than the number required for the complete collapse of the structure. For the case of critical damage scenario, the number of plastic hinges formed is 58 which is equal to that observed for the plastic analysis (Table 3.1). Further, Fig. 3.27 shows the spread of plastic hinges beyond the damaged zone for all damaged scenarios;

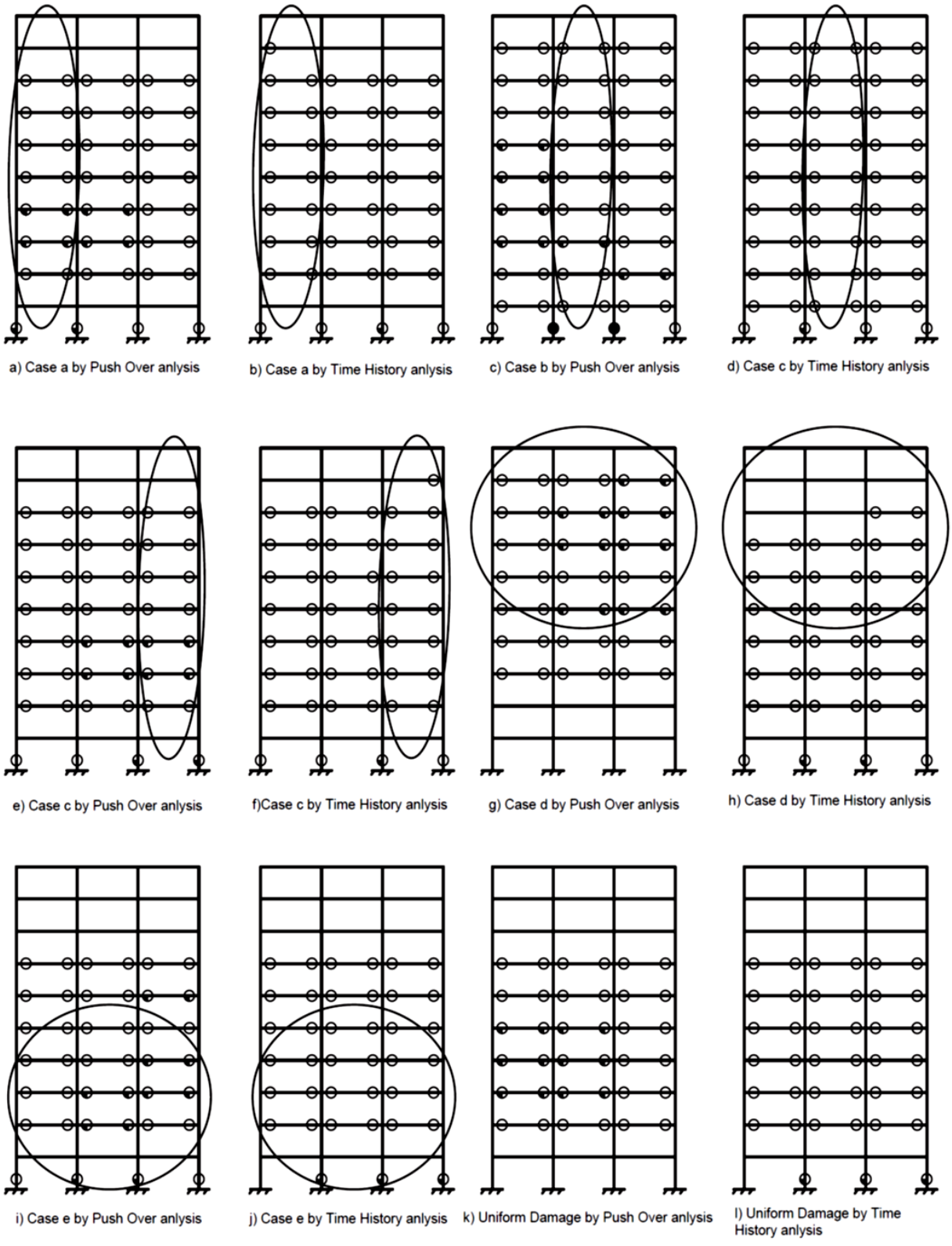

Fig. 3.27 Plastic Hinge Location and State for Different Damage Scenarios.

initial damage states are encircled. It is seen from figures that the formation of plastic hinges is not only confined within the encircled zone but beyond that zone indicating the spread (or progress) of the collapse of members under seismic excitation. The severity of the damage is indicated by the plastic rotations taking place in plastic hinge which is shown with the color of hinges. As expected, the maximum plastic rotations have taken place for hinges within the initial damage zone. Further, it is seen from the figures that except the case b, which corresponds to the initial critical damage state, the spread of the plastic hinge is arrested at some state before the state of the complete collapse.

3.3.2 VALIDATION OF THE PROPOSED METHOD

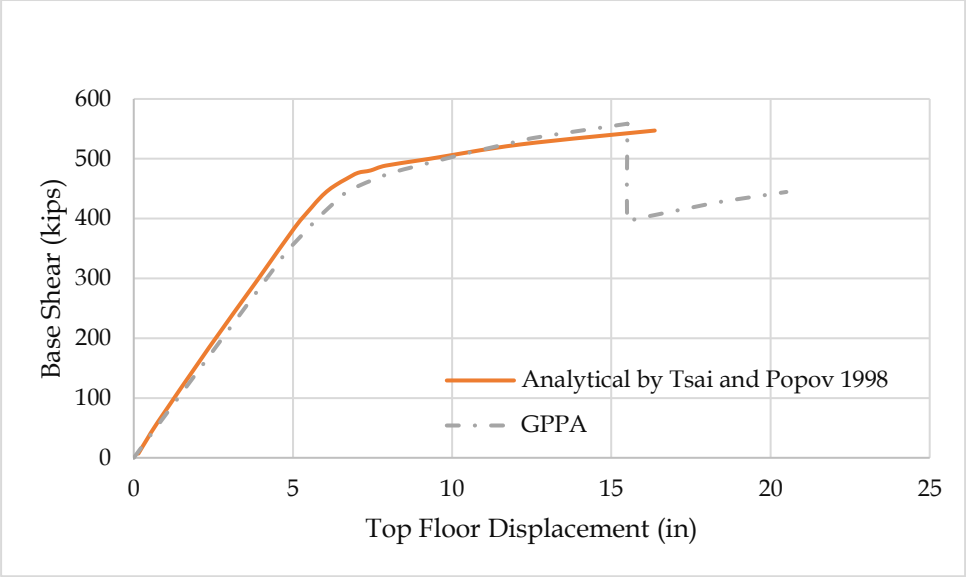

Fig. 3.28 Comparisons of Capacity Curve for Steel Buildings.

The proposed GPPA is new in the sense that it predicts the ultimate load carrying capacity of the frame using the genetic algorithm and then, uses the pushover analysis to verify the predicted ultimate load in the sway mode of failure. In order to validate the proposed method, results of two example problems published in the literature are considered. In the first, comparison of ultimate load predicted by Tsai and Popov 1988 using a pushover analysis for a steel frame with that predicted by proposed GPPA is made. In the second, the comparison of the GPPA with the experimental pushover capacity curve presented by Sharma et al. 2011, is made.

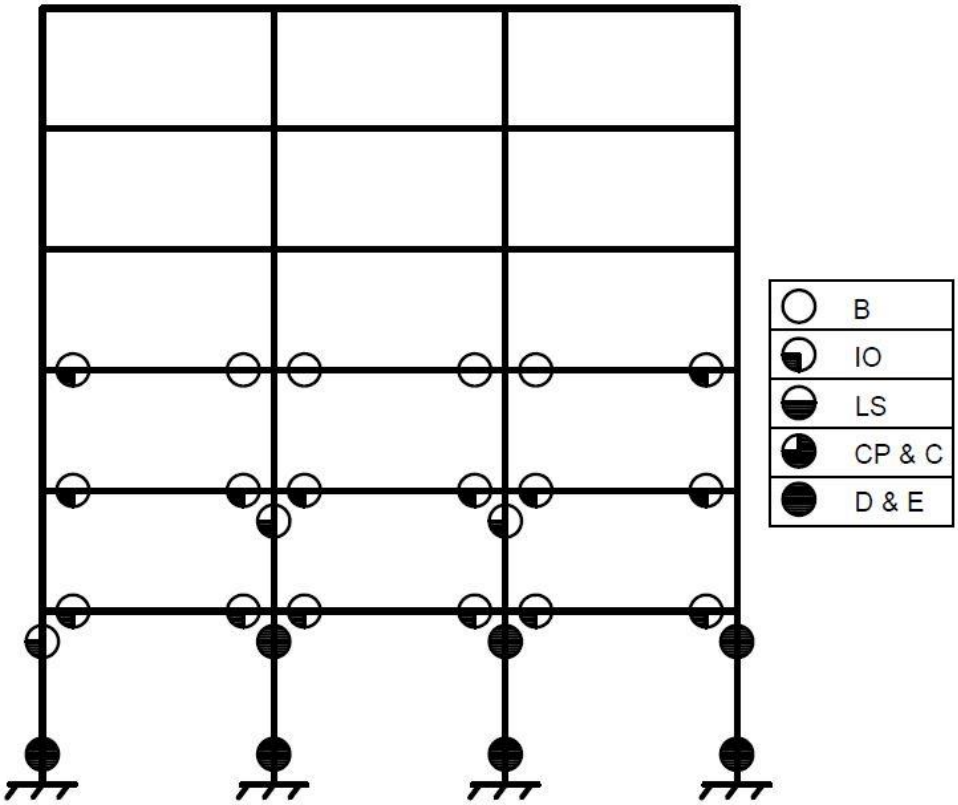

Fig. 3.29 Hinge Locations obtained by the pushover analysis for the reference 6 storey building.

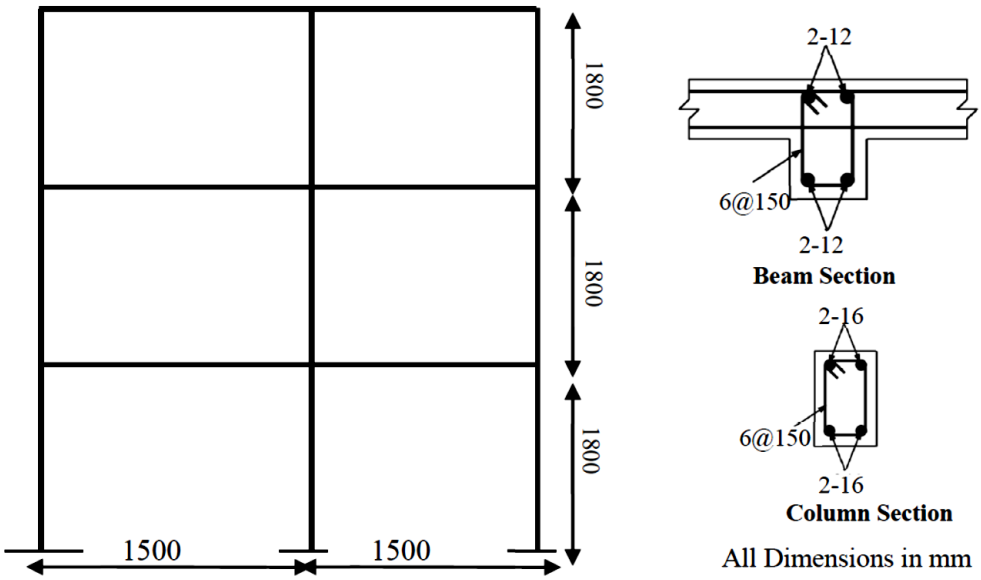

Fig. 3.30 Reinforced concrete reference building.

The properties of steel frame analyzed are given in Tsai and Popov 1988. No experimental curve showing a variation of the top displacement of the frame with

the base shear (capacity curve) is presented in the cited reference. However, the capacity curve obtained analytically for different rigidities of the joints are given for triangular load distribution pattern. The capacity curve obtained by the pushover analysis and the collapse load predicted by GPPA following sway mechanism of failure and those given by Tsai and Popov are compared in Fig. 3.28 for zero rigidity of the joints. It is seen from the figure that both capacity curves compare very well, and the collapse loads obtained by Tsai and Popov and the GPPA are nearly the same. Note that the failure mechanism is a partial sway mechanism of failure as shown in Fig. 3.29.

Sharma et al. 2011 conducted an experimental study on the 3-storey RC frame model as a part of a benchmark study conducted by Bhaba atomic research centre (BARC) in India. The properties of frames are shown in Fig. 3.30 and more details are available in a paper by Sharma et al. 2011. The capacity curve obtained experimentally and that obtained by the proposed method (GPPA) are compared in Fig. 3.31. It is seen from the figure that there is a good agreement between the two-capacity curves.

3.3.3 IMPLEMENTATION

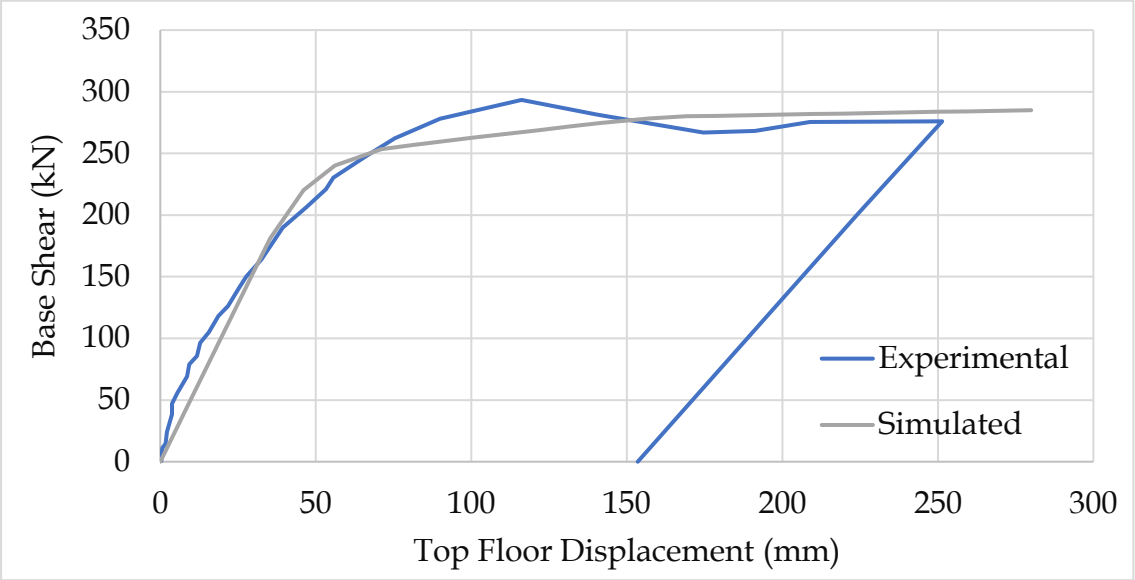

Fig. 3.31 Comparisons of the Capacity curve for the Reinforced concrete building.

In order to implement the proposed GPPA method for identifying the critical initial damage state of the frame which would collapse under a probable

earthquake, the following steps may be adopted. The properties of the undamaged state of the frame with anticipated damage are obtained from the original drawing of the structure. Different possible damage scenarios for the undamaged frame can be simulated as described in Section -3.2.6. A pushover analysis for each damage condition is performed to find the performance point to coincide with the collapse point of the capacity curve and accordingly, the PGA of the response spectrum (demand curve) compatible earthquake to cause a complete collapse of the frame having the same damage may be ascertained. Actual damage state of the frame is then assessed by a prototype experimental test on the frame. Actual damage state is compared with the simulated ones in order to find if there exists a possibility of the frame to collapse under a response compatible earthquake. If a possibility exists, then the PGA value for which such an episode would take place can be easily estimated. Further, a lower limit of the PGA value of the response spectrum compatible earthquake can be predicted for which the collapse of the frame under earthquakes can take place if the evaluated damage state is close to the simulated critical damage scenario.

3.4 CONCLUSION

The possibility of the collapse of damaged building frames under earthquake is investigated in order to demonstrate that certain existing localized damages expressed in terms of the percentage reduction of the total plastic moment capacity of the frame may trigger either complete or partial collapse of the structure. There could be other localized damage scenarios having the same total damage, in which the progression of the damage under the earthquake is arrested much before the collapse. An analysis called GPPA is proposed for the analysis. It identifies the damage scenario which is most likely to fail by the complete sway mechanism formed in the structure, for the response spectrum compatible earthquake used to find the performance point in the pushover analysis. The nonlinear time history analysis is carried out to verify the collapse mechanisms formed. Further, the proposed methodology is validated using the

existing test data that has been published in the literature. Following conclusions can be drawn from the numerical study:

- There exist certain localized damage states for a building frame which may trigger sway mode of collapse under an earthquake; this explains why one of the two identical buildings built at the same time and site collapse, while the other survives under the same earthquake.
- It is possible to identify these localized damage states using the GPPA proposed here.
- The nonlinear time history analysis with response spectrum compatible earthquake confirms that the sway mode of collapse of the frame takes place for the critical initial damaged state of the frame identified by the GPPA.
- For the same earthquake, similar building frames may have progression of the initial damages, depending upon their initial location and states other than the critical damage state, without collapsing the frame.
- If the damage state of a building can be evaluated beforehand, the vulnerability of the building to collapse under future earthquakes can be predicted using the methodology presented here.
- The methodology may be usefully employed for retrofitting the damaged building to withstand specific levels of earthquake intensity.

CHAPTER-4
EFFECTS OF AFTERSHOCKS ON THE PERFORMANCE OF STEEL BUILDING FRAMES

4.1 INTRODUCTION

Earthquake resistant design is based on the lateral deformation capacity of the structure and the demand imposed by an earthquake. A moment resisting frame (MRF) is damaged during an earthquake due to its limit to resist lateral deformation. As a consequence, evaluations of existing structures (e.g., FEMA 356, FEMA 355f American Society of Civil Engineers (ASCE) 2000; Federal Emergency Management Agency (FEMA) 2000) are based on the estimation of peak lateral displacement demands that structures could suffer under seismic excitation. These evaluation procedures are not explicit about the aftershock effects. In real life, a structure located in high seismic regions not only experiences a single seismic event (i.e., mainshock), but also to a seismic sequence consisting of foreshocks, mainshock, and aftershocks.

Recent evidence of aftershocks of significant magnitudes are those associated with the Kathmandu valley earthquake and Mexico earthquake. After the earthquake, on 25th April 2015 (Mw=7.8), that violently shook the Kathmandu valley causing the collapse of several structures, several earthquakes of magnitude higher than Mw of 4.0 were observed within first 45 days (Adhikari et al. 2015). On 12th May 2016, weeks after the main earthquake, an aftershock of Mw of 7.3 hit the region. Similarly, after a few days of the Mexico earthquake (Mw=7.1) on 19th September 2017, an earthquake of Mw= 6.1 was observed. Moreover, there were nearly 150 earthquakes in 450 km radius of Matias Romero between 2nd September 2017 and 13th October 2017 including an earthquake of Mw =8.1.

Post-1994 Northridge earthquake, research on the response of a structure subjected to mainshock and aftershock events has gained momentum. After a seismic event, damage assessments are performed visually by trained professionals which may not be accurate. Different professionals may take

different decisions. Therefore, the confirmed decision is unachievable. Nevertheless, most of the current seismic risk assessment tools only consider mainshock effects without considering aftershocks. After the mainshock, the threat to life safety for building occupants and risk of building damage are higher than before the occurrence of the mainshock due to the permanent deformation or hinge formation in the building during a mainshock. Collapse in successive earthquakes because of the damage from the mainshock was demonstrated by van de Lindt on a shake table (Han et al. 2016; Nazari et al. 2015). Most of the building codes on the earthquake resistant design of structures do not provide any clear-cut guideline for aftershock effects. The value of the reduction factor 'R' specified in the code for different types of buildings might cater to this effect. However, no explicit recommendation is available on this issue.

In this chapter, a detailed investigation of the nonlinear behavior and damage of the steel moment resisting frame (MRF) subjected to a series of Indian Standard (Standard 1893) response spectrum compatible mainshock-aftershock sequence is presented. The mainshocks and aftershocks are artificially generated using SeismoArtif 2016 (SEiSMOSOFT 2016.). Three designed building frames, 4-storey, 8-storey and 12-storey (Santa-Ana & Miranda 2000) are considered for the study.

4.2 ANALYSIS

The building frames are subjected to the response spectrum compatible earthquakes consisting of one mainshock followed by a number of aftershocks. The mainshock is assumed to be of duration 40s, while the aftershocks are assumed to be one-fourth the duration of the mainshock. These durations are considered based on general observations. Further, based on baths law (Ruiz-García 2012; Shcherbakov et al. 2005), it is assumed that aftershock has the magnitude 1.2 less than that of the mainshock. Nonlinear time history analysis of the frames is carried out for the mainshock and series of aftershocks. Analysis for the aftershock duly considers the deformed configuration of the structure, after the mainshock is over, as the initial state. Similarly, each aftershock duly considers the cumulative

deformed configuration of the structure due to the episodes that occurred prior to it. This is achieved by joining the two-time history records by a series of zeros sampled at an interval of Δt, which is used to sample the time history records. Sufficient interval of time is created between the two-time history records, so that damped free oscillation after the previous episode completely dies down. Thus, a long-time history record is simulated by joining the mainshock and aftershock sequences. The total length of the time history depends upon the numbers of mainshock and aftershocks considered. The mainshock and aftershock sequence is simulated considering that (Ruiz-García 2012) i) the predominant period of the mainshock is longer than that of the corresponding aftershock, ii) the bandwidth of the mainshock is larger than that of the subsequent aftershock, and iii) the significant duration of the mainshock is longer than that of the aftershock.

The three-building frames with stories 4, 8 and 12 are modelled as two dimensional MRF steel frames, originally designed by Santa-Ana & Miranda (2000), are analyzed for the mainshock-aftershock sequences. The frames were designed to resist the lateral load distribution as prescribed in the UBC 1994. At the joints, column to beam strength ratio (CBSR) is maintained more than 1 for all the storey except the roof. Nonlinear properties of the material have been modelled using lumped plasticity model (ASCE 41-13 2014). Hinges are embedded at discrete locations (ends) of the beams and columns. The yield and post-yield behaviors have been modelled using the strength deterioration model as prescribed in section 3.2.2. In order to incorporate the sudden strength loss, hinge overwrites have been assigned in all the frames. Moment hinges have been specified in the beam ends and coupled axial force – moment hinges are provided in column ends. Different performance points, Intermediate Occupancy (IO), Life Safety (LS) and Collapse Prevention (CP) are defined based on the rotation of the hinges as given in ASCE 41-13 (2014).

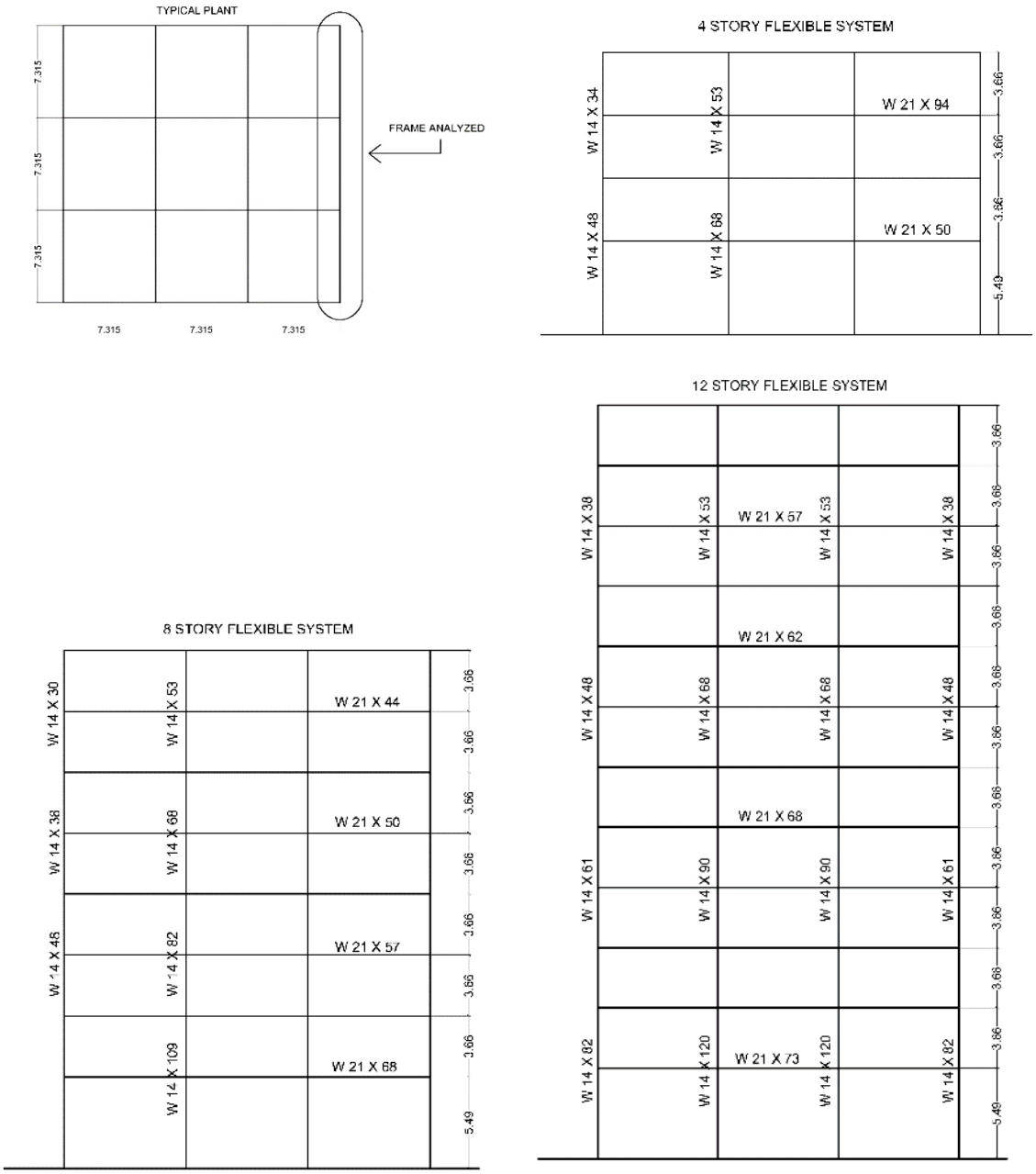

Fig. 4.1 Plan and East-West elevation of building Frames

4.3 NUMERICAL STUDY

The designed MRFs have a non-uniform distribution of the mass. Details of the frames are shown in the Fig. 4.1. The time periods for the first three modes of vibration of frames are given in Table 4.1. Both computed and reported (Santa-Ana & Miranda 2000) values are shown in the table. It can be seen from the table that time periods for the both are almost the same. The sum of mass participation factors for all the three-building frames for the first three modes are about 98%. In order to verify the modelling of building frames and the analysis procedure, the

modelled 4-storey MRF is subjected to the near-fault seismic sequence as considered by Ruiz-García & Negrete-Manriquez (2011). The seismic sequence considered is the 228° component of 1994 Northridge earthquake recorded at Rinaldi receiving station. The mainshock is having Mw=6.7, whereas the aftershock has Mw=5.7. The seismic sequence (the mainshock and one aftershock) is separated by 60secs as shown in the Fig. 4.2. From the figure, it is seen that PGA of the mainshock is higher than that of the aftershock.

Table 4.1 Modal Properties (time periods in secs) of the building Frames

Modes	4-storey		8-storey		12-storey	
	Modeled	reported	Modeled	reported	Modeled	Reported
First	1.23	1.23	1.92	1.92	2.60	2.61
Second	0.38	0.39	0.67	0.68	0.91	0.91
Third	0.20	0.20	0.39	0.39	0.53	0.53

Note: Reported results are from Santa-Ana & Miranda (2000)

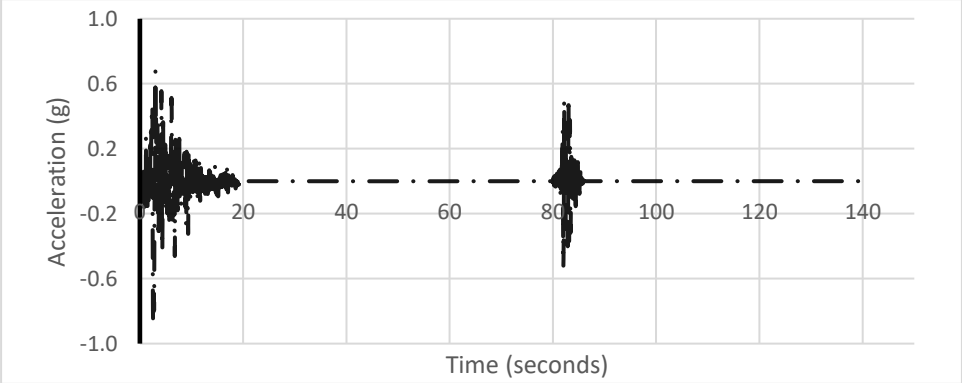

Fig. 4.2 Seismic Sequence at Rinaldi receiving station, Component 228.

The time histories of the first storey displacement of the 4-storey MRF as obtained by the present analysis and that reported by Ruiz-García & Negrete-Manriquez (2011) are compared in Fig. 4.3. Mainshock transients for the two-time histories differ to some extent, but the residual displacement for the two are the same. There is no difference between the two aftershock transients and the consequent residual displacements. Further, aftershocks are found to have the least effect on the top storey displacement. The response of the structure is dominated by the mainshock; there is no further damage to the structure during

the aftershock. The present study focuses on the damage to buildings during an aftershock and their accumulation during subsequent aftershocks. The mainshocks and aftershocks are artificially generated. The mainshock and aftershock represent any random seismic sequence that can occur during the lifespan of a building constructed in the active seismic zone.

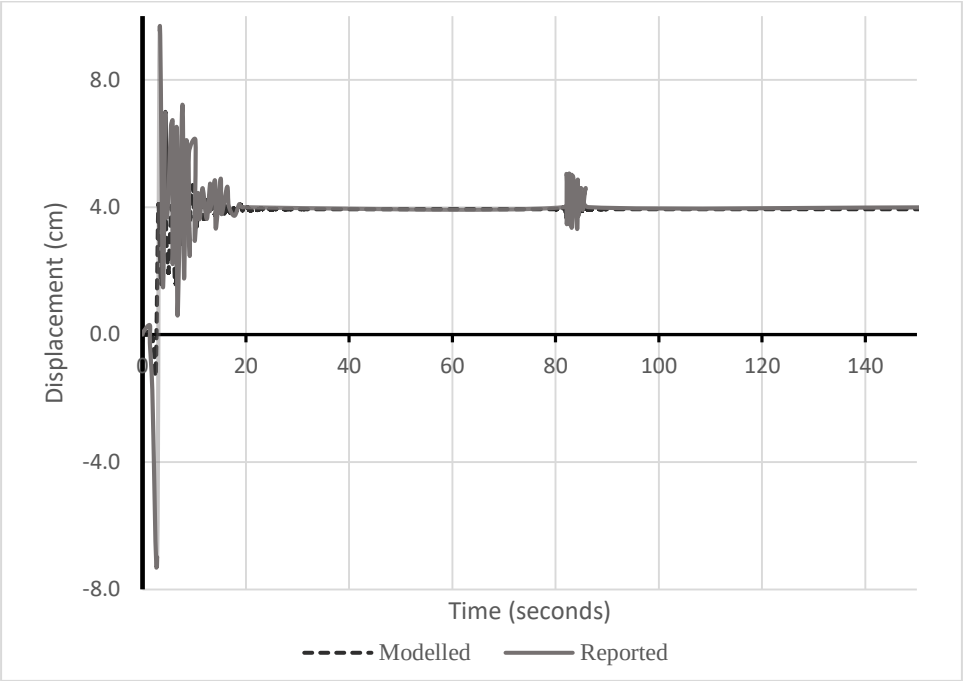

Fig. 4.3 Comparison of First-floor displacement time-histories of the 4-storey frame subject to Rinaldi 228

4.3.1 EFFECTS OF MAINSHOCK AND AFTERSHOCK SEQUENCES

The three-building frames designed according to UBC as shown in Fig. 4.1 are subjected to the IS-Spectrum compatible mainshock and aftershock sequences. The reason for choosing the building frames designed according to UBC is to validate the analysis procedure using the published results. The response spectrum compatible mainshocks and aftershocks are used in order to include any desirable number of earthquakes in the mainshock-aftershock sequence which can only be achieved by simulation. These artificially generated earthquakes are far-field in nature produced by inter-plate regime having linear site effects. The building frame is assumed to be on the hard rock having a Joyner-Boor distance of 10 Km. The mainshock and aftershock are having Mw=7.8 and 6.5 respectively. Different physical parameters of the artificially generated earthquake are given in

Table 4.2. It is evident from the table that the mainshock and the aftershock follow the relation proposed by Ruiz-García (2012). Eight mainshocks and seven aftershocks are generated synthetically. It can be observed that the difference between average PGAs of the mainshock and aftershock is very small. As observed by Ruiz-García (2012), there is no relation between the PGAs of both events. It had been noticed in a few real earthquakes that the PGAs of aftershocks are higher than those of the mainshock (e.g., Mexico City Earthquake (Astiz et al. 1987).

Table 4.2 Mainshock and Aftershock characteristics

Parameters	Mainshock	Aftershock
Magnitude (Mw)	7.8	6.5
Average mean error (%)	9.11	9.27
Average PGA(g)	0.41	0.34
Average Intensity(cm/s)	3.05	1.08
Significant Duration(s)	20.88	5.45
Duration (s)	40.56	10.05

The normalized acceleration response spectrums of the mainshock, aftershock, and the normalized Indian standard response spectrum are plotted in Fig. 4.4. It can be seen that for the periods of interest (time period greater than and equal to the fundamental period of 4-storey building considered), all the response spectra nearly match that of the Indian standard response spectrum. It can also be seen that in the periods of interest, there is no spike in the response spectra. The artificially generated mainshocks and aftershocks are shown in Fig. 4.5 and 4.6 respectively. The PGA and root mean square (RMS) of all mainshocks and aftershocks considered in the study are given in Table 4.3. It can be seen from the figures that different seismic events are different in time, but they have nearly the same PGA. Therefore, the suite of mainshock and aftershock events form different time history records. Fig. 4.7 shows the relationship between the predominant period and the bandwidth of the generated earthquake records. Bandwidth is a function of the spectral velocity and time period given by Vanmarcke (1972).

$$\Omega = \left[1 - \frac{(\lambda_1^*)^2}{\lambda_0^* \lambda_2^*}\right]^{\frac{1}{2}} \quad (4\text{-}1)$$

Where, λ_0^*, λ_1^* and λ_2^* are given by $\lambda_0^* = \sum_{i=1}^{n} S_{v,i}^2 \cdot \Delta T$; $\lambda_1^* = \sum_{i=1}^{n} T_i \cdot S_{v,i}^2 \cdot \Delta T$; and $\lambda_2^* = \sum_{i=1}^{n} T_i^2 \cdot S_{v,i}^2 \cdot \Delta T$. S is defined as the velocity spectrum ordinate for 5% damped SDOF system.

Table 4.3 PGA and RMS of the mainshocks and aftershocks considered

Mainshock	PGA(g)	RMS (g)	Aftershocks	PGA(g)	rms(g)
mainshock_1	0.394	0.067	Aftershock_1	0.289	0.083
mainshock_2	0.494	0.068	Aftershock_2	0.410	0.092
mainshock_3	0.341	0.071	Aftershock_3	0.408	0.092
mainshock_4	0.353	0.066	Aftershock_4	0.333	0.081
mainshock_5	0.346	0.068	Aftershock_5	0.346	0.086
mainshock_6	0.455	0.064	Aftershock_6	0.367	0.087
mainshock_7	0.410	0.069	Aftershock_7	0.328	0.088
mainshock_8	0.366	0.076			

The predominant periods of most of the earthquakes are in the vicinity of 0.35 - 0.5 Secs. Only two ground motions have a predominant period in the range of 5 secs. The predominant periods of all the ground motions are away from the fundamental periods of the structure. Therefore, the structures are not near resonating conditions. The responses of the three different MRFs subjected to these mainshocks and aftershocks are obtained to investigate the effects of the mainshock-aftershock sequence on the structures.

The building frames are subjected to one of the eight mainshocks and a series of seven aftershocks after each mainshock. A typical sequence of a mainshock followed by two aftershocks is shown in Fig. 4.8. Each shock is separated by 40 secs from the previous one. The time delay of 40 secs is to ensure that the building is at rest before the next aftershock is applied. In this manner, as shown in Fig. 4.8, the mainshock is succeeded by a maximum of 7 aftershocks, each in series with the other time histories.

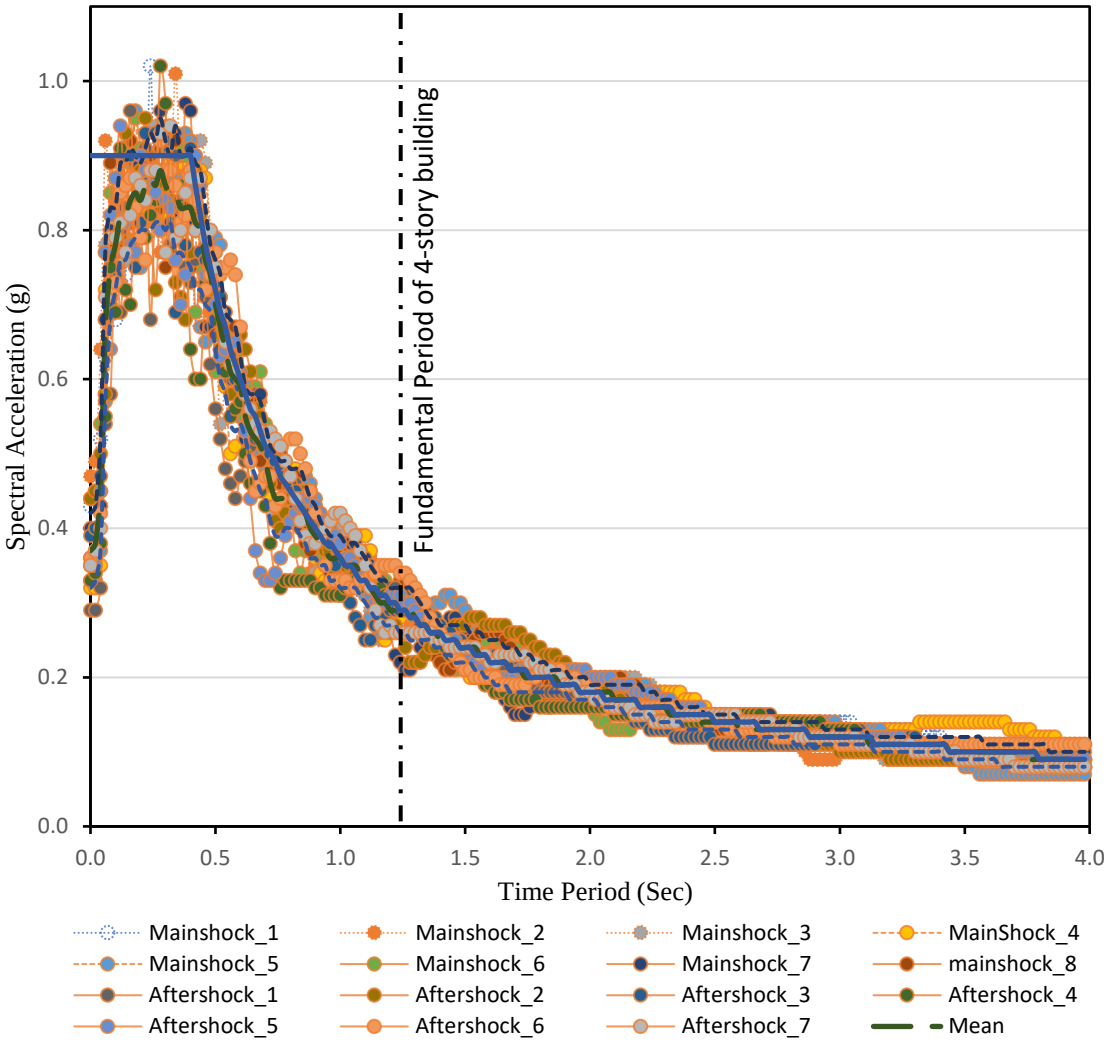

Fig. 4.4 Response Spectrum for a suite of mainshock and aftershock considered

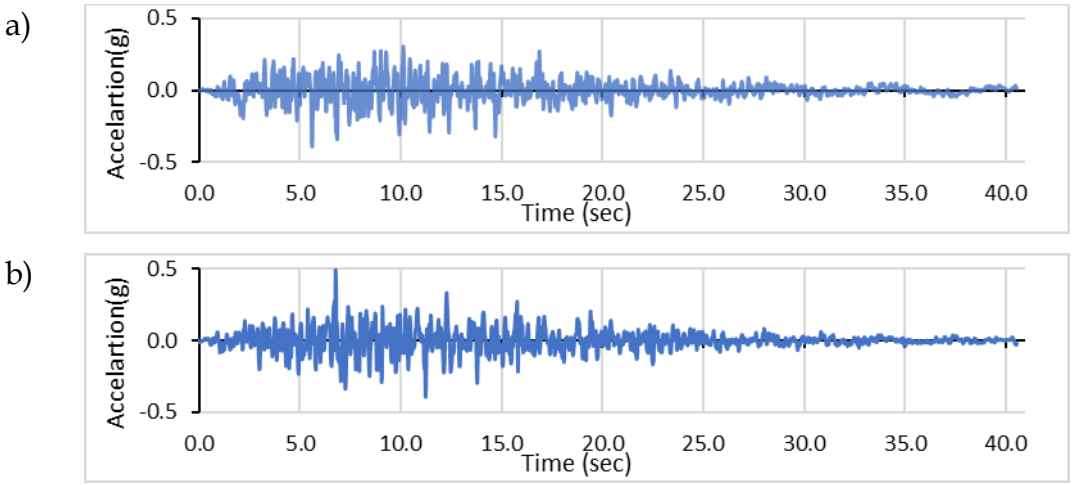

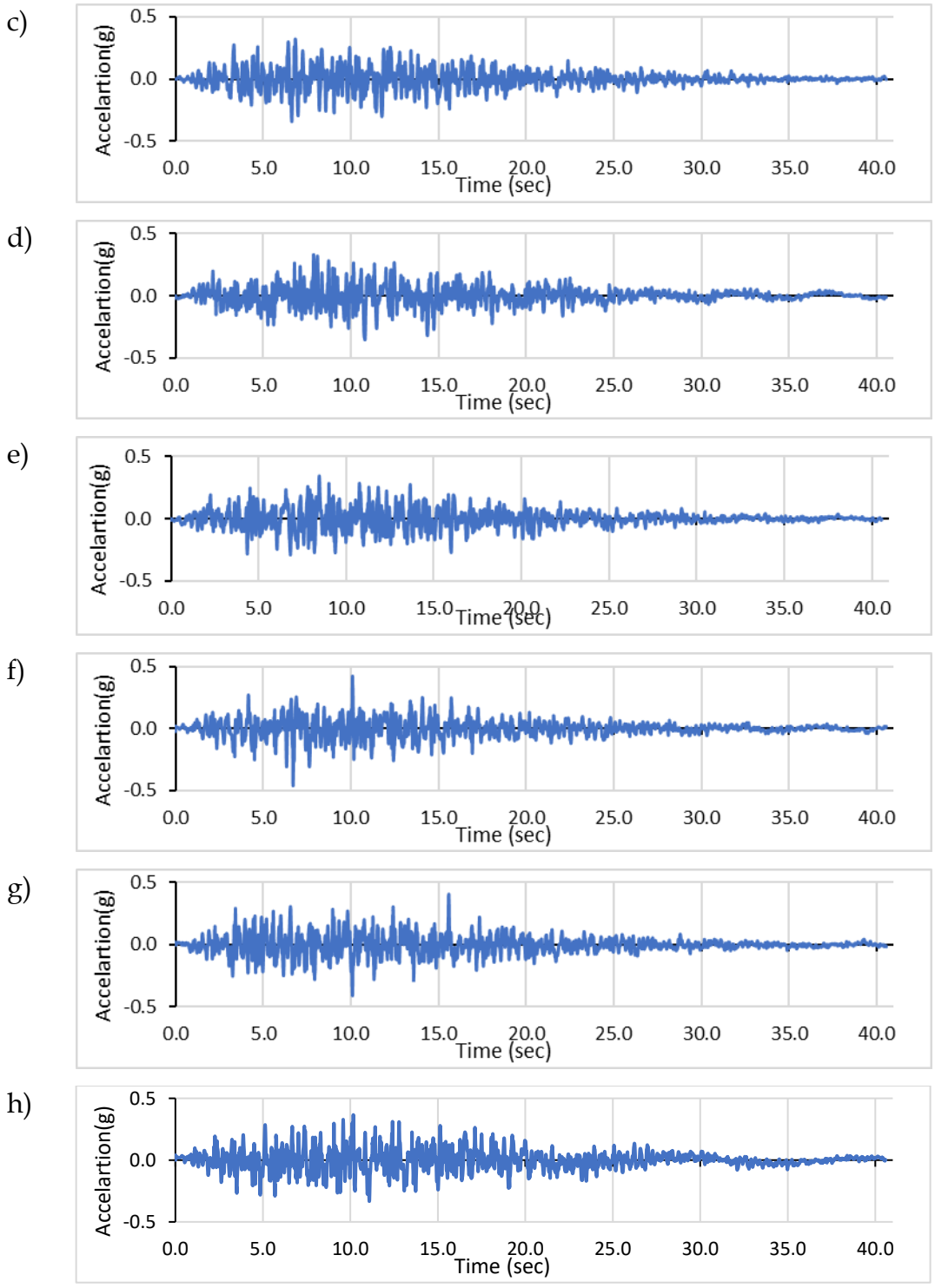

Fig. 4.5 Response spectrum compatible mainshocks of Mw=7.8 generated. a) Mainshock_1 b) Mainshock_2 c) Mainshock_3 d) Mainshock_4 e) Mainshock_5 f) Mainshock_6 g) Mainshock_7 h) Mainshock_8

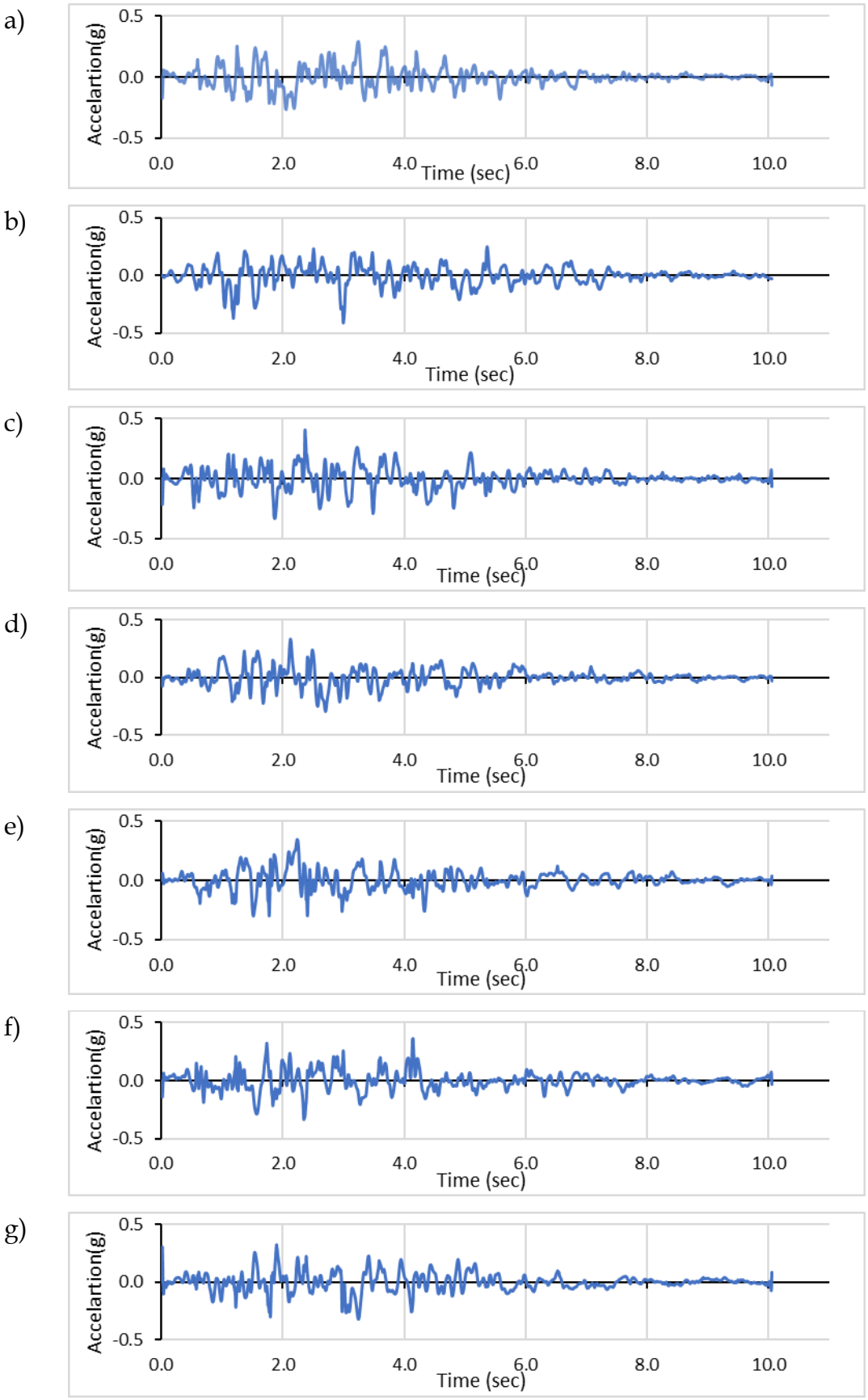

Fig. 4.6 Response spectrum compatible generated Aftershock of Mw=6.5. a) Aftershock_1 b) Aftershock_2 c) Aftershock_3 d) Aftershock_4 e) Aftershock_5 f) Aftershock_6 g) Aftershock_7

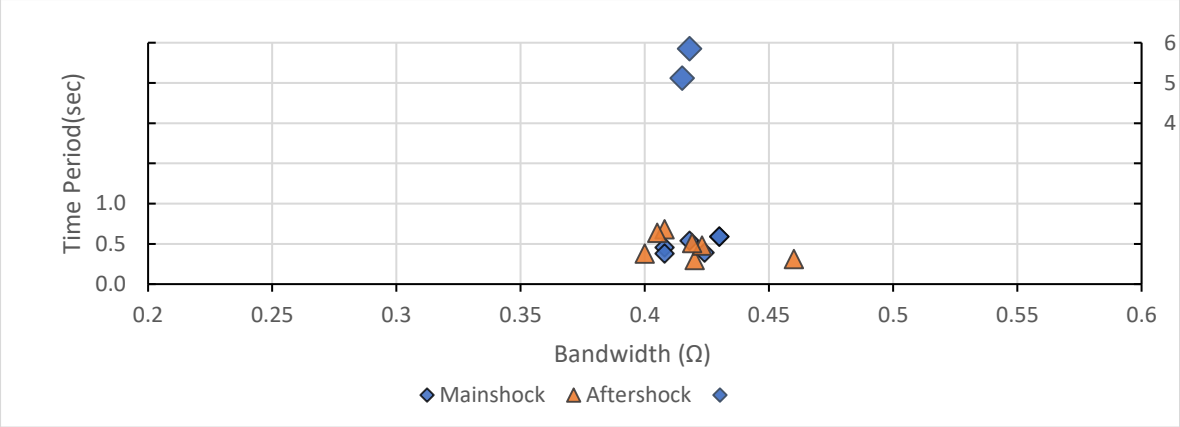

Fig. 4.7 Relationship between Predominant period and bandwidth of generated artificial earthquakes

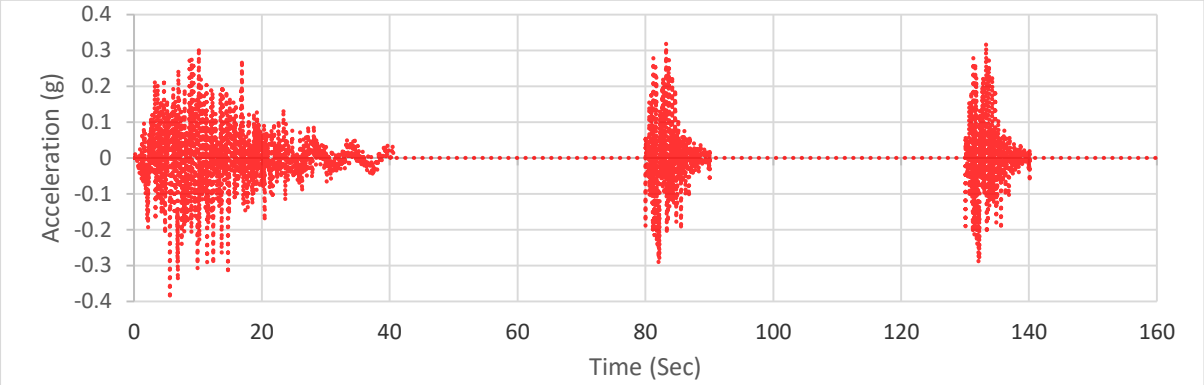

Fig. 4.8 A series of mainshock and aftershock

Table 4.4 MIDR of the first floor for different numbers of aftershocks

	Aftersh ock_1	Aftersh ock_2	Aftersh ock_3	Aftersh ock_4	Aftersh ock_5	Aftersh ock_6	Aftersh ock_7
Mainshock_1	1.18%	1.77%	2.16	2.78%	3.81%	4.62%	5.44%
Mainshock_2	1.37%	1.97%	2.60%	3.62%	5.13%	6.44%	9.72%
Mainshock_3	1.02%	1.63%	2.17%	2.97%	4.20%	5.21%	6.37%
Mainshock_4	1.30%	1.91%	2.47%	3.37%	4.75%	5.93%	7.60%
Mainshock_5	1.29%	1.88%	2.36%	3.13%	4.37%	5.40%	6.58%
Mainshock_6	1.01%	1.60%	2.00%	2.61%	3.60%	4.36%	5.12%
Mainshock_7	1.37%	1.97%	2.53%	3.46%	4.88%	6.09%	7.64%
Mainshock_8	1.04%	1.64%	2.14%	2.90%	4.08%	5.04%	6.02%

The variation of the maximum inter-story drift ratio (MIDR) along the height of the 4 storey MRF after the mainshock and every aftershock are shown in Fig. 4.9. It is seen from the figures that the MIDR is not very sensitive to the number

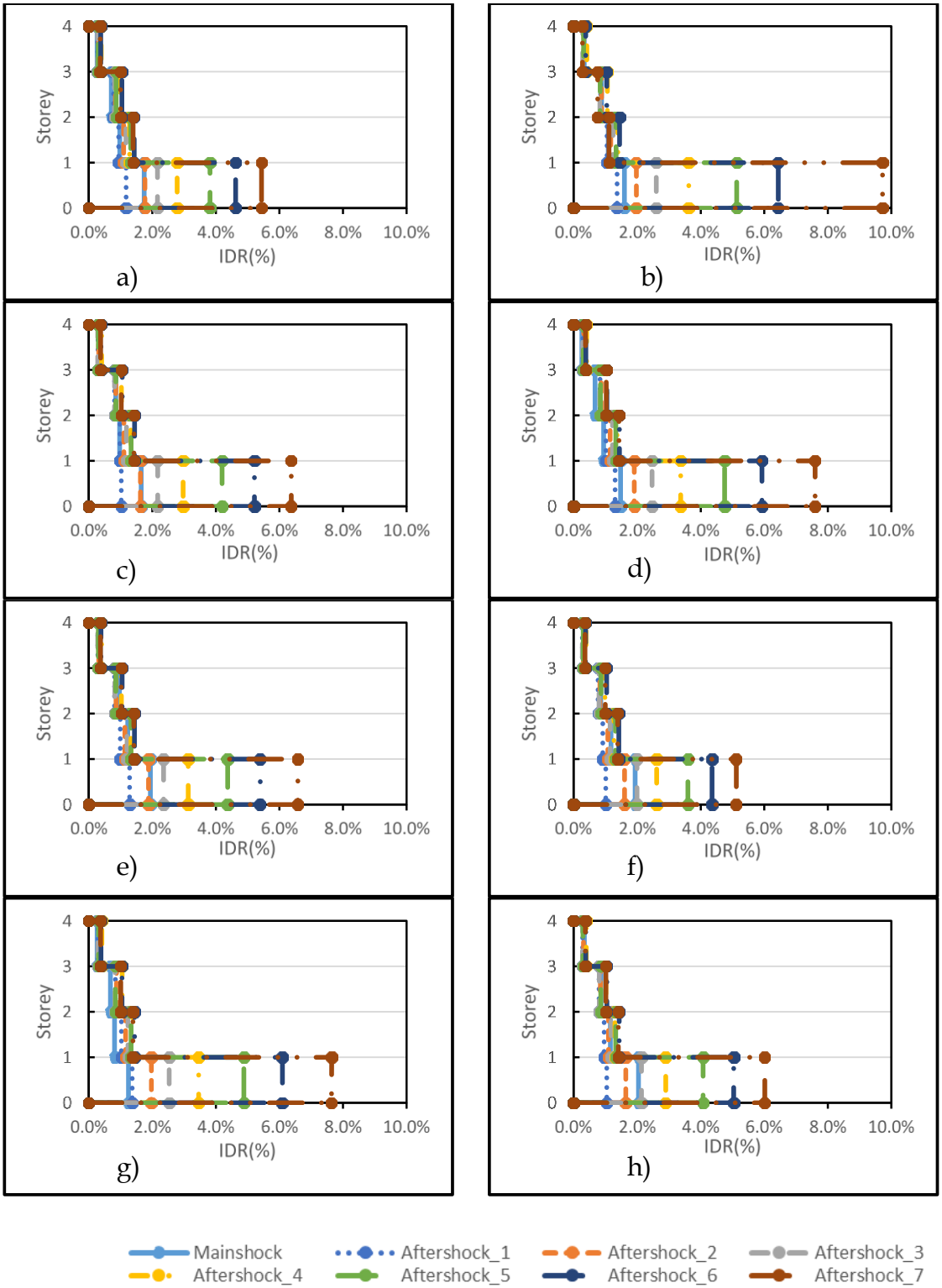

Fig. 4.9 Maximum transient inter-story drift distribution over height for series of aftershocks following the a) Mainshock_1 b) Mainshock_2 c) Mainshock_3 d) Mainshock_4 e) Mainshock_5 f) Mainshock_6 g) Mainshock_7 h) Mainshock_8

of aftershocks above the first storey. The MIDR of the first floor significantly varies with the number of aftershocks. Table 4.4 shows the MIDR of the first floor for different numbers of aftershocks following each of the eight different mainshocks.

The MIDR of the first floor after the seventh aftershock varies with different mainshocks considered in the study. The variation is about 5 to 10% and appears to be random; no consistent pattern is observed. However, the MIDR of 10% is observed for the simulated mainshock having a maximum PGA (0.494g).

The variation of the residual inter-story drift ratio (RIDR) along the height of the 4 storey MRF after the mainshock and every aftershock are shown in Fig. 4.10. It is seen from the figure that the RIDR, like the MIDR, is very small after the mainshock above the first storey level. At the first storey level, it increases with the number of aftershocks. This is attributed to the formation of new hinges during each aftershock, especially after the third aftershock. With a greater number of plastic hinges and more plastic hinge rotations, the RIDR is expected to increase. Fig. 4.11 shows the plastic hinges formed in the frame after different numbers of aftershocks for one of the case of mainshocks.

Table 4.5 RIDR of the first floor for different numbers of aftershocks

	Aftersh ock_1	Aftersh ock_2	Aftersh ock_3	Aftersh ock_4	Aftersh ock_5	Aftersh ock_6	Aftersh ock_7
Mainshock_1	0.25%	0.40%	1.01%	1.69%	2.52%	3.52%	3.84%
Mainshock_2	0.44%	0.73%	1.56%	2.73%	4.03%	5.91%	8.71%
Mainshock_3	0.19%	0.34%	1.09%	1.96%	2.98%	4.20%	4.94%
Mainshock_4	0.37%	0.63%	1.39%	2.42%	3.60%	4.98%	6.49%
Mainshock_5	0.36%	0.55%	1.25%	2.12%	3.16%	4.39%	5.18%
Mainshock_6	0.13%	0.23%	0.85%	1.50%	2.28%	3.23%	3.50%
Mainshock_7	0.44%	0.69%	1.46%	2.53%	3.75%	5.19%	6.33%
Mainshock_8	0.17%	0.33%	1.04%	1.86%	2.84%	4.00%	4.48%

Table 4.5 shows the RIDR of the first floor for different numbers of aftershocks following each of the eight different mainshocks. The RIDR of the first floor could be very large after the seventh shock (about 9%). It is seen from Table 4.4 and 4.5 that the MIDR at the first-floor level is of the order of 2% and the RIDR at the same level is of the order of 0.5% or more after 3 aftershocks. Thus, the frame is pushed to the life safely limit after three aftershocks according to the prescribed limits of the FEMA 355f.

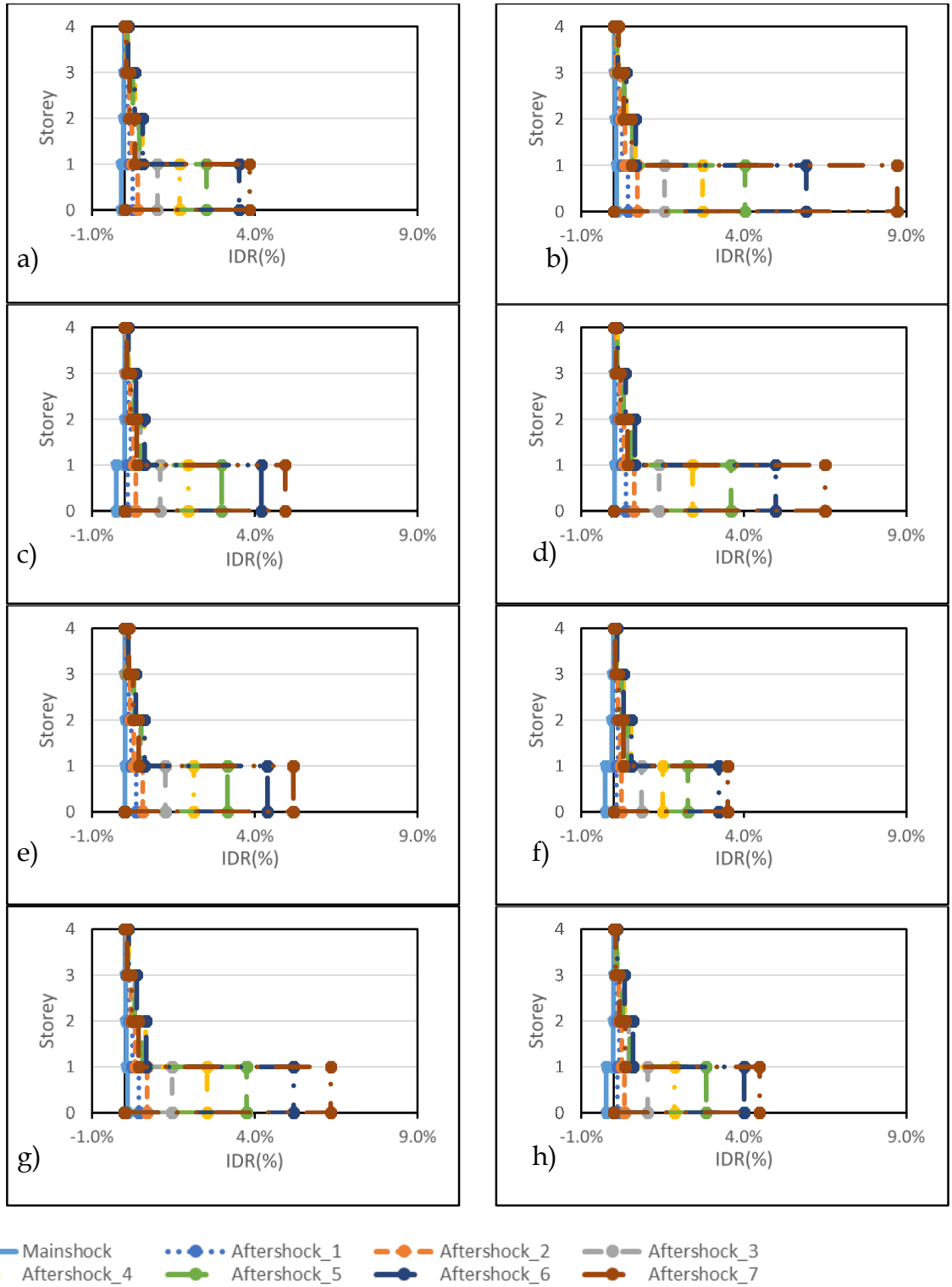

Fig. 4.10 Residual inter-story drift ratio distribution over height for series of aftershocks following the a) Mainshock_1 b) Mainshock_2 c) Mainshock_3 d) Mainshock_4 e) Mainshock_5 f) Mainshock_6 g) Mainshock_7 h) Mainshock_8

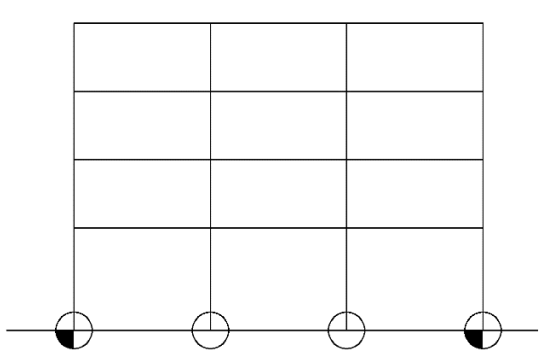

a) Mainshock

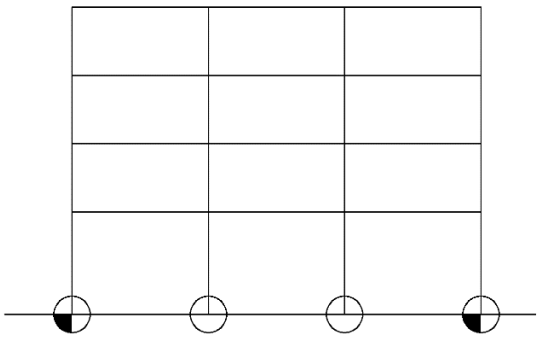

b) Aftershock_1

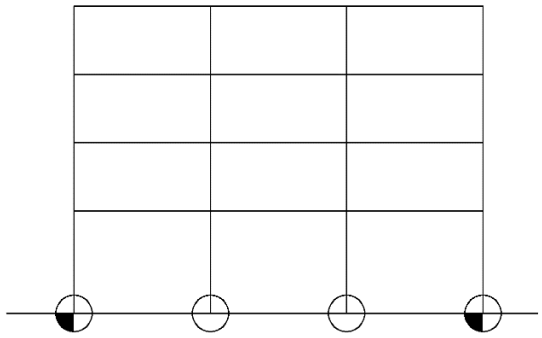

c) Aftershock_2

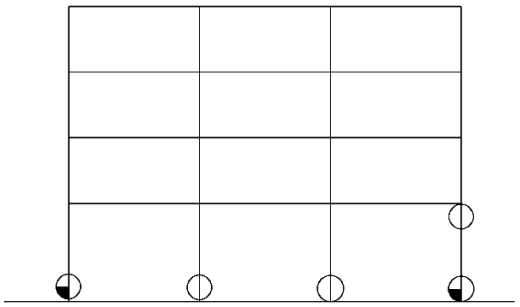

d) Aftershock_3

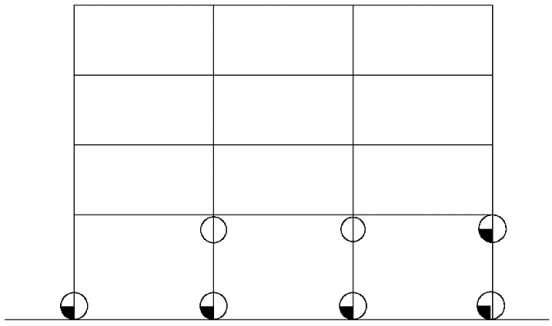

e) Aftershock_4

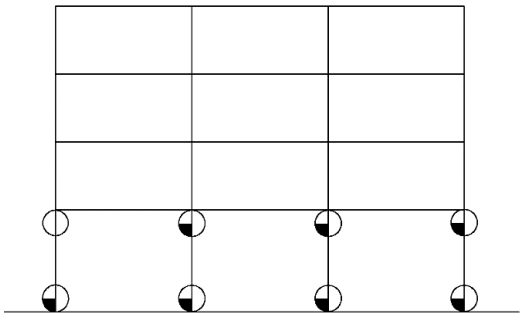

f) Aftershock_5

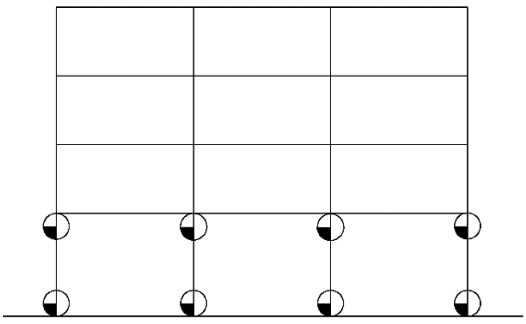

g) Aftershock_6

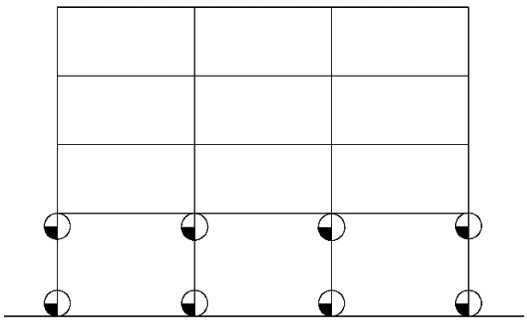

h) Aftershock_7

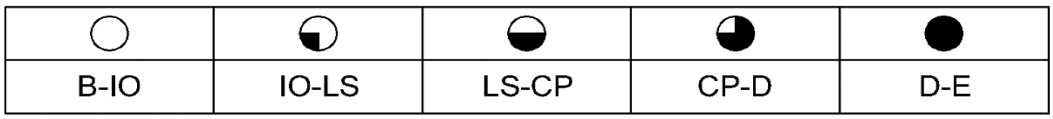

Fig. 4.11 Hinge location and state after different mainshock and aftershock

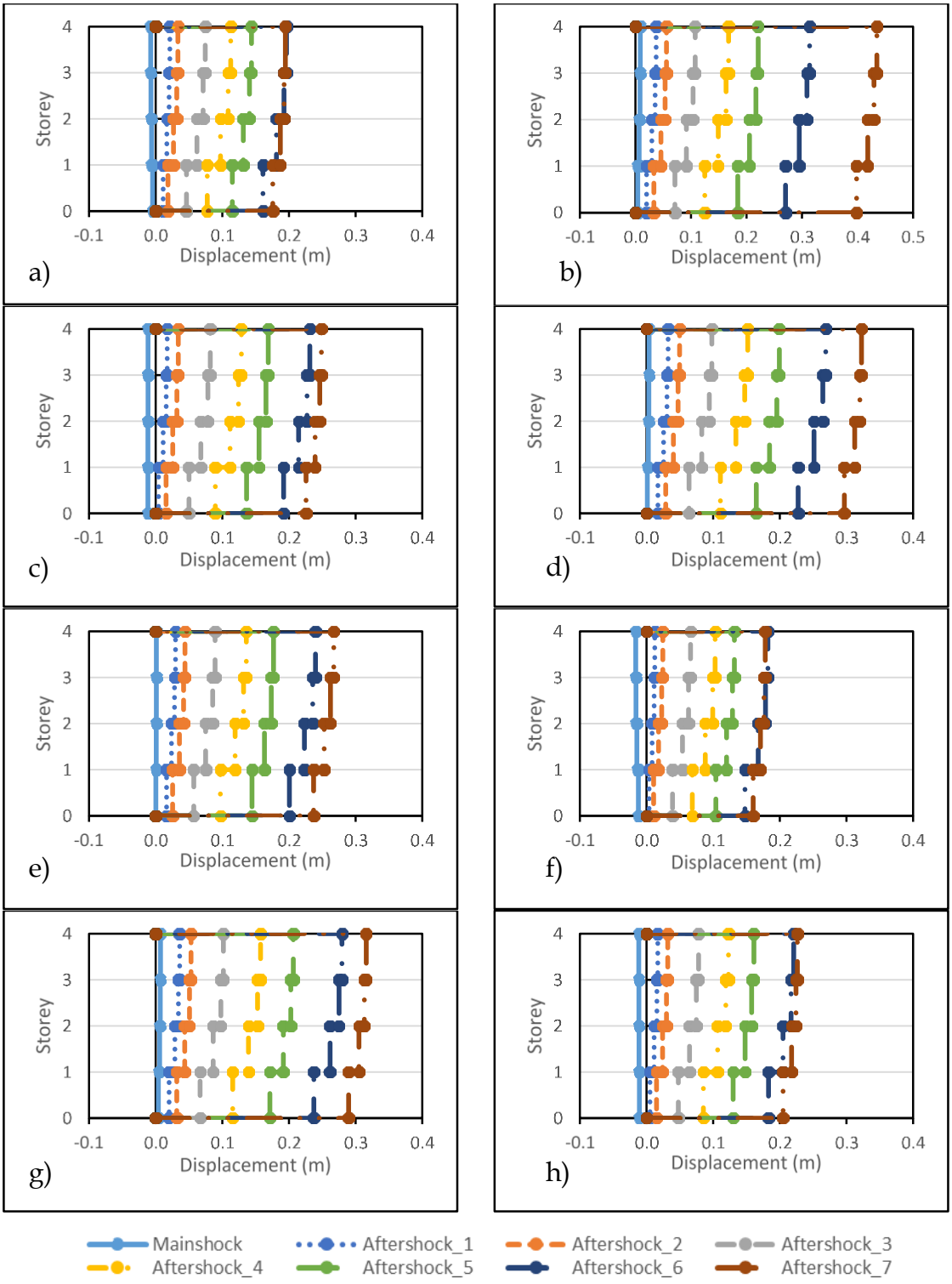

Fig. 4.12 Residual story displacement of building subjected to series of aftershock subsequent to the a) Mainshock_1 b) Mainshock_2 c) Mainshock_3 d) Mainshock_4 e) Mainshock_5 f) Mainshock_6 g) Mainshock_7 h) Mainshock_8

Table 4.6 Top storey displacement (mm) for different numbers of aftershocks

	Aftersh ock_1	Aftersh ock_2	Aftersh ock_3	Aftersh ock_4	Aftersh ock_5	Aftersh ock_6	Aftersh ock_7
Mainshock_1	2.12	3.33	7.43	11.25	14.36	19.63	19.46
Mainshock_2	3.74	5.60	10.76	16.79	22.10	31.35	43.49
Mainshock_3	1.72	3.39	8.18	12.85	16.89	23.13	24.86
Mainshock_4	3.25	4.95	9.80	15.18	19.93	26.90	32.27
Mainshock_5	2.97	4.39	8.90	13.60	17.68	23.98	26.71
Mainshock_6	1.24	2.44	6.60	10.30	13.19	18.22	17.81
Mainshock_7	3.59	5.30	10.16	15.73	20.64	27.95	31.59
Mainshock_8	1.69	3.19	7.81	12.30	16.11	22.09	22.64

Fig. 4.12 shows a few typical plots of the variation of the residual storey displacements along the height of the 4 storey MRF after the mainshock and every aftershock. It is seen from the figure that the residual storey displacement increases with the number of aftershocks. Further, the increase in the residual displacement after each aftershock depends upon the PGA value of the aftershock as evident from Table 4.6. The increase in the residual displacement with the number of aftershocks is apparently due to the formation of more numbers of plastic hinges and more rotations in the plastic hinges, as the number of aftershocks is increased (see Fig. 4.11).

The top floor displacement and ground storey inter-story drift ratio of 4-storey building subjected to the series of seismic sequence is shown in Fig. 4.13 and 4.15 respectively. Till the second aftershock, the residual displacement or drift is negligible (cannot be perceived in the visual inspection). The buildings will remain safe, and with repairs and retrofit, the building can be reoccupied. The residual inter-story drift ratio increases with each aftershock. This is also attributed to the formation of extra hinges during the third aftershock, where there is a reduction in the moment carrying capacity of the beams and large hinge rotations are observed at the plastic hinges. It is observed that for the third aftershock the transient MIDR is more than 1.5%, i.e., the damage level of the building is in life safety zone. At the end of the third aftershock, hinges were observed only at the column bases of the ground storey.

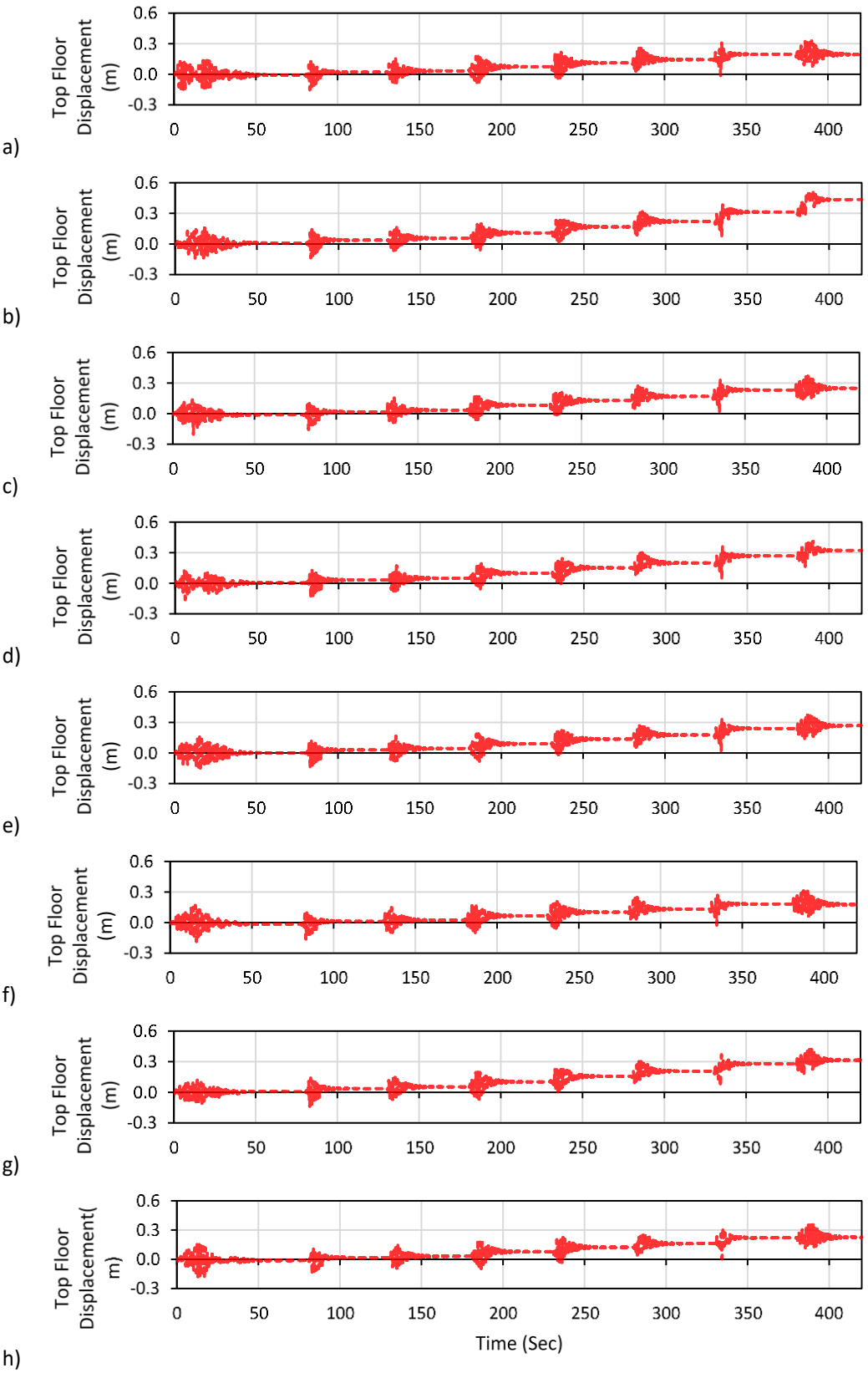

Fig. 4.13 Top floor displacement variation with time of building subjected to series of aftershock subsequent to a) Mainshock_1 b) Mainshock_2 c) Mainshock_3 d) Mainshock_4 e) Mainshock_5 f) Mainshock_6 g) Mainshock_7 h) Mainshock_8

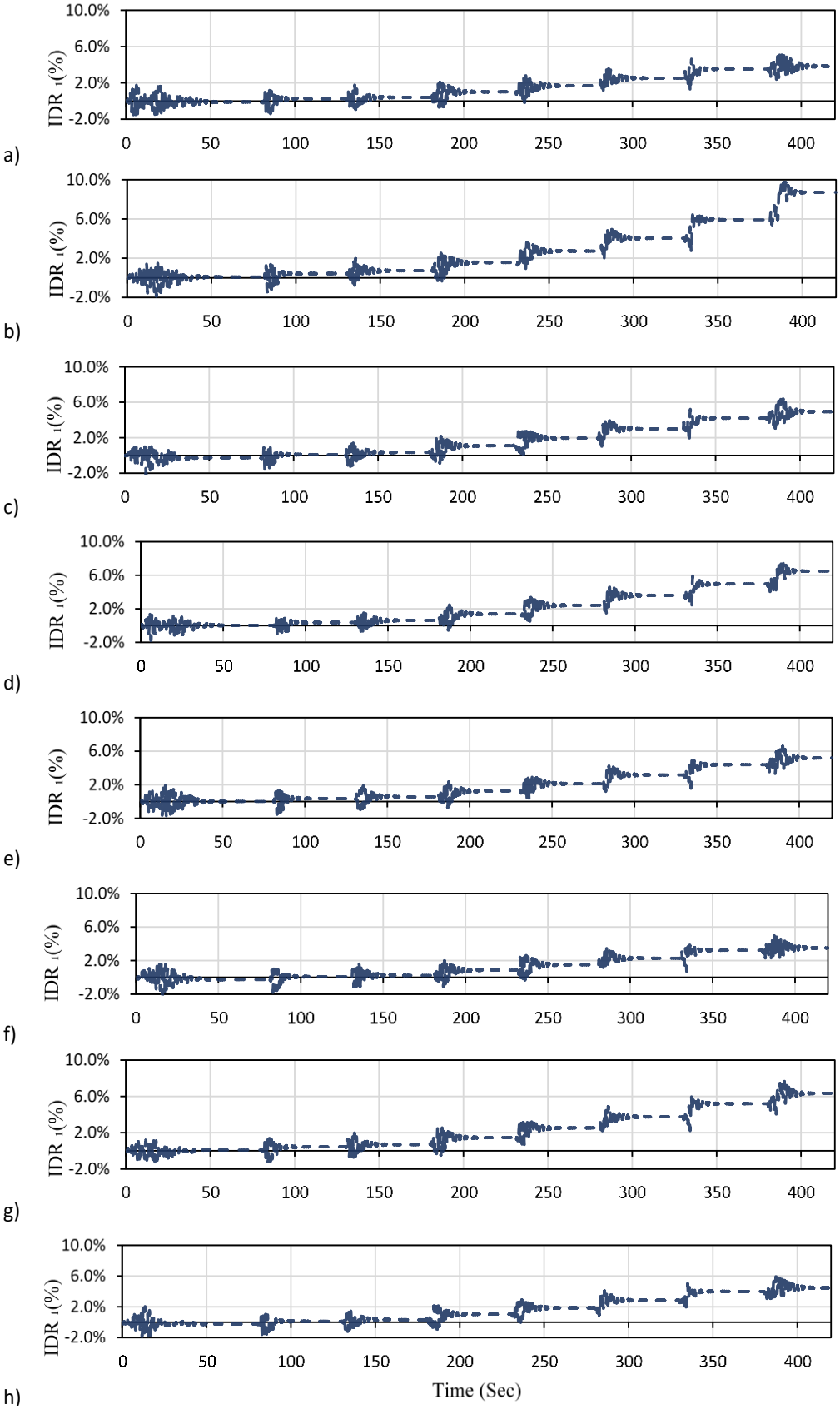

Fig. 4.14 Inter story drift ratio variation with time for ground story of the building subjected to series of aftershock subsequent to a) Mainshock_1 b) Mainshock_2 c) Mainshock_3 d) Mainshock_4 e) Mainshock_5 f) Mainshock_6 g) Mainshock_7 h) Mainshock_8

Figs 4.15 to 4.17 show the variations of MIDR, RIDR and residual storey displacements along the heights of the three MRFs (4,8 and 12 storey) after the mainshock-aftershock sequence, side by side, for the sake of comparison. For the purpose of illustration, the aftershocks are applied to the 4th mainshock of the ensemble of 8 mainshocks. The pattern of variations of the MIDR along the height of the three buildings is different. For the 12-storey frame, which fails after 3 aftershocks, the effects of the first two mainshocks are not large, and except for the top two storeys, other storey MIDRs are quite comparable. After the third aftershock, the MIDR of the first storey becomes excessively large compared to other storeys. For the 8-storey frame, the MIDRs are nearly uniform over the middle portion of the frame. Further, the polarity of the MIDRs of the first aftershock is opposite to that of the mainshock. Note that both 4 and 8 storey frames do not collapse after the entire- sequence of the mainshock-aftershock although MIDR at the first storey level exceeds the permissible limit specified by the FEMA recommendation.

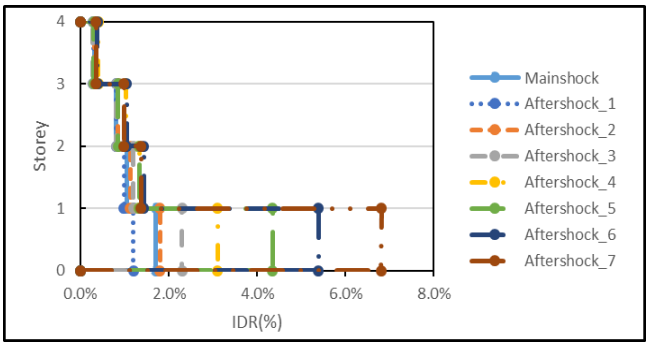

4 Storey building frame

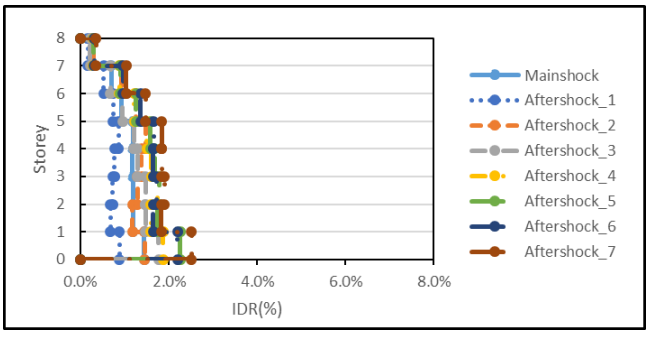

8 Storey building frame

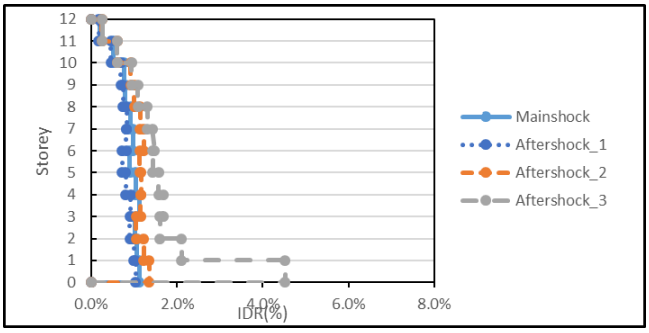

12 Storey building frame

Fig. 4.15 Average Maximum transient inter-story drift ratio for different series of seismic sequence

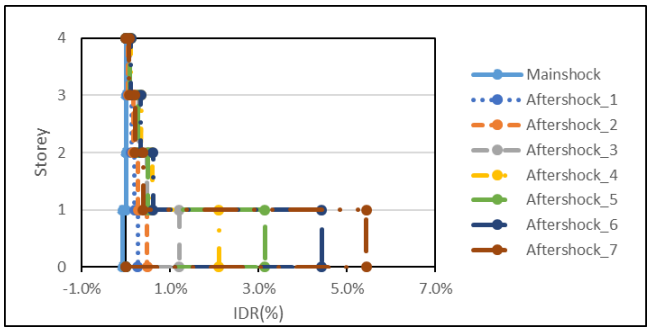

4 Storey building frame

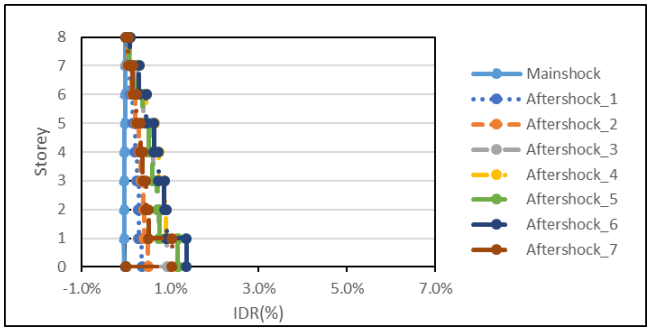

8 Storey building frame

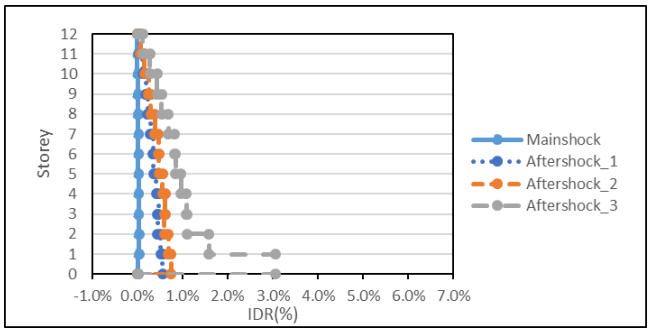

12 Storey building frame

Fig. 4.16 Average residual inter-story drift ratio for series of seismic sequence

Moreover, it is seen from the figures that MIDR at the first storey level is maximum for the 4-storey frame. Formation of the plastic hinges in the 8 (after the 7th aftershock) and 12 (after the 3rd aftershock when it fails) storey frames are shown in Fig. 4.18 and 4.19. It is seen from Fig. 4.11, 4.18 and 4.19 that the numbers of plastic hinges formed in the 4 and 8 storey frames are less as compared to the 12-storey frame. Note that the numbers of hinges formed in the 12-storey frame are shown after the 3rd aftershock. The failure is caused due to the formation of sufficient number of plastic hinges.

It is seen from Fig. 4.15 that the variations of the RIDR for the three frames follow nearly the same pattern as those of the MIDR. Although RIDRs are smaller than MIDRs, the RIDRs are significant, and they exceed the limits provided by the FEMA 355f for 4 and 12 storey frames at the first storey level.

In Fig. 4.17, the variations of the maximum story displacements with height are shown for the three frames. It is seen from the figure that the patterns of variations of the maximum story displacements are different for the three frames. For the 8 and 12 storey frames, the maximum story displacements in the first aftershock are greater than those of the mainshock. After the second, the maximum story displacements continuously increase with each aftershock; for the 4 and 8 story frames, the increase in the displacement after each aftershock is comparable. For the 12-storey frame, the increase in the displacement disproportionally changes compared to the first and second shocks. This is due to the fact that the frame collapses at the third aftershock. Further, it is seen that the increase in the maximum story displacement at each aftershock increases with the height of the storey for the 8 and 12 storey frames; the increase is significantly large toward the top storey. For the 4-storey frame, this increase is relatively uniform starting from the first storey of the frame. The reason for this difference is attributed to the pattern of the formation of plastic hinges in the frame. It is seen from Fig. 4.11, 4.18 and 4.19 that the spread of plastic hinges is more uniform for the case of 4 storey frame as compared to the 8 and 12 storey frames.

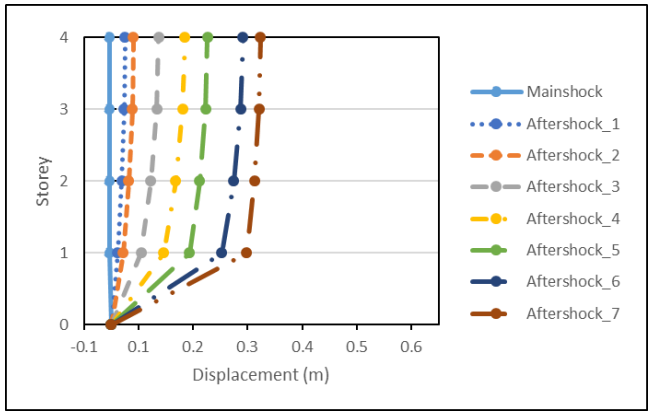

4 Storey building frame

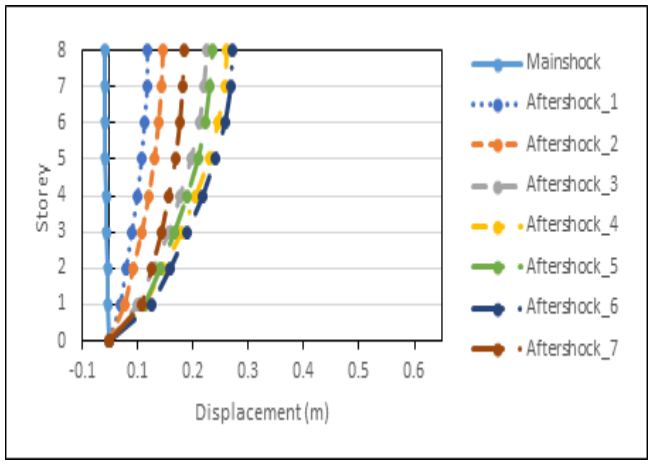

8 Storey building frame

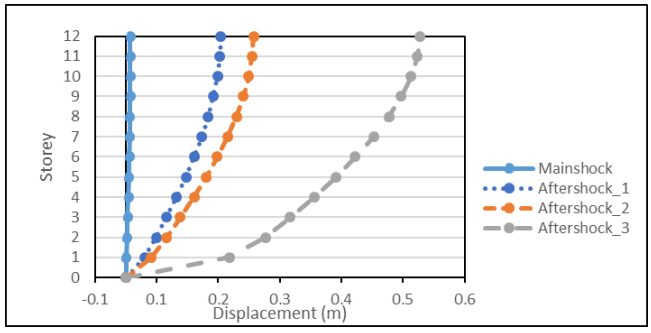

12 Storey building frame

Fig. 4.17 Average residual story displacement for a series of seismic sequence

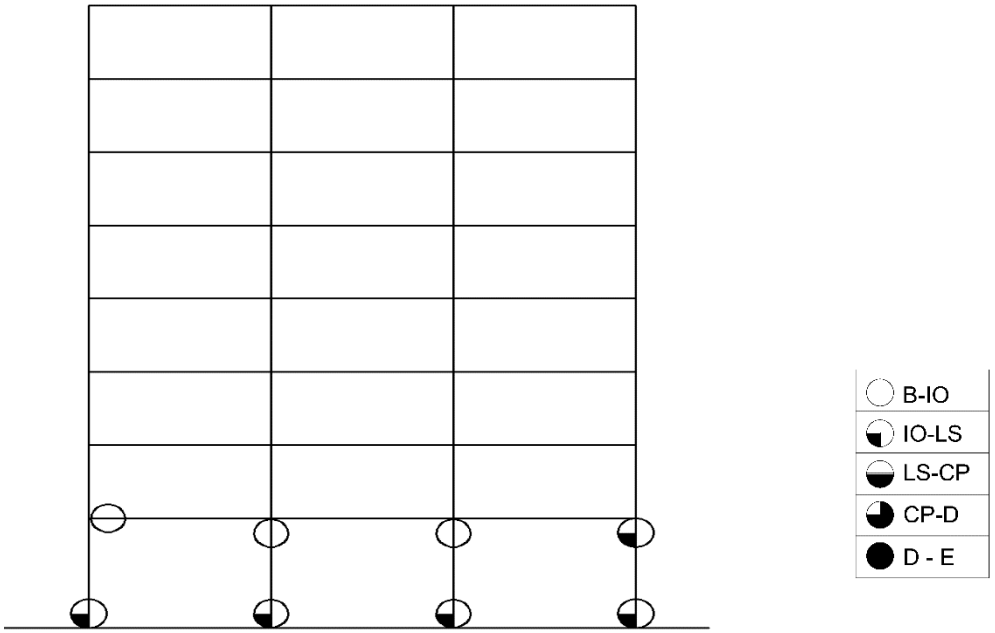

Fig. 4.18 spread of hinges for 8-storey building frame after 7th aftershock

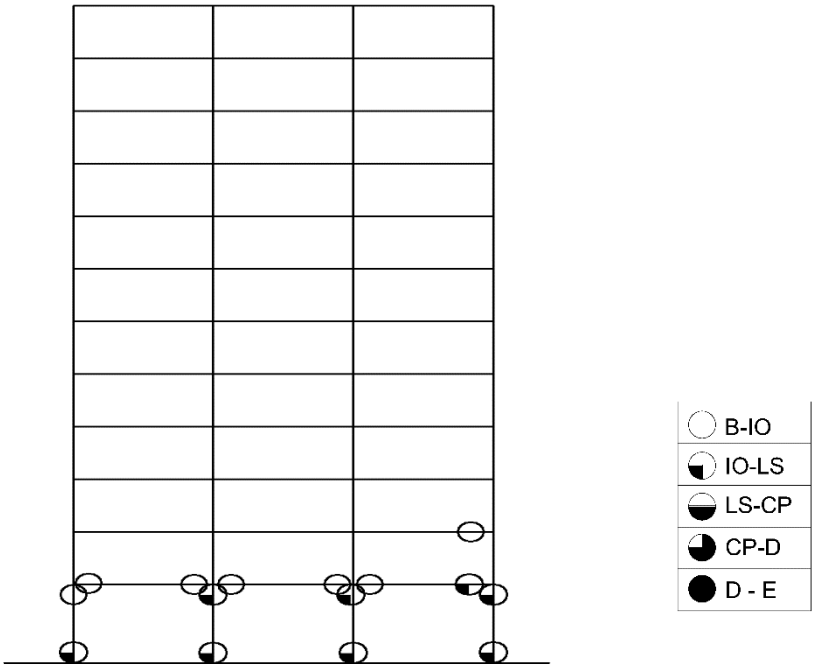

Fig. 4.19 Spread of hinges for 12 storey building frame after 3rd aftershock

4.4 CONCLUSION

Effects of aftershock on the moment resisting frames are investigated by subjecting the frames to a simulated sequence of mainshock and aftershock events.

The artificially generated ground motions compatible with the Indian standard response spectrum are used to simulate the sequences of the mainshock and aftershocks. For the study, the low rise (4-storey), medium rise (8-storey) and high rise (12-storey) frames are considered, designed according to the Indian standard earthquake design practice for a PGA value as the average PGA of mainshocks. Nonlinear time history analysis of the frames is carried out for the sequence of mainshock and aftershock events. The behaviors of the frames are investigated after each episode by studying the residual story displacement, maximum inter-story drift (both transient, MIDR, and residual, RIDR) and number of plastic hinges. The results of the numerical study lead to following conclusions:

- Damages (indicated by the MIDR, RIDR, and number of plastic hinges) caused by aftershocks could be significant and should be accounted for in the seismic design of structures; the present codes do not have this provision in explicit form.
- Damages increase significantly with the number of aftershocks as it would be expected; they increase with the height of the building also.
- Damages caused up to two aftershocks may not be significant; after that, they become significant indicating the necessity of retrofitting.
- For the high-rise buildings, the collapse may take place at a less number of aftershocks; in the present case of the 12-storey frame, the collapse took place at the third aftershock.
- For the low and medium rise buildings, after the third aftershock, the maximum inter-story drifts (both MIDR and RIDR) are found to exceed the limit proposed by FEMA.
    - With more number of aftershocks, the increase in MIDR and RIDR at the first storey level is much greater compared to the other storeys; it is not very significant at the upper levels. This feature is more pronounced for the low-rise frame (4-storey).

CHAPTER-5
PERFORMANCE OF RETROFITTED BUILDING UNDER THE SEQUENCE OF MAINSHOCK AND AFTERSHOCKS

5.1 INTRODUCTION

In the previous chapter, it is observed that the 12-storey building frame designed according to the seismic designed code could not withstand the expected number of aftershocks. These observations attracted the attention of researchers to develop good retrofitting techniques which could allow structures to withstand earthquakes episodes, including mainshock- aftershock events, more effectively. Further, they extended their researches to provide alternate effective retrofitting strategies to upgrade a damaged structure or an inadequately designed structure. Seismic Retrofitting is defined as "judicious modification of the structural properties of an existing building in order to improve its performance in a future earthquake" (Wyllie 1983). Several techniques such as the local modification of components, removal or reduction of existing irregularities, global structural stiffening, global structural strengthening, mass reduction, seismic isolation and installation of energy dissipation devices are currently available to retrofit and strengthen buildings (ASCE 41-13 2014). Addition of new structural elements such as structural walls or steel braces, and selective strengthening of deficient structural elements such as the use of concrete or steel jackets and fibre reinforced polymers are the two popular retrofitting approaches to upgrade the seismic performance of existing structures (Li et al. 2009; Di Sarno and Elnashai 2009).

Among several global seismic retrofit techniques, the bracing system is widely used to strengthen the steel moment resisting frames (MRFs) as well as the reinforced concrete framed structures (Di Sarno and Elnashai 2006, 2009; Youssef et al. 2007). Moment resisting frames are not efficient in resisting sequences of earthquakes (the sequence of the mainshock aftershocks) for tall steel buildings (such as more than 10 storey MRFs). The diagonal bracings are often used to brace steel frameworks to maintain lateral drifts within acceptable limits (Liang et al.

2000). The buildings retrofitted using steel braces have higher strengths and stiffnesses than those retrofitted with energy dissipation devices (Tena-colunga and Vergara 1997). Higher stiffness significantly reduces both deformation and acceleration demands of the structure during an earthquake. Tremblay (2002) observed that hollow bracing members were efficient in providing the required ductility during the seismic excitation.

Most of the above studies focused on the performance of retrofitted structures to withstand a single earthquake episode (the mainshock). In this Chapter, the performance of a retrofitted 12-storey building frame during the mainshock-aftershock sequence is evaluated. The 12-storey steel building frame is retrofitted with the X-bracing in order to withstand a mainshock and several aftershock sequences. The bracings made of hollow sections are used in order to investigate its advantage in terms of the performance of the building during the seismic sequence. The performance is measured in terms of transient maximum inter-storey drift ratio, residual inter-storey drift ratio, transient maximum storey displacement and residual top storey displacement. The sizes and locations of bracings are varied to evaluate the efficiency of the bracing system. Further, both an iterative technique and a genetic algorithm (GA) based optimization technique are used to effectively retrofit the building frame for upgrading the seismic performance of the 12-storey building frame for the considered mainshock-aftershock seismic sequence.

5.2 METHODOLOGY

The 12-storey building frame considered for retrofitting is shown in Fig. 5.1. The building frame is retrofitted with Hollow Steel Section (HSS) as a preventive measure. For the initial study, an iterative method is used to select the locations of the cross bracings. The HSS member in a bay is selected such that the cross-sectional area of the member is much less (less than 15%) as compared to those of the column and beam sections. This is adopted to ensure that the strength of bracing members is less than that of the adjoining beams and columns. The low cross-sectional area also confirms that the foundation of the original structure

supports the increased mass of the structure. The lower strength of the braces does not drastically affect the stiffness of the MRF. Moreover, a lower strength of bracing members also ensures that the yielding first occurs in the braces rather than in beams or columns. Out of the different bracing configurations available in the literature, X-bracing is selected for the study. A typical X-bracing is shown in Fig. 5.1. The X-braces are confined in the central bay of the building frame. The locations of bracings can be decided by a) an iterative technique and b) an optimization technique. Both methods use the nonlinear time history analysis (NTHA) of the frame structure. The NTHA is performed for a long-time history of ground motion connecting all the aftershocks with the mainshock. Analysis for the aftershock duly considers the deformed configuration of the structure as the initial state. The method of constructing the time history is the same as discussed in section 4.2.

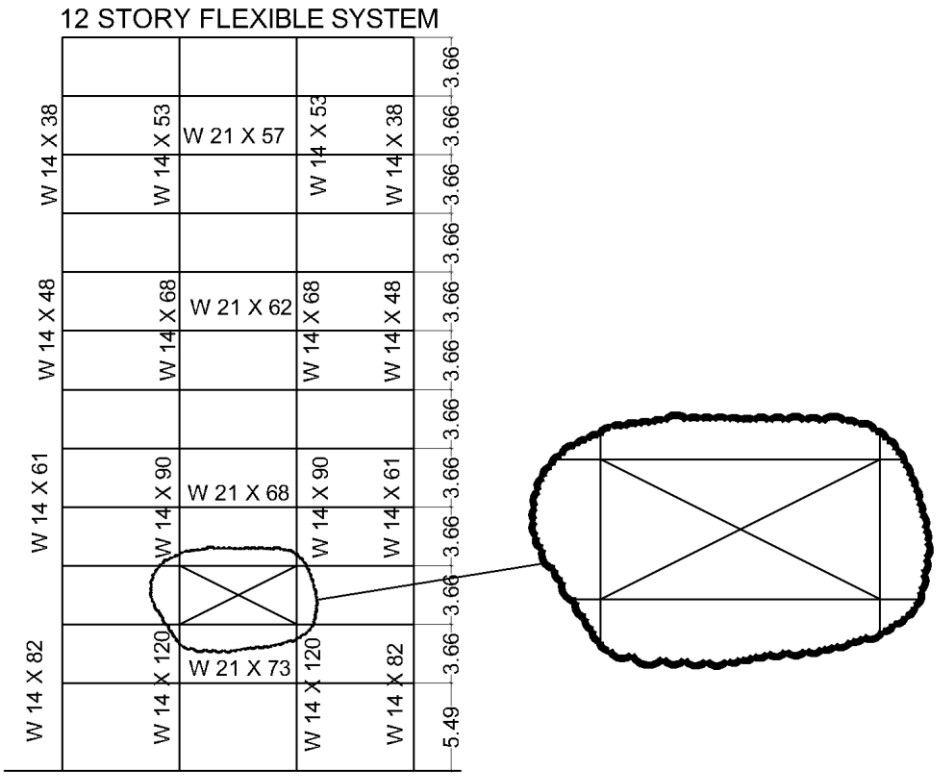

Fig. 5.1 Building Frame considered for retrofitting

5.2.1 ITERATIVE METHOD

Three different sizes of HSS are used as a bracing member. Should the building frame require retrofitting is decided based on its nonlinear time history

response to the generated long -time history record of ground motion as described before. the placement of braces is based on controlling the transient maximum inter-storey drift ratio and residual inter-storey drift ratio to the state of immediate occupancy level (IO). If the responses are such that they are below IO level, then the building frame is not retrofitted else, it is retrofitted. If the original building

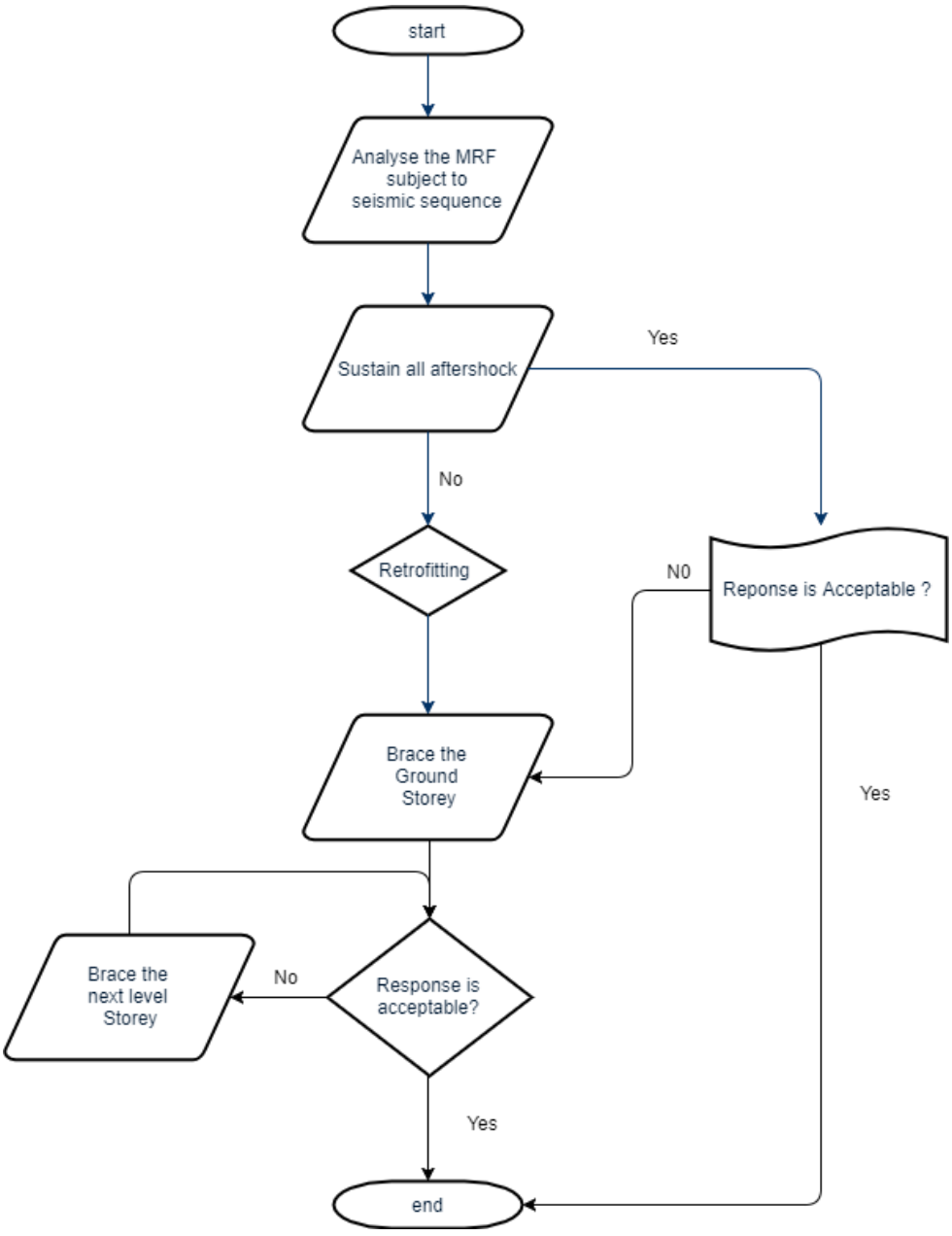

Fig. 5.2 Flow chart for iterative retrofitting technique

frame fails to satisfy limits on the responses imposed, then it is first retrofitted with cross braces in the ground storey. Once the building frame is fitted with braces in the ground storey, then the building frame is again subjected to the same long -

time history of ground motion and responses are evaluated. If the responses of building frame are beyond the limits considered, then the next story is retrofitted. The process is continued until the nonlinear time history responses are within the acceptable limit. The limit on both transient maximum inter-storey drift ratio and residual inter-storey drift ratio to fix at IO level is in conformity with FEMA 355f. Fig. 5.2 shows a flow chart of the iterative process involved in retrofitting.

5.2.2 OPTIMIZATION METHOD

The bracing locations can be optimized using a genetic algorithm (GA). The GA is also an iterative process; details on genetic algorithm are discussed in section 3.2.3. Since optimization of multi-objective functions is intricate and highly time-consuming in the GA, optimization of a single objective function is attempted here.

Since the optimization with multi objective functions is intricate and highly time consuming in the GA, a single objective optimization technique is attempted here. The roof displacement is considered as the single objective function. Using the GA, the roof displacement is minimized under the constraint that the transient maximum inter-story drift ratio and residual inter-story drift ratio remain within the specified limit. The location of the bracing is considered as a state variable. The location vector consists of zeros and ones. Zeros are representing that the bay is not braced and one represents that the bay is braced with hollow steel sections. The constraint of the optimization is taken as the number of bracing required to keep the transient maximum inter-story drift ratio and residual inter-story drift ratio within IO level. The problem is solved using a GA toolbox in MATLAB and SAP 2000. The application program interface (API) of SAP2000 with MATLAB is exploited to achieve the same. One of the pitfalls of the API is that hinge locations and property can't be provided through it in the SAP2000. This is overcome by initially providing braces of desired property in all the bays of the frame with desired hinge properties at the desired locations using the graphical user interface of the SAP 2000. The frame with bracing and hinge properties are saved and the GA toolbox of MATLAB is extended with an initial choice taken as saved properties of the frame. The NTHA is performed at each stage to find the transient

maximum inter-storey drift ratio and limit imposed on it is checked. Optimized locations of the bracing members are achieved by putting the zeros in the state variable where the bracings are deleted.

5.3 NUMERICAL RESULTS

The designed MRFs have varying section sizes along the height. Thus, the distribution of the mass and stiffness along the height is nonuniform. Details of the frame are shown in Fig. 5.1. Time periods for the first, second, and third modes of vibration are 2.60secs, 0.91secs and 0.53 secs respectively. The dynamic properties of the frame are discussed detail in section 4.3. Three hollow steel sections, namely, HSS 3X0.250, HSS 4X0.250 and HSS 5X0.250 are chosen for retrofitting. The properties of the sections are also given in Table 5.1. Each of the hollow sections is used as braces, and the responses of the retrofitted building frame are evaluated in terms of transient maximum inter-storey drift ratio and residual inter-storey drift ratio. For the present study, the mainshock-aftershock sequence is taken as the same as that of the sequence considered in the previous chapter. The mainshock considered in the study is the first mainshock and seven aftershocks used in the previous chapter. The time series of the mainshock is shown in Fig 4.5a. The aftershocks considered are shown in Fig 4.6 a-g. The peak ground acceleration (PGA) of the mainshock considered is 0.394g and the PGA of the aftershock varies from 0.289g to 0.410g with mean PGA as 0.34g. Details of mainshock and aftershock are presented in the previous chapter. It was observed in chapter 4 that the un-retrofitted building collapses after 3 aftershocks for the sequence of mainshock-aftershock considered here. It is retrofitted using the stiffness bracing comprising of hollow cross-sections shown in Table 5.1.

Table 5.1 Hollow steel section properties

Section Name	HSS3X0.250 (SEC-I)	HSS 4X0.250 (SEC-II)	HSS 5X0.250 (SEC-III)
Outer Diameter (cm)	7.62	10.16	12.7
Wall Thickness (cm)	0.635	0.635	0.635
Cross sectional Area (cm^2)	13.10	17.81	22.52
Moment of Inertia (cm^4)	811.7	2044	4137

5.3.1 SIMPLE ITERATIVE SCHEME

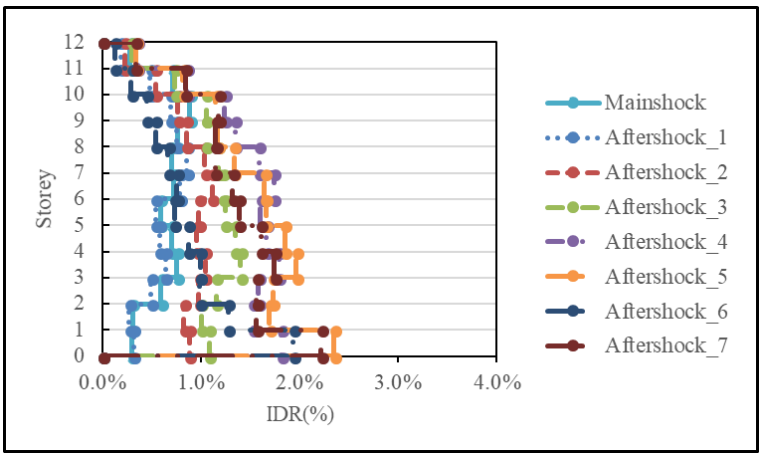

Fig. 5.3 Maximum Inter-storey drift ratio after each aftershock.

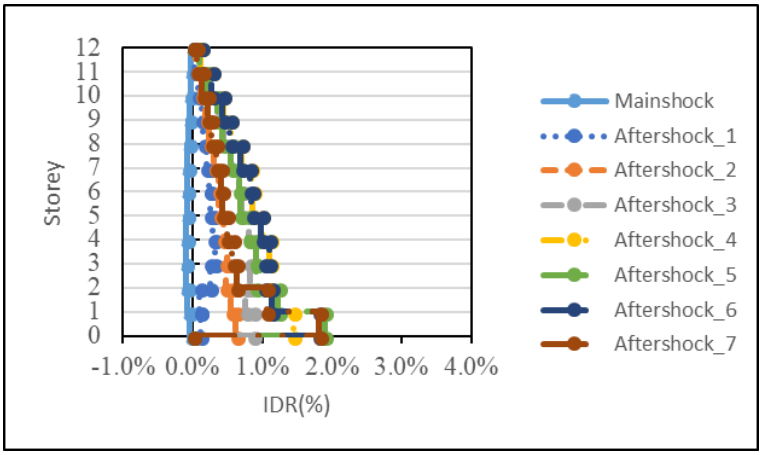

Fig. 5.4 Residual inter-storey drift ratio after each aftershock for HSS3X0.250

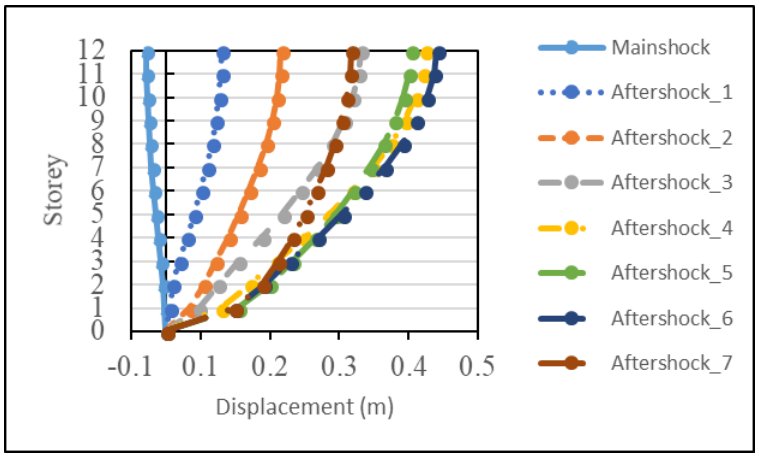

Fig. 5.5 Residual storey displacement after each aftershock for HSS3X0.250

For the first trial, HSS3X0.250 is considered as the bracing. The retrofitted building is then subjected to a NTHA. When the bracing is placed in the bottom storey only, then the test frame fails after four aftershocks. The retrofitted frame cannot sustain all the aftershocks. The frame is then retrofitted with bracings at the

bottom two storeys. It is seen that the retrofitted frame can withstand all seven aftershocks.

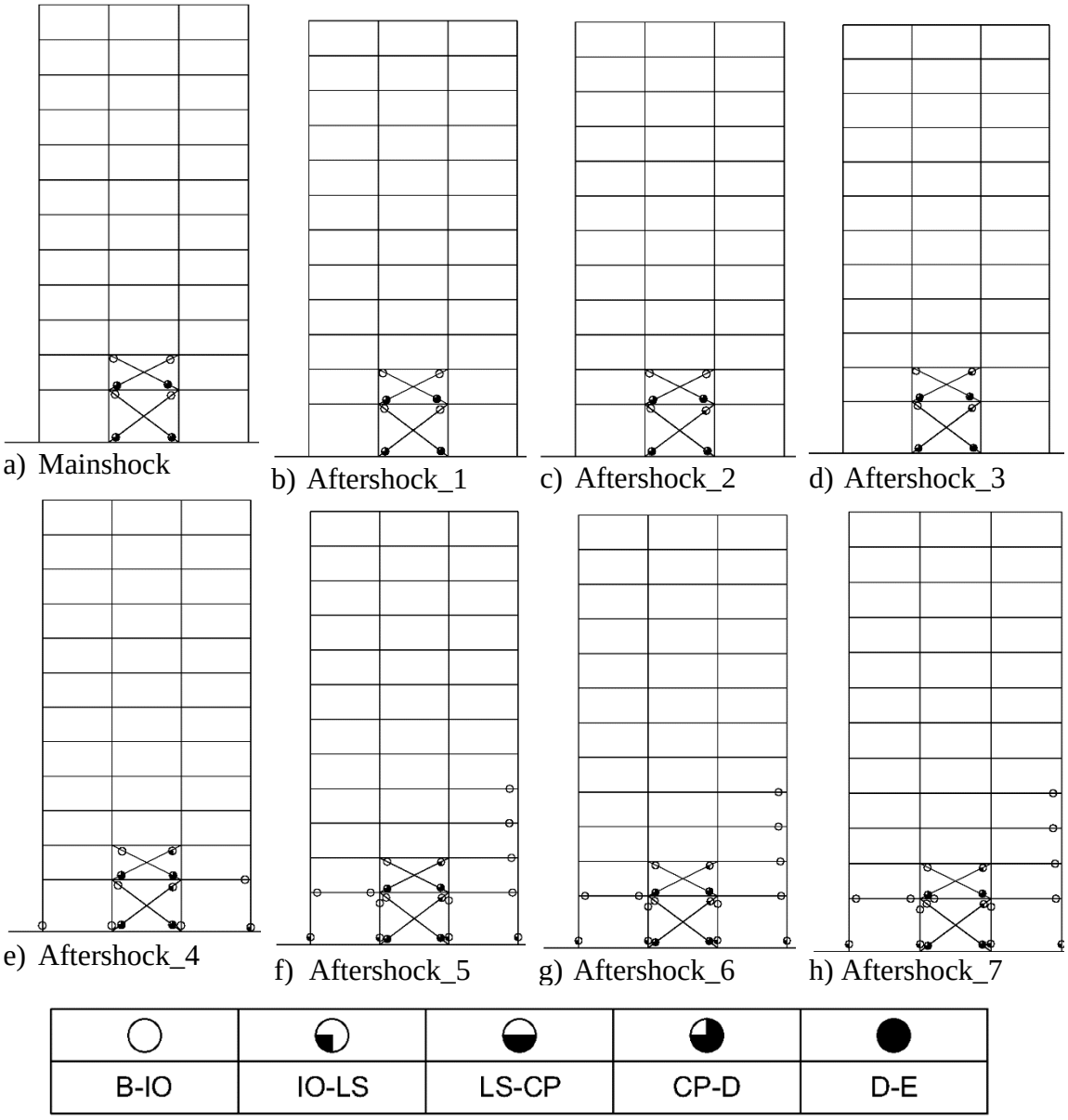

Fig. 5.6 Spread of hinges for HSS3X0.250

The variations of the transient maximum inter-story drift ratio, residual interstorey drift ratio and residual storey displacement along the height of the 12 storey MRF after the main-shock and every aftershock are shown in the figs 5.3, 5.4 and 5.5 respectively. It is seen from the Fig. 5.3 that the transient maximum inter-story drift ratio at the ground storey and fourth storey are relatively greater compared to other storeys. Further, the transient maximum inter-story drift ratio in general is more toward the bottom of the frame as it would be expected. The

same trend is observed for the residual inter-story drift ratio as shown in fig 5.4. However, the patterns of variation of the transient maximum inter-story drift ratio and residual inter-story drift ratio along the height of the frame are different.

Table 5.2 MIDR values for MRF braced with 2 HSS 3X0.250

Storey No.	Mainshock	Aftershocks						
		First	Second	Third	Fourth	Fifth	Sixth	Seventh
1	0.29%	0.31%	0.88%	1.08%	1.81%	2.35%	2.22%	2.45%
2	0.30%	0.27%	0.83%	1.00%	1.52%	1.69%	1.56%	1.71%
3	0.59%	0.49%	0.97%	1.15%	1.58%	1.73%	1.56%	1.73%
4	0.75%	0.64%	1.04%	1.40%	1.79%	1.96%	1.74%	1.93%
5	0.70%	0.58%	0.95%	1.34%	1.66%	1.85%	1.60%	1.81%
6	0.59%	0.54%	0.98%	1.24%	1.60%	1.66%	1.38%	1.67%
7	0.72%	0.78%	1.11%	1.22%	1.74%	1.64%	1.32%	1.70%
8	0.70%	0.86%	1.04%	1.17%	1.58%	1.34%	1.14%	1.56%
9	0.76%	0.75%	0.85%	1.05%	1.34%	1.17%	1.14%	1.50%
10	0.88%	0.69%	0.77%	1.05%	1.24%	1.15%	1.18%	1.45%
11	0.71%	0.48%	0.54%	0.74%	0.86%	0.81%	0.84%	0.97%
12	0.28%	0.18%	0.22%	0.29%	0.35%	0.34%	0.33%	0.39%

Table 5.3 RIDR for MRF braced with 2 HSS 3X0.250

Storey	Mainshock	Aftershocks						
		First	Second	Third	Fourth	Fifth	Sixth	Seventh
1	-0.04%	0.11%	0.63%	0.86%	1.45%	1.89%	1.81%	1.81%
2	-0.07%	0.10%	0.55%	0.76%	1.13%	1.23%	1.13%	1.06%
3	-0.09%	0.24%	0.47%	0.82%	1.04%	0.91%	1.03%	0.63%
4	-0.10%	0.31%	0.49%	0.90%	1.11%	0.90%	1.10%	0.57%
5	-0.09%	0.29%	0.44%	0.82%	0.99%	0.80%	0.98%	0.49%
6	-0.08%	0.25%	0.38%	0.71%	0.86%	0.69%	0.85%	0.42%
7	-0.08%	0.24%	0.37%	0.69%	0.84%	0.66%	0.82%	0.40%
8	-0.07%	0.20%	0.31%	0.57%	0.70%	0.55%	0.69%	0.34%
9	-0.06%	0.15%	0.24%	0.45%	0.54%	0.43%	0.53%	0.26%
10	-0.05%	0.12%	0.19%	0.36%	0.44%	0.35%	0.43%	0.21%
11	-0.03%	0.07%	0.12%	0.22%	0.28%	0.22%	0.27%	0.13%
12	-0.02%	0.03%	0.05%	0.10%	0.12%	0.10%	0.12%	0.06%

On the other hand, the residual storey displacement increases with the height; with each aftershock, the relative increase in the storey displacement toward the top increases significantly. The reason for the increase in the response quantities after each aftershock is clearly due to the formation of more number of

hinges and greater hinge rotations with increasing number of aftershocks as shown in the fig 5.6. Further, it is seen from the figure that hinges are first formed in the bracings as desired and then, they spread to the beams and columns.

Table 5.4 Maximum transient storey displacement (mm) for MRF braced with 2 HSS 3X0.250

		Aftershocks						
Storey	Mainshock	First	Second	Third	Fourth	Fifth	Sixth	Seventh
1	0.03	0.04	0.05	0.06	0.10	0.13	0.12	0.13
2	0.05	0.07	0.08	0.10	0.15	0.19	0.18	0.20
3	0.07	0.10	0.11	0.14	0.21	0.25	0.23	0.26
4	0.09	0.13	0.15	0.18	0.27	0.32	0.29	0.33
5	0.12	0.16	0.18	0.22	0.32	0.38	0.35	0.39
6	0.15	0.19	0.21	0.27	0.37	0.44	0.39	0.45
7	0.17	0.22	0.23	0.31	0.42	0.50	0.43	0.51
8	0.19	0.24	0.26	0.35	0.47	0.55	0.46	0.56
9	0.19	0.26	0.29	0.37	0.52	0.59	0.48	0.60
10	0.19	0.28	0.31	0.39	0.56	0.61	0.51	0.64
11	0.19	0.30	0.33	0.42	0.59	0.63	0.53	0.67
12	0.20	0.31	0.34	0.43	0.60	0.64	0.53	0.68

Table 5.5 Residual storey displacement (m) for MRF braced with 2 HSS 3X0.250

		Aftershocks						
Storey	Mainshock	First	Second	Third	Fourth	Fifth	Sixth	Seventh
1	0.00	0.01	0.03	0.05	0.08	0.10	0.10	0.10
2	0.00	0.01	0.05	0.08	0.12	0.15	0.14	0.14
3	-0.01	0.02	0.07	0.10	0.16	0.18	0.18	0.16
4	-0.01	0.03	0.09	0.14	0.20	0.22	0.22	0.18
5	-0.01	0.04	0.11	0.17	0.24	0.24	0.25	0.20
6	-0.02	0.05	0.12	0.19	0.27	0.27	0.29	0.22
7	-0.02	0.06	0.13	0.22	0.30	0.29	0.32	0.23
8	-0.02	0.07	0.14	0.24	0.32	0.31	0.34	0.24
9	-0.03	0.07	0.15	0.26	0.34	0.33	0.36	0.25
10	-0.03	0.08	0.16	0.27	0.36	0.34	0.38	0.26
11	-0.03	0.08	0.16	0.28	0.37	0.35	0.39	0.27
12	-0.03	0.08	0.17	0.28	0.37	0.35	0.39	0.27

Table 5.2, and 5.3 record the transient maximum inter-story drift ratio and residual inter-story drift ratio after the main-shock and after each aftershock. The transient maximum inter-story drift ratio increases with each storey for the mainshock. However, for the aftershocks there is no definite pattern observed. From the fourth aftershock, hinges are observed in the ground storey column

bases. Therefore, maximum transient maximum inter-story drift ratio is observed in the ground storey and it decreases up to the third storey. Then it again assumes a higher value at the fourth storey, after which it decreases continuously up to the top storey. The maximum value of the transient maximum inter-story drift ratio observed after the seventh aftershock is 2.45%, which is lower than the collapse prevention level. The formation of a large number of hinges in the beams and columns contributes to high inter-storey drift ratio.

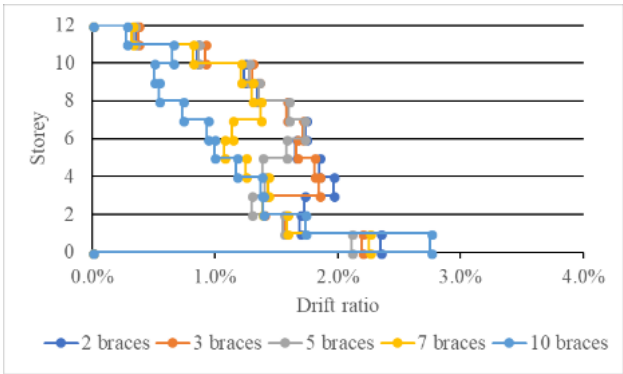

a) HSS 3X0.250

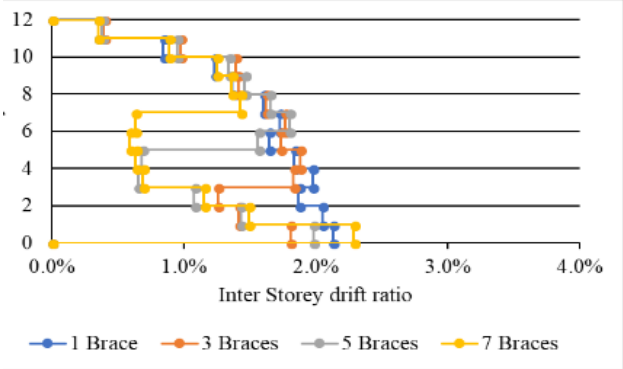

b) HSS 4X0.250

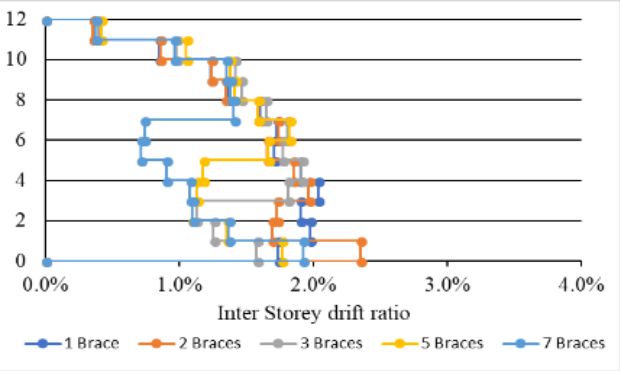

c) HSS 5X0.250

Fig. 5.7 MIDR for different number and locations of braces

From the table 5.3, it is observed that the residual inter-story drift ratio, like the transient maximum inter-story drift ratio, is very small after the mainshock. At

the third storey level, it is maximum for the first two aftershocks, and the residual inter-story drift ratio continuously increases with the number of aftershocks up to fifth aftershock. After the third aftershock, residual inter-story drift ratio is the maximum at the ground storey. This is the case because new hinges are formed during each aftershock, after the third aftershock. This results in the formation of more number of plastic hinges and rotations; consequently, the residual inter-story drift ratio increases.

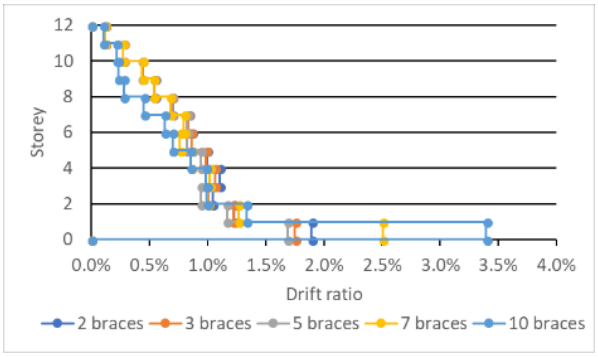

a) HSS 3X0.250

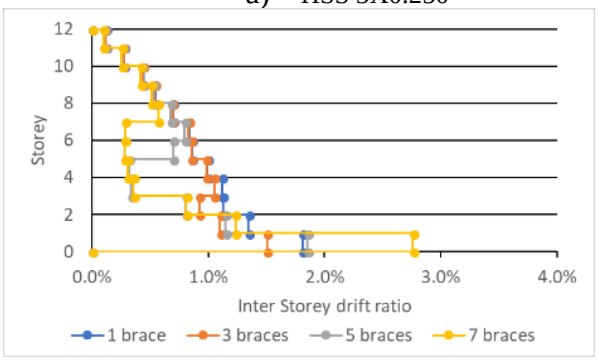

b) HSS 4X0.250

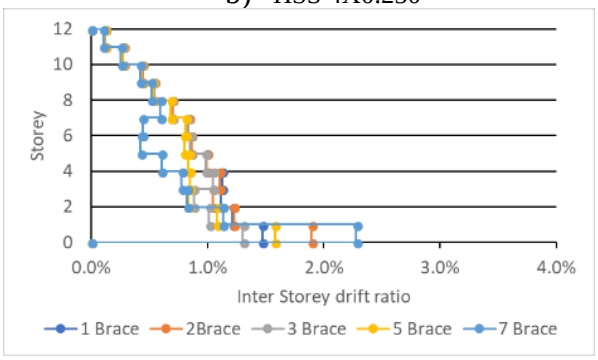

c) HSS 5X0.250

Fig. 5.8 RIDR for different number and locations of braces

Table 5.6 Maximum MIDR for HSS 3X0.250 after all aftershocks

storey	2braces	3braces	5braces	7 braces
1	2.35%	2.19%	2.11%	2.26%
2	1.69%	1.57%	1.55%	1.59%
3	1.73%	1.40%	1.30%	1.38%
4	1.96%	1.84%	1.41%	1.43%
5	1.85%	1.81%	1.38%	1.25%
6	1.66%	1.66%	1.58%	1.07%
7	1.74%	1.71%	1.73%	1.14%
8	1.58%	1.58%	1.60%	1.37%
9	1.34%	1.36%	1.36%	1.30%
10	1.24%	1.30%	1.28%	1.21%
11	0.86%	0.92%	0.87%	0.82%
12	0.35%	0.37%	0.34%	0.32%
Maximum	2.35%	2.19%	2.11%	2.26%

Table 5.7 Maximum MIDR for HSS 4X0.250 after all aftershocks

storey	1brace	3braces	5braces	7 braces
1	2.13%	1.81%	1.98%	2.29%
2	2.05%	1.41%	1.43%	1.49%
3	1.87%	1.26%	1.08%	1.15%
4	1.98%	1.83%	0.65%	0.69%
5	1.84%	1.88%	0.68%	0.63%
6	1.64%	1.73%	1.56%	0.59%
7	1.73%	1.77%	1.80%	0.63%
8	1.60%	1.62%	1.65%	1.43%
9	1.37%	1.41%	1.46%	1.36%
10	1.23%	1.39%	1.34%	1.25%
11	0.84%	0.97%	0.95%	0.89%
12	0.35%	0.39%	0.38%	0.35%
Maximum	2.13%	1.88%	1.98%	2.29%

The maximum transient storey displacement and residual storey displacement after the main-shock and after each aftershock are shown in the Tables 5.4 and 5.5 respectively. It is seen that the storey displacement increases with the increase in the number of aftershocks up to the fifth aftershock. During the sixth aftershock, the maximum storey displacement is reduced, but the maximum is observed at the end of the seventh aftershock. The residual top storey displacement is maximum after the sixth aftershock and is nearly the same for the top two storeys. The variation of the transient maximum inter-story drift ratio and maximum residual inter-story drift ratio along the storey for different numbers of braces provided at different locations are shown in Fig. 5.7the Fig. 5.7 and 5.8

respectively. It can be seen from the figures that the maximum drift (residual or transient) is highest at the ground storey. The storey just above the braced storey has more drift than the storey below. This is caused due to the sudden change of unbraced storey stiffness immediately above the last braced storey.

Table 5.8 Maximum MIDR for HSS 5X0.250 after all aftershocks

storey	1brace	3braces	5braces	7 braces
1	1.73%	1.58%	1.76%	1.92%
2	1.97%	1.25%	1.35%	1.37%
3	1.90%	1.12%	1.09%	1.09%
4	2.03%	1.81%	1.13%	1.07%
5	1.90%	1.91%	1.18%	0.90%
6	1.71%	1.77%	1.66%	0.71%
7	1.73%	1.80%	1.82%	0.74%
8	1.60%	1.64%	1.58%	1.40%
9	1.36%	1.46%	1.41%	1.38%
10	1.23%	1.41%	1.38%	1.35%
11	0.85%	0.98%	1.05%	0.96%
12	0.36%	0.39%	0.41%	0.37%
Maximum	2.03%	1.91%	1.82%	1.92%

Table 5.9 Maximum RIDR for HSS 3X0.250 after all aftershocks

Storey	2braces	3braces	5braces	7 braces
1	1.89%	1.75%	1.69%	2.51%
2	1.23%	1.22%	1.16%	1.27%
3	1.04%	1.01%	0.94%	1.00%
4	1.11%	1.06%	1.02%	1.02%
5	0.99%	0.99%	0.94%	0.86%
6	0.86%	0.86%	0.82%	0.76%
7	0.84%	0.83%	0.82%	0.80%
8	0.70%	0.70%	0.69%	0.68%
9	0.54%	0.54%	0.54%	0.54%
10	0.44%	0.44%	0.44%	0.44%
11	0.28%	0.27%	0.27%	0.27%
12	0.12%	0.12%	0.12%	0.12%
Maximum	1.89%	1.75%	1.69%	2.51%

Tables 5.6, 5.7 and 5.8 present the transient maximum inter-story drift ratio values for different number and sizes of bracings after all the aftershocks. From the table 6, it is clearly seen that there exists an optimum number of bracings which provides the minimum transient maximum inter-story drift ratio on the first floor. For the SEC-I, SEC-II and SEC-III, they are found to be 5, 3 and 5 respectively. An increase in the number of bracing beyond the optimum number increases the

transient maximum inter-story drift ratio on the first floor. The same observations hold true for the residual inter-story drift ratio, which are shown in tables 5.9 -5.11. Note that the increase in RIDR and MIDR may take place with increased number of bracings beyond the optimum number. It may happen because of the change in the mode shape with increased number of bracings and also, because of the contribution of higher modes.

Table 5.10 Maximum RIDR for HSS 4X0.250 after all aftershocks

Storey	1 Brace	3 Braces	5 Braces	7 Braces
1	1.81%	1.51%	1.85%	2.76%
2	1.35%	1.10%	1.15%	1.23%
3	1.13%	0.92%	0.81%	0.81%
4	1.12%	1.05%	0.34%	0.36%
5	0.99%	0.98%	0.32%	0.31%
6	0.86%	0.86%	0.70%	0.28%
7	0.84%	0.83%	0.80%	0.29%
8	0.70%	0.69%	0.68%	0.57%
9	0.54%	0.54%	0.53%	0.51%
10	0.44%	0.44%	0.43%	0.42%
11	0.28%	0.27%	0.26%	0.26%
12	0.12%	0.12%	0.11%	0.10%
Maximum	1.81%	1.51%	1.85%	2.76%

Table 5.11 Maximum RIDR for HSS 5X0.250 after all aftershocks

storey	1 Brace	3 Braces	5 Braces	7 Braces
1	1.47%	1.31%	1.58%	2.28%
2	1.22%	1.01%	1.08%	1.13%
3	1.11%	0.88%	0.84%	0.83%
4	1.13%	1.05%	0.85%	0.78%
5	1.00%	0.98%	0.84%	0.60%
6	0.86%	0.85%	0.80%	0.43%
7	0.84%	0.83%	0.81%	0.44%
8	0.70%	0.69%	0.68%	0.59%
9	0.54%	0.54%	0.53%	0.52%
10	0.44%	0.44%	0.43%	0.42%
11	0.28%	0.27%	0.27%	0.26%
12	0.12%	0.12%	0.11%	0.11%
Maximum	1.47%	1.31%	1.58%	2.28%

It is seen from the above numerical illustrations that with the increase in the number of aftershocks, the transient maximum inter-story drift ratio and the residual inter-story drift ratio increases. By putting more number of bracings, the transient maximum inter-story drift ratio and residual inter-story drift ratio are

controlled after each aftershock. However, With the increase in the number of bracings, more material is used for retrofitting. Therefore, a more systematic optimization procedure for bracing the frames should be adopted in place of the simple trial method presented in the previous section. An optimum retrofitting strategy based on certain performance criteria is presented in the following section.

5.3.2 PERFORMANCE BASED OPTIMUM RETROFITTING STRATEGY

In this section, an optimum placement of bracings using the GA is presented. Since multiobjective optimization technique using GA is difficult to implement, a single objective optimization procedure is adopted. The objective function is to minimize the top storey displacement with the constraint that the number of braces is not more than '*n*'. less the value of n, less is the cost of material for retrofitting. Further, for a specified value of *'n'*, the performance levels of the plastic hinge are checked. If they remain within IO - level after each aftershock up to the last aftershock, the value of 'n' is not changed. Otherwise, the value of 'n' is changed.

The objective function is formulated by the NTHA of the braced frames in SAP2000. With each population generated in the GA, the NTHA is performed in SAP2000. The state variable, which is taken as the locations of the bracings (one set of diagonal bracing) is a vector of size 36X1. The number of possible locations of placing one bracing in the frame is 36 (12storey X 3bays). The entities of the state variables are *'1'* and *'0'*, where *'1'* represents that bracing is placed at a particular location, and *'0'* represents that the bracing is not placed in that location. The constraint is that the sum of all the entities of the vector should be less than or equal to *'n'*. That means that the population generated should have no more than *'n'* entities whose values are *'1'*. The GA toolbox is used for generating the constrained generations and SAP2000 is used for the NTHA. The API of SAP2000 is employed for interacting MATLAB with SAP2000. For the numerical study of the 12-storey frame *'n'* is taken as 8 and HSS3X0.250 bracings are used.

The optimized locations for the braces are shown in fig. 5.9. It is observed that the locations of the braces do not follow any definite pattern. The bracings are

irregularly distributed over the height. The irregular distribution of stiffness along the height of the unbraced frame has led to the irregular distribution of bracings in the optimized solution. For example, the ground storey being the soft storey, two numbers of bracings appear in it. Similarly, the sixth storey being a relatively

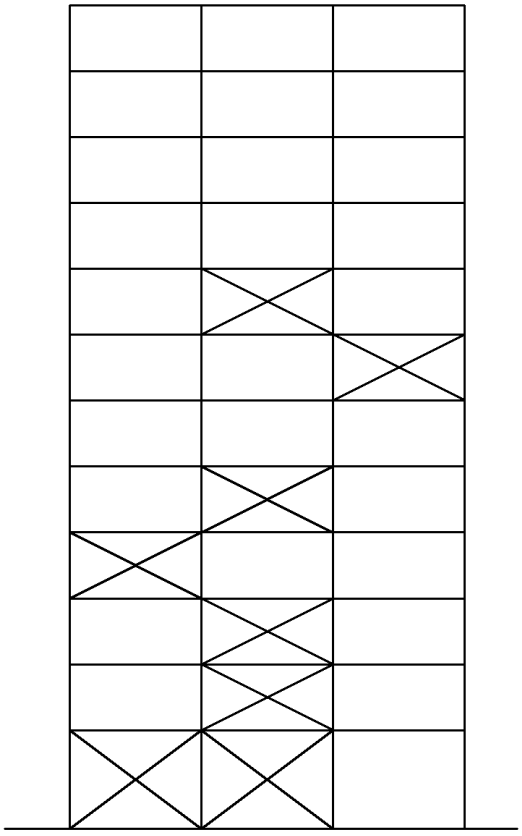

Fig. 5.9 Optimised location of braces

stiff storey, no bracing is found in that storey. For the optimized bracing pattern, the maximum top storey displacement (which is minimized) is 0.56m.

The variation of the transient maximum inter-story drift ratio and residual inter-story drift ratio along the height of the 12-story frame, retrofitted optimally, after the main-shock and every aftershock are shown in Figs 5.10 and 5.11. The transient maximum inter-story drift ratio values for the ground storey increase with the onset of aftershocks. The transient maximum inter-story drift ratio values are maximum at the first storey level for all the aftershocks and it decreases at higher storey. The residual inter-story drift ratio is the maximum at the ground storey for all the aftershocks and decreases with height. However, the patterns of the variation of the transient maximum inter-story drift ratio and residual inter-

story drift ratio look different. Fig 5.12 shows the variation of inter-storey drift ratio with time for the ground storey. It is observed that with each aftershock the transient maximum inter-story drift ratio increases. The residual inter-story drift ratio also increases.

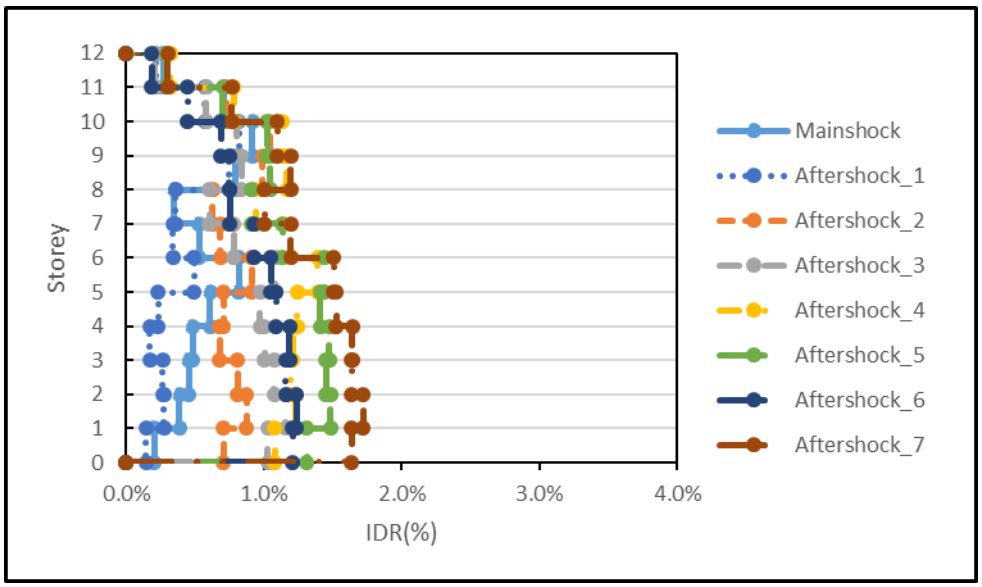

Fig. 5.10 MIDR for 12-storey MRF retrofitted with the optimised location of bracing

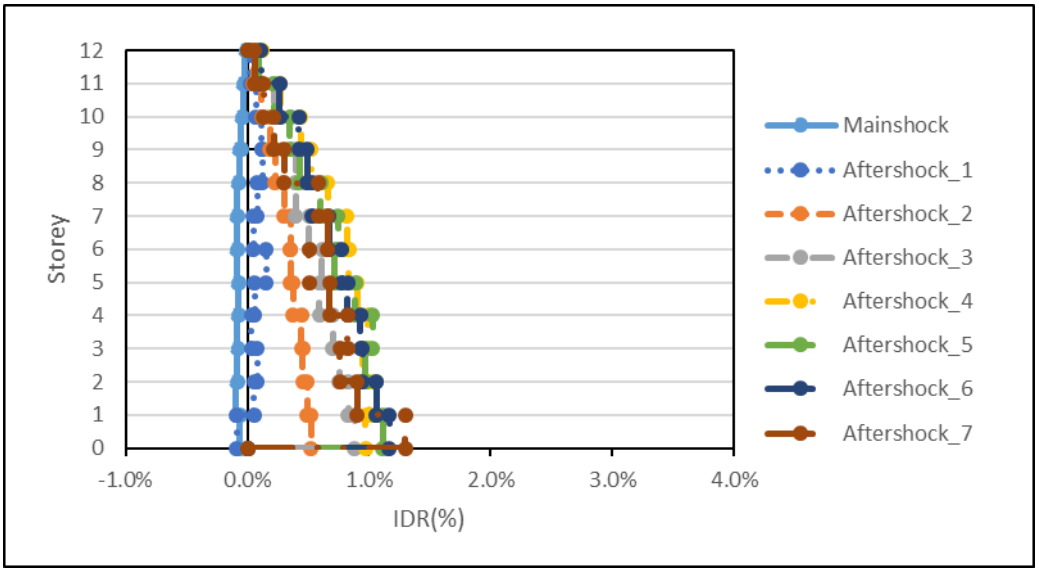

Fig. 5.11 RIDR for 12-storey MRF retrofitted with the optimised location of bracing

The variation of the residual top storey displacement along the height is shown in Fig. 5.13. The residual top storey displacement for the mainshock has opposite polarity of that of the aftershock. In other words, the residual displacement after the mainshock is opposite in direction to those of the aftershocks. It can also be observed that the residual top floor displacement after

the fourth aftershock is the maximum. The residual displacement decreases after the fourth aftershock. The variation of the top floor displacement with respect to time is shown in Fig 5.14. It can be observed that the maximum top floor displacement increases with the onset of each aftershock as it would be expected.

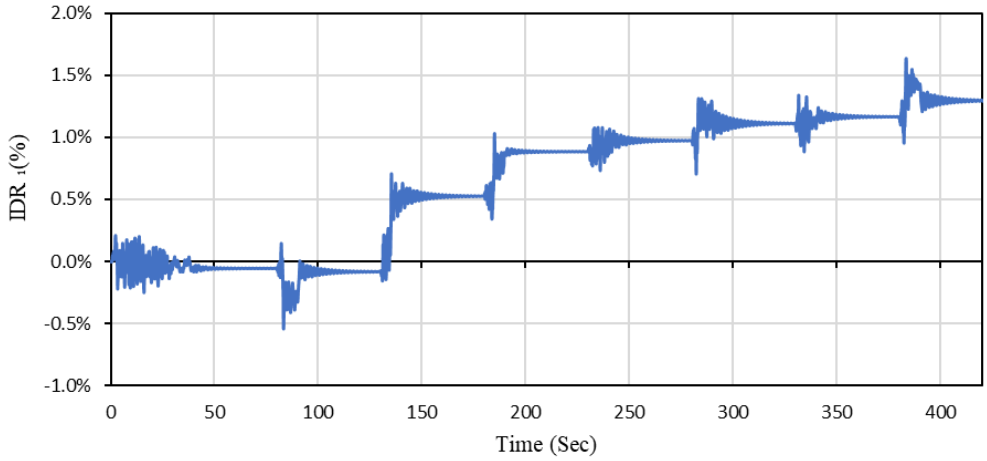

Fig. 5.12 variation of ground storey inter-storey drift ratio with time

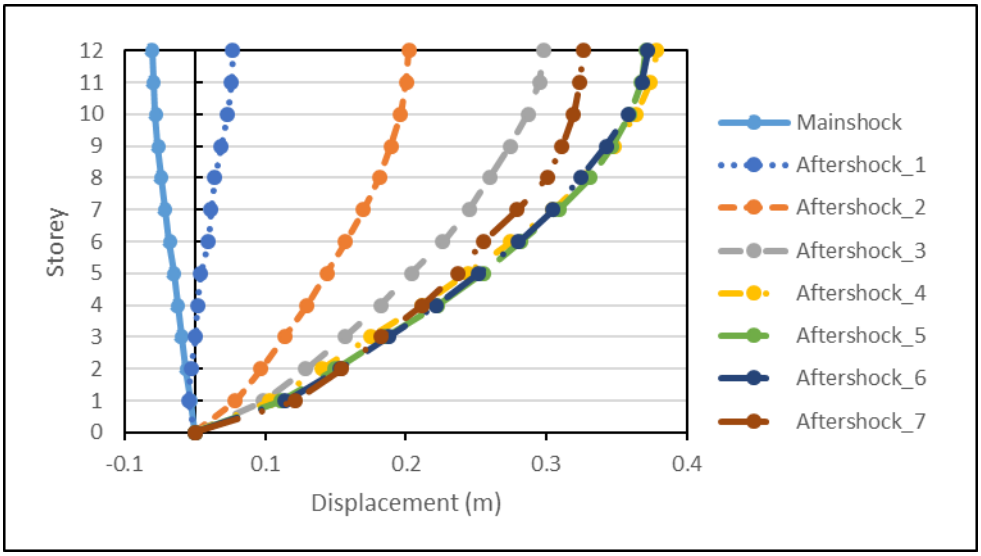

Fig. 5.13 residual top storey displacement for 12-storey MRF retrofitted with the optimised location of bracing

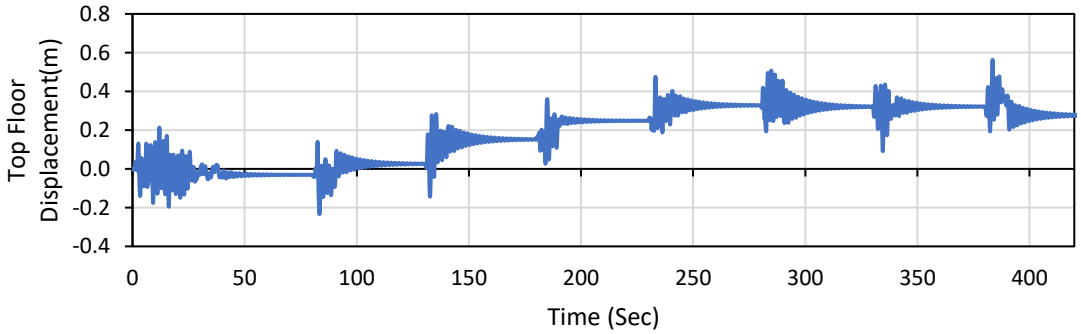

Fig. 5.14 variations of top storey displacement ratio with time

Table 5.12 MIDR values for optimally braced MRF with HSS 3X0.250

		Aftershocks							
Storey	Mainshock	First	Second	Third	Fourth	Fifth	Sixth	Seventh	N
1	0.21%	0.14%	0.71%	1.03%	1.08%	1.31%	1.34%	1.64%	
2	0.39%	0.28%	0.88%	1.16%	1.23%	1.49%	1.43%	1.72%	3,5,6,7
3	0.46%	0.27%	0.81%	1.07%	1.20%	1.45%	1.33%	1.64%	
4	0.48%	0.17%	0.68%	1.01%	1.21%	1.47%	1.30%	1.64%	
5	0.61%	0.23%	0.71%	0.97%	1.24%	1.41%	1.22%	1.53%	
6	0.82%	0.50%	0.91%	1.08%	1.39%	1.44%	1.26%	1.51%	4
7	0.53%	0.34%	0.68%	0.78%	1.15%	1.13%	1.00%	1.19%	
8	0.35%	0.36%	0.63%	0.61%	0.94%	0.91%	0.80%	1.01%	
9	0.79%	0.75%	0.99%	0.84%	1.17%	1.05%	0.98%	1.20%	
10	0.92%	0.82%	1.04%	0.80%	1.13%	1.02%	0.99%	1.10%	1,2
11	0.71%	0.57%	0.73%	0.58%	0.78%	0.70%	0.65%	0.77%	
12	0.27%	0.21%	0.29%	0.21%	0.32%	0.30%	0.26%	0.30%	

Table 5.13 RIDR values for optimally braced MRF with HSS 3X0.250

		Aftershocks							
Storey	Mainshock	First	Second	Third	Fourth	Fifth	Sixth	Seventh	N
1	-0.06%	-0.09%	0.52%	0.88%	0.97%	1.11%	1.17%	1.30%	2,3,5,6,7
2	-0.09%	0.05%	0.49%	0.83%	1.00%	1.06%	1.06%	0.91%	4
3	-0.08%	0.08%	0.46%	0.76%	0.95%	0.97%	0.94%	0.76%	
4	-0.08%	0.04%	0.44%	0.70%	0.99%	1.03%	0.93%	0.82%	
5	-0.07%	0.06%	0.38%	0.59%	0.90%	0.89%	0.82%	0.68%	
6	-0.08%	0.15%	0.36%	0.61%	0.83%	0.72%	0.77%	0.51%	1
7	-0.09%	0.05%	0.36%	0.51%	0.82%	0.75%	0.67%	0.66%	
8	-0.08%	0.08%	0.30%	0.40%	0.66%	0.61%	0.54%	0.58%	
9	-0.07%	0.13%	0.23%	0.40%	0.52%	0.43%	0.49%	0.30%	
10	-0.05%	0.12%	0.19%	0.35%	0.44%	0.35%	0.43%	0.22%	
11	-0.03%	0.07%	0.12%	0.22%	0.27%	0.22%	0.27%	0.13%	
12	-0.02%	0.03%	0.05%	0.09%	0.12%	0.09%	0.11%	0.06%	

Table 5.12, and 5.13 record the transient maximum inter-story drift ratio and residual inter-story drift ratio after the main-shock and after each aftershock for the optimally braced frame. it is seen from the table that the maximum transient maximum inter-story drift ratio occurs at the 10^{th} storey in the mainshock, but in the subsequent aftershocks the maximum transient maximum inter-story drift ratio occurs in other storeys. The last column of the table shows the number (N) of aftershock at which the transient maximum inter-story drift ratio is observed in a storey. It is observed that in four aftershocks, the transient maximum inter-story

drift ratio occurs in the second storey. This illustrates that the storey in which the transient maximum inter-story drift ratio takes could be different in the mainshock from that of the aftershocks. Further, it may be different in different aftershocks. The reason for this is attributed to the formation of plastic hinges and the relative stiffnesses of the storeys computed after the main-shock and after each aftershock. Moreover, the maximum transient maximum inter-story drift ratio of 1.72% (underlined in the table) is lower than IO-level as specified in the FEMA 355F. Table 5.13, shows the residual inter-story drift ratio after the main-shock and after each aftershock. At the end of the main-shock, residual inter-story drift ratio has opposite polarity as compared to those of the aftershocks. The rest of the observations remain the same as those for the transient maximum inter-story drift ratio.

Table 5.14 Residual storey displacements (m) for optimally braced MRF with HSS 3X0.250

		Aftershocks						
Storey	Mainshock	First	Second	Third	Fourth	Fifth	Sixth	Seventh
0	0.00	0.00	0.00	0.00	0.00	0.00	0.00	0.00
1	0.00	0.00	0.03	0.05	0.05	0.06	0.06	0.07
2	-0.01	0.00	0.05	0.08	0.09	0.10	0.10	0.10
3	-0.01	0.00	0.06	0.11	0.12	0.14	0.14	0.13
4	-0.01	0.00	0.08	0.13	0.16	0.17	0.17	0.16
5	-0.02	0.00	0.09	0.15	0.19	0.21	0.20	0.19
6	-0.02	0.01	0.11	0.18	0.22	0.23	0.23	0.21
7	-0.02	0.01	0.12	0.19	0.25	0.26	0.25	0.23
8	-0.02	0.01	0.13	0.21	0.28	0.28	0.27	0.25
9	-0.03	0.02	0.14	0.22	0.30	0.30	0.29	0.26
10	-0.03	0.02	0.15	0.24	0.31	0.31	0.31	0.27
11	-0.03	0.03	0.15	0.25	0.32	0.32	0.32	0.27
12	-0.03	0.03	0.15	0.25	0.33	0.32	0.32	0.28

The residual storey displacement along the height of the 12 storey MRF after the main-shock and every aftershock are presented in table 5.14. It is seen from the table that the residual top storey displacement for the mainshock has again the opposite polarity compared to those of the aftershocks. As expected, the residual storey displacement is maximum at the top storey for both the mainshock and aftershocks. After the third aftershock, the residual storey displacements remain nearly the same after subsequent aftershocks.

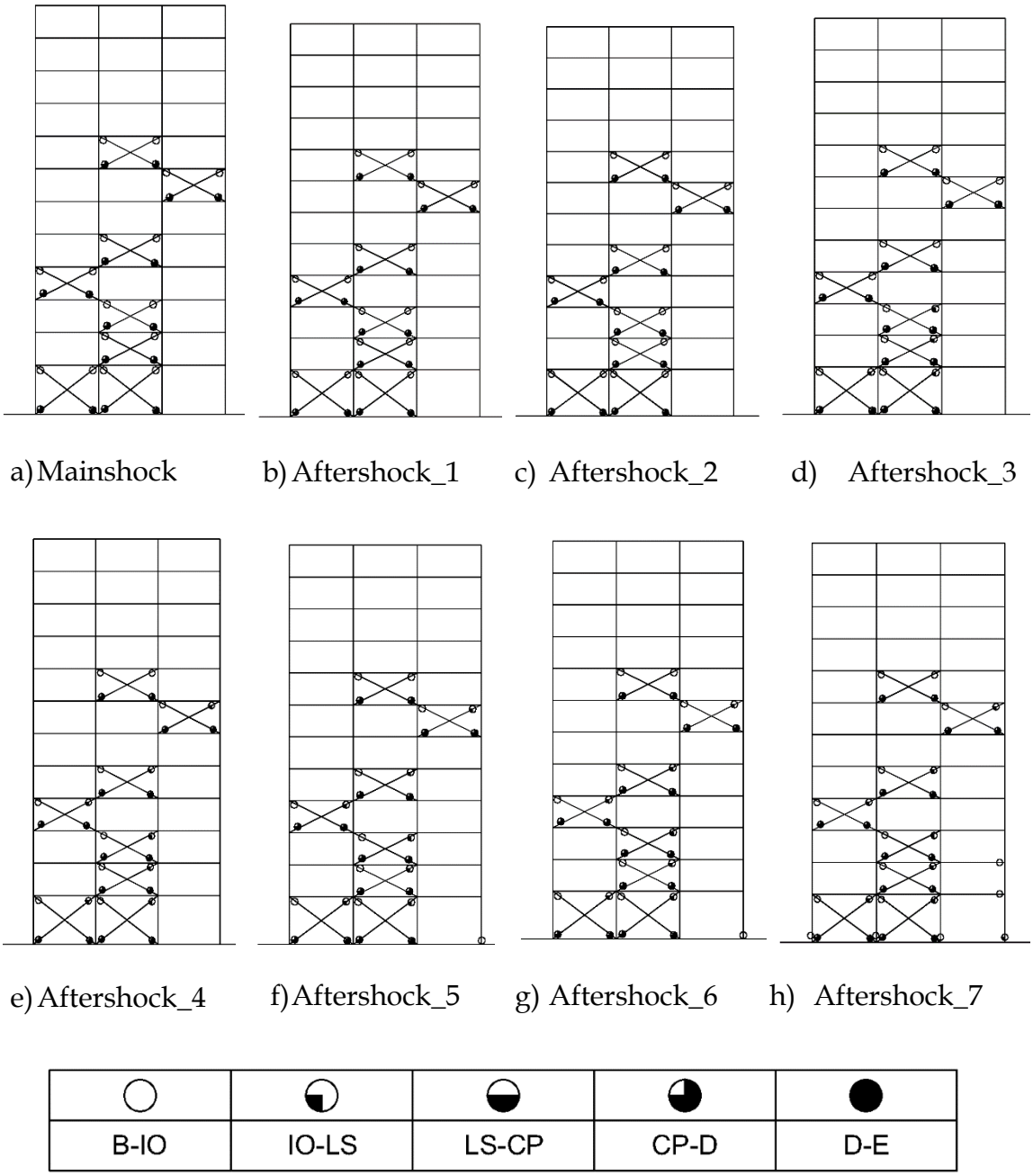

Fig. 5.15 Spread of hinges for the optimal bracing locations during the mainshock and aftershock sequence

The spreading of hinges after the main-shock and subsequent aftershocks are shown in Fig. 5.15. It can be observed from the figure that hinges are formed in braces up to the fourth aftershock. At the fifth aftershock on hinge is formed at the base of the rightmost column. During the seventh aftershock, hinges are formed in all the column bases and hinges at few beam ends are also formed. Hinges in the bracings range from IO to CP levels, while those in the beams and columns remain at IO level only. Because of the retrofitting of the frame optimally with bracings, not only the frame sustains all the seven aftershocks, but also it suffers very small

damages only in a few beams and columns. Most damages are confined to the bracings which can be easily replaced.

5.3.3 EVALUATION OF THE PERFORMANCE OF THE OPTIMALLY BRACED FRAME

In order to evaluate the performance of the optimally braced frame, four other patterns of bracings keeping the total number of bracings the same as that of the optimal pattern are considered. The patterns are shown as the case 1 to case 4 in Fig. 5.16. The optimal pattern of the bracings is shown in Fig 5.9.

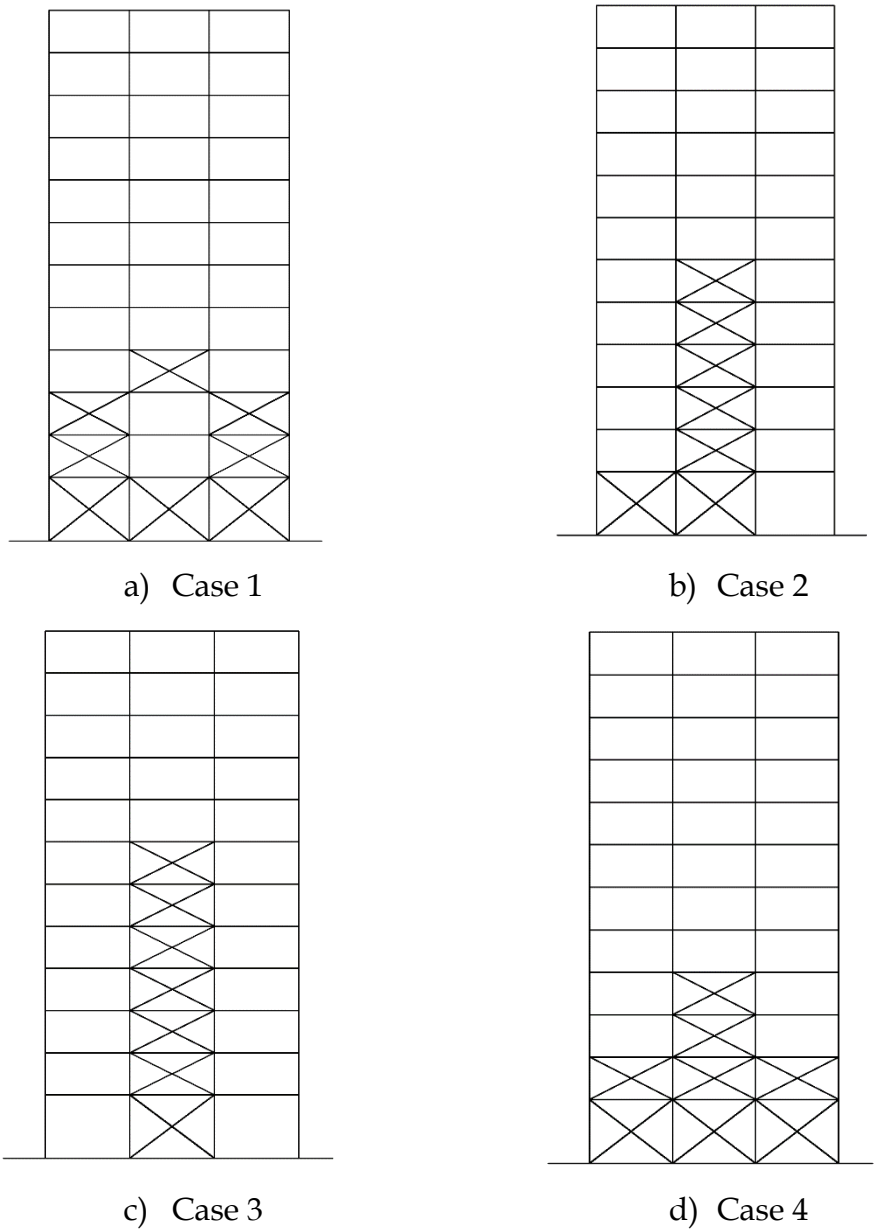

Fig. 5.16 Different configurations of bracing considered

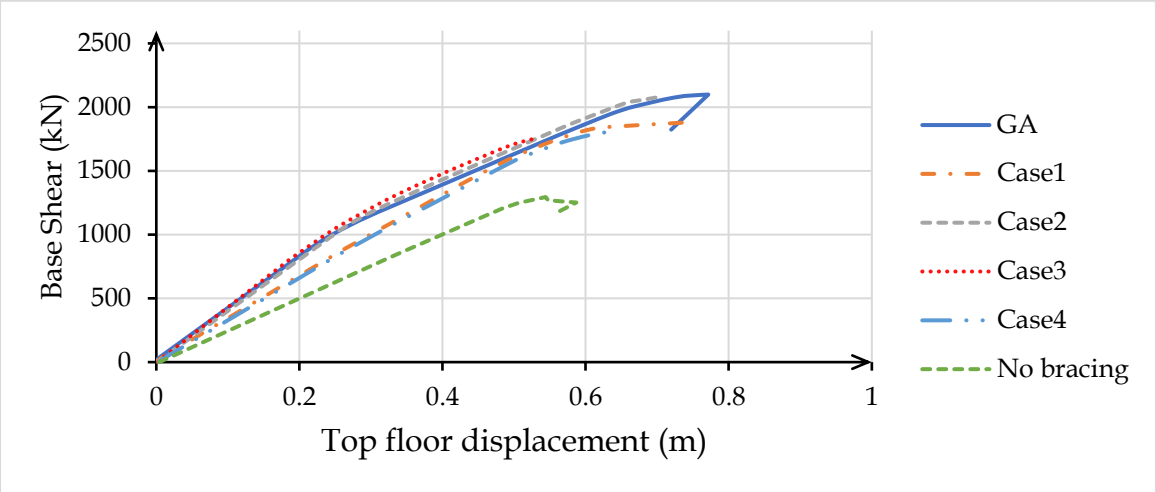

Fig. 5.17 Capacity curve for all the cases considered

Table 5.15 Maximum transient top storey displacement (m) values for different cases considered

	GA	Case 1	Case 2	Case 3	Case 4
Mainshock	0.21	0.24	0.24	0.23	0.23
Aftershock_1	0.23	0.28	0.23	0.21	0.28
Aftershock_2	0.28	0.30	0.29	0.28	0.30
Aftershock_3	0.36	0.36	0.37	0.35	0.35
Aftershock_4	0.48	0.49	0.49	0.48	0.48
Aftershock_5	0.51	0.54	0.52	0.53	0.53
Aftershock_6	0.44	0.51	0.45	0.62	0.50
Aftershock_7	0.56	0.61	0.59	0.62	0.61

Table 5.16 MIDR values for different cases considered

	GA	Case 1	Case 2	Case 3	Case 4
Mainshock	0.92%	1.07%	0.97%	0.88%	1.02%
Aftershock_1	0.82%	0.91%	0.87%	0.78%	0.90%
Aftershock_2	1.04%	1.35%	1.15%	1.12%	1.31%
Aftershock_3	1.16%	1.39%	1.18%	1.42%	1.39%
Aftershock_4	1.39%	1.75%	1.44%	1.65%	1.73%
Aftershock_5	1.49%	1.85%	1.55%	2.26%	1.82%
Aftershock_6	1.43%	1.60%	1.50%	2.43%	1.55%
Aftershock_7	1.72%	1.92%	1.83%	3.33%	1.91%

The response obtained from NTHA for all the cases are compared with those of the optimal one. Further, the push over analysis for the frames with all types of bracing is performed. The capacity curve for all the cases along with the un-retrofitted building frame are shown in Fig. 5.17. It can be seen from the figure that the capacity curves for all the cases are nearly the same; however, the optimal

one can resist more base shear. Further, the initial stiffnesses of the retrofitted frames are significantly higher than the unbraced frame as it would be expected.

Table 5.17 RIDR values for all cases considered

	GA	Case 1	Case 2	Case 3	Case 4
Mainshock	0.09%	0.10%	0.12%	0.10%	0.09%
Aftershock_1	0.15%	0.25%	0.15%	0.18%	0.25%
Aftershock_2	0.52%	0.39%	0.57%	0.51%	0.40%
Aftershock_3	0.88%	0.76%	0.83%	0.89%	0.76%
Aftershock_4	1.00%	0.94%	1.02%	1.38%	0.96%
Aftershock_5	1.11%	0.90%	1.18%	1.83%	0.95%
Aftershock_6	1.17%	0.94%	1.23%	1.97%	0.98%
Aftershock_7	1.30%	0.78%	1.46%	2.58%	0.71%

Table 5.18 Residual top storey displacement (m) for all cases considered

	GA	Case 1	Case 2	Case 3	Case 4
Mainshock	0.03	0.02	0.03	0.01	0.02
Aftershock_1	0.03	0.05	0.02	0.04	0.06
Aftershock_2	0.15	0.11	0.15	0.13	0.11
Aftershock_3	0.25	0.22	0.25	0.25	0.21
Aftershock_4	0.33	0.28	0.33	0.34	0.28
Aftershock_5	0.32	0.26	0.33	0.36	0.26
Aftershock_6	0.32	0.31	0.34	0.38	0.30
Aftershock_7	0.28	0.20	0.28	0.36	0.19

The responses of the NTHA of the retrofitted building frames with different types of bracings are compared in Tables 5.15 to 5.19. From the tables 5.15-5.18, it is observed that the maximum top storey displacement and transient maximum inter-story drift ratio are consistently the least for the optimally braced frame (using GA) in the main-shock and all aftershocks. However, the residual top storey displacement and residual inter-story drift ratio are not found to be the least in the optimally braced frame. this is the case, because the objective function for the optimization is taken as the transient peak top storey displacement during each event in the sequence. If the residual displacement or the residual inter-storey drift ratio is taken as the objective function, then the optimally braced frame would have yielded the least value of residual inter-story drift ratio or the least value of the residual top storey displacement. Therefore, the response of the optimally braced frame depends upon the selected objective function. In Table 5.19, the maximum

values of the response in all the cases of the study are reported. It is seen from the table that the overall performance of the optimally braced frame is very satisfactory.

Table 5.19 Maximum of different response quantity during a sequence of mainshock and series of aftershocks

	GA	Case 1	Case 2	Case 3	Case 4
Roof displacement (m)	0.56	0.61	0.59	0.62	0.61
Residual roof displacement (m)	0.33	0.31	0.34	0.38	0.30
Residual IDR (%)	1.30	0.94	1.46	2.58	0.98
Transient IDR (%)	1.72	1.92	1.83	3.33	1.91

5.4 CONCLUSION

Enhanced seismic performance of the retrofitted building frame with stiffness bracings is investigated by considering the effects of aftershocks which are not usually considered for the seismic design of the building frames. For this purpose, a 12-storey steel building frame designed according to the Indian standard (IS) code is considered. The frame is designed for a PGA of 0.394g. The unbraced frame withstands the mainshock but fails after three aftershocks. The sequence of the mainshock and aftershock is synthetically generated from the IS response spectrum. The frame is retrofitted with stiffness bracing using hollow sections comprising of HSS 3X0.250, HSS 4X0.250 and HSS 5X0.250. Two different techniques of stiffness bracings are proposed, namely, a simple iterative approach and an optimization approach. In the iterative approach, a systematic trial of putting a minimum number of bracings is used in order that braced frame can sustain all the aftershocks with damage remaining within the IO level. In the optimization approach, the frame is optimally braced using the GA for a specified number of bracings. In the example problems, 8 numbers of bracings are used. The results of the numerical study lead to the following conclusions:

- The undamaged building frame is damaged to the collapse state after 3 aftershocks, while the retrofitted building frames sustain all the seven aftershocks considered in the study and remain at the desired performance levels.

- The retrofitted building frames sustain three aftershocks without the formation of plastic hinges in the beams or columns.
- In the iterative approach, only two numbers of bracings placed in the central bay successively at the bottom two storeys are adequate to retrofit the frame to the desired performance level. The above observations indicate that with very nominal retrofitting using bracings at the lower levels of the frame the effects of the aftershocks can be adequately mitigated.
- The transient maximum inter-story drift ratio and residual inter-story drift ratio at the ground storey increases significantly with the increase in the number of aftershocks.
- There exists an optimum number of bracings beyond which no significant gain is achieved in the seismic performance of the frame.
- The locations of bracing for the optimally braced MRF does not follow a definite pattern; they depend on the storey stiffness.
- The maximum transient roof displacement and transient maximum inter-story drift ratio of the optimally braced frame are found to be the least for the main-shock and all aftershocks, when compared with those of the other alternative patterns of bracings.
- The optimized pattern of bracings depends upon the objective function selected. The optimal pattern only ensures that the response, which is selected as the objective function, becomes the least out of those obtained with other arbitrarily selected patterns. Other responses of the optimally braced frame may not be the least.
- The damages in the form of inelastic deformation of the optimally retrofitted frame remain below the immediate occupancy level up to the last aftershock; the damages remain mostly confined to the bracings.

CHAPTER-6

SEISMIC RELIABILITY ANALYSIS OF STEEL BUILDING FRAMES FOR MAINSHOCK AFTERSHOCK SEQUENCE.

6.1 INTRODUCTION

Earthquake events often consist of a sequence of shocks, i.e., a mainshock and several aftershocks. The mainshock in most cases imparts the most significant amount of energy and thus, causes the most damage. Aftershocks, however, have also been known to cause considerable damages and may be detrimental to structures that have been weakened by the mainshock and have not been repaired or rehabilitated. It has been observed in chapters 3 and 4 that when a building is subjected to a sequence of the mainshock and a series of aftershocks, the damage resulting from the mainshock increases the vulnerability of the building to more damages in the subsequent aftershocks. The damage accumulation during the mainshock and aftershocks leads to the instability of the structure and finally to collapse.

The damage to the structure during the strong ground motion depends upon the dynamic properties of the structure and characteristics of the seismic waves. There are uncertainties in the characteristics of strong ground motion, such as the spectral shape, duration and frequency contents. These uncertainties lead to a probabilistic assessment of the risk of the collapse of structures. Current damage estimation methods consider the effects of the mainshock only on building frames without explicitly considering the aftershock effects. The structures damaged during the mainshock behave differently during the aftershock since the performance of the damaged structures is completely different from that of the virgin structure exposed to the same earthquake. This difference is likely because of the significant (i) the uncertainty in the capacity of damaged buildings after mainshocks, (ii) the complexity of the characteristics of aftershocks and their occurrence probability, and (iii) a general lack of accurate system fragility models to evaluate building performance.

In this Chapter, the contribution of aftershocks to the structural damage is considered in the damage estimation method. A probabilistic approach to quantify the earthquake-induced damage and collapse, considering the sequence of the mainshock and aftershocks are presented. The probability of occurrence of different damage states of steel building frames, both undamaged and retrofitted, produced due to a single mainshock-aftershock episode is presented using fragility analysis. The response of each building frame is simulated with a nonlinear MDOF model, which can capture the strength and stiffness degradation of building components as damage progresses, potentially leading to the collapse. For carrying out the analysis, the building frame is subjected to an ensemble of the mainshock-aftershock sequences. Damage is quantified by physical damage indicators such as the maximum inter-story drift and roof drifts experienced during the ground motion time history, residual inter-story drift and roof drift at the end of the ground motion.

6.2 THEORY

The seismic fragility analysis of the frame is performed using the concept of probabilistic hazard analysis of the frame under an ensemble of earthquake records. The development of the fragility function involves measures of ground motion (Intensity measure) and structural response parameter (Damage measure). The different salient features of the analysis are outlined below.

6.2.1 INTENSITY MEASURES AND DAMAGE MEASURES

The fragility analysis requires unified quantification of the earthquake as well as damage. The earthquake is quantified by intensity measures (IM). Intensity measure is an indicator of the intensity of ground motion. The intensity measures, whichever chosen should be efficient, sufficient and be scaling robust. If the response of the structure has less variability at a given IM, the IM is efficient. The IM is sufficient if the conditional probability distribution of the IM is independent of the other parameters used in the seismic hazard analysis. One of the essential features for good IM is that the earthquake time history should easily be scaled to

different levels of intensity measures. The intensity measures satisfying the three properties may be based on the acceleration, velocity, displacement or energy. There are several ground-motion intensity measures (IMs) that have been used in assessing the seismic performance of a structure which satisfies the above parameters. The peak ground acceleration, spectral acceleration at the fundamental period, arias intensity, effective peak acceleration, earthquake power index, peak ground velocity, spectral velocity, effective peak velocity, peak ground displacement, peak spectral displacement are few examples of IMs.

The collapse of the structure is quantified by the damage measure (DM). In the literature, engineering demand parameter is also used as an alternative terminology to the damage measure. The DMs are chosen such that it relates to structural and non-structural damages. Damage measures are indicators of the performance of a structure based on the performance assessment of structures. The different damage indexes are roof displacement, roof drifts, storey drift, storey ductility, residual roof displacement, residual roof drift, residual storey drift, plastic rotation and the square root of the sum of squares of maximum plastic rotations. These parameters are evaluated by the nonlinear time history analysis of the structure.

The damage to structural and non-structural elements is a quantification of the damage parameters. This quantification of the damage at different discrete levels is termed as damage states. If the response of the structure is beyond a threshold value of a damaged state, then the structure is generally assumed to collapse for a practical purpose. The damage states are sometimes also related to the occupancy of the structure after the structure has sustained the earthquake. These damage states may be associated with the immediate occupancy (IO), life safety (LS), collapse prevention (CP) and collapse of the structure.

In this analysis, the different intensity measures, damage measures and damage states considered are mentioned in section 6.3.2. For the purpose of analysis, the intensity measure and damage measure are considered to follow a lognormal distribution.

6.2.2 FRAGILITY CURVES

The fragility curve is defined as "the conditional failure probability of a structure, element or component, given the seismic load intensity (IM) α". In other words, a fragility function postulates the probability of failure of a structure as a function of some ground motion intensity measure, IM. In this regard, the failure may not be indicated by the collapse of the structure, rather it is described by the damage measure (DM). Different failure levels are expressed by damage states (D_s) given by threshold values of the DM. The fragility curve is defined by a lognormal cumulative distribution function given by the following equation.

$$P_f(\alpha) = P_f(DM > D_s|IM = \alpha) = \Phi\left(\frac{\ln \alpha/\theta}{\beta}\right) \quad (6\text{-}1)$$

Where $P_f(DM > D_s|IM = \alpha)$ is the probability that a ground motion with the intensity measure as $IM = \alpha$ will cause a damage of the structure greater than or equal to the damage measure; Φ is the normal cumulative distribution function (CDF); θ is the intensity measure with 50% probability of collapse, β is the dispersion of the intensity measure in terms of the standard deviation. The intensity measure, damage measure and damage state are discussed in the section 6.2.1. In the above equation, the distribution of the intensity measure is also assumed to be lognormal.

For a given structure and set of ground motion, θ *and* β are necessary and sufficient to uniquely define the fragility function for the given damage state and needs to be evaluated. There are two commonly used approaches to collect the data for estimating θ *and* β to develop the fragility function consistent with the observed data. One common approach is incremental dynamic analysis (IDA), and the second common approach is multiple stripe analysis.

6.2.2.1 INCREMENTAL DYNAMIC ANALYSIS

Incremental dynamic analysis (IDA) is a widely used seismic probabilistic risk assessment methodology for the evaluation of the seismic risk. In the IDA, nonlinear building models are subjected to a ground motion with a predefined intensity measure. The response of the building following the nonlinear time

history analysis (NLTHA) is obtained. The ground motion is then scaled by a scaling factor to different values of the intensity measure, and the response is recorded. This process is repeated up to the collapse of the structure for the ground motion. In the process, the response of the structure is recorded ranging from the yield point to the collapse. The value of the intensity measure is plotted with respect to the extent of damage (magnitude of the response quantity of interest). The curve is known as the IDA curve. A typical IDA curve is shown in Fig. 6.1. The collapse capacity is reached when the IDA curve becomes flat, which means that with a small increase in the intensity of the earthquake there will be a significant amount of the response generated in the structure.

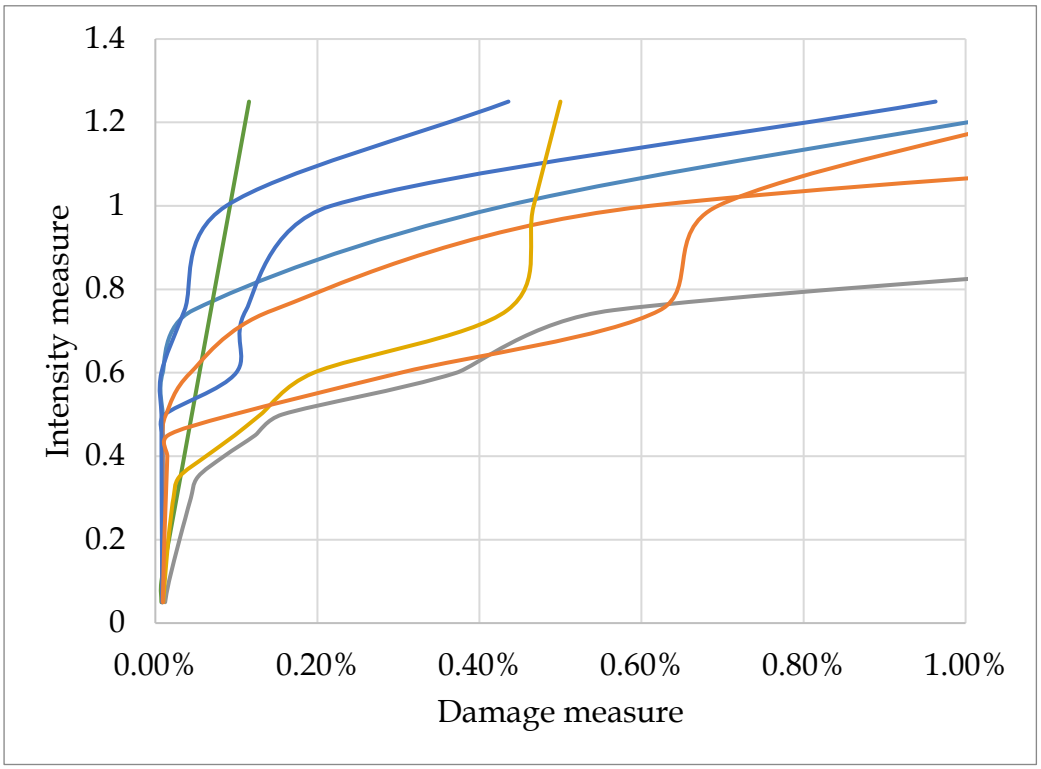

Fig. 6.1 An example of Incremental dynamic analysis curve

The probability of collapse at a predefined intensity measure level, α, can be estimated after an estimate of θ *and* β. The IDA is based on N-sample, generally $N \geq 10$, of earthquakes considered. Sometimes, the probability is estimated as the fraction of records for which the collapse occurs at a level lower than α. Since the records considered is a sample taken from the population of earthquakes, this estimate may be misleading until the value of N is large and samples are homogenous. So, the parameters of the fragility curve are chosen as the median

(θ) and the log- standard deviation (β) of the log normal distribution and is given by the following equations.

$$\ln \theta = \frac{1}{n}\sum_{i=1}^{n} \ln IM_i \tag{6-2}$$

$$\beta = \sqrt{\frac{1}{n-1}\sum_{i=1}^{n} (\ln(IM_i/\theta))^2} \tag{6-3}$$

Where n is the number of ground motions considered, and IM_i is the IM value associated with the onset of collapse for the i^{th} ground motion. A fragility curve is shown in Fig 6.2.

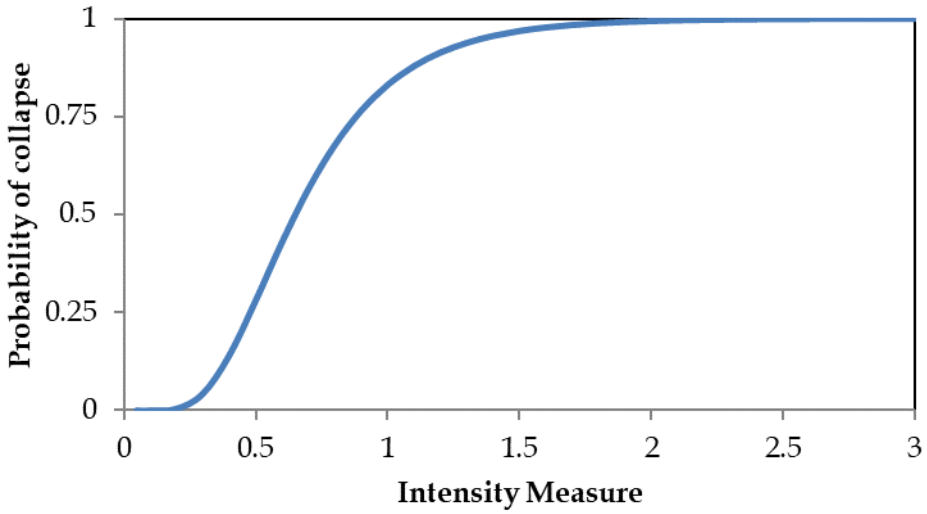

Fig. 6.2 An example of Fragility curve using IDA

6.2.2.2 MULTIPLE STRIPE METHOD

Incremental dynamic analysis requires intensity measures to be continuous monotonically increasing. Whereas, in the multiple stripe method the response of the structure is measured at discrete levels of the intensity measure. The method is widely used and efficient when the ground motions are selected using the conditional spectrum. In other words, when the sample of ground motions is biased, multiple stripe method is useful in determining the probable seismic risk. In this approach, it is not necessary that all the ground motions are scaled to a precisely defined level at which the building is globally collapsed. The increment for different intensity measure levels may not be the same.

Multiple stripe analysis (MSA) is based on a group of stripe-based fragility analysis. In the stripe analysis, the ground motions considered are scaled to the same intensity measure, IM_i, and NLTHA is performed on the structural model. The damage measure obtained from the NLTHA is fit to the lognormal distribution function. The response of structure for some ground motions may be beyond the damage state (collapse). There may be an instance at a lower value of IM_i, that the response is not beyond the damage state. The probability of observing z_i collapses out of N earthquake considered at the intensity measure, IM_i, is given by binomial distribution as:

$$P(z_i) = \binom{N}{Z_i} {P_i}^{z_i}(1 - P_i)^{N - z_i} \tag{6-4}$$

Where P_i is the probability of collapse at IM_i and $\binom{N}{Z_i} = \frac{N!}{Z_i!(N-Z_i)!}$. P_i is given by Eq. 6.1. For multiple stripes, the probability of collapse for the set of earthquakes at different levels of an earthquake is given by the product of Eq. 6.4 for different intensity measures IM_i and termed as the likelihood and given as:

$$Likelihood = \prod_{i=1}^{m} \binom{N}{Z_i} {P_i}^{z_i}(1 - P_i)^{N - z_i} \tag{6-5}$$

Where m is the number of levels of intensity measures considered in the analysis. The estimates of parameters $\theta \; and \; \beta$ are obtained by maximising the likelihood function. Once the estimates are determined, fragility function can be uniquely defined by Eq. 6.1.

6.3 NUMERICAL RESULTS AND DISCUSSION

The seismic risk probability is determined for the 12-storey building frame under the action of as-recorded mainshock and aftershocks. Two different building frame models, one the un-retrofitted moment resisting frame and the other the optimally braced moment resisting frame are considered. The building model is the same as mentioned in chapter 5. The two building frames are shown in Figs. 5.1 and 5.9. The nonlinear time history analysis is performed on the building frames to obtain the data set required for determining the fragility function. Multiple stripe analysis is used for evaluating the desired seismic risk analysis.

Different earthquake records recorded at the different stations are considered and detailed in the section 6.3.1.

6.3.1 EARTHQUAKE RECORDS

In this study, the ground motions recorded at different sites have been used. The real ground motions were selected since the other approaches such as the back to back, and random approaches generally overestimate the effect of the aftershocks. The site was selected such that the aftershock records were available at the site. The ground motion time histories were downloaded from the cosmos website (https://strongmotioncenter.org/vdc/scripts/default.plx). The aftershocks considered were recorded within a few days from the mainshock. Some of the aftershocks were recorded within a few hours of the mainshock.

6.3.1.1 SELECTION OF GROUND MOTIONS

The details of the ground motions considered are given in Table 6.1. The effect of site conditions was not explicitly studied in the present work. In total, nine different earthquakes were considered for the study with two components in each. The two components of the earthquake were treated as independent ones. So, in total 18 earthquakes were considered for the present study. The details of the earthquake time histories considered are listed in Table 6.1.

The PGAs reported in Table 6.1 are PGAs experienced at the site. In most of the instances, the PGA of the mainshock is greater than that of the aftershocks. There are a few instances where the peak ground acceleration of the aftershock is greater.

Table 6.1 Details of earthquake records considered

Year	Event Name	Station	Component	Mainshock		Aftershock	
				MW	PGA (g)	MW	PGA (g)
2001	El Salvador	Hospital Santa Teresa, Zacatecoluca, La Paz - office	NS	7.6	0.27	6.6	0.40
			EW		0.25		0.22
1999	Mexico City	UNR: Papanoa, Mexico Guerrero Array Stn PPN	EW	8.1	0.15	7.6	0.18
			NS		0.09		0.24
1985	Kozani	GSC station NAH3	EW	6.4	0.21	5.3	0.09
			NS		0.14		0.13
1988	Spitak	Gukasyan, Armenia	NS	7.1	0.19	5.9	0.09
			EW		0.19		0.06
1994	Northridge	CSMIP: Tarzana, CA Cedar Hill Nursery A	90	6.7	1.74	5.3	0.37
			360		0.84		0.21
1986	Taiwan	IES: Lotung, Taiwan SMART1 array, south extension	NS	7.3	0.18	6.2	0.17
			EW		0.20		0.13
1985	Chile	DGG: Valparaiso, Chile	160	7.8	0.16	6.3	0.04
			70		0.17		0.03
2016	New Zealand	GNS: Hanmer Springs Emergency Centre Emergency Centre	N10E	7.8	0.24	6.5	0.17
			N80W		0.26		0.14
1999	Chichi	CWB: Taichung, Taiwan	NS	7.6	0.25	6.3	0.31
			EW		0.41		0.25

6.3.1.2 SCALING OF MAINSHOCK AFTERSHOCK SEQUENCE

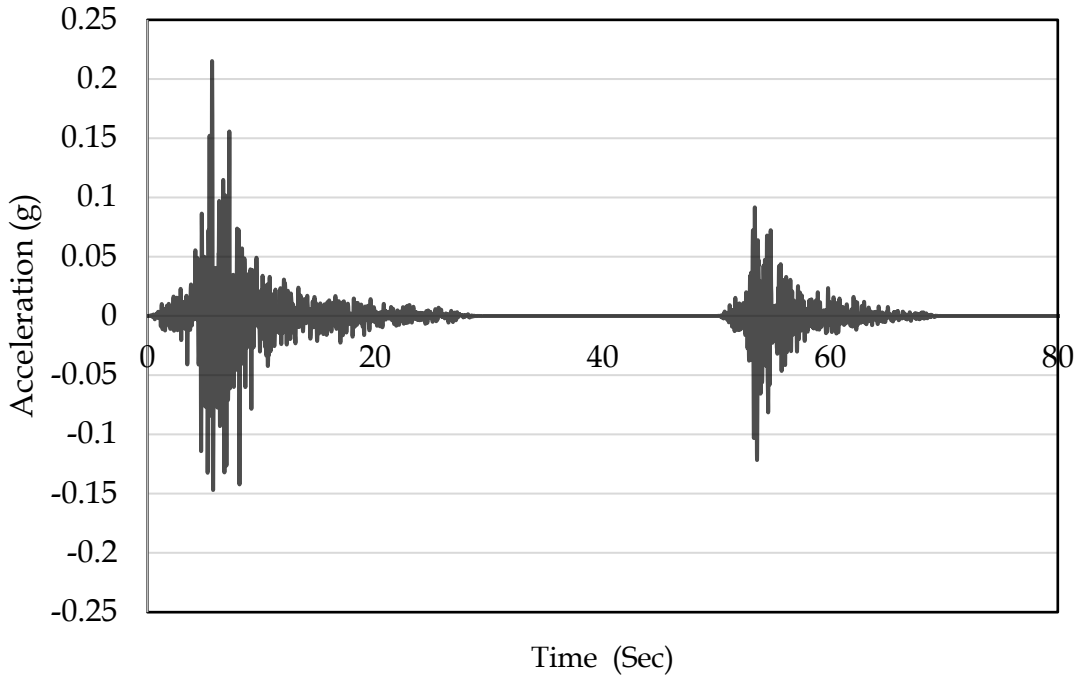

Fig. 6.3 Mainshock and Aftershock sequence of Kozani earthquake in longitudinal direction

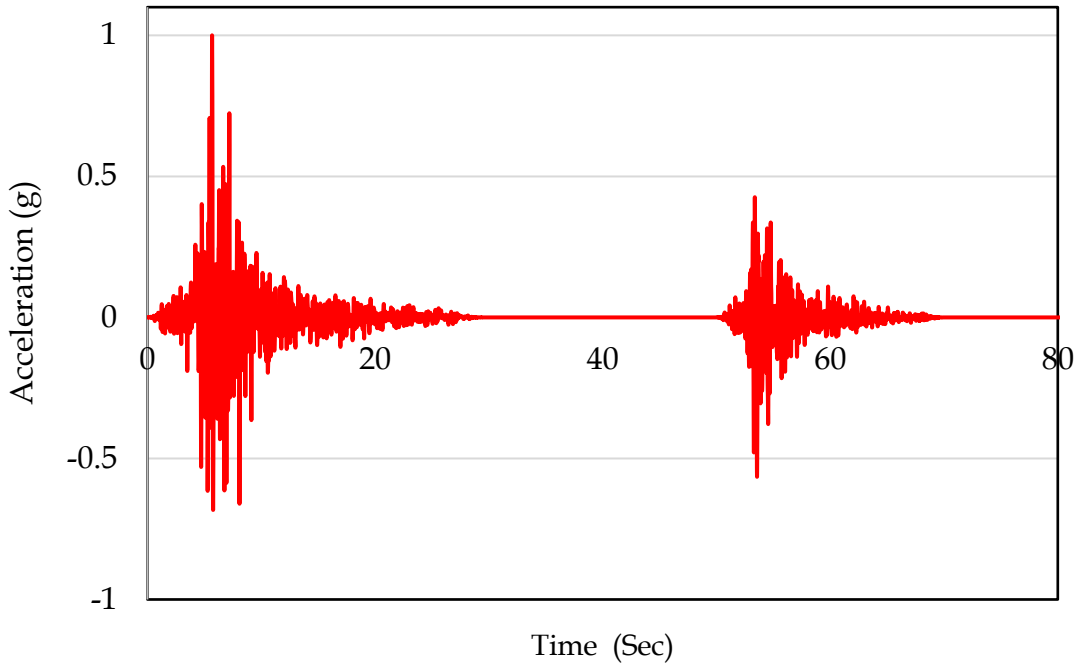

Fig. 6.4 Normalised sequence of Kozani earthquake in longitudinal direction

The time series of the mainshock and aftershock were joined together in chronological order from back to back. One of the ground motion records containing the mainshock and aftershock is shown in Fig. 6.3. The mainshock and

aftershock are joined after a time gap. This time gap is necessary to model the mainshock aftershock effects. The gap is chosen such that the building is at rest after the mainshock event is over.

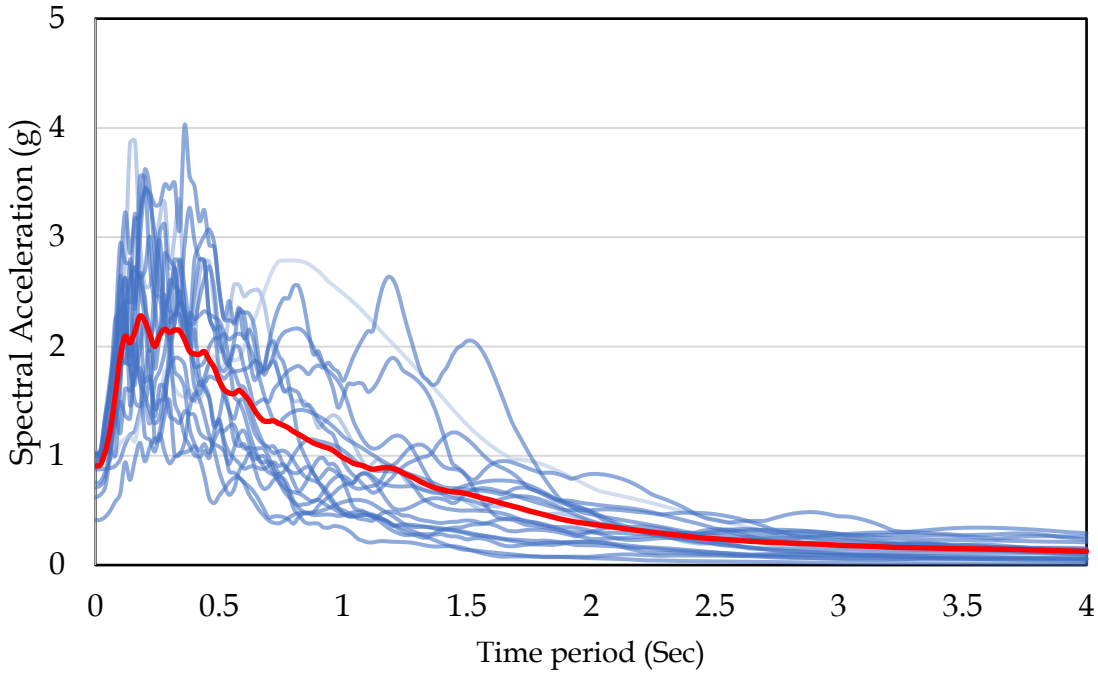

Fig. 6.5 Response spectra of mainshock from the normalized sequence

The mainshock and aftershock sequence is scaled based on the PGA of the combined time history instead of only the time history of the mainshock or aftershock. The mainshock and aftershock sequence is normalized by the peak ground accelerations of the mainshock-aftershock sequence. The normalized mainshock-aftershock sequence is shown in Fig. 6.4.

The response spectra of the mainshocks of the normalized 18 mainshock-aftershock sequence are shown in Fig. 6.5. The elastic response spectra are plotted for the 5% damped SDOF system. The dark solid line represents the median of the response spectra for the mainshocks. The elastic response spectra for aftershocks of the mainshock-aftershock sequence are shown in Fig. 6.6. The dark solid line represents the median of the response spectra for the aftershocks.

Fig. 6.7 shows the comparison between the mean response spectra of the mainshock and aftershock. It can be observed that the spectral ordinates for the aftershock are less than those of the mainshock. The difference between the two is maximum in the period range of 0.1s to 2.55s. Further, it is seen that the spectral

ordinate at zero time period for the aftershock is less than 1 indicating that the PGA of the mainshock is higher than that of the aftershocks.

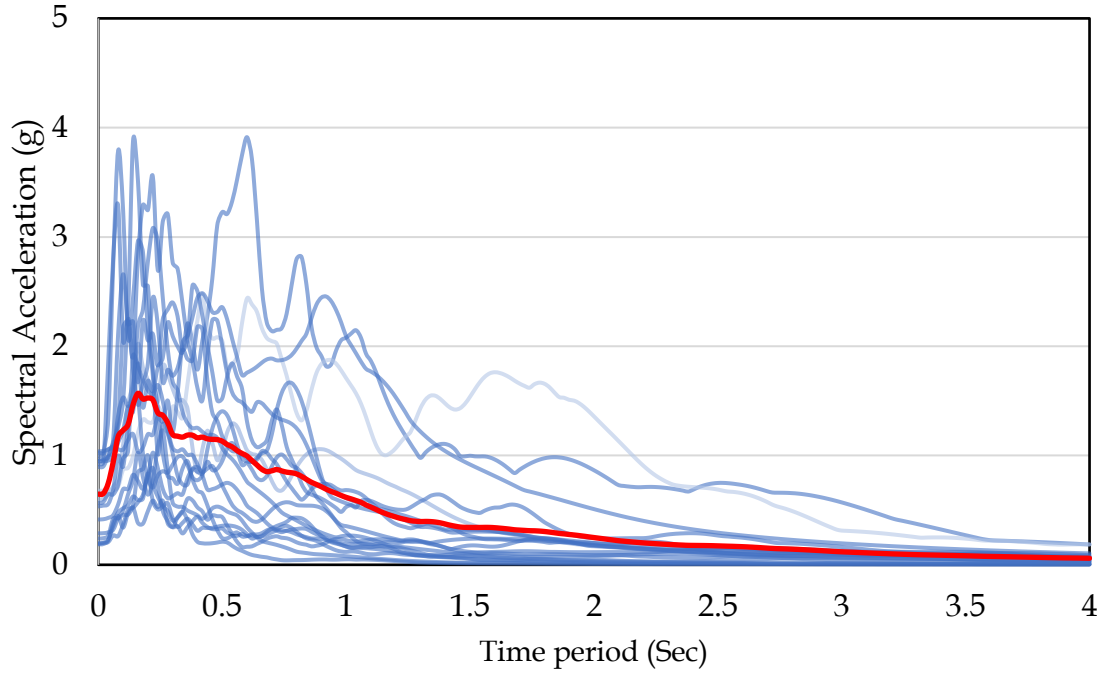

Fig. 6.6 Response spectra of Aftershocks from the normalized sequence

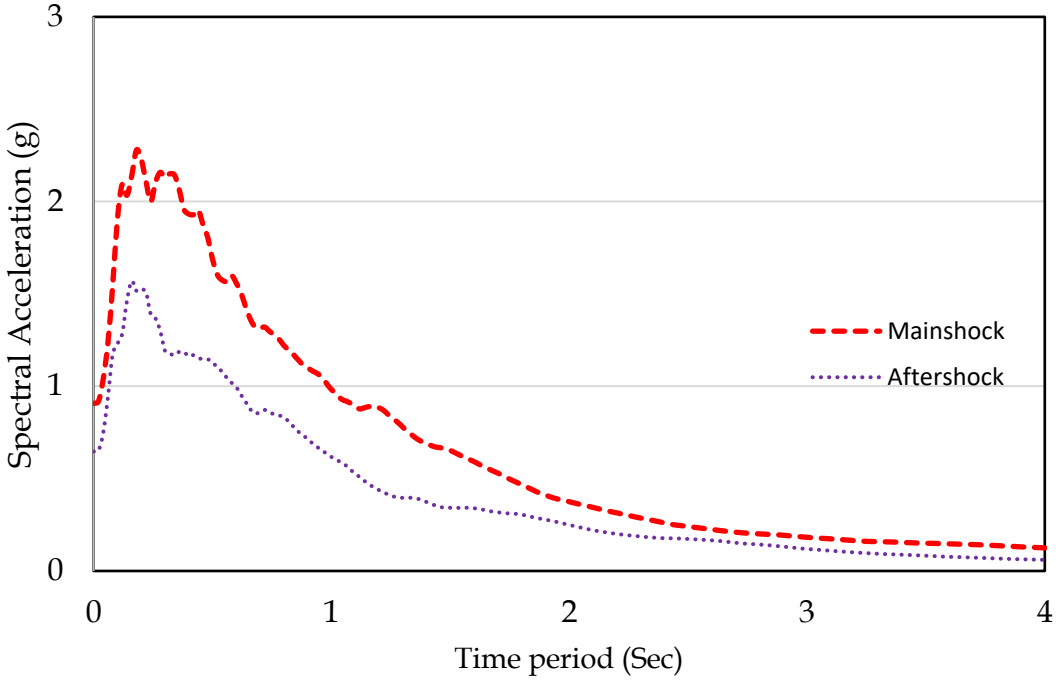

Fig. 6.7 comparison of mean response spectra of mainshock and aftershock

6.3.2 INTENSITY MEASURE AND DAMAGE MEASURE

The peak ground acceleration and spectral acceleration at the fundamental period have been widely used in the seismic risk probability analysis than those of the other parameters mentioned in the section 6.2.1. In the present study, the peak ground acceleration (PGA) has been considered as the intensity measure. The mainshock-aftershock sequence is scaled based on the PGA ranging from 0.05g to 1.25g. The range 0.05-1.25g is divided into equal intervals with an increment of 0.05g. The scaling of the mainshock-aftershock sequence is done by multiplying the normalized mainshock-aftershock sequence by the scaling factor. The NLTHA of the building frames is performed for each scaled mainshock-aftershock sequence. The NLTHA is performed as described in the section 3.2.4.

Table 6.2 Threshold values of damage measures for different damage states

	Immediate Occupancy (D_{s1})	Life safety (D_{s2})	Collapse Prevention (D_{s3})
Transient	0.7%	2.5%	5%
Permanent	0.1%	1%	5%

The damages in the structure, represented by the global response of the building frame, are quantified by the damage measures. In the present study, the transient maximum roof drift and residual roof drift are the two most important damage measures considered. The threshold values of the roof drift can reasonably be quantified for different damage states. Three damage states have been considered in the study, which are D_{s1}, D_{s2} and D_{s3}. These damage states correspond to immediate occupancy (IO), life safety (LS) and collapse prevention (CP) respectively. The threshold values of different damage states as per FEMA 356 are given in Table 6.2. One may note that the threshold values for the permanent roof drift are lower than those of the transient maximum roof drift.

6.3.3 SEISMIC RISK ANALYSIS OF THE BUILDING FRAME

The un-retrofitted MRF is titled as MRF and optimally braced MRF as braced MRF hereafter. Both MRFs are subjected to the recorded mainshock-aftershock sequences as shown in Table 6.1. The seismic sequence is scaled to different intensity measures as mentioned in the section 6.3.2. The response parameters in terms of the transient roof drift and permanent roof drift are recorded for the mainshock as well as aftershocks. Fragility analysis as described in section 6.2.2.2 is performed for both building frames. In the process of determining the risk probability, the likelihood function given by Eqn. 6.5 is minimized to determine θ *and* β.

6.3.3.1 PROBABILITY OF COLLAPSE OF THE UN-RETROFITTED FRAME

The fragility curves for the MRF are shown in Figs. 6.8 and 6.9. Fig. 6.8 shows the collapse probability of the un-retrofitted building frame with the transient maximum roof drift as a damage measure for the three different damage states (IO, LS, CP). It is observed from Fig. 6.8 that the collapse probability for LS and CP is practically zero up to a PGA level of 0.8g in the mainshock. At a PGA level of 1.25g, it increases to only 25%. The same observation holds true for the aftershock. Thus, the probability of collapse (from the consideration of roof drift) in terms of LS and CP is practically very low in the mainshock as well as aftershock for the example problem selected. However, the probability of the collapse in terms of IO is significantly high for both the mainshock and aftershock. At a PGA level of 1.25g, the collapse probability is nearly of the order of 75%. For the aftershock, the values are a little more than those of the mainshock. The reason for the increased probability of collapse for the aftershocks is primarily due to the damage state of the frame in the mainshock. Even very minor damages caused in the mainshock can get significantly amplified in the aftershock leading to the higher probability of the collapse of the frame.

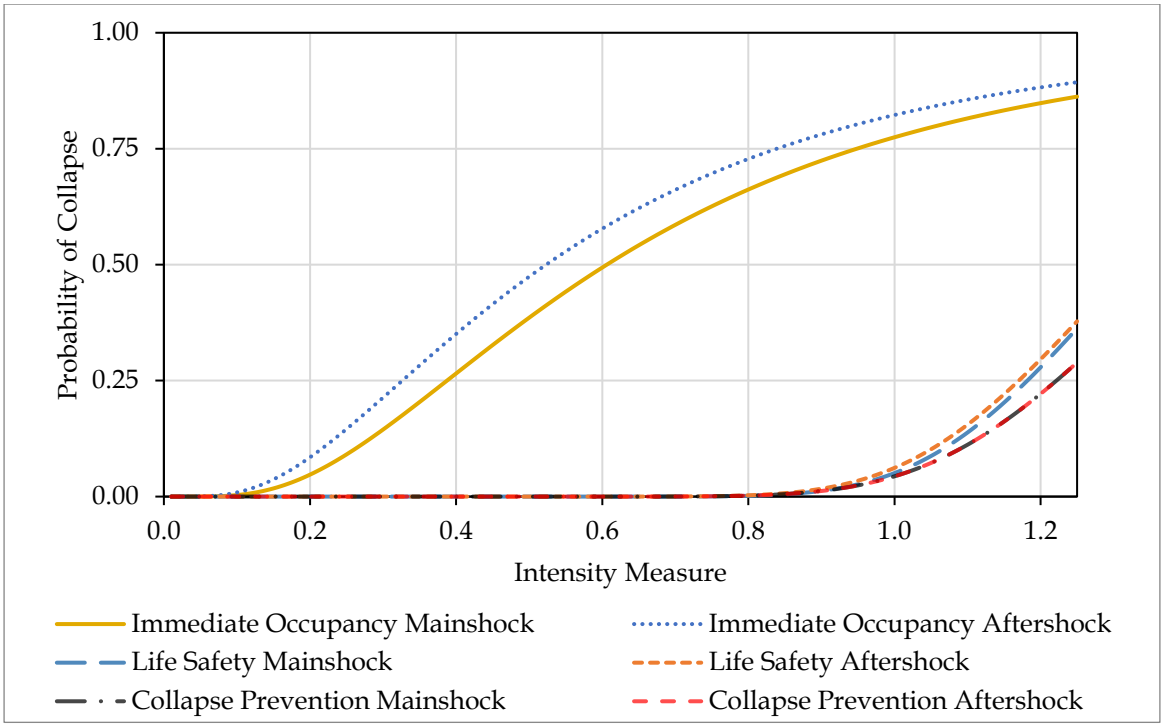

Fig. 6.8 Collapse probability of MRF subjected to mainshock and aftershock based on transient maximum roof drift

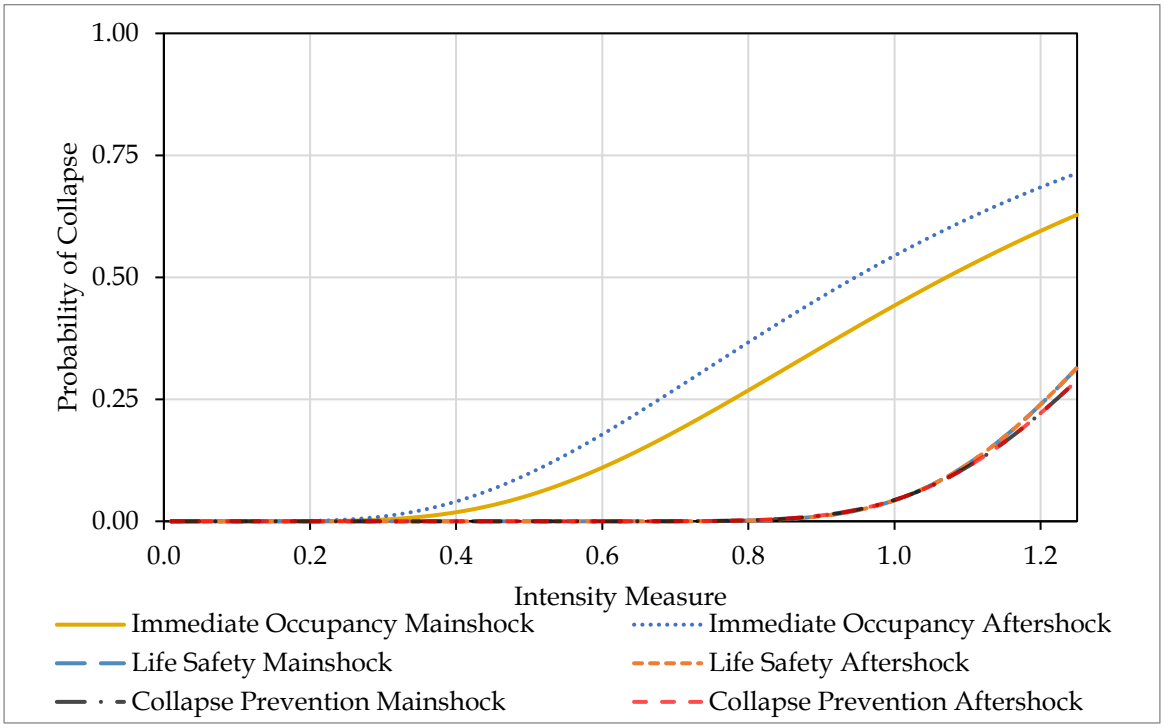

Fig. 6.9 Collapse probability of MRF subjected to mainshock and aftershock based on the residual roof drift

Fig 6.9 shows the fragility curve for the residual roof drift. Comparing Figs. 6.8 and 6.9, it is seen that the probability of the collapse in terms of the residual roof drift is less as compared to the maximum transient roof drift. This is the case

because the maximum transient roof drift is expected to be more than the residual roof drift. Besides the above difference, the nature of the fragility curves for the two damage measures is nearly the same with the exception that the difference between the fragility curves of the mainshock and aftershock for the IO damage state is more for the residual drift as compared to the transient maximum drift.

6.3.3.2 BRACED MOMENT RESISTING FRAME

Figs 6.10 and 6.11 show the fragility curves of the optimally braced building frame for the transient maximum roof drift and residual roof drift. The features of the fragility curves may be summarized as:

i) The probability of collapse in terms of residual drift is significantly less for the braced frame as compared to the unbraced frame.

ii) For the braced frame, the probability of collapse for the residual drift is also much less compared to the maximum transient drift.

iii) The probability of collapse in terms of both the maximum transient and residual roof drifts are extremely small for the damage states LS and CP.

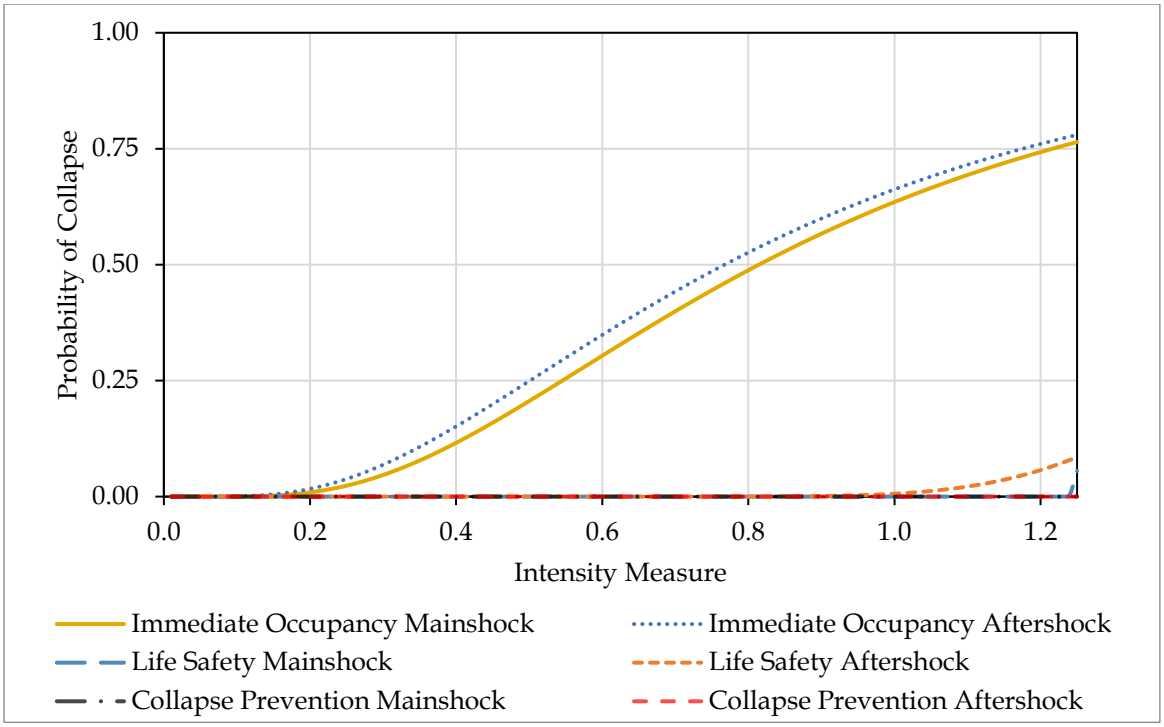

Fig. 6.10 Collapse probability of braced MRF subjected to mainshock based on the transient maximum roof drift

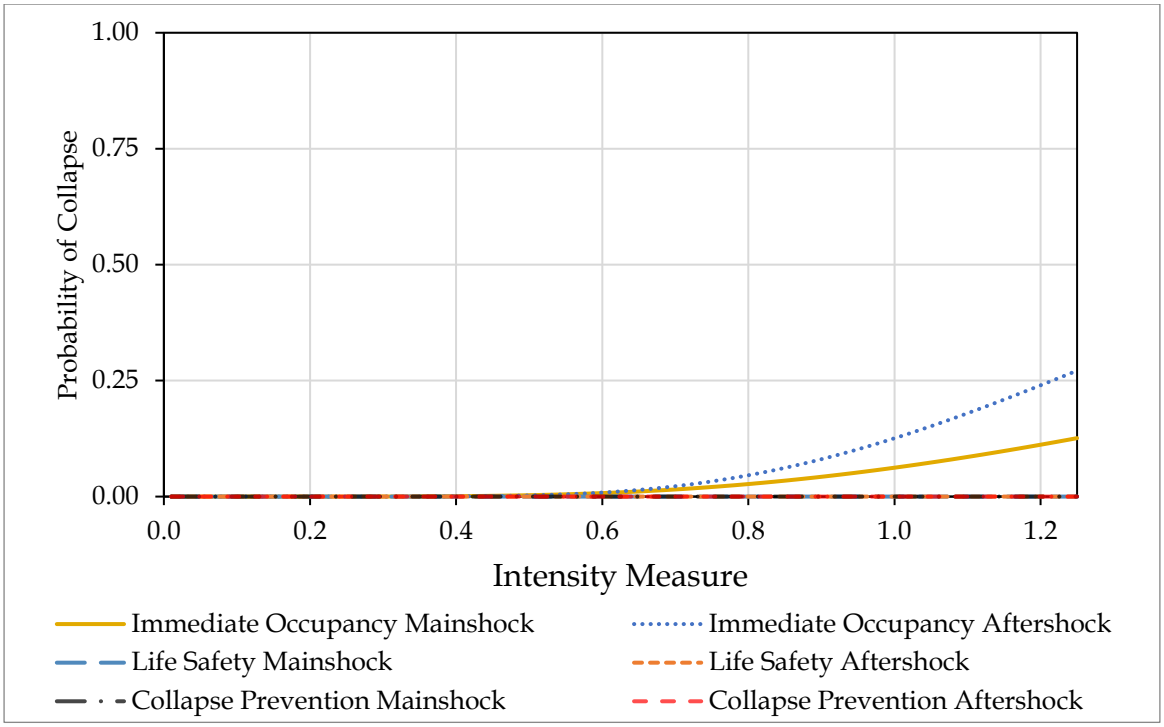

Fig. 6.11 Collapse probability of braced MRF subjected to aftershock based on the residual roof drift

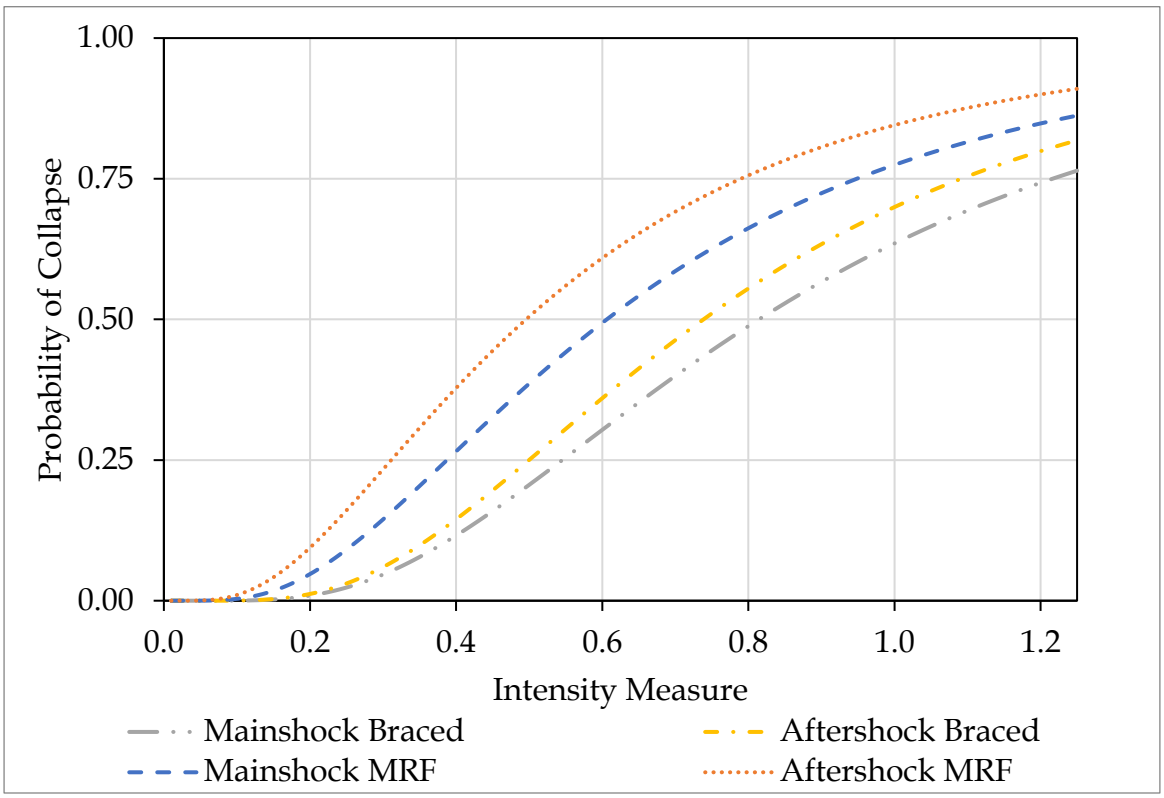

Fig. 6.12 Comparisons of collapse probability for intermediate occupancy

Since the probabilities of collapse in terms of damage states, LS and CP are very small, the comparison is shown for the probabilities of collapse in terms of

the damage state IO between the un-retrofitted and retrofitted frame in Fig 6.12. The maximum transient roof displacement is considered as the seismic demand parameter. The figure clearly shows that the probability of collapse of the braced frame is much less compared to the unbraced frame for both the mainshock and aftershock.

Table 6.3 PGA values (g) for 50% probability of collapse (θ) for different cases considered

		MRF		Retrofitted MRF	
		Mainshock	Aftershock	Mainshock	Aftershock
Transient Roof Drift	DS1	0.6063	0.5232	0.8145	0.7675
	DS2	1.3285	1.3227	1.2652	1.6386
	DS3	1.392	1.392	4.6061	4.6061
Permanent Roof Drift	DS1	1.0712	0.9465	2.4054	1.6081
	DS2	1.3639	1.3639	4.6061	4.6061
	DS3	1.392	1.392	4.6061	4.6061
Roof Drift	DS1	0.6063	0.4958	0.8145	0.7386
	DS2	1.3285	1.3227	1.2652	1.6386
	DS3	1.392	1.392	4.6061	4.6061

Table 6.4 Spread of intensity measure (β) for different cases considered

		MRF		Retrofitted MRF	
		Mainshock	Aftershock	Mainshock	Aftershock
Transient Roof Drift	DS1	0.6635	0.6998	0.5946	0.632
	DS2	0.1733	0.1817	0.0076	0.1973
	DS3	0.1935	0.1935	0.0869	0.0869
Permanent Roof Drift	DS1	0.4725	0.494	0.5715	0.4143
	DS2	0.1808	0.1808	0.0869	0.0869
	DS3	0.1935	0.1935	0.0869	0.0869
Roof Drift	DS1	0.6635	0.6903	0.5946	0.5789
	DS2	0.1733	0.1817	0.0076	0.1973
	DS3	0.1935	0.1935	0.0869	0.0869

The intensity measure (PGA) for 50% probability of collapse, denoted by θ and spread of intensity measure, denoted by β for different cases considered are presented in Tables 6.3 and 6.4 respectively. It can be seen from the table that the θ values are higher for the retrofitted building frame than those of the un-retrofitted

building frame. Moreover, the θ values during the mainshock are higher than those of the aftershocks for all the damage states. Further, it is observed that the θ values for the un-retrofitted frame for the LS damage state (DS3) are 1.392 for both the mainshock and aftershock whereas, it is 4.60 for the retrofitted building frame. Thus, the retrofitted building frame withstands the earthquake effects with minor damage in a much better way than the un retrofitted frame. Table 6.4 also indicates that the β values decrease with the increase in damage states.

6.4 CONCLUSION

The probability of seismic collapse (in terms of damage states) of un-retrofitted and retrofitted building frames subjected to a mainshock and aftershock sequence is evaluated. The retrofitted frame is optimally braced to withstand a sequence of mainshock and aftershock events. An ensemble of 18 recorded mainshock and aftershock sequences is selected for the probability seismic collapse analysis. For determining the failure probability, the multiple stripe method is utilized to generate the fragility curves. For this purpose, the PGA is taken as the intensity measure. Two different seismic demand parameters, namely, the transient maximum roof drift and residual roof drift are considered. The three damage states, the immediate occupancy, life safety and collapse prevention as per FEMA 356, are used to define the collapse states. Using a nonlinear time history analysis for the earthquake events, the fragility curves are prepared. The results of the numerical study lead to the following conclusions:

- The probability of collapse for the aftershock, in general, is higher than that of the mainshock.
- Very less probability of collapse in terms of the collapse prevention and life safety is exhibited for both retrofitted and un-retrofitted frame; in particular, it is almost negligible for the retrofitted frame. Therefore, the collapse is primarily governed by the IO damage state.
- The transient maximum roof drift is always found to be greater than the residual roof drift.

- The probability of collapse for different damage states is underestimated if the residual roof drift is taken as the damage measure; therefore, the transient maximum roof drift is a preferred choice for the fragility analysis.
- The probability of collapse of the un-retrofitted frame is greater than that of the optimally retrofitted frame; with marginal retrofitting of a frame (as shown in the chapter 5), the reliability against the seismic collapse of the frame may be considerably alleviated even if the effects of aftershocks are considered.

CHAPTER-7
SUMMARY AND CONCLUSION

7.1 SUMMARY

The seismic behaviors of the damaged, undamaged, and retrofitted steel MRFs are studied at different damage states starting from the initial occupancy state (IO) to the collapse prevention state (CP). While the behaviors of the damaged MRFs are investigated considering the mainshock effect of the earthquake, those of the undamaged and retrofitted ones are investigated considering both mainshock and aftershock effects. The first study is aimed at finding the critical damage scenario, out of all the damage scenarios having the same total damage, which leads to the sidesway collapse of the MRF under a given earthquake. This is obtained by an innovative approach (GPPA) in which the plastic analysis, pushover analysis and genetic algorithm are combined. The results of the proposed method of analysis are verified by the nonlinear time history analysis. A ten-storey building frame having a number of artificially generated damage scenarios is taken as an illustrative example.

The second study is primarily carried out to illustrate the need for considering the aftershock effects of earthquakes in defining the collapse state of a structure consistent with different damage states. Three MRFs are analyzed under the sequence of the mainshock and a number of aftershocks. The performances of the MRFs during and at the end of each shock are evaluated in terms of a number of seismic demand parameters such as the peak top floor displacement, maximum inter-story drift ratio, maximum base shear, number of plastic hinges and residual inter story drift ratio.

In the third study, the performance of the retrofitted MRFs in the aftershocks are investigated. The MRFs are retrofitted optimally to enhance their performance in the aftershocks. A simple iterative scheme and an optimization scheme are employed for optimal retrofitting. The seismic performances of both

un-retrofitted and retrofitted frames are evaluated in order to illustrate the efficiency of the optimal retrofitting scheme.

Finally, a fragility analysis of both un-retrofitted and retrofitted MRFs are performed with the help of an ensemble of 18 recorded mainshock and aftershock sequences in order to investigate the probability of the collapse of the frames in terms of the seismic damage states (IO, LS, CP). The results of the study are useful in asserting the seismic performance of both un-retrofitted and retrofitted frames probabilistically.

7.2 CONCLUSIONS

The major conclusions obtained from different numerical investigations carried out in each of the studies summarized as above are presented below:

- There exist certain localized damage states for a building frame which may trigger sway mode of collapse under an earthquake; this explains why one of the two identical buildings built at the same time and site collapse, while the other survives under the same earthquake.
- It is possible to identify these localized damage states using the GPPA proposed here.
- The nonlinear time history analysis with response spectrum compatible earthquake confirms that the sway mode of collapse of the frame takes place for the critical initial damaged state of the frame identified by the GPPA.
- The methodology may be usefully employed for retrofitting the damaged building to withstand specific levels of earthquake intensity.
- Damages (indicated by the MIDR, RIDR, and number of plastic hinges) caused by aftershocks could be significant and should be accounted for in the seismic design of structures; the present codes do not have this provision in explicit form.
- For the high-rise buildings, the collapse may take place at a less number of aftershocks; in the present case of the 12-storey frame, the collapse took place at the third aftershock.

- For the low and medium rise buildings, after the third aftershock, the maximum inter-story drifts (both MIDR and RIDR) are found to exceed the limit proposed by FEMA.
- With more number of aftershocks, the increase in MIDR and RIDR at the first storey level is much greater compared to the other storeys; it is not very significant at the upper levels. This feature is more pronounced for the low-rise frame (4-storey).
- In the iterative approach, only two numbers of bracings placed in the central bay successively at the bottom two storeys are adequate to retrofit the frame to the desired performance level. The above observations indicate that with very nominal retrofitting using bracings at the lower levels of the frame the effects of the aftershocks can be adequately mitigated.
- The transient maximum inter-story drift ratio and residual inter-story drift ratio at the ground storey increases significantly with the increase in the number of aftershocks.
- There exists an optimum number of bracings beyond which no significant gain is achieved in the seismic performance of the frame.
- The locations of bracing for the optimally braced MRF does not follow a definite pattern; they depend on the storey stiffness.
- The maximum transient roof displacement and transient maximum inter-story drift ratio of the optimally braced frame are found to be the least for the main-shock and all aftershocks, when compared with those of the other alternative patterns of bracings.
- The optimized pattern of bracings depends upon the objective function selected. The optimal pattern only ensures that the response, which is selected as the objective function, becomes the least out of those obtained with other arbitrarily selected patterns. Other responses of the optimally braced frame may not be the least.
- The damages in the form of inelastic deformation of the optimally retrofitted frame remain below the immediate occupancy level up to the last aftershock; the damages remain mostly confined to the bracings.

- The probability of collapse for the aftershock is much greater than that of the mainshock.
- The transient maximum roof drift is always found to be greater than the residual roof drift.; it provides a good seismic demand parameter for the fragility analysis.
- The probability of collapse for different damage states is underestimated with the residual roof drift as the damage measure.
- The probability of collapse of the un-retrofitted frame is greater than that of the optimally retrofitted frame. For the later, the probability of collapse by considering the aftershock event is observed to be small even for a considerably high PGA level.
- Marginal retrofitting of a frame may considerably elevate the reliability against the collapse of the frame even for aftershock effects.

7.3 LIMITATIONS OF THE PRESENT WORK

The nonlinear time history analysis, pushover analysis and plastic analysis are carried out using the idealizations used for the two-dimensional center line model. Therefore, the limitations of the findings of the study are primarily confined to neglecting 3D modelling of the frame which may predict different responses. They and other limitations of the study may be summarized as:

- The building frames considered represent a class of building frames, but not all types of the building frames. The results may be different for other classes of building models.
- The building frame is modelled as a 2-D MRF idealization of 3-D building frame; thus, out of the plane motion of the frame is ignored.
- The center of mass and center of stiffness is assumed as concentric. Torsional effects produced due to the eccentricity is not considered.
- The present work is limited to regular buildings without any vertical discontinuities. The initiation and progression of the collapse of a building with a vertical discontinuity are entirely different from that of the building without the discontinuity.

- The columns and beams are modelled as I-Section; local failures of the I-sections are not considered in the study.
- The joints are assumed to be sufficiently rigid and with enough strength that the joints will remain in the elastic region during the entire seismic event.
- Composite action of beams and slabs have not been considered in the study. Some part of the slab in the vicinity of the beam act as part of the beam leading to higher strengths and stiffness.
- Material plasticity is assumed to be concentrated at discrete locations instead of distributed plasticity.
- The nonlinear behavior of the material is assumed to be bilinear instead of the experimental or exact behavior of the material.
- Foundations have not been modelled; the bases are assumed to be fixed.

7.4 RECOMMENDATION FOR FUTURE WORK

The present work briefly elaborates the effects of damages on the building frames. As an extension of the present work and to overcome the limitations mentioned above, the following are recommended for the future work.

- The seismic risk of the building by means of fragility analysis considering the sequence of many aftershocks should be carried out.
- The performance of other retrofitting techniques such as base isolators to withstand a sequence of the mainshock and aftershock is recommended.
- The performance of control techniques such as Tuned Mass Dampers in the building frames should be carried out for the sequence of the mainshock and aftershocks.
- The Effect of the presence of slab in withstanding the aftershocks and the consequent fragility analysis should be carried out.
- Shape and size optimization of braces considering other engineering demand parameter is also recommended.

BIBLIOGRAPHY

1. Adhikari, L. B., Gautam, U. P., Koirala, B. P., Bhattarai, M., Kandel, T., Gupta, R. M., Timsina, C., Maharjan, N., Maharjan, K., Dahal, T., Hoste-Colomer, R., Cano, Y., Dandine, M., Guilhem, A., Merrer, S., Roudil, P., and Bollinger, L. (2015). "The aftershock sequence of the 2015 april 25 Gorkha-Nepal earthquake." *Geophysical Journal International*, 203(3), 2119–2124.
2. AISC Committee. (2010). Specification for structural steel buildings (ANSI/AISC 360-10). American Institute of Steel Construction, Chicago-Illinois.
3. Amadio, C., Fragiacomo, M., and Rajgelj, S. (2003). "The effects of repeated earthquake ground motions on the non-linear response of SDOF systems." *Earthquake Engineering and Structural Dynamics*, 32(2), 291–308.
4. American Society of Civil Engineers (ASCE). (2000). "FEMA 356 Prestandard and Commentary for the Seismic Rehabilitation of Building." *Rehabilitation*, (November).
5. Anderson, J. G., Bodin, P., Brune, J. N., Prince, J., Singh, S. K., Quaas, R., and Onate, M. (1986). "Strong ground motion from the michoacan, Mexico, earthquake." *Science (New York, N.Y.)*, 233(4768), 1043–1049.
6. ANSI, B. (2005). AISC 360-05-specification for structural steel buildings. *Chicago! AISC*.
7. ASCE 41-13. (2014). *Seismic Rehabilitation of Existing Buildings*. American Society of Civil Engineers, Reston, Virginia.
8. Astiz, L., Kanamori, H. & Eissler, H., (1987). "Source characteristics of earthquakes in the Michoacan seismic gap in Mexico". *Bulletin of the Seismological*, 77(4), pp.1326–46.
9. Baker, J. W. (2013). "Trade-offs in ground motion selection techniques for collapse assessment of structures." *Vienna Congress on Recent Advances in Earthquake Engineering and Structural Dynamics*, 2013(123), 28–30.
10. Baker, J. W. (2015). "efficient analytical fragility function fitting using dynamic structural analysis." *Earthquake Spectra*, 31(1), 579–599.

11. Baker, J. W., and Cornell, C. A. (2005). "A vector-valued ground motion intensity measure consisting of spectral acceleration and epsilon." *Earthquake Engineering and Structural Dynamics*, 34(10), 1193–1217.
12. Baker, S. J., and Heyman, J. (1969). *Plastic Design of Frames. 1. Fundamentals. Vol. 1*, Cambridge University Press, New York, 144–168.
13. Bandyopadhyay, M., Banik, A. K., and Datta, T. K. (2008). "Progressive Collapse of Three-Dimensional Semi-Rigid Jointed Steel Frames." *Journal of Performance of Constructed Facilities*, *30*(3), 04015051.
14. Bartera, F., and Giacchetti, R. (2004). "Steel dissipating braces for upgrading existing building frames." *Journal of Constructional Steel Research*.,60(3-5),751-769.
15. Broderick, B. M., Elnashai, A. S., Ambraseys, N. N., Barr, J. M., Goodfellow, R. G., and Higazy, E. M. (1994). "The Northridge (California) earthquake of 17 January 1994: observations. Strong motion and correlative response analysis." *Engineering seismology and earthquake engineering, Research Report No. ESEE*, 94(4).
16. Burton, H. V., Sreekumar, S., Sharma, M., and Sun, H. (2017). "Estimating aftershock collapse vulnerability using mainshock intensity, structural response and physical damage indicators." *Structural Safety*, Elsevier, 68, 85–96.
17. Carreño, M., Cardona, O., and Barbat, A. (2010). "Computational tool for post-earthquake evaluation of damage in buildings." *Earthquake Spectra*, 26(1), 63–86.
18. Champion, C., and Liel, A. (2012). "The effect of near-fault directivity on building seismic collapse risk." *Earthquake Engineering & Structural Dynamics*, Wiley-Blackwell, 41(10), 1391–1409.
19. Code, T. E. (2007). Specifications for buildings to be built in seismic areas. Ministry of Public Works and Settlement, Ankara (in Turkish).
20. Del Carpio, R., Mosqueda, G., and Lignos, D. G. (2016). "Seismic performance of a steel moment frame subassembly tested from the onset of damage

through collapse." *Earthquake Engineering & Structural Dynamics*., 45(10), 1563–1580.

21. Di Sarno, L., and Elnashai, A. S. (2006). "Bracing systems for seismic retrofitting of steel frames." *First European Conference on Earthquake Engineering and Seismology*, 3–8.
22. Di Sarno, L., and Elnashai, A. S. (2009). "Bracing systems for seismic retrofitting of steel frames." *Journal of Constructional Steel Research*, Elsevier Ltd, 65(2), 452–465.
23. Di Sarno, L., and Manfredi, G. (2010). "Seismic retrofitting with buckling restrained braces: Application to an existing non-ductile RC framed building." *Soil Dynamics and Earthquake Engineering*, Elsevier, 30(11), 1279–1297.
24. Domingues Costa, J. L., Bento, R., Levtchitch, V., and Nielsen, M. P. (2007). "Rigid-plastic seismic design of reinforced concrete structures." *Earthquake Engineering & Structural Dynamics*, 36(1), 55–76.
25. Dreger, D. (1997). "The large aftershocks of the Northridge earthquake and their relationship to mainshock slip and fault-zone complexity." *Bulletin of the Seismological Society of America, 87*(5), 1259-1266..
26. Dulinska, J. M., and Murzyn, I. J. (2016). "Dynamic behavior of a concrete building under mainshock-aftershock seismic sequence with a progressive damage and failure material model." *Civil Engineering and Urban Planning IV - Proceedings of the 4th International Conference on Civil Engineering and Urban Planning, CEUP 2015*, Taylor & Francis, 7(1), 695–700.
27. Ellingwood, B. R., and Kinali, K. (2009). "Quantifying and communicating uncertainty in seismic risk assessment." *Structural Safety*, Elsevier Ltd, 31(2), 179–187.
28. Elnashai, A. S., Bommer, J., Baron, I., Salama, A., and LEE, D. (1995). "Selected engineering seismology and structural engineering studies of the Hyogo-ken Nanbu (Great Hanshin) earthquake of 17 January 1995". *ESEE research report ; no. 95-2*.
29. Eshelman, L. J., R. A. Caruana and J. D. Schaffer (1989). Biases in the crossover

landscape. Proceedings of the third international conference on Genetic algorithms, Morgan Kaufmann Publishers Inc.

30. Federal Emergency Management Agency (FEMA). (2000). "FEMA 355F - State of the Art Report on Performance Prediction and Evaluation of Steel Moment-Frame Buildings." *Fema-355F*, 1, 1–367.
31. Fereshtehnejad, E., Banazadeh, M., and Shafieezadeh, A. (2016). "System reliability-based seismic collapse assessment of steel moment frames using incremental dynamic analysis and Bayesian probability network." *Engineering Structures*, Elsevier, 118, 274–286.
32. Folz, B., and Filiatrault, A. (2004). "Seismic Analysis of Woodframe Structures. II: Model Implementation and Verification." *Journal of Structural Engineering*, 130(9), 1361–1370.
33. Fragiacomo, M., Amadio, C., and Macorini, L. (2004). "Seismic response of steel frames under repeated earthquake ground motions." *Engineering Structures*, 26(13), 2021–2035.
34. Fu, F. (2012). "Response of a multi-storey steel composite building with concentric bracing under consecutive column removal scenarios." *Journal of Constructional Steel Research*, *70*, 115-126.
35. Gee Liek Yeo and C. Allin Cornell. (2012). "Post-quake decision analysis using dynamic programming." *Earthquake Engineering & Structural Dynamics*, 41(11), 1549–1568.
36. Goda, K. (2012). "Nonlinear response potential of mainshock–aftershock sequences from Japanese earthquakes." *Bulletin of the Seismological Society of America,* 102(5), 2139-2156.
37. Goda, K. (2015). "Record selection for aftershock incremental dynamic analysis." *Earthquake Engineering & Structural Dynamics*, 44, 1157–1162.
38. Goda, K., and Taylor, C. (2012). "Effects of aftershocks on peak ductility demand due to strong ground motion records from shallow crustal earthquakes." *Earthquake Engineering & Structural dynamics,*41, 2311-2330.
39. Goda, K., Kurahashi, S., Ghofrani, H., Atkinson, G. M., and Irikura, K. (2013). "Nonlinear Response Potential of Real versus Simulated Ground Motions for

the 11th March 2011 Great East Japan Earthquake." *Earthquake Spectra*, 31(3), 1711–1734.

40. Goldberg, D. E. and J. H. Holland (1988). "Genetic algorithms and machine learning." Machine learning 3(2): 95-99.
41. Haddad, M. (2018). "Intermediate HSS bracing members during seismic excitations: modeling, design, and behavior." *Frontiers of Structural and Civil Engineering*, 12(1), 148–162.
42. Haddad, M., Brown, T., and Shrive, N. (2011). "Experimental cyclic loading of concentric HSS braces." *Canadian Journal of Civil Engineering*, 38(1), 110–123.
43. Hamidia, M., Filiatrault, A., and Aref, A. (2014a). "Simplified seismic sidesway collapse analysis of frame buildings." *Earthquake Engineering & Structural Dynamics*, 43(3), 429–448.
44. Hamidia, M., Filiatrault, A., and Aref, A. (2014b). "Simplified seismic sidesway collapse capacity-based evaluation and design of frame buildings with linear viscous dampers." *Journal of Earthquake Engineering*, Taylor & Francis, 18(4), 528–552.
45. Hamidia, M., Filiatrault, A., and Aref, A. (2015). "Seismic Collapse Capacity – Based Evaluation and Design of Frame Buildings with Viscous Dampers Using Pushover Analysis." *Journal of Structural Engineering*, 141(6), 1–12.
46. Han, R., Li, Y., and van de Lindt, J. (2015). "Impact of aftershocks and uncertainties on the seismic evaluation of non-ductile reinforced concrete frame buildings." *Engineering Structures*, Elsevier Ltd, 100, 149–163.
47. Han, R., Li, Y., and van de Lindt, J. (2016). "Seismic Loss Estimation with Consideration of Aftershock Hazard and Post-Quake Decisions." *ASCE-ASME Journal of Risk and Uncertainty in Engineering Systems, Part A: Civil Engineering*, 2(4), 04016005.
48. Han, R., Li, Y., and van de Lindt, J. W. (2014). "Seismic risk of base isolated non-ductile reinforced concrete buildings considering uncertainties and mainshock-aftershock sequences." *Structural Safety*, 50, 39–56.
49. Hashemi, B., and Naserpour, A. (2014). "Performance Evaluation of the Damaged Steel Moment Frames under Mainshock-Aftershock Sequences

Considering Plastic Hinge Modification Factors." *Journal of Seismology and Earthquake Engineering,* 16(4), 261-270.

50. Hatzigeorgiou, G. D., and Beskos, D. E. (2009). "Inelastic displacement ratios for SDOF structures subjected to repeated earthquakes." *Engineering Structures*, 31(11), 2744–2755.
51. Holland, J. (1975). "Adaption in natural and artificial systems." Ann Arbor MI: The University of Michigan Press.
52. Hou, X., and Tagawa, H. (2009). "Displacement-restraint bracing for seismic retrofit of steel moment frames." *Journal of Constructional Steel Research*, Elsevier Ltd, 65(5), 1096–1104.
53. Hua, W., and Chen, Z. (2009). "A Study on Segmentation Characteristics of Aftershock Source Parameters of the Wenchuan M8. 0 Earthquake in 2008." *Chinese Journal of Geophysics*, 52(2), 365–371.
54. Huang, Y., Wu, J. P., Zhang, T. Z., and Zhang, D. N. (2008). "Relocation of the M8.0 Wenchuan earthquake and its aftershock sequence." *Science in China, Series D: Earth Sciences*.
55. Hueste, M. B. D., and Bai, J. W. (2007). "Seismic retrofit of a reinforced concrete flat-slab structure: Part I - seismic performance evaluation." *Engineering Structures, 29*(6), 1165-1177.
56. Hwang, S.-H., and Lignos, D. G. (2017). "Effect of Modeling Assumptions on the Earthquake-Induced Losses and Collapse Risk of Steel-Frame Buildings with Special Concentrically Braced Frames." *Journal of Structural Engineering*, 143(9), 04017116.
57. Ibarra, L. F., and Krawinkler, H. (2005). "Global Collapse of Frame Structures under Seismic Excitations." *Evaluation*, (152), 1–301.
58. International Conference of Building Officials. (1997). *Uniform building code*. International Conference of Building Officials.
59. IS-1893. (2007). Criteria for earthquake resistant design of structures.
60. Ito, A., Uçer, B., Baris, S., and Nakamura, A. (2002). "Aftershock activity of the 1999 Izmit, Turkey, earthquake revealed from microearthquake observations." *Bulletin of the Seismological Society of America*, 92(1), 418–427.

61. Jalayer, F., De Risi, R., and Manfredi, G. (2015). "Bayesian Cloud Analysis: efficient structural fragility assessment using linear regression." *Bulletin of Earthquake Engineering*, Springer Netherlands, 13(4), 1183–1203.
62. Karamanci, E., and Lignos, D. G. (2014). "Computational Approach for Collapse Assessment of Concentrically Braced Frames in Seismic Regions." *Journal of Structural Engineering*, 140(8), A4014019.
63. Kiani, J., Camp, C., and Pezeshk, S. (2018). "Does the number of applied ground motions matter on the structural responses ?" *Eleventh U.S. National Conference on Earthquake Engineering*.
64. Kim, J., Park, J. H., & Lee, T. H. (2011). "Sensitivity analysis of steel buildings subjected to column loss" *Engineering Structures*, *33*(2), 421-432.
65. Koboevic, S., Rozon, J., and Tremblay, R. (2012). "Seismic Performance of Low-to-Moderate Height Eccentrically Braced Steel Frames Designed for North American Seismic Conditions." *Journal of Structural Engineering*, 138(12), 1465–1476.
66. Kojima, K., and Takewaki, I. (2016). "A Simple Evaluation Method of Seismic Resistance of Residential House under Two Consecutive Severe Ground Motions with Intensity 7." *Frontiers in Built Environment*, Frontiers, 2(July), 1–11.
67. Koopaee, M. E., Dhakal, R. P., and MacRae, G. (2017). "Effect of ground motion selection methods on seismic collapse fragility of RC frame buildings." *Earthquake Engineering & Structural Dynamics*, 46(11), 1875–1892.
68. Krishnan, S., and Muto, M. (2012). "Mechanism of Collapse of Tall Steel Moment-Frame Buildings under Earthquake Excitation." *Journal of Structural Engineering*, 138(11), 1361–1387.
69. Kumar, R., and Gardoni, P. (2014). "Effect of seismic degradation on the fragility of reinforced concrete bridges." *Engineering Structures*, 79, 267–275.
70. Kwasniewski, L. (2010). "Nonlinear dynamic simulations of progressive collapse for a multistory building." *Engineering Structures*, Elsevier Ltd, 32(5), 1223–1235.

71. Lai, J. W., and Mahin, S. A. (2014). "Steel concentrically braced frames using tubular structural sections as bracing members: Design, full-scale testing and numerical simulation." *International Journal of Steel Structures*, 14(1), 43–58.
72. Li, J., Gong, J., and Wang, L. (2009). "Seismic behavior of corrosion-damaged reinforced concrete columns strengthened using combined carbon fiber-reinforced polymer and steel jacket." *Construction and Building Materials* , *23*(7), 2653-2663.
73. Li, Q., and Ellingwood, B. R. (2007). "Performance evaluation and damage assessment of steel frame buildings under main shock-aftershock earthquake sequences." *Earthquake Engineering and Structural Dynamics*, *36*(3), 405–427.
74. Li, Y., Song, R., and Van De Lindt, J. W. (2014). "Collapse Fragility of Steel Structures Subjected to Earthquake Mainshock-Aftershock Sequences." *Journal of Structural Engineering*, 140(12), 04014095.
75. Liang, Q. Q., Xie, yi M., and Steven, G. P. (2000). "Optimal topology design of bracing systems for multistory steel frames." *Journal of Structural Engineering*, 126(7), 823–829.
76. Lignos, D. G., Hikino, T., Matsuoka, Y., and Nakashima, M. (2013). "Collapse assessment of steel moment frames based on e-defense full-scale shake table collapse tests." *Journal of Structural Engineering*, 139(1), 120–132.
77. Lignos, D. G., Krawinkler, H., and Whittaker, A. S. (2011). "Prediction and validation of sidesway collapse of two scalemodels of a 4-story steel moment frame." *Earthquake Engineering & Structural Dynamics*, Wiley-Blackwell, 40(7), 807–825.
78. Liu, J. L. (2010). "Preventing progressive collapse through strengthening beam-to-column connection, Part 1: Theoretical analysis." *Journal of Constructional Steel Research*, Elsevier Ltd, 66(2), 229–237.
79. López, S. E., Ayala, A. G., and Adam, C. (2015). "A novel displacement-based seismic design method for framed structures considering P-Delta induced dynamic instability." *Bulletin of Earthquake Engineering*, 13(4), 1227–1247.
80. Luco, N., Bazzurro, P., and Cornell, C. (2004). "Dynamic versus static computation of the residual capacity of a mainshock-damaged building to

withstand an aftershock." *13th World Conference on Earthquake Engineering*, 2405.

81. Maheri, M. R., Kousari, R., and Razazan, M. (2003). "Pushover tests on steel X-braced and knee-braced RC frames." *Engineering Structures*, 25(13), 1697–1705.
82. Mahin, S. A. (1980). "Effects of duration and aftershocks on inelastic design earthquakes." *Proceedings of the 7th world conference on earthquake engineering*.
83. Mai, C., Konakli, K., and Sudret, B. (2017). "Seismic fragility curves for structures using non-parametric representations." *Frontiers of Structural and Civil Engineering*, Higher Education Press, 11(2), 169–186.
84. Málaga-Chuquitaype, C., Elghazouli, A. Y., and Bento, R. (2009). "Rigid-plastic models for the seismic design and assessment of steel framed structures." *Earthquake Eng. Struct. Dyn.*, 38(14), 1609–1630.
85. Malaga-Chuquitaype, C., Elghazouli, A. Y., and Enache, R. (2016). "Contribution of secondary frames to the mitigation of collapse in steel buildings subjected to extreme loads." *Structure and Infrastructure Engineering*, 12(1), 45–60.
86. Marjanishvili, S. M. (2004). "Progressive Analysis Procedure for Progressive Collapse." *Journal of Performance of Constructed Facilities*, 18(2), 79–85.
87. MATLAB [Computer software]. MathWorks, Natick, MA.
88. Montejo, L. A., and Kowalsky, M. J. (2008). "Estimation of Frequency-Dependent Strong Motion Duration Via Wavelets and Its Influence on Nonlinear Seismic Response." *Computer-Aided Civil and Infrastructure Engineering*, 23(4), 253–264.
89. Moustafa, A., and Takewaki, I. (2011). "Response of nonlinear single-degree-of-freedom structures to random acceleration sequences." *Engineering Structures*, 33(4), 1251–1258.
90. Moustafa, A., and Takewaki, I. (2012). "Characterization of earthquake ground motion of multiple sequences." *Earthquake and Structures*, 3(5), 629–647.
91. Muntasir Billah, A. H. M., and Shahria Alam, M. (2015). "Seismic fragility

assessment of highway bridges: a state-of-the-art review." *Structure and Infrastructure Engineering*, Taylor & Francis, 11(6), 804–832.

92. Nasional, B. S. (2002). Standar Perencanaan Ketahanan Gempa Untuk Gedung. SNI, 3, 1726.
93. Nazari, N., van de Lindt, J. W., and Li, Y. (2015a). "Effect of Mainshock-Aftershock Sequences on Woodframe Building Damage Fragilities." *Journal of Performance of Constructed Facilities*, 29(1), 04014036.
94. Nazari, N., van de Lindt, J. W., and Li, Y. (2015b). "Quantifying Changes in Structural Design Needed to Account for Aftershock Hazard." *Journal of Structural Engineering*, 141(11), 04015035.
95. NBCC, N. (2005). National building code of Canada. National Research Council of Canada (NRCC), Ottawa, Canada.
96. Oliver, I., D. Smith and J. R. Holland (1987). Study of permutation crossover operators on the traveling salesman problem. Genetic algorithms and their applications: proceedings of the second International Conference on Genetic Algorithms: July 28-31, 1987 at the Massachusetts Institute of Technology, Cambridge, MA, Hillsdale, NJ: L. Erlhaum Associates, 1987.
97. Özel, A. E., and Güneyisi, E. M. (2011). "Effects of eccentric steel bracing systems on seismic fragility curves of mid-rise R/C buildings: A case study." *Structural Safety*, 33(1), 82–95.
98. Pang, Y., and Wu, L. (2018). "Seismic Fragility Analysis of Multispan Reinforced Concrete Bridges Using Mainshock-Aftershock Sequences." *Mathematical Problems in Engineering*, 2018.
99. Park, S. W., Park, H. S., Oh, B. K., and Choi, S. W. (2018). "Fragility Assessment Model of Building Structures Using Characteristics of Artificial Aftershock Motions." *Computer-Aided Civil and Infrastructure Engineering*, *33*(8), 691-708.
100. Patil, D. M., and Sangle, K. K. (2015). "Seismic Behaviour of Different Bracing Systems in High Rise 2-D Steel Buildings." *Structures*, Elsevier B.V., 3, 282–305.

101. Pei, S., and van de Lindt, J. W. (2010). "Influence of structural properties and hazard level on seismic loss estimation for light-frame wood structures." *Engineering Structures*, 32(8), 2183–2191.

102. Powell, G. (2005). "Progressive Collapse: Case Studies Using Nonlinear Analysis." *Structures Congress 2005*, 1(1), 1689–1699.

103. Raghunandan, M., and Liel, A. B. (2013). "Effect of ground motion duration on earthquake-induced structural collapse." *Structural Safety*, 41, 119–133.

104. Raghunandan, M., Liel, A. B., and Luco, N. (2015). "Aftershock collapse vulnerability assessment of reinforced concrete frame structures." *Earthquake Engineering & Structural Dynamics*, Wiley-Blackwell, 44(3), 419–439.

105. Renzi, E., Perno, S., Pantanella, S., and Ciampi, V. (2007). "Design, test and analysis of a light-weight dissipative bracing system for seismic protection of structures." *Earthquake Engineering & Structural Dynamics*, 36(4), 519–539.

106. Roeder, C. W., and Popov, E. P. (1978). "Eccentrically Braced Steel Frames for Earthquakes." *Journal of the Structural Division*, ASCE, 104(3), 391–412.

107. Ruiz-García, J. (2012). "Mainshock-Aftershock Ground Motion Features and Their Influence in Building's Seismic Response." *Journal of Earthquake Engineering*, 16(5), 719–737.

108. Ruiz-García, J. (2014). "Discussion on 'Effects of multiple earthquakes on inelastic structural response.'" *Engineering Structures*, 58, 110–111.

109. Ruiz-García, J., and Aguilar, J. D. (2015). "Aftershock seismic assessment taking into account postmainshock residual drifts." *Earthquake Engineering and Structural Dynamics*, 44(9), 1391–1407.

110. Ruiz-García, J., and Negrete-Manriquez, J. C. J. (2011). "Evaluation of drift demands in existing steel frames under as-recorded far-field and near-fault mainshock-aftershock seismic sequences." *Engineering Structures*, 33(2), 621–634.

111. Safarizki, H. A., Kristiawan, S. A., and Basuki, A. (2013). "Evaluation of the use of steel bracing to improve seismic performance of reinforced concrete building." *Procedia Engineering*, Elsevier B.V., 54, 447–456.

112. Salami, M. R., and Goda, K. (2014). "Seismic Loss Estimation of Residential Wood-Frame Buildings in Southwestern British Columbia Considering Mainshock-Aftershock Sequences." *Journal of Performance of Constructed Facilities*, 28(6), A4014002.
113. SAP 2000 [Computer software]. Computers and Structures, Inc., Berkeley, CA.
114. Santa-Ana, P.R. & Miranda, E., 2000. Strength reduction factors for multi-degree-of-freedom systems. *Proceedings of the 12th world conference on Earthquake Engineering*, (2), pp.1–8.
115. Sarno, L. Di. (2013). "Effects of multiple earthquakes on inelastic structural response." *Engineering Structures*, 56, 673–681.
116. Scholz, C. (2002). *The Mechanics of Earthquakes and Faulting*. Cambridge university press.
117. Shaback, B., and Brown, T. (2003). "Behaviour of square hollow structural steel braces with end connections under reversed cyclic axial loading." *Canadian Journal of Civil Engineering*, 30(4), 745–753.
118. Sharma, A., Reddy, G. R., Eligehausen, R., and Vaze, K. K. (2011). "Experimental and analytical investigation on seismic behavior of RC framed structure by pushover method." *Structural Engineering and Mechanics*, 39(1), 125–145.
119. Shcherbakov, R., Turcotte, D. L., and Rundle, J. B. (2005). "Aftershock statistics." *Pure and Applied Geophysics*, 162(6–7), 1051–1076.
120. Song, R., Li, Y., and van de Lindt, J. W. (2014). "Impact of earthquake ground motion characteristics on collapse risk of post-mainshock buildings considering aftershocks." *Engineering Structures, 81*, 349-361.
121. Song, R., Li, Y., and Van De Lindt, J. W. (2016). "Loss estimation of steel buildings to earthquake mainshock-aftershock sequences." *Structural Safety*, *61*, 1-11.
122. Syswerda, G. (1989). "Uniform crossover in genetic algorithms".

123. Sun, C., Chen, J., and Zhang, Y. (2016). "Damage-based Strength Reduction Factor for Sequence-type Ground Motions." *the 2016 world congress on the 2016 structures congress*.

124. Tamai, H., and Takamatsu, T. (2005). "Cyclic loading tests on a non-compression brace considering performance-based seismic design." *Journal of Constructional Steel Research, 61*(9), 1301-1317.

125. Tena-colunga, A., and Vergara, A. (1997). "Comparative Study on The Seismic Retrofit of A Mid-Rise Steel Building : Steel Bracing vs Energy Dissipation." *Earthquake engineering & structural dynamics*, *26*(6), 637-655.

126. Tsai, K. C., and Popov, E. P. (1988). *Steel beam-column joints in seismic moment resisting frames, Vol. 2*, Univ. of California, Berkeley, CA.

127. Tremblay, R. (2002). "Inelastic seismic response of steel bracing members." *Journal of Constructional Steel Research 58*(5-8), 665-701.

128. Tremblay, R., Archambault, M.-H., and Filiatrault, A. (2003). "Seismic Response of Concentrically Braced Steel Frames Made with Rectangular Hollow Bracing Members." *Journal of Structural Engineering, 129*(12), 1626-1636.

129. Vafaei, D., and Eskandari, R. (2015). "Seismic response of mega buckling-restrained braces subjected to fling-step and forward-directivity near-fault ground motions." *The Structural Design of Tall and Special Buildings*, *24*(9), 672-686.

130. Vanmarcke, E., 1972. Properties of spectral moments with applications to random vibration. *Journal of the engineering mechanics division*, 98(2), pp.425–446.

131. Vargas, Y. F., Pujades, L. G., Barbat, A. H., and Hurtado, J. E. (2013). "Capacity, fragility and damage in reinforced concrete buildings: a probabilistic approach." *Bulletin of Earthquake Engineering*, Springer Netherlands, 11(6), 2007–2032.

132. Wittrick, W. H. (1968). "Sidesway Collapse modes for Groups of Vertical Columns." *International Journal of Mechanical Sciences*, 10, 549–562.

133. Wyllie, L. (1983). "Seismic strengthening procedures for existing buildings."

Strengthening of building structures-Diagnosis and Theory, International association of bridge and structural engineering symp., Venice, Italy, 363–370.

134. Xie, Q. (2005). "State of the art of buckling-restrained braces in Asia." *Journal of Constructional Steel Research, 61*(6), 727-748.

135. Yin, Y. J., and Li, Y. (2010). "Seismic collapse risk of light-frame wood construction considering aleatoric and epistemic uncertainties." *Structural Safety*, Elsevier Ltd, 32(4), 250–261.

136. Youssef, M. A., Ghaffarzadeh, H., and Nehdi, M. (2007). "Seismic performance of RC frames with concentric internal steel bracing." *Engineering Structures, 29*(7), 1561-1568.

137. Zareian, F., Krawinkler, H., Ibarra, L., and Lignos, D. (2010). "Basic concepts and performance measures in prediction of collapse of buildings under earthquake ground motions." *Struct. Des. Tall Special Build.*, 19(1–2), 167–181.

138. Zentner, I., Gündel, M., and Bonfils, N. (2017). "Fragility analysis methods: Review of existing approaches and application." *Nuclear Engineering and Design*, Elsevier B.V., 323, 245–258.

139. Zhao, X. L., and Zhang, L. (2007). "State-of-the-art review on FRP strengthened steel structures." *Engineering Structures*, 29(8), 1808–1823.

BIO-DATA

The author is currently serving as Assistant Professor (Civil Engineering) at the National Institute of Technology Uttarakhand, Srinagar Garhwal. He obtained his bachelor's degree in Civil Engineering from Malaviya National Institute of Technology, Jaipur in 2010. He completed his master's degree in Structures with dissertation on "*Smooth Finite Element Methods with Polynomial Reproducing Shape Functions*", from the Indian Institute of Science Bengaluru in 2013. His area of specialization is "Earthquake Engineering".

Following is the list of the publications from his Doctoral work

List of publications

Journals

S. Narayan, M.K. Shrimali, S.D. Bharti, T.K. Datta, "Collapse of damaged steel building frames because of earthquakes". Journal of Performance of Constructed Facilities, 32 (1), 04017128.

S. Narayan, M.K. Shrimali, S.D. Bharti, T.K. Datta, "Effects of mainshock-aftershocks sequence on the performance of steel building frames". International Journal of steel structures (under review).

S. Narayan, M.K. Shrimali, S.D. Bharti, T.K. Datta, "Retrofitting of Building frames for Enhanced performance under a sequence of aftershocks". Journal of Earthquake engineering (under review).

Conferences

S Narayan, M K Shrimali, SD Bharti and TK Datta, "Seismic Behavior of Damaged Building Under Second Episode of Earthquake" 10th Structural Engineering Convention by SERC CSIR Chennai at Chennai / 1164-1169 / 2016

S. Narayan, M.K. Shrimali, S.D. Bharti and T.K. Datta, "Progressive collapse of damaged structures under seismic excitation" Sixteen World Conference on Earthquake Engineering by IEA at Santiago, Chile / 1-12 / 2017

S. Narayan, M.K. Shrimali, S.D. Bharti and T.K. Datta, “Performance of Retrofitted Building under the Sequence of Mainshock and Aftershocks" Sixteen Symposium on Earthquake Engineering by IIT Roorkee at Roorkee / paper id 211/ 2018